Università degli Studi di Padova

Dipartimento di Ingegneria Industriale
Corso di Laurea in Ingegneria Aerospaziale

Preliminary Dimensioning and Design of an Ultralight Acrobatic Motor-Glider Powered by a Self-Sufficient Electric Solution

Dimensionamento e Design Preliminare di un Moto-Aliante Acrobatico Propulso Mediante una Soluzione Elettrica Autosufficiente

Relatore:
Ch.mo Prof. Ugo Galvanetto

Laureando:
Marco Marzari

Corelatore:
Ch.mo Prof. Francesco Picano

Academic Year 2017/2018

Contents

1 Introduction **1**
1.1 Why Researching on Electric Propulsion Aircraft 2
1.2 Motivation and Objectives 3
1.2.1 Phases of an Aeronautical Project 5
1.3 The Electric Powered Flight 6
1.4 Brief Summarize on Solar Powered Aircraft Prototypes 7
1.4.1 First Conceptual and Experimental Prototypes 7
1.4.2 The Beginning of Solar Aviation 9
1.4.3 From Model-Scale Aircaft to H.A.L.E. 9
1.4.4 State of the Art in Conceptual Methodology Design . . 16
1.5 Structure of this Work 17

2 General and Fundamental Concepts **19**
2.1 Basic Sailplane Aerodynamics Laws 20
2.1.1 Introduction 20
2.1.2 Airfoil and Wing Aerodynamic Theory 22
2.1.3 Typical Sailplane Wing Geometry 28
2.2 Aeronautic Structures: First Aspect Considerations 30
2.3 The Innovative Purpose: The Electric Propulsion Solution . . 32
2.3.1 Photovoltaic Cell: Working Principle and Typology . . 33
2.3.2 Power Accumulator: Electrochemical Batteries 37
2.3.3 Electric Engine: New Motion Way 37
2.3.4 AC Motor Equations 40

3 Aerodynamic and Structural Conceptual Design **43**
3.1 Design : Requirements and Approach 44
3.1.1 Glider Airworthiness: Rules for a Safety Project 46
3.1.2 Force Balance for in-Flight Glider 46
3.1.3 L/D Efficiency Parameter 48
3.2 Preliminary Weight Estimation 50
3.3 Preliminary Airfoil Design 66

3.3.1 Introduction: Main Airfoil Parameters 67
3.3.2 Aerodynamic Considerations on Finite Wings 68
3.3.3 List and Properties of Chosen Airfoils 69
3.3.4 The Airfoil Polar Graph 72
3.3.5 Wing Geometry 77
3.3.6 Tail Dimensioning and Design 82
3.3.7 Correction of Aerodynamic Parameters 84
3.4 The Flight Envelope Diagram 87
3.4.1 Spiral Flight Performance 94
3.4.2 Climbing Flight Performance 99
3.4.3 Maximum Efficiency Velocity $V_{L/D_{BEST}}$ 102
3.4.4 *Lofting* the Solar Powered Motorglider 102

4 Computational Fluid Dynamics Simulations 107
4.1 Introduction to Computational Fluid Dynamics 108
4.2 Governing Equation 109
4.3 Pre-Processing 112
4.4 Solution Set-Up 114
4.5 Post-Processing: Results 120
4.5.1 Airfoil CFD Results 120
4.5.2 Complete Wing C_L CFD Results 121
4.5.3 Comparison with Theoretical Results 137
4.5.4 Glider With and Without Winglet Comparison 137
4.6 Verification and Validation 138
4.6.1 Airfoil C_l Verification 144

5 The Self-Sufficient Electric Solution 149
5.1 Introduction 150
5.1.1 Requirements for Energy Devices 150
5.2 Estimation of *Flying Power* Required 150
5.2.1 Take-Off Ride 152
5.2.2 Levelled Flight with Velocity Increment 153
5.2.3 Increase in Altitude 154
5.2.4 Levelled Flight at $V_{L/D_{MAX}}$ 155
5.3 Photovoltaic Panel Choice and Configuration 155
5.4 Solar Radiance Evaluation 157
5.4.1 Photovoltaic Panel Mass Estimation 167
5.5 Electric Motor Choice and Configuration 168

6 Results Summary and Future Developments 175
6.0.1 Future Developments 179

7 Appendix **181**
Appendix A 181
Appendix B 184
Appendix C 196

List of Figures

1.1 Design process structures,divided in three macro-areas including preliminary design, project design and detail design[22]. . . 5
1.2 Some of the newest electric aircraft presented at AERO 2017 in Friedrichshafen[1]. 8
1.3 The first solar-electric powered fly machine, a model scale prototype edveloped thanks to Astro Flight Inc in collaboration with ARPA. It open the way of solar powered aircraft future [18]. 10
1.4 The solar powered model wih held actually world records in longest rectilinear distance and duration[18]. 10
1.5 The Gossamer Penguin was designed and built on 1980 by Dr. Paul B. McCready. Was the first solar aircraft piloted directly by human and demonstrated the possibility to conceive the solar flight[18]. 12
1.6 The Solar Riser was a improved version of the Easy Rider hang glider which combine aerodynamic facility with solar propulsion implant[18]. 12
1.7 Helios project, designed to be the ultimate eternal plane and made by NASA. Improved from the previous project Centurion, it achieve the incredible altitude of 30 000 m (2001) before crashing on Pacific Ocean caused by structural fail in 2003[11]. 14
1.8 Little HALE model that break the barrier of 24 hours flight with only solar energy and batteries[18]. 14
1.9 Solar Impulse 1, considered as a prototype for the successor Solar Impulse 2. Wingspan of 63 m, long 21.85 m and a takeoff speed of 35 km/h. It weigh 2000 kg and has a cruise speed of 70 km/h. His funder and investor Bertand Piccard tested it flighting from Switzerland to Spain and then to Marocco in 2010[12]. 15

1.10 Solar Impulse 2 has a wingspan of 71 m, 22.4 m length, a cruise speed of 90 km/h during daytime and 60 km/h during night to save batteries. With it, Bertrand Piccard established new world record of circumnavigation in a solar airplane taking 16 months and 42000 km.[12]. 15

2.1 The principle of aerodynamic sustentation : on the left the equilibrium condition of a GA airplane[18]; on the right the equilibrium condition of a sailplane[24]. 21
2.2 Forces and moment acting on an ideal 2D airfoil immersed in a flow. Centre of pressure is positioned at a quarter of the chord length, Drag is opposed to the freestream velocity while the Lift is perfectly orthogonal to it. 23
2.3 The two reference points, the aerodynamic centre and the centre of pressure of the airfoil[24]. 23
2.4 Three images of the same ideal profile at different angle of incidence[25]. 24
2.5 Skin friction drag very closed to wing surface(a) and in a global airfoil view(b)[25]. 26
2.6 Induced drag is a part of the total drag, derived from the fact that real wing has finite wingspan and subsequently to the lift generation[25]. 27
2.7 Types of wing shape used in aviation[24]. 29
2.8 Structures comparison between two different categories of aircraft. 31
2.9 Typical glider airframe. 32
2.10 Typical wing structure[26]. 32
2.11 Working principle of photovoltaic cell https://www.nrel.gov/docs/legosti/old/1448.pdf[36]. 34
2.12 Solar radiation Spectrum[18]. 35
2.13 The energy budget diagram shows best understanding of energy flows into and away from the Earth. https://science-edu.larc.nasa.gov/energy_budget/. 35
2.14 Efficiency chart of photovoltaic cell technologies updated until year 2017. Source https://www.nrel.gov/. 36
2.15 Graph on different types of batteries technologies at the state of the art[18]. 38
2.16 Quick and easy picture of main differences between brushed and brushless DC motor. https://www.youtube.com/watch?v=RsqHr2cpp4M. 39
2.17 Basic principal function of AC motor [58]. 41

3.1 The Design Wheel [39]. 45
3.2 Forces acting on in-flight aircraft[40]. 47
3.3 Required Thrust to V_∞ diagram [40]. 49
3.4 First order design method [39]. 52
3.5 Empty weight fraction versus W_0 [39]. 52
3.6 *empty weight* in [kg] expressed as a function of wingspan b on the top; Wingspan as a function of aircraft's length. Both for only Motorglider. 54
3.7 *empty weight* in [kg] expressed as a function of wingspan b on the top; Wingspan as a function of aircraft's length. Both for only Glider. 55
3.8 Wingspan as a function of aircraft's length on the top; *empty weight* in [kg] expressed as a function of wingspan b. Both for all aircraft. 56
3.9 Wing Aspect ratio as a function of wingspan [m] on the top and empty weight[kg] for only motorglider. 57
3.10 Wing surface[m^2] as a function of wingspan [m] for only motorglider. 58
3.11 Evaluation through interpolation equation of main design parameters. 60
3.12 Evaluation through interpolation equation of main design parameters. 61
3.13 Stender equation[16] and database data in logarithmic graphs which variable is S [m^2] and dependant parameter is W [kg]. It is clear the good alignment between data and Stender's equation. 64
3.14 Noth equation[18] and database data in logarithmic graphs which variable is S [m^2] and dependant parameter is W [kg]. Noth's equation overstate glider's weight data containing in database. 65
3.15 the airfoil geometry and principal features [39]. 67
3.16 Typical sailplane operating condition, in terms of Reynolds number. 69
3.17 Polar graphs example, relative to NACA 44415 airfoil. 75
3.18 Graphs developed thanks to Delft University which help to perform best wing shape with minor induced drag. 78
3.19 Wing geometry designed in **SolidWorks**®with quoted measure and mean aerodynamic chord length evaluation. 80
3.20 Conceptual and qualitative force distribution on a sailplane;Dimension in meters. 82
3.21 Flight Envelope Diagram example and load factor limit for acrobatic glider[34]. 89

3.22 Reymar's method [39] for *Flight Envelope Diagram* estimation. 91
3.23 *Flight Envelope Diagram* using Pajno's Method [34] referenced to wing only. 92
3.24 *Flight Envelope Diagram* using Pajno's Method [34] referenced to complete Glider. 93
3.25 Polar velocity graphs at different Reynolds Number referred only to $C_{L_{Wing}}$. 96
3.26 Polar velocity graphs at different Reynolds Number referred only to $C_{L_{Glider}}$. 97
3.27 Spiral Flight Performance evaluated with $C_{L_{Wing}}$ and $C_{L_{Glider}}$ to characterize the dive velocity as a function of spiral radios. 98
3.28 Evaluation of glider compared with only wing climb performance, Re=1E6. 100
3.29 Evaluation of glider compared with only wing climb performance, Re=1E6. 101
3.30 Evaluation of Best L/D evaluating first the induced and parasite drag composition, second the distribution of L/D against TAS; The C_d value use is associated to that of the glider. . . . 103
3.31 Useful suggestion provide by [34] and [39] on the tail plan position and winglets design. 104

4.1 Summarize scheme of correct analysis procedure. 108
4.2 Solved set equation process in FLUENT [50]. 111
4.3 Control fluid volume dimension. 113
4.4 Different type of mesh on different models, from 2D airfoil to 3D Glider. 115
4.5 3D mesh parameters describing discretization quality onEntire Glider. 117
4.6 2D mesh parameters describing discretization quality on FX 61-147 118
4.7 2D mesh parameters describing discretization quality on FX 63-137. 119
4.8 C_l and C_d convergence graphs, at different angle of attack, same Reynolds number=1E6 123
4.9 C_l and C_d convergence graphs, at high AoA: 15 degree for FX 61-147 and 12.5 degree for FX 63-137; same Reynolds number=750k. 124
4.10 Example of difference residuals tendency as a function of simulation parameters. 125
4.11 Post-Process results: Pressure, Velocity field and Velocity stream for FX 61-147 airfoil at AoA=0 and 12.5 degree; Re=1E6. . . 126

4.12 Post-Process results: Pressure, Velocity field and Velocity stream for FX 61-147 airfoil at AoA=-2 and 12.5 degree; Re=750k. . 127
4.13 Post-Process results:Pressure, Velocity field and Velocity stream for FX 63-137 airfoil at AoA=0 and 12.5 degree; Re=1E6. . . 128
4.14 Post-Process results: Pressure, Velocity field and Velocity stream for FX 63-137 airfoil at AoA=0 and 12.5 degree; Re=750k. . . 129
4.15 Post-Process results: Turbolence Kinetic Energy for FX 63-137 and FX 61-147 airfoil at AoA=12.5 degree; Re=1E6 and 750k. 130
4.16 Boundary Layer mesh not good approximation. Best compromise between Hardware resources and results quality. 131
4.17 Table containing Airfoil CFD simulation Results at Re=1E6 and Re=750k when varying AoA. 132
4.18 C_l and C_d Graph which represents Airfoil CFD simulation Results at Re=750k and 1E6 when varying AoA. 133
4.19 C_l and C_d variation graphs vs iteration for 3D glider model with winglet. 134
4.20 C_l and C_d variation graphs vs iteration for 3D glider model without winglet. 135
4.21 CFD results at Re= 1E6 on glider with and without winglet. . 136
4.22 Difference between C_l values referred to glider with and without winglet. 136
4.23 Pressure distribution over fuselage and wings for Glider model with winglet; Re=1E6 along flight direction over wings at 0, 10 and 15 degree. 139
4.24 Force distribution over fuselage and wings for Glider model with winglet; Re=1E6 along flight direction over wings at 0, 10 and 15 degree. 140
4.25 Velocity Streamline over the entire aircraft; Re=1E6 along flight direction over wings at 0, 10 and 15 degree. 141
4.26 Streamline of fluid particles on specific aircraft region to observe vortices and fluid interferences;Re=1E6 comparison between glider with and without winglets. 142
4.27 Other post-processing images on wing-fuselage interference and wing-tip vorticity. 143
4.28 Airfoil FX 63-137 experimental data graphs on wind tunnel facilities [53]. 145
4.29 Value gap between results given from **Profili2**®and **FLUENT**®against the experimental data obtained in a wind tunnel facilities [53]. 146

5.1 Compromise choice based on a surface curve radiance evaluation; minimize losses, maximize energy acquisition[56]; image for qualitative purpose. 156
5.2 Comparison between photovoltaic silicon monocrystalline area respect to photovoltaic silicon amorphous technologies. Dimension in meters. 157
5.3 Solar radiation evaluated thanks to PVGIS[55] interactive web program for different locations. 159
5.4 Solar radiation and horizon height evaluated thanks to PVGIS[55] interactive web program for different locations. 160
5.5 Horizon height on July and December in Siracusa[55]. 161
5.6 Solar Radiation specific energy [W/m^2] for different location at different latitude evaluated thank to PVGIS considering *Global Real Sky*[54]. 161
5.7 Comparison between the total and available($\eta_{Monocrustalline} = 25\%$, $\eta_{Amorphous} = 15\%$) energy can be acquired on exposed surface [54]. 162
5.8 Energy can be acquired in different location on silicon monocrystalline and amorphous technology-based photovoltaic panel[54]. 163
5.9 Direct comparison between energy acquired from monocrystalline and amorphous silicon technology-based photovoltaic panel[54]. 164
5.10 Li-Ion cell performance variation, depending on time discharge and temperature[58]. 165
5.11 Define rechargeable temporal limits based on energy required for take-off. 166
5.12 Possible location for electric brushless motor. 169
5.13 The electric brushless motor device, develop to satisfy motor-glider requirements. 172
5.14 FES propellers created to obtain best performance from the electric motor. 173

List of Tables

3.1 Reymar's equation results for total weight and empty weight fraction estimation. 53
3.2 Average value of main geometric and mass parameters belonged to the created database and available in appendix A. . 59
3.3 Chosen value for predicting aerodynamic performance. 63
3.4 Table relative to the correction process of wing and tail airfoil main parameters[34]. 88

4.1 Number of Nodes and Elements for the two set of 2D simulation for both airfoil and for the 3D simulation. 113
4.2 2D Mesh statistics on FX 61-147 airfoil. 114
4.3 2D Mesh statistics on FX 63-137 airfoil. 114
4.4 Set Up environment conditions(ρ,velocity and viscosity) evaluated with characteristic length of 1 m to obtain Re=1E6 and Re=750k. 120
4.5 3D simulation boundary conditions. 133
4.6 Comparison between hand calculation performance [34] and simulation results provided by **ANSYS**®;Re=1e6; percentage deviation from hand calculation. 137

5.1 Take-off ride initial Value. 152
5.2 Levelled flight with velocity increment initial value. 153
5.3 Increase in altitude flight configuration initial value. 154
5.4 Maximum efficiency velocity and initial value. 155
5.5 Comparison between commercial flexible and rigid photovoltaic alternatives 167
5.6 Mass estimation based on available surface for energy absorption. 168
5.7 Evaluation of the ultimate required power from motor, knowing the flight power and assuming reasonably η_{motor} and $\eta_{propeller}$ equal to 0.95%. 170
5.8 Motor requirements and specifications. 170

Dedication

To my father Stefano, who inspired me and supported my ambition in this journey
To my mother Lauretta who taught me to live and not to demise
To my brother Carlo, a friend of life
To my grandmothers Antonia and Celidonia for their love, support and generosity
To my girlfriend Astrid, who always be without asking anything, for the wisdom and kindness, which every day colours the pages of my life
To Antonio, Donatella, Daris, Giulia, for their friendliness, comprehension and taught me to be myself
To my University colleagues, for the long days spent together on projects and thanks to whom I am here
To my friends, for happy memories, dreams and future hopes

To all, thank you for believe in me.

Acknowledgement

The synthesis of this project from the ambitious but valid claims, required a series of analysis and considerations that span three distinct macro areas, namely aerodynamics, energy and structure. The achievement of the presented results, although of a preliminary nature, was made possible thanks to the support of Prof. Galvanetto, who motivated me in this journey, finding out which were the best ways to go; to Prof. Picano, who thanks to his aerodynamic knowledge, taught me the best techniques of calculation and helped in validating formulas; to Prof. Bianchi and Bignucolo, Professors of the Energy Department, which I was able to confront on alternative and sustainable technologies and how to dimension them to better meet the requirements of this project; last but not least the prof. Sambin, who thanks to his personal experience and matured with "Il Merlo", supported the project by collaborating with Prof. Galvanetto. Thanks for giving an identity to this job.

Abstract

The University of Padua, in pursuit of the "Merlo" project being built by the Aerolab team, has decided to invest in a semi-autonomous solar-powered motorglider. The requirements are: mass less than 200 kg, wingspan from 8 to 12 meters, rise speed limit 2 m/s, self-picking capacity. The objective is to identify constraints and specifications for subsequent studies through an analysis and a preliminary dimensioning, aimed at analysing in depth each sector: propulsion, aerodynamics, structure.
The aircraft category was set up, and by means of a historical-statistical design approach, a database of motorglider and their technical characteristics was created. Database analysis allow to chose first design parameters: 'Aspect Ratio'=20, usual value in gliders, and wingspan b=12 meter for which it has a length of 5 meter and 255 kg of mass. Aerodynamics was then investigated by **Profili2**®software that implements the *XfoiL* code. It is a Low-Re aircraft, operating on the transition layer between laminar and turbulent. The Lift curves of an airfoil group were studied for Reynolds varying from 100k to 1E6 in order to evaluate different environment types, and two were selected to meet the requirements of high efficiency, high lift and flight power. So we used the design techniques of prof. Pajno to estimate the best wing configuration. The result is a double tapered wing twisted negatively 2.5 degree, 7.26 m^2 wing surface. The Xfoil values were corrected to take account the finite wing and the preliminary performance values were derived. At the same time, a 3D representation with **SolidWorks**®has been developed that summarizes all the choices made. 2D and 3D CFD analyses were carried out for the in-depth study of the selected profiles and the 3D model created. For these analysis was adopted the $k - \omega$ SST algorithm and it is evident that above 10 degrees, the data is not very reliable. Therefore it is required experimental investigation. The 3D analysis has allowed to study complex three-dimensional geometry and evaluate the turbulence effects. Finally, the propulsion apparatus was dimensioned. For the choice of photovoltaic panels, it was necessary to investigate the intensity of radiation for different latitudes and on this basis choose the optimal compromise between monocrystalline or amorphous silicon photovoltaic technology. Amorphous silicon technology has been chosen for this configuration due to its versatility and flexibility to cover multiple surface wings. Flight configurations were studied, from which the flight powers were extracted, information needed to dimension the batteries and the engine. 250 Wh/kg lithium batteries and high performance brushless motor was selected. Following a comparison between different electric motors, it was found that the FES (Front Electric Sustainer) best meet requirements.

Abstract Italiano

L'Università degli Studi di Padova, in prosecuzione del progetto *Merlo* sviluppato dal team Aerolab, intende sviluppare un motoaliante a ricarica solare e spinto, quando necessario, da un motore elettrico. I requisiti sono: massa inferiore a 200 kg, apertura alare da 8 a 12 metri, velocità di salita limite 2 m/s, capacità di decollo autonomo. L'obiettivo è identificare mediante un analisi preliminare i vincoli e le specifiche per realizzare un primo dimensionamento e fornire le basi per approfondire: propulsione, aerodinamica, struttura.
Una volta fissata la categoria di velivolo, è stato adottato un approccio storico-statistico di design e si è generato un database di motoalianti con relative caratteristiche tecniche. Dallo studio del database si sono potuti fissare i seguenti parametri: *Aspect Ratio*=20, valore usuale negli alianti, ed apertura alare di 12 metri; lunghezza di 5 metri e 255 kg di massa. Si è investigata l'aerodinamica mediante il software **Profili2**®che implementa il codice *XfoiL*. Si tratta di un aereo che opera in regime Low-Reynolds, nella zona di transizione tra moto laminare e turbolento. Si sono studiate le curve di portanza di una famiglia di profili alari al variare del numero di Reynolds da 100k a 1E6, al fine di considerare più tipologie di flusso. Sono stati selezionati due profili della stessa famiglia che soddisfano i requisiti di alta efficienza, alta portanza e fattore di potenza. Quindi si sono utilizzate le tecniche di progettazione del prof. Pajno per stimare la migliore configurazione d'ala. Il risultato è un'ala a doppia rastremazione con svergolamento di 2.5 gradi e superficie di 7.26 m^2. I valori di Xfoil sono stati corretti per tener conto degli effetti d'ala finita e si sono ricavate le prestazione di volo preliminari. Contemporaneamente si è sviluppata una rappresentazione 3D con **SolidWorks**®che sintetizza tutte le scelte effettuate. Sono state svolte delle analisi CFD 2D e 3D dei profili scelti e dell'aliante creato. Per queste analisi è stato adottato l'algoritmo $k - \omega$ SST e si è notato come al di sopra dei 10 gradi di angolo d'attacco, i dati non siano molto attendibili. Per questi valori di angoli sarebbe necessaria una valutazione sperimentale. Infine è stato dimensionato l' apparato propulsivo. Per i pannelli fotovoltaici è stato necessario investigare l' intensità di radiazione per diverse latitudini e sulla base di ciò scegliere il compromesso d'ottimo tra tecnologia fotovoltaica a silicio monocristallino o amorfo. La tecnologia al silicio amorfo è stata scelta per questa configurazione data la versatilità e flessibilità che permettono di coprire più superficie alare. Sono state studiate delle configurazioni di volo tipiche per le quali si sono valutate le potenze di volo, informazioni necessarie per dimensionare le batterie e il motore. Batterie agli ioni di litio da 250 Wh/kg e motore brushless ad alte prestazioni. A seguito di una comparazione fra prodotti di varie industrie operanti nel campo dei motori elettrici, si è riscontrato che il motore brushless FES soddisfa meglio i requisiti di volo.

Chapter 1

Introduction

1.1 Why Researching on Electric Propulsion Aircraft

"We know that dreams fuel innovation"
Bertrand Piccard

Humanity's interest in heavens has been universal and enduring. Humans are driven to explore the unknown, push the boundaries of our scientific and technical limits. The desire to explore and challenge the boundaries of what we know and where we have been has provided benefits to our society for centuries. Space exploration, for example, could helps to address fundamental questions about our place in the Universe and the history of our solar system, expand technology, create new industries, and help to foster a peaceful connection with other nations. Curiosity and exploration are vital to the human spirit.
This is the beginning of a new era in space exploration in which NASA,ESA and others space agencies has been challenged to develop systems and capabilities required to explore beyond low-Earth orbit, including destinations such as translunar space, near-Earth asteroids and eventually Mars. To achieve these goals it is necessary a rigid method enabling to proceed gradually.
Inventions and prototypes developed during important researches, as described above, will be available in everyday life in order to reach better and certainly innovative lifestyle. There are examples of this kind that can be found from hospitals to the "World Wide Web". The photovoltaic cell technology used during the space missions of the 1970s is nowadays used in common domestic installations. Widespread progress is anticipated in research laboratories and on average over 20-30 years it has been made available throughout the world. Around the early millennium, the automotive market was overwhelmed by a new hybrid vehicle prototype. Nearly two decades, hybrid technology has undergone a huge leap forward, thanks to carbon-based emissions treaties signed by industrialized countries and the constant and necessary awareness of the pollution problem. Despite the countries' disbelief about the actual harmfulness of smog, the improper use of fossil fuels and its consequences on the viability of this planet (greenhouse, global warming), the road that is facing the Humanity is started, and electricity as a feed to a combustion engine or even as main propulsion is real. The use of hybrid or electric propulsion is also spreading in the aeronautical sector. It is necessary to know that the number of commercial tracts, both for the carriage of stuffs and people, is constantly increasing and the search for new

drivers, larger fleets, could become an element of criticism from the point of view of pollution. Certainly the number of aircraft in circulation is less than the number of road vehicles and a comparison between the pollution produced by a civil aircraft with a car would not be correct. All over the world, aircraft manufacturers such as Boeing and Airbus have recently concluded agreements with energy industries to come in a few decades to the first hybrid vehicle. This is a sign of progress and of release from the matter that had opened the past industrial revolution.
There are many benefits of using an electric vehicle, as are the disadvantages, especially from the point of view of design. Nevertheless, responsibility for the planet Earth and its resources is becoming increasingly heavy. One of the key issues that have to be clarified and resolved is "how do we produce electricity?", "Is it an efficient and ecologically sustainable technique?", "What are the impacts of this technology?" This issue will not be argument in this project. However the improving methodology adopted from these major air company, it's also linked to the better efficiency of the energy that could be stored and used directly in motion of the engine parts. As with terrestrial vehicles, and commercial aircraft, electric propulsion solutions are also gaining ground in the private aeronautics industry. Engineering design issues on the efficiency of these devices as a much smaller scale, as well as for the masses, has brought some results.

1.2 Motivation and Objectives

With new electrical and hybrid technologies, the continuous advancement in research to optimize fuel consumption by boosting performance, over the last decades an incredible increase in fully developed or prototype projects has been observed in order to combine electrical technology with the aviation world. One of the main goals that major airlines and government hopes to reach is a plane that can travel for long periods of time around Earth at high altitude and remote controlled. Recently, HALE experiments have yielded positive results and the private project Solar Impulse has confirmed the feasibility of flight 24 hours with an aircraft powered by only electricity derived from Sun. The potential of an aircraft powered solely by direct solar energy or stored in batteries was originally acquired by NASA, while civilian airlines such as Boeing and Airbus are opting for a hybrid alternative. That technology would hopefully low the consumption and emissions while maximizing efficiency in power delivery. One of the factors contributing to the adoption of this technology in the civil transport sector is certainly awareness of the human footprint on the climate change, and also the increase

in population and resource consumption will also lead to an increase in flights and air traffic. As we have already seen in the automotive world, where the hybrid and the pure electricity are already marketed, the world of aeronautics and the naval industry are also moving in this direction. Not only for ethical or moral judgement but also (and above all) for a reduction in consumption, maintenance costs, greater transmission efficiency and energy delivery. The first prototypes developed are small aeromodels belonging to the category of experimental ultralight aircrafts and in this direction the University of Padua is also to be set up, aiming at the realization of an electric airplane powered by solar energy. In particular the project aim to developed an aerobatic motorglider which is propulsed by an electric motor, feed from solar cell positioned on wing surfaces. Indeed the University of Padua has developed yet an acrobatic ultralight airplane called *Merlo* and for the preliminary design of aerodynamic, structural and weight would be used some topics of these researches[20][21].
Below is a list of the main objectives to be achieved with this project:

- Search history background on solar aircraft
- Define the main features in a preliminary way in terms of weight and aerodynamics
- Define the feasibility of the project considering various configuration of airfoil and geographical zone
- Prove with simulation first-approach model, by taking in consideration the previous results
- Treat in general three principal aspect: Aerodynamics, Structure and Energy hardware

Concerning motivation aspects, the combination between low cost fuel (even free) and civilian flight transport is becoming a reality and it'is important to continue researching and testing new prototypes that could be used in future or that will help to define a new design approach for developing the aircraft of tomorrow. It will be clear when Reader come closer to the end of this thesis. Until that moment, some interesting results, extracted from previous investigation and prototypes, have confirmed the following features:

- Better efficiency on delivering energy from batteries to electric motor
- Soundless system with low impact sound wave

- Reliability of the entire system and consequently of the machine indeed there's no fluid or violent combustion that could be problematic
- Security requirement less severe than turbojet engine
- No pollution or poison substances product by the machine
- Reduce supply costs with an integration of solar cells and hangars that could provide a rapid charging during the wait time.
- Reduce maintenance costs

These are a small amount of the global possibility that could be achieved with the implementation of solar energy driven propulsion in a modern civil plane.

1.2.1 Phases of an Aeronautical Project

The production process of an aircraft, either military, civil or GA, is the result of a homogeneous and coherent organization among the project's responsible parts who use method and rigid criteria to meet the company's interests. The sever control which aeronautical projects are completed, leads to the ac-

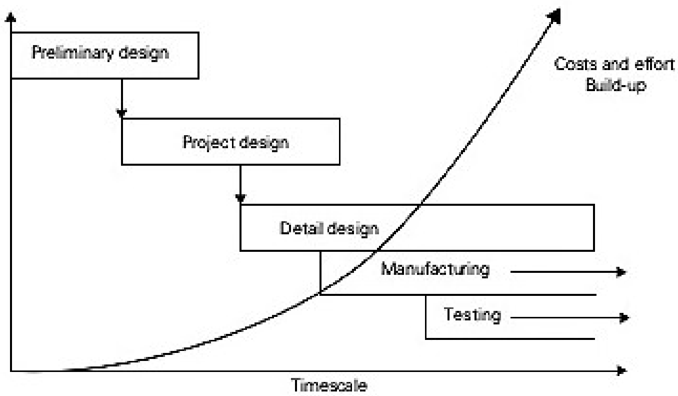

Figure 1.1: Design process structures,divided in three macro-areas including preliminary design, project design and detail design[22].

quisition of the quality certificate for the manufacturer and this entails new opportunities for contracting and investment. The development of any item, especially for an aircraft, is articulated through successive phases that can be summarized in Figure 1.1. The project begins with *Feasibility Studies*, which are part of the **Preliminary** or **Conceptual Design** phase, which demonstrates the feasibility of the aircraft based on the project data provided by the contracting entity or the specific customer through request for proposal. The general architecture is defined. Designers working at this stage developing new conceptual prototypes continuously, aware that only a small part of their proposals will exceed the preliminary exam. The result is a technical document that specifies the individual project subsystems, however, with a general view and not in depth. Specifically, it identifies the architecture that best meets the requirements, especially the minimum weight that is obtained at this stage by statistical data by acquiring similar aircraft data. It follows the **Project Design** phase in which expert technicians are tasked with concretizing the ideas contained in the preliminary documents. In this case, they are people with specializations in different sectors and rarely related. At the end of project phase, starts the **Detail Design** phase, in which the first prototype is built and then the **Industrialization**. The process does not end here, as the company also works to provide support to users and customers. Typically, the life cycle of an aeronautical program is average thirty years with a trend towards fifty years[23].

In this paper we will try to provide the reader with a broader view on electric airplanes field, by developing a virtual model of solar powered motor-glider for an additional propulsion to be used in case of emergency or need. This thesis will focus, from a technical point of view, in the preliminary phase of conceptual development and feasibility study, explaining choices and parameters with different levels of formalities in order to facilitate understanding for a general public.

1.3 The Electric Powered Flight

This year was held in Friedrichshafen, the German city, the twenty-fifth edition of the world exhibition of aeronautical vehicles and the latest developments in the industry. This event was also attended by Frank Anton, vice president of Siemens and aeronautical industry who commented on the presence of a large amount of electrical ultra-light aircraft and prototypes with the phrase: "In 2030 we will fly with electric motors and a hybrid battery charging system. " This statement was immediately transformed into the news of the fair[1][2]. Siemens®'s collaboration with Airbus and Andrè Borschberg[1] has led to the development of an acrobatic electric drive that will be used for serial production. But it is no less the Pipistrel company that with its *Alpha Electro* was awarded the best electric airplane of the year with a cruising speed of 108 knots and a 60 minute autonomy reserve. Over

[1] co-founder of Solar Impulse project, the first ever round-the-world solar flight

to the innovative solutions offered at the fair, the one that is most likely to succeed is surely the hybrid motor, that is affected by endothermic motor generator sets, in particular conventional fuel engines that recharge batteries connected to the electric motors. Not only airplanes but also helicopters have begun to undertake the electric road, for example the *Aquinea Volta*, which has an empty weight of 420 kilograms and is powered by two continuous 70 kW engines and 90 kilowatts of peak. One of the real problems lies in the flight autonomy of the aircraft, linked to aerodynamic efficiency,engine power efficiency and battery technology that nowadays is the bottle neck of these kind of projects.

The revolutionary idea of using electric power to move an airplane is not recent but is to be attributed around the 1970s, when NASA was planning to develop an airplane capable of resettling hours or days flying only with convex flux and electric engine, powered by solar panels. This configuration can be adopted in those aircraft that have a high sun exposure. The electrical configuration can be imagined as that of a satellite where solar energy is stored in accumulators that, on demand, provide energy to the load. In the aeronautical world, the load mentioned above is an electric engine.

1.4 Brief Summarize on Solar Powered Aircraft Prototypes

In the following sections, it will be explain the development process through the year since early 50th. Researches about the solar technology and its linkage with electric motors is not really recent as we can think. Only in the last decades was globally diffused the possibility to fly with hybrid or pure electric solution thanks to the trust of main aircraft building company, how ever the studies on this new field were initiated thanks to great researchers and few persons.

1.4.1 First Conceptual and Experimental Prototypes

The use of electric power on flying vehicle is attributed to Colonel H. J. Taplin, who on June 1957 made the first officially and historical recorded radio controlled flight with his model "Radio Queen", which used a permanent-magnet motor ad a silver zinc battery. Then Fred Militky achieved a succesfull flight with an uncontrolled model in October of the same year. Since this new project, battery and electric motor technology continue improving[3].

The *Equator P2*, hybrid aircraft within the motor-generator *Engiro G60*[1].

The Swiss made*H55*, single seat and acrobatic electric aircraft developed by Andrè Borshberg [1].

The *Alpha Electro*, of *Pipistrel*[1].

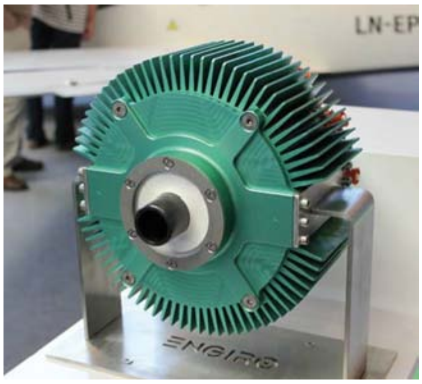

The *Engiro G60*,97 kW and 32 kg weight, air and liquid cooled[1].

Figure 1.2: Some of the newest electric aircraft presented at AERO 2017 in Friedrichshafen[1].

Although the electric motor-solar cells link was not already began. Photovoltaic technology was born at Bell Telephone Laboratories where Daryl Chapin, Calvin Fuller and Gerald Pearson developed the first silicon photovoltaic cell[3].

1.4.2 The Beginning of Solar Aviation

On 1974 the Sunrise I, developed by Astro Flight Inc in collaboration with ARPA, flew for 20 minutes at an altitude of 100m. This was the first flight of a solar powered aircraft. It had a wingspan of 9.76 m, weighed 12.25 kg, 4096 solar cells and a power output of 450 W[4]. Later the Sunrise II was tested on September 1975 that distinguished from Sunrise I for less mass, better solar cells in terms of efficiency and more power output(approx. 600W). Over the next decades, the improvement in design, electric motors and batteries technology, pushed many government research centers and free professionals on the road of electric flight. A recent example is that of Dave Beck, a US citizen who established two records in 1996 with his solar-powered aircraft model called Solar Solitude, F5 category in the FAI[5][6]. It reached the altitude of 1283 m and flew a distance of 38,84 km. The current record is held by Wolfgang Schaeper with his model Solar Excel in terms of flight duration(11 h 34 min 18 s) and distance(48.31 km) from 1990 to 1999[7].

1.4.3 From Model-Scale Aircaft to H.A.L.E.

With the first scale models prototypes, was demonstrated the possibility of conceiving the flight of an aircraft propelled by the only energy extracted from solar irradiation. The positive outcomes of these first researches led the first pioneers of this sector in large-scale experimentation. It has moved from the development of electric models to cover long distances or participate in amateur championships on real manned ultralight aircraft.
On 1979, Larry Mauro flew for the first time the Solar Riser, a solar version of Easy Rider hang glider. Although the 350 W were insufficient to power the airplane and so on was decided to insert a battery package. His longest flight covered about 800 m at altitudes varying between 1.5 e 5 m. The manned solar aviation was started. On 1980, Dr. Paul B. McCready and his society AeroVironment Inc realized the first controlled-long endurance fly with the Gossamer Penguin. At this point there were other crucial consideration in design to investigate and solve. The good result hold with Gossamer Penguin, motivated AeroVironment Inc to ask finances and search for investors with the final purpose to go across the English Channel. The Gossamer Penguin successor called Solar Challenger was a 14.2 m wingspan with 16128 solar

Figure 1.3: The first solar-electric powered fly machine, a model scale prototype edveloped thanks to Astro Flight Inc in collaboration with ARPA. It open the way of solar powered aircraft future [18].

Figure 1.4: The solar powered model wih held actually world records in longest rectilinear distance and duration[18].

cells offering 2500 W at sea level. On 1981 flew from Puntoise-Cormeilles to Manston RAF Base near London in 5 hours 23 minutes covering 262.3 km with only solar energy and no storage equipment as battery on-board. When they arrived in England, heard about a German, Gunter Rochelt, who was trying to realize the same record with a solar aircraft called Solair I. However the features of Solair I, even if innovative in design, were no sufficient to realize the England Channel crossing, that was reached several years later in 1983. In 1986, Eric Raymond began to design a competitive and aerodynamic clear aircraft called Sunseeker, which established an other world record for this new typology of air vehicle: the entire cross country of U.S. in 21 days and 121 hours in flight[8]. Later on 1996 in Germany, in the town of Ulm, was organized a special competition exclusively for electric and solar aircraft. This match provided a money prize for the prototype which should be able to stay up with at least half of the solar energy a good summer day with clear sky[9]. The winner was the motorglider Icarè 2 from Stuttgart University[10]. There were other two important competitors : *O Sole Mio* from the italian team of Dr. Antonio Bubbico and *Solair II*, second generation prototype of the Prof. Gunter Rochelt.
Government and important research centres as NASA, understood rapidly the potential usage of these kind of machine, powered exclusively from solar energy, noiseless and invisible at high altitudes, remote controlled and full time available with rarely maintenance and completely stand-alone. The idea to conceive solar aircraft as a low altitude satellite substitution was on go. US Government take a deal with AeroVironment Inc., company that realized Gossamer Penguin, Gossamer Albatross, to study the feasibility of long duration flight at altitude above 20000 km. A first prototype called HALSOL was built to test the aerodynamic and structure features but it defect on energy storage and propulsion performance. In 1993 was built *Pathfinder*, a 30 m wingspan and 254 kg aircraft define officially the new NASA's programme called ERAST (Environmental Research Aircraft Sensor Technology). In 1995 it reach the Solar challenger altitude at 15392 m and in 1995 break the wall of 20000 m. The NASA's programme ERAST signed the future research on solar-powered aircraft because the entry of this major and technology advance centre in this kind of project would be attractive for investors, provided a great deal of support for researches. The next step was to improving the energy subsystems, propulsion hardware and optimize aerodynamic for low velocity,high altitude and low mass. From 1997 to 1999 scientist and engineer were busy on the new project Centurion, developed as demonstrator of new low orbit remote aircraft that could stay in flight for months. It reached altitude over 24 000 m but the low efficiency of lithuym battery used, doesn't allowed the flight during night[11]. The successor called *Helios* was the first

Figure 1.5: The Gossamer Penguin was designed and built on 1980 by Dr. Paul B. McCready. Was the first solar aircraft piloted directly by human and demonstrated the possibility to conceive the solar flight[18].

Figure 1.6: The Solar Riser was a improved version of the Easy Rider hang glider which combine aerodynamic facility with solar propulsion implant[18].

solar aircraft to achieve 30000 m recorded. Secondarily it would do an entire flight during 24h but for structure failure it collapse on Pacific Ocean. Helio's unfinished target was reached in 2005 by an unmanned aircraft called Solong, made thanks to Alan Cocconi, president of AcPropulsion. The autonomous aircraft model flew for over 24 hours with the only solar energy directly used or stored for the night. It was 4.75 m wingspan, 11.5 kg mass. While Dr. Cocconi try to establish the longest duration flight record, an other company called QinetiQ based on California, was developing Zephyr, which arrived at an altitude of 17 786m with a weigh of 30 kg for 18 m wingspan. Recently it was selected for a new project called Pegasus, to use as a platform for next generation HALE UAV. The main purpose of Pegasus project is to maintain the same feature of Zephyr and improve the payload capability to 100 kg.

The development evolution process of solar aircraft started from little prototypes model, coming through first ultralight aircraft with discrete performances and the realization of unmanned, relatively little HALE, achieved the best configuration with Solar Impulse project[12], a manned and huge solar airplane, with a wingspan bigger than a Boeing 747, capable to carry one person. It is a privately financed project led by Swiss engineer Andrè Borschberg and Swiss psychiatrist and balloonist Bertrand Piccard, last one held the world record to circle the world no stop in a balloon. Solar Impulse 1 was the prototypes to investigate the capability of this new kind of solar aircraft. Researcher and scientist who worked for this project ascertain that Solar Impulse 1 can stay airborne for 26 hours in 2010. Although Piccard flew from Switzerland to Spain and then to Morocco in 2012 and realize a successful cross country flight in USA. It was clear that Solar Impulse Project was the right wasy to prove the feasibility of continuous flight with only solar energy. The next generation aircraft called Solar Impulse 2 signed the aviation history with a great flight around the entire world on 2015 taking 16 months to travel approximately 42000 km.

Future Development and Perspectives for Solar Aircraft

In many areas of research, it has already been possible to use HALE aircraft[26]. The development paths are started and soon we will see the first results. Among the applications expected for this type of aircraft are the exploration of planetary atmosphere. Recently, some scientists from NASA and ESA agencies are designing drones to explore the surface of a planet and allow mapping much faster than a rover on wheels and more defined image of an orbiting satellite[32]. In addition to the purely aerospace research field with exploratory mission, there are also military uses with ISR applications. Given the unsustainable solar source at high altitude, the theoretical duration of

Figure 1.7: Helios project, designed to be the ultimate eternal plane and made by NASA. Improved from the previous project Centurion, it achieve the incredible altitude of 30 000 m (2001) before crashing on Pacific Ocean caused by structural fail in 2003[11].

Figure 1.8: Little HALE model that break the barrier of 24 hours flight with only solar energy and batteries[18].

Figure 1.9: Solar Impulse 1, considered as a prototype for the successor Solar Impulse 2. Wingspan of 63 m, long 21.85 m and a take-off speed of 35 km/h. It weigh 2000 kg and has a cruise speed of 70 km/h. His funder and investor Bertand Piccard tested it flighting from Switzerland to Spain and then to Marocco in 2010[12].

Figure 1.10: Solar Impulse 2 has a wingspan of 71 m, 22.4 m length, a cruise speed of 90 km/h during daytime and 60 km/h during night to save batteries. With it, Bertrand Piccard established new world record of circumnavigation in a solar airplane taking 16 months and 42000 km.[12].

a flying plane is infinite if not interrupted by mechanical failures[27]. There is also interest from civil telecommunication agencies whose goal is to exploit HALE technology to ensure better medium-range coverage in a higher quality and superior extension than a terrestrial infrastructure[28]. The close observation of the Earth's wide surface area would also allow for more accurate algorithms to prevent natural disasters such as floods or large-scale fires than those based on current satellite imagery[29]. Finally, it is also trying to implement solar technology to promote agricultural development, allowing long-term observation of cultivated soils for extensive analysis on large-scale optics. Cheaper than using a satellite, more accurate for image resolution and coverage, more extensive than sample testing that a lab technician might accomplish[30][31].

1.4.4 State of the Art in Conceptual Methodology Design

Before the realization of a prototype, it is necessary to establish a theoretical-preliminary development method in order to demonstrate the feasibility of the project. Although the theories used are the simplest as a preliminary study and are simplified for an ideal reality, it is crucial to obtain the first data as a comparison. The projects so far described are property of private companies and very often they do not provide information about the conceptual method employed, or the large number of existing methods stops at the theoretical level without validating it with a practical experiment. In the development of solar airplanes as HALE or UAV long-lasting , there are papers dating back to the early 1980's, when NASA started the first projects. Here they are remembered as example, even if this thesis will be less near to the HALE projects. R. J. Boucher published in 1979 a description of performances and hardware used in the Sunrise project, with no explanation of the design process[13]. Unfortunately this behaviour is also presented on McCready's papers which talks about Gossamer Penguin and Solar Challenger[14]. How ever some papers give informations or tips about guidelines on design process as the oldest of them, written by F.G. Irving in 1974. He presented a manned airplane design[15] using weight prediction models for the airframe, the propulsion group and solar cells. To estimate the airframe weight he used Stender's equation based on statistical data for sailplane[16]. David and Stan Hall developed in 1984 a new method to predict the airframe weight of solar aircraft but it reveals to be valid only for airplane weight of 450 to 1360 kg. In 2005 Rizzo developed an interesting method but limited to big airplanes. Concerning only weight models, authors consider the weight of all the elements as proportional to the wing surface, such as Brandt in 1995 using iterative design process[17]. Guglieri in 1996 simplifies excessively the problem, saying that the wing structural weight is linear proportional to the surface. Rehmet also consider a wing weight proportional to its surface, revised after the Berblinger contest on 1996 with a polynomial formula between surface and wingspan. It is still valid for 15 to 40 m wingspan and it was used on Icarè 2 project. The design of solar powered airplane was also studied by many students during bachelor or master project but them results poor in some parts or not completely depth. An interesting research conducted by Andrè Noth[18] during his doctorate period explains an other typology of conceptual design methodology, based on previous work that it seems to be functional and valid because he had tested it on a amateur model called Sky-Sailor under a contract with ESA, capable to flight over 24 hours autonomously. His conceptual and theoretical method could be used on model solar prototypes as big airplane. Mehdi Hajianmaleki of Mississippi State University defined a conceptual method design for solar powered aircrafts based on traditional design technologies but modified to include special features of solar vehicles. In depth he has defined an iterative method and used a linear extrapolation between take-off weight versus wing area to obtain the first step parameters[19]. In this works the contribution of all these researches, in particular Andrè Noth investigation, will be taken into account and used in some parts, especially on the electrical features.

1.5 Structure of this Work

After this general and not at all complete but wide introduction, explaining motivations and the state of the art on technological level of improving the link between the electric field and aviation, the next chapter will define some theories and concepts on aerodynamics and structures of a plane, in a general way, and the energetic devices such as batteries, motor and control hardware. In chapter three we will go inside specific field, exposing the development process considered in this project, the specific formulas, aerodynamics and structural configurations. At this point will be fixed some design elements, basing on previous works or valid and consolidated textbooks. Will be shown data and results of the configurations considered and explain why the project have to be realize with these parameters. Although with the software **Profili2**®will be exposed some graphics on the critical parameters just talk about before. In chapter 4, readers will be able to see the results of design process done until now, in a three-dimensional and bi-dimensional rendering using the software **Solidworks**®. Also some general and essential simulation using CFD and FEM numerical solution will be realized and explained using the software **Ansys®**. In chapter 5 will be observed the electrical solution in a general and systematic way, analysing in depth what was previously described in chapter 2, which device and hardware configuration will satisfied the propulsion and weight requirements. At the end, in chapter 6, the results obtained on precedent chapters will be presented synthetically and also what have to be depth or improve in section *Future Developments* to continue the research and choose the best design.

Chapter 2

General and Fundamental Concepts

2.1 Theory and Basic Concepts on Gliders' Aerodynamic Laws

2.1.1 Introduction

In this chapter we will provide the reader with the aerodynamic basics needed to understand simple formulas that will be used in subsequent chapters for design. The previously illustrated project is very ambitious, though not impossible. As mentioned in the paragraphs above, the development of a motor-glider powered by an electrical technology that allows the overcoming of a fundamental physical barrier such as the *maximum efficiency distance*[1] to reach the landing track in adverse conditions or, in extreme cases, an off-site location make the difference to the pilot's health. By neglecting for a moment the aforementioned conditions in which a pilot can be, without however ignoring, the propulsion infrastructure will be designed to support the pilot in a flight that can be defined under nominal conditions to facilitate translation and to eliminate partially the dependence on convective currents[2] to fly. For this reason, the link between the energy-propulsion and the aerodynamic-structural apparatus is not mixed and coexisted, as it would be for an HALE, an aircraft that have different requirements, flight targets and specifications.

Like any other aircraft, sailplane also comply with the laws of macroscopic physics that affect any object present on the Earth's surface, with particular reference to the phenomena that are most present between surface and tropopause, until an average altitude of 12 km, where most of civil aircraft flies. Among the main forces that govern the dynamics of a plane in level flight conditions we recognize **Gravity**, the aerodynamic forces of **Lift** and **Drag**, **Thrust**. In Figure 2.1 it is possible to understand the equivalence between these forces to keep a plane, from general aviation to turbojet, in flight. A glider for the specific definition is an aircraft heavier than air, which is supported in flight due to the dynamic air reaction against wing surfaces and whose free flight does not depend on a motor[25]. In this case the dynamics of the glider in the absence of convective currents is determined by the gravity that acts as on any object in fall. However, due to the geometry of the wings,

[1] maximum distance on ground that can be reach by an airplane with no thrust; this condition can be satisfied if the aircraft fly at the maximum efficiency velocity, define by the airfoil and the general architecture

[2] air mass that goes up, reaching altitude. The intensity of ascension flux become more strong with the increment of solar irradiation during the day and it will be more probable to identify under a cumulus or where there are light colour field, due to the best reflection conditions to the upper fluid mass

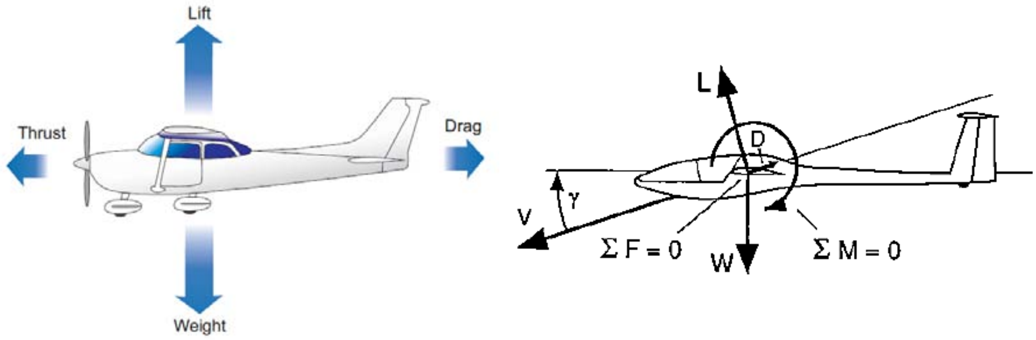

Figure 2.1: The principle of aerodynamic sustentation : on the left the equilibrium condition of a GA airplane[18]; on the right the equilibrium condition of a sailplane[24].

a pressure force called lift that is opposed to weight is generated. Because of the friction, there is a loss on potential energy, initially possessed by a glider, during the conversion into kinetic energy that impose to land. A motorglider is distinguished from the glider simply for the installation of a small endothermic engine or in the more recent cases of an electric motor that gives greater flexibility to the pilot than a normal sailplane.

Physical Properties of the Atmosphere

The flow of air around a sailplane in flight is determined by the laws of fluid mechanics. The state of the air is determined by a number of physical properties such as pressure, density, temperature, compressibility, kinematic viscosity and relative humidity. Due to gravity, solar radiation and topography, these properties vary considerably, especially at low altitudes. Several standard atmospheric models exist, used to describe the atmosphere environment and dynamics. They are also used to design aircraft indeed there's a great change on performance from ground to ten thousand meters, for example caused by a reduction of density. One of the most consolidated atmosphere model is the 1964 ICAO Standard atmosphere, which represents an atmosphere free from meteorological influences and will be described well in the next chapters. How ever these standard atmospheric models are idealization based on empirical data and focused on the *Perfect Gas Law*

$$p = \rho RT \tag{2.1}$$

that links pressure variation[Pa] to density[kg/m^3] and temperature[K], through the specific gas constant R. Obviously the fluid mechanics of particles that flow on aircraft surfaces is not so simple. Acceleration leads to inertia forces, compression to elastic forces and shearing to viscous forces. The relation between these three forces and geometric form of the aircraft is defined by the *Navier-Stokes Equation* that will be not presented or demonstrated here but the reader could find a lot of information and clearly explained on [33].

2.1.2 Airfoil and Wing Aerodynamic Theory

Any moving object that is affected by a pressure difference between two opposing surfaces also undergoes the effect of generating an aerodynamic force. In the case where the motion is horizontal and the two surfaces are one upper and lower, a force is able to support the body. As it is moving, there will also be a force component that is opposed to the horizontal motion due to friction that must be counterbalanced by a propulsion force. A first justification for the development of pressure difference can be found in the Bernoulli theorem[3] properly modified which states that the pressure exerted by a fluid moving around a body is inversely proportional to the speed of the fluid itself[24].

$$p_T = p_\infty + \frac{1}{2}\rho v_\infty^2 \tag{2.2}$$

It is possible to interfere constructively with the genesis of the pressure difference not only by changing the contour geometry but also by varying the incidence angle. Typically, the pressure forces observed to act in a profile are sunk according to a Cartesian reference system where horizontal axes is among the v_∞ direction, conventionally centred at one quarter of the chord length from the attachment edge. The source point of this reference is the *aerodynamic centre*, point about which the moment remains constant as the lift varies, that is, the moment gradient is zero. Absolutely different, Figure 2.3, from the *Centre of pressure*, point on the airfoil at which the lift acts. That is the reference point about which the pitching moment is zero and moves along the profile when changing the velocity toward the attachment edge. However, for low Mach values, we can accept the previous assumption. The forces in question are lift and drag, draw on Figure 2.2.

Lift: Brief Analysis

Below is a general introduction to the concept of Lift in intuitive considerations so that the elaborate is easy to understand. Try to imagine, with the knowledge just learned, a wing profile immersed in a stream of air. It

[3]The resulting equation of the integration process on Euler Equation. Hypothesis:fluid has to be steady, incompressible and inviscid

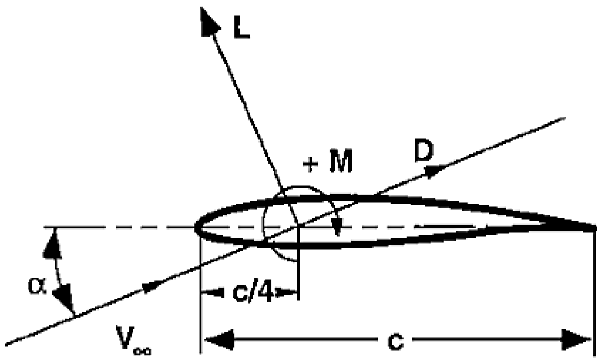

Figure 2.2: Forces and moment acting on an ideal 2D airfoil immersed in a flow. Centre of pressure is positioned at a quarter of the chord length, Drag is opposed to the freestream velocity while the Lift is perfectly orthogonal to it.

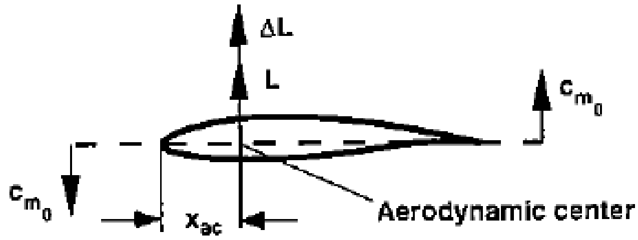

(a) the aerodynamic centre and zero-lift moment

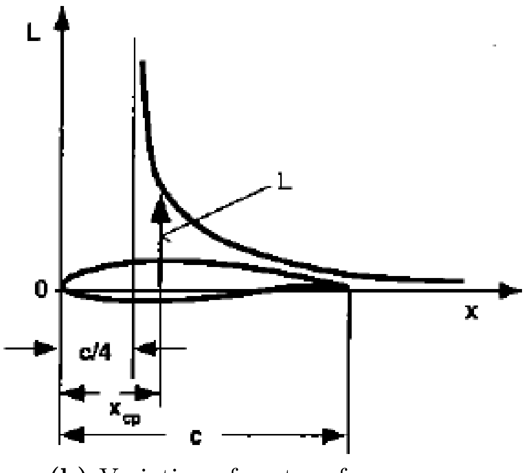

(b) Variation of centre of pressure

Figure 2.3: The two reference points, the aerodynamic centre and the centre of pressure of the airfoil[24].

appears intuitive as the incidence angle increases,would do the same also the lift and this can be justified by the fact that the particles moving on the upper surface need to travel at a higher speed to reach the particles that flow to the lower surface and this results in an increase in the variation of pressure that ,as it was conceived, generates the Lift. However, this profile's aptitude has limits, and in particular there is a limit beyond which the profile is no longer capable of generating lift and performance fall. Start the Stall effect. This phenomenon is related to the behaviour of fluid threads running on the upper surface of the wing for which, besides a certain angular value, they no longer remain attached as the centrifugal force of the various particles is higher than the cohesive force. You can appreciate it in Figure 2.4. At this stage, the simplest aerodynamic theories can no longer be applied as outside the ideal field traced by the underlying hypotheses and therefore it is necessary to run into numerical advanced analyses based on turbulence models. Typical angular values in which the stall occurs are between 15 and 20 degrees. To calculate lift we can use this formula:

$$L = \frac{1}{2}\rho v^2 S c_L \tag{2.3}$$

where c_L is the Lift coefficient, which depends heavily on airfoil chosen, the angle of attack and the Reynolds Number.

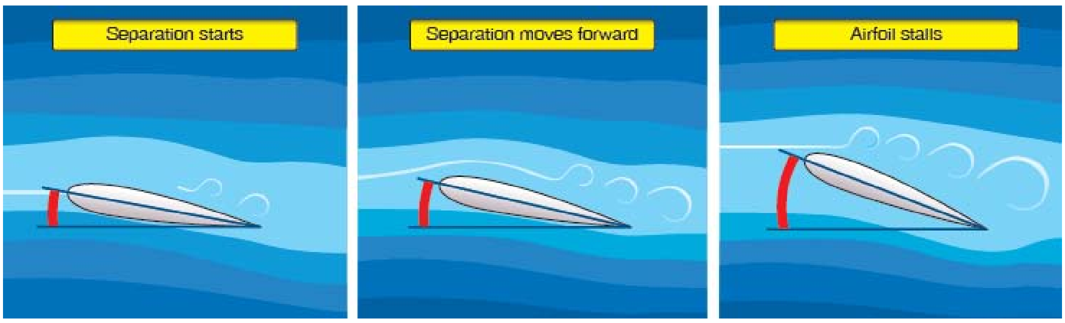

Figure 2.4: Three images of the same ideal profile at different angle of incidence[25].

Drag: Brief Analysis

As we previously said, Drag is the force generated with Lift, caused by the pressure variation between upper and lower surface of an airfoil. Similarly to Lift, it is possible tu use simplified equation tu calculate it:

$$D = \frac{1}{2}\rho v^2 S c_D \tag{2.4}$$

where c_D is the Drag coefficient, which depends heavily on airfoil chosen, the angle of attack and the Reynolds Number. Drag is composed of multiple terms:

- **Parasite Drag**: is the resistance offered by the air to anything moving through it. Typically the wing of the sailplane alone has very low parasite drag, but when the total drag of the glider is added to it, the amount of drag becomes significant. Parasite drag increases with the square of velocity. it is divided in three types:

    1. *Form Drag* : results from the turbulent wake caused by the separation of airflow from the surface of a structure. Any object moving through the air, push the air in front of it out of the way. the difference in pressure between the front and back surfaces of the object results in the parasite drag. It could be reduce by reducing the object's cross sectional area or by streamlining it;
    2. *Skin Friction Drag* : caused by the roughness of the glider's surfaces and depends on the skin material and superficial treatment realized. This roughness allows a thin layer of air to stay attached to the surface, contributing drag generation. this layer then slows the layer above it and so on. This layer of decelerated air is called *Boundary Layer*, as you can see in Figure 2.5. It is possible to distinguished the Laminar Boundary Layer and the Turbolent Boundary Layer, since the latter has five to ten times skin friction produced;
    3. *Interference Drag* : Occurs when varied current of air over glider meet and interact. For example the mixing air over structures such the junction between fuselage and wing or fuselage and tail. It could be reduce by designing the glider in such way that can penetrate better the airflow;

- **Induced Drag** : Caused for the directly consequence of lift generation. Every aerodynamic theories as Kutta-Joukowsky, are based on simplification. This Drag term born as the natural passage from the

Infinite length wing to the *Finite length wing* proposed on the lifting-line theory of L. Prandtl. For a real wing vortices are produced at the wing tip. As the higher pressure air on the lower surface of the airfoil curves around the end of the wing and fills in the lower pressure area on the upper surface, the lift is lost, yet the energy to produce the different pressures is still expended. The coefficient of Induced drag $C_{D_{ind}}$ is proportional to the square of the lift coefficient and inversely proportional to the aspect ratio. For better and intuitively comprehension see Figure 2.6.

At the end, global drag coefficient can be expressed with the formula:

$$C_{D_{ind}} = \frac{C_L^2}{e\pi AR} \tag{2.5}$$

where:
C_L : Lift Coefficient, defined by the airfoil geometry chosen;
e : is the Oswald efficiency factor that has a value between 0 and 1; 1 being the ideal case where the load distribution on the wing is elliptical.
Glider designers attempt to reduce drag by increasing the aspect ratio of the glider. The greatest aspect ratio of the wing is, the lower the induced drag is. However is not convenient increasing with no attention the aspect ratio, to avoid excessive mass.

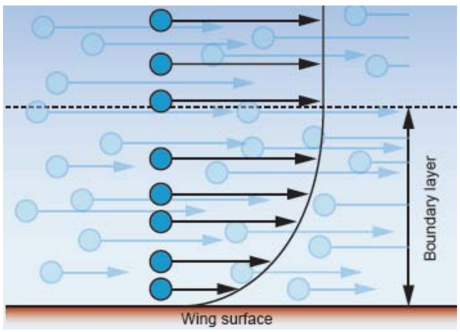

(a) Layer of decelerated air called the boundary layer.

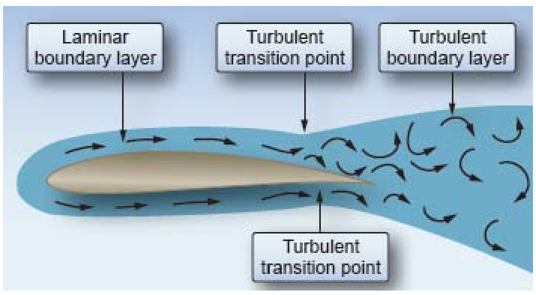

(b) Skin friction increases due to the turbolent boundary layer.

Figure 2.5: Skin friction drag very closed to wing surface(a) and in a global airfoil view(b)[25].

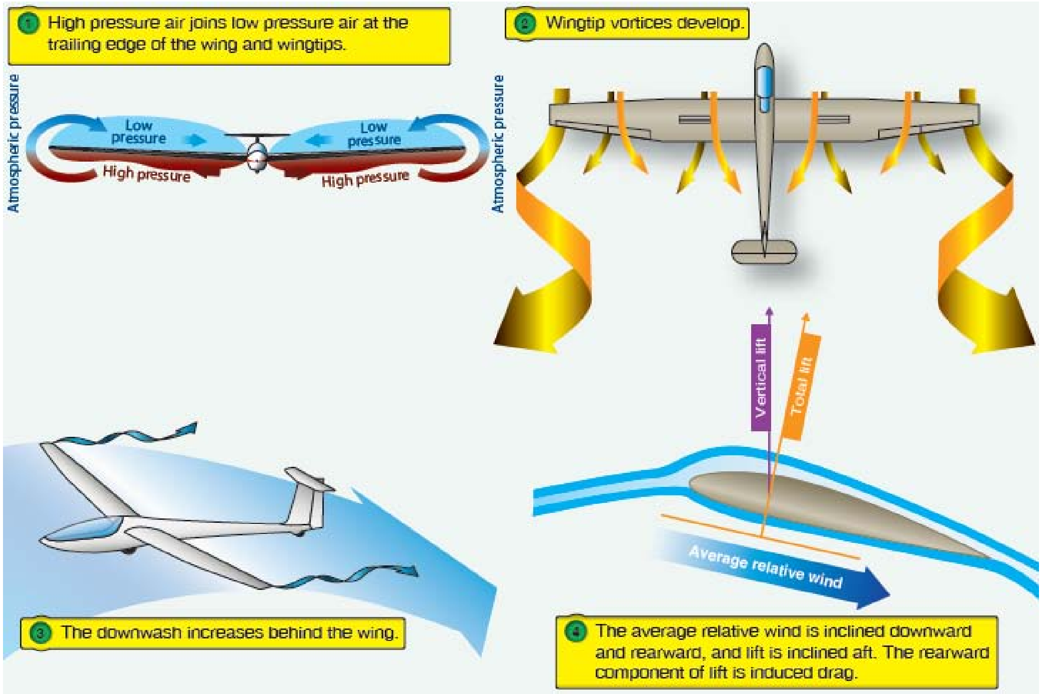

Figure 2.6: Induced drag is a part of the total drag, derived from the fact that real wing has finite wingspan and subsequently to the lift generation[25].

The Reynolds Number

Due to their complexity, the Navier-Stokes Equations are not solved in closed form for use in calculating the aerodynamic properties of a sailplane. It's interesting to observe that given the particular condition and behaviour of fluid where sailplanes in most cases fly, it is possible to reduce the Navier-Stokes equation to obtain results very near to reality. The first simplification derives from the fact that inertial forces are more significant than viscous forces, since we are interested in a preliminary design in which we can obtain most significant results and not go in deep on perfect representation of the boundary layer. The term which synthesize the relation between these two forces is the *Reynolds Number* :

$$Re = \frac{v_\infty l}{\nu} \tag{2.6}$$

where:
v_∞ : Freestream velocity [m/s];
l : characteristic length [m]
ν : kinematic viscosity of the air [m/s^2]

This topic will be explained in detail in chapter three where first results will be presented, largely influenced by the Reynolds Number ranges choice for simulation.

2.1.3 Typical Sailplane Wing Geometry

Since the beginning of aviation, research the perfect wing geometry that allowed a flight and optimized design was the focus of various studies. First wing theories were empirical, based on the observation of prototypes. Joukowsky was the first to identify a mathematical correlation to justify the geometry of the wings, and from that moment a whole set of geometries, that were still widespread and whose performance was consolidated by laboratory tests, was developed. The choice of wing shape is of utmost importance to allow a clear and stable flight and this choice has important consequences on lift and drag, as well as structural. The most common wing geometries in gliders design are: elliptical wing, rectangular wing, trapezoidal wing and swept forward[25].

Rectangular Wing

The rectangle is the simplest planform that we can see in aeronautical products. How ever it is not the best solution to optimize the glider performance. Indeed from experimental observation and Prandtl theories, it is possible to observe that vortices at the wingtip are very strong and this cause a great amount of energy loss. Experts says that this type of wing has some parts that not realize the expected lift. For this reason the glider's weight is supported by less lift than theoretical. The positive thing of rectangular wing shape is the smooth and stable stall. Example of rectangular wing planform are in Figure 2.7(a).

Trapezoidal Wing

The highly tapered trapezoidal wing has the advantage of having a long root chord and so with a relatively high thickness that allows the designer to insert a lighter and stiffer wing spar. Stall problem can be controlled by twisting the whole half wing in such a way that the geometric angle of attack of the tips is reduced by the required amount needed to equalize the deflection along the half span. This kind of twist allows for a more proportionate distribution of the load to the area and a reduction in vortex induced drag. If the wing tip twisting is done by rotating it by a positive angle,the behaviour of the entire aircraft would be critical because the stall will be anticipated and the vortex intensity greater. The wing tip twist has to be counter-clockwise, observing the fuselage. This property will be taken into account on this project.

Elliptical Wing

The elliptical wing shape has the advantage that minimizes the induces drag, demonstrated also by Prandtl theories. The effective angle of attack is constant along the span and the maximum lift coefficient affects the whole span simultaneously. The perfect distribution load is interrupted by fuselage in such way that in central zone lift could be zero. How ever elliptic wing-shape is an idealization of the the wing planform that every designers have to achieved. The disadvantage of this kind of planform live on the manufacturing and flight-stability. The best compromise between aerodynamic

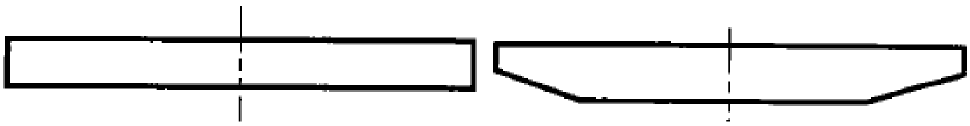

(a) Rectangular wing

(b) Tapered wing

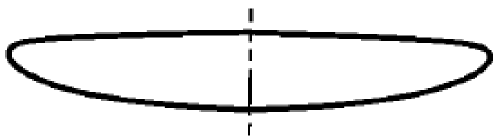

(c) Elliptical wing

Figure 2.7: Types of wing shape used in aviation[24].

performance and simplicity manufacturing is a combination of rectangular and trapezoidal wing planform, which will be taken into account on this project and developed in depth in next chapters.

2.2 Aeronautic Structures: First Aspect Considerations

To understand the functionality of aerospace structures, consider the following examples. As you can observe in Figure 2.8, the structural conformation of a plane from hundreds of passenger seats, it is globally similar to that in a common general aviation plane. In aeronautical jargon the structure acts as a skeleton. However without any coverage you will never be able to fly. This is the reason that aircraft's structure have to be coated with a membrane so that the pressure forces integrated on a closed surface can generate the required lift. This coating is defined as the skin of the plane. Aerospace structures generally consist of thin wall beams that must be able to meet the rigidity and resistance requirements of aerodynamic and structural evaluations. As can be seen from the Figure 2.9, which suggests the skeleton of a glider's fuselage, longitudinal elements are observed whose purpose is to provide rigidity in the direction of the length or plan of symmetry of the airplane and transverse elements which instead provide rigidity along orthogonal directions to the plan of symmetry. The main functions of aeronautical structures can be summarized as follows:

- transmitting and resisting loads
- ensure an aerodynamic shape
- protect passengers and payload from the extreme in-flight environment

In addition, the outer coating, generally thin aluminum plates and the most modern passenger aircraft, carbon fibre plates, while in smaller aircraft the use of the composite is wider, it is to ensure waterproofness and to withstand the pressure difference that comes exerted by fluid on the way. Skin is an excellent element for shear and traction resistance, but deforms when subjected to compression loads. In such situations, the buckling condition of the plates rises, particularly when the wing is bent up due to lift, which leads to the corrugation of the plates by drastically reducing the aerodynamic effects as it changes the shape of wing. Structural dimensioning follows a number of requirements that arise from customer expectations in terms of expected performance. Based on operational conditions such as supersonic military, combat, payload release, passenger transport at maximum performance and minimum cost, high altitude flight,invisible recognizing, are defined the most critical parameters that lead to the development of a product that meets the needs. Everything is enclosed within specific norms that make up the good project standard: airworthinesses, vary based on geopolitical considerations,

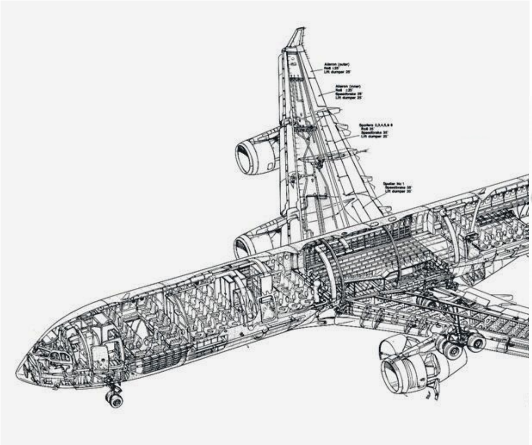

(a) The Airbus A340-300 airframe

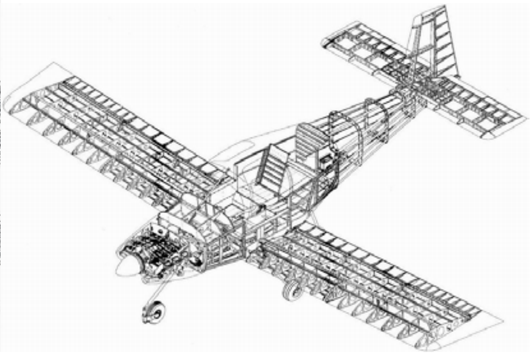

(b) Typical ultralight, high wing, fixed lanfing gear, two seat, airframe

Figure 2.8: Structures comparison between two different categories of aircraft.

operational conditions and the primary mission required. Specifically, it is to identify the performance limits per aircraft category, based on the past design experience. Each designer must draw up a chart that includes the expected flight performance, called *flight envelope diagram*, and which will be further elaborated. To conclude the introductory part on aeronautical structures, briefly define some of the fundamental elements that make up the skeleton of the wings, visible in Figure 2.10. The rigidity and flexural strength of the aircraft surfaces are bars that cross the plane orthogonal to its length. In particular, they can withstand the main flexural tension that comes from the generation of the lift. In fact, from a general point of view, wings can be compared in the first approximation to beams fixed at one end, for which the application of a distributed load causes the inflection. The wings are geometrically complex as they must be able to promote a difference in pressure between the upper and lower surfaces. This is why they can be defined as the airfoil envelope through parallel plans. At a fixed distance, the winged holes that place the skin between the root and the wing tip are positioned. Thanks to these elements it is possible to secure a fixing point of the skin, increasing the buckling load and thus avoiding corrugation of the skin for abnormal loads.

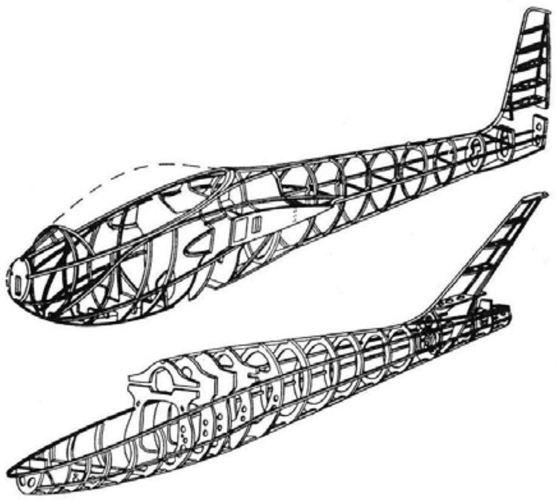

Figure 2.9: Typical glider airframe.

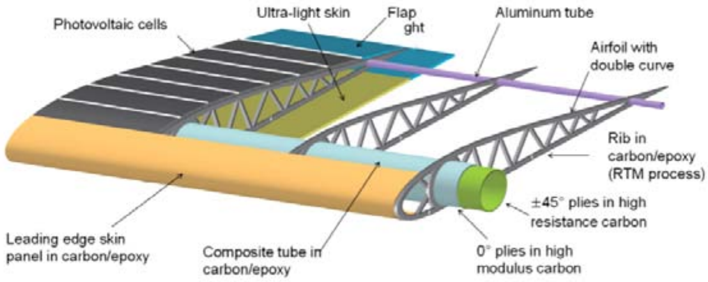

Figure 2.10: Typical wing structure[26].

2.3 The Innovative Purpose: The Electric Propulsion Solution

This section will provide the reader with a general and synthetic scheme of the technology underlying operation of photovoltaic cells, batteries and electric motors, which will be further discussed in subsequent chapters. The electrical infrastructure inherent in the avionics of this project is very important as it will have the role of providing the necessary power to level the downsink rate and allow the pilot to be less dependent on the nature of glider flight, for playful or emergency motifs. I would like to emphasize that such propulsive compartment is the adaptation of an already capable aircraft and therefore not strictly dependent as a HALE aircraft. For further details, please refer to the bibliography below.

2.3.1 Photovoltaic Cell: Working Principle and Typology

A photovoltaic cell is a device capable of converting solar energy into electrical energy by ionizing the materials of which it is composed. This technology, whose first experiments were performed by Einstein for which he was awarded the Nobel Prize, is largely employed in the aerospace industry. Indeed, the technology currently used in the private commercial market is similar to that used for the first exploration space missions of the 1970s. The ability to extract energy from the sun by converting it into electricity in environments where lighting is always present and at high density with respect to the ground, such as space, has allowed a rapid consolidation of this technology, constantly evolving. The most common photovoltaic cells are silicon, which is well suited for this purpose as a semiconductor. A semiconductor is a material that has a different conductive behavior based on the contour conditions that are placed on it. It can preset a better conductivity of many metals or also act as an insulator. In the production of photovoltaic cells, silicon is doped, ie contaminated with other chemical species to ionize it. In particular, doping type "P" is defined if the silicon is contaminated with elements containing the last five orbital electrons (phosphorus, arsenic), while it is said of type "n" if it is combined with trivalent atoms.

Reference to the Figure 2.11, when light hits the surface of the cell, transmits energy to electrons migrating leaving voids. The electrons move in the direction of the path of less resistor and instead of crossing the junction, they flow to the external load. The holes behave as positive particles and flow to the positive layer, while the electrons make way through the load to get into the negative layer. This process is only possible when the photovoltaic cell receives the right amount of energy to allow the electrons to migrate, for siliceous the *Energy Gap* from the spectral curve is around 1,1 eV. Justifications for this behaviour can be found in solar radiation. With reference to the Figure 2.12, showing the sunlight power as a function of the wavelength, it is noted that the available ground energy is different from that in space, that could be located in the absence of atmosphere. In fact, the atmosphere, consisting of different chemicals substances including water vapor and oxygen, absorbs part of the energy, thus reducing the overall power available. From the following calculation with reference to the curve in the absence of atmospheric absorption:

$$\int_0^\infty P(\lambda)d\lambda = 1367[W/m^2] \tag{2.7}$$

for an orthogonal surface. The same formula applied considering radiation

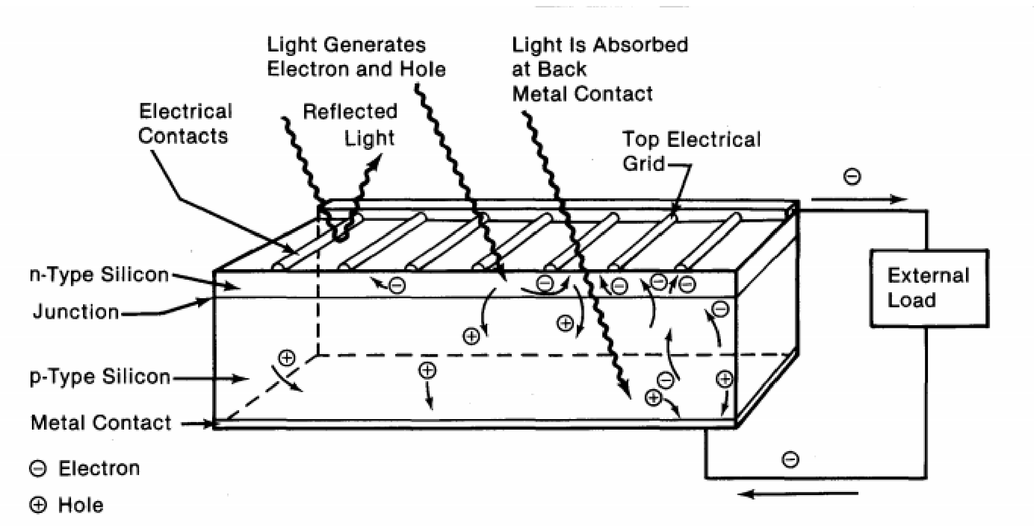

Figure 2.11: Working principle of photovoltaic cell `https://www.nrel.gov/docs/legosti/old/1448.pdf`[36].

intensity on the ground, give conventionally $1000[W/m^2]$. An ideal perfect solar cell that would cover the entire spectrum and convert all this energy into electricity would have an efficiency of 100 %. In reality, depending on the semiconductors used, only a part of this spectrum is covered. It is interesting to note from Figure 2.13, that of all the energy coming from the sun, about fifty percent is absorbed by the atmosphere or reflected. Of the rest, only ten to twenty percent are converted from the photovoltaic panel, at first approximation, without considering any transmission losses. The ability of this technology to reach a level of converted energy to be considered competitive with other forms of energy conversion is far but not excessively. Thanks to the continuous research and development of new junction types that represent the heart of the photovoltaic cell, a continuous percentage increase in efficiency is being observed. At this point, we describe the types of cells most widely used in commerce and through which will be choose the best solution for this work.

1. **Monocrystalline**: it has a great efficiency that stay around 25 % and during the lifecycle it remains stable. The main disadvantages are cost and the saturation of technological development. Humans have extract all of possible capabilities for this technology. From the other hand, how ever, it has a commercial maturity and it is a consolidated PV cell;

2. **Polycrystalline**: it has little less percentage efficiency but a more

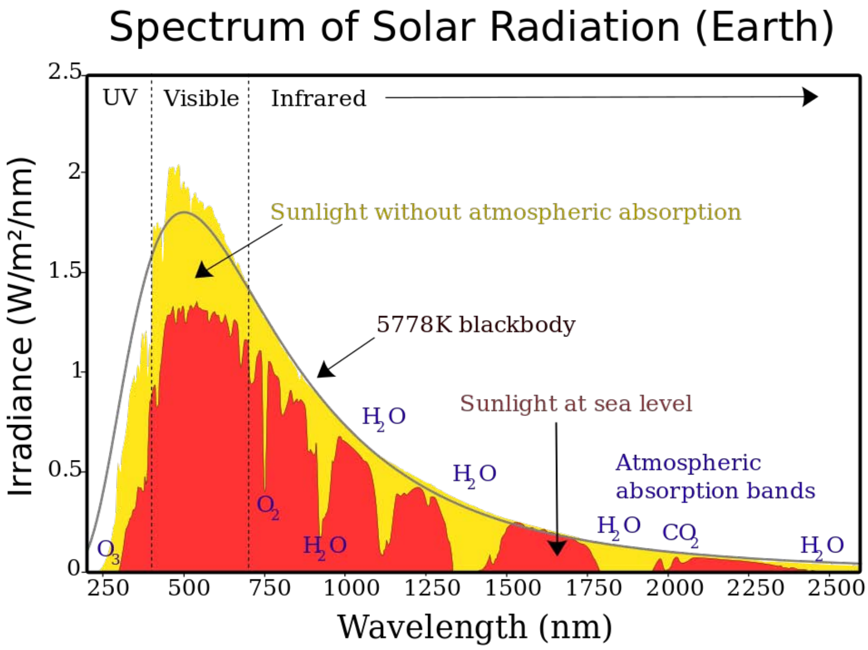

Figure 2.12: Solar radiation Spectrum[18].

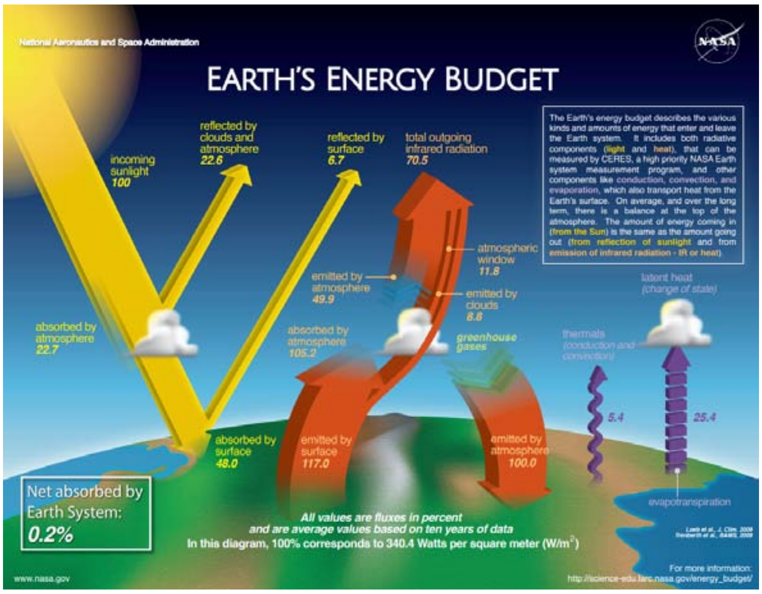

Figure 2.13: The energy budget diagram shows best understanding of energy flows into and away from the Earth. `https://science-edu.larc.nasa.gov/energy_budget/`.

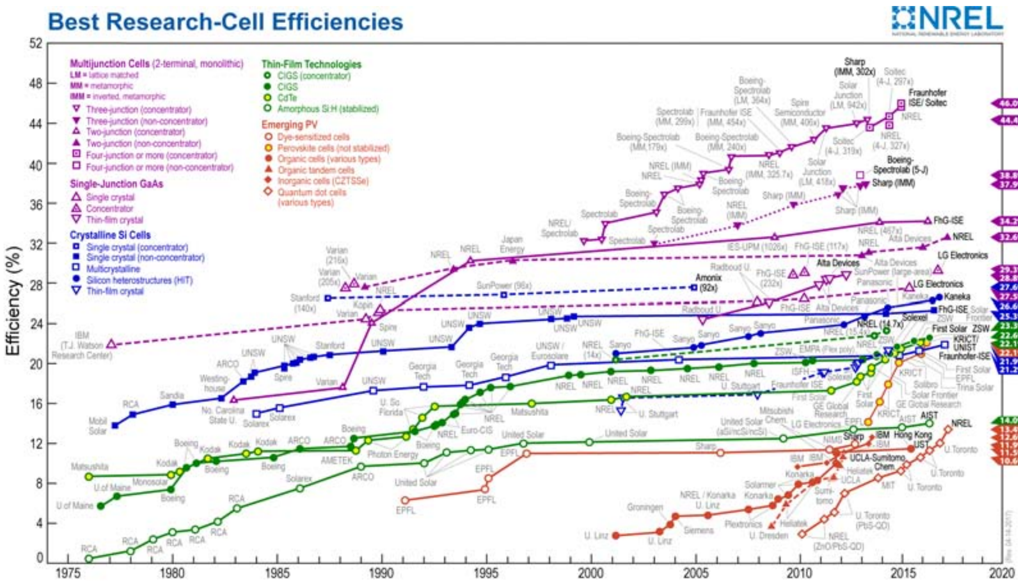

Figure 2.14: Efficiency chart of photovoltaic cell technologies updated until year 2017. Source `https://www.nrel.gov/`.

simplified assembling and production process and it has improvement margin. But for the same required energy it needs a more sun-exposed surface than the monocrystalline siliceous;

3. **Amorphous** : limited use of primary resources, simplified process and great argin of improvement are the advantage points of this technology. But the efficiency is estimated about 10 %.

For others technical insight, the reader could examine the *NREL* advises. Indeed the National Renewable Energy Laboratory provided every year an evolution chart in terms of cell efficiency improvement since 1975 that it is reported in Figure 2.14 and contain a much more types of PV cell respect to these cited in this elaborate paper. The best technology at the state of the art is the three-junction photovoltaic cell which allow to convert 45% of sun energy. This technology is widely used on aerospace hardware on the energetic acquisition compartment.

2.3.2 Power Accumulator: Electrochemical Batteries

Energy storage devices are indispensable for the good functioning of the propulsion apparatus involved in this project. The energy taken from the photovoltaic panels would not be enough to power an electric motor in a direct way, for such motivation it will be uses the strategy of electrochemical batteries, that allow to have available for a limited time, based on the stored energy, the power needing to tackle, for example, a level flight or forcing a climb. The key parameter in the preliminary characterization of the accumulators is the energy density. For high-energy batteries with the same output power required, they will have a smaller mass than competitors with lower energy density. From a constructive point of view, it can be stated that typically the batteries are constituted by a cathode, an anode and an electrolytic transition barrier. When the anode and cathode circuit is externally closed, the existing potential difference is liberated through a stream of electrons in the direction of the cathode. Among the multitude of existing batteries, those that maximize power output at the expense of mass are lithium-ion batteries, widely adopted in previous projects of solar aircraft. This type of battery is capable of reaching average density value of about 200 $[Wh/kg]$. Also belonging to this family of batteries are lithium-sulphurous and lithium polymers. For example, Zephyr 7 used lithium-sulphurous batteries with an energy density of 350 $[Wh/kg]$, while the solar aircraft developed by NASA called Helios used fuel cells, a technology adopted on satellites, Moon exploration and others missions, that is now spreading also in futuristic projects such as those reported on the introduction. In fact, the Figure 2.15, shows the peak power according to the energy density for various battery technologies. It is noted that the fuel cells occupy the area to the right, as they are most efficient accumulators and secondly probably, only to gasoline and fuel oil derivatives. In this thesis, will be adopted the lithium-ion batteries, widely exposed and studied later in particular will be argue about performances and the technological choice for the best link with the other electrical items.

2.3.3 Electric Engine: New Motion Way

To allow a velocity increase, it is necessary to transform the stored energy into mechanical energy. This is through the use of an electric motor that converts electrical energy into mechanical energy. The reverse process, that is, the conversion from electrical to mechanical, is made by tools called generators. In this thesis we will choose a specific engine or otherwise identify the technical specifications based on the requirements required by the aerodynamic analysis of the motorglider. In the state of the art, the propulsion

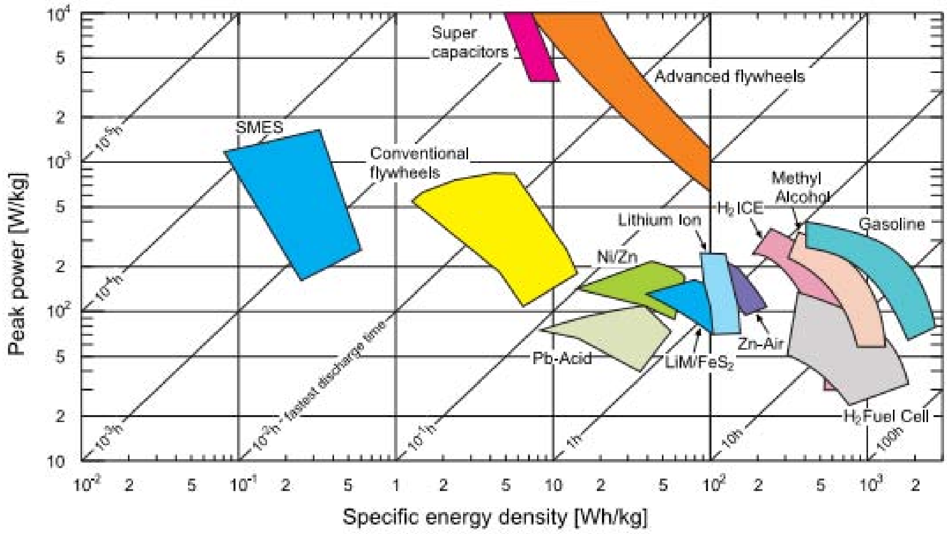

Figure 2.15: Graph on different types of batteries technologies at the state of the art[18].

devices are equipped with a motor, a gearbox and a propeller. The efficiency in the conversion made by the engine is very important, as it would allow for the same applied load to decrease the electrical input. The most popular types of electric motors are brushed and brushless, which use mechanical and electronic switching to create a magnetic field that moves a permanent magnet or electromagnetic magnet. The fundamental laws that an electric motor responds to can be, in an elementary approximation, gathered in: Ampere Law, Gauss Law, Faraday-Lenz Law. A classic DC electric motor consists of three main parts: stator, rotor, air gap. The gap is a space immersed in the air or in the vacuum that wraps the rotor. Instead, the stator transports the magnetic field and therefore needs to be made of a material with high magnetic permeability to minimize leakage. The inner part is the rotor, which consists in a wound coil generating a rotating magnetic field or a permanent magnet. The electrical connection between the rotor and the external power supply are ensured by brushes, in a typical DC motor. The rotation will continuously change the coil polarity, thus generating an oscillating current. The main limitation of DC motors are due to the need for brushes to press against the commutator, that creates friction, sparks and electrical noise. Their speed control is easily achieved by varying the constant voltage or the duty cycle by a Pulse Width Modulated signal(PWM). In a brushless DC motor, the permanent magnets rotate and the armature remain static, Figure 2.16. This gets the problem of how to transfer current to a moving armature. The brushed commutator is replaced with electronic controller that performs the same power distribution found in a brushed DC motor. The drive electronics is more complicated in a brushless system because it has to activated one coil at times, and this process has to be very synchronize to the rotor's position. The main advantages of brushless DC motor are: very precise speed control, high efficiency, reliability, reduced noise, no ionizing sparks.

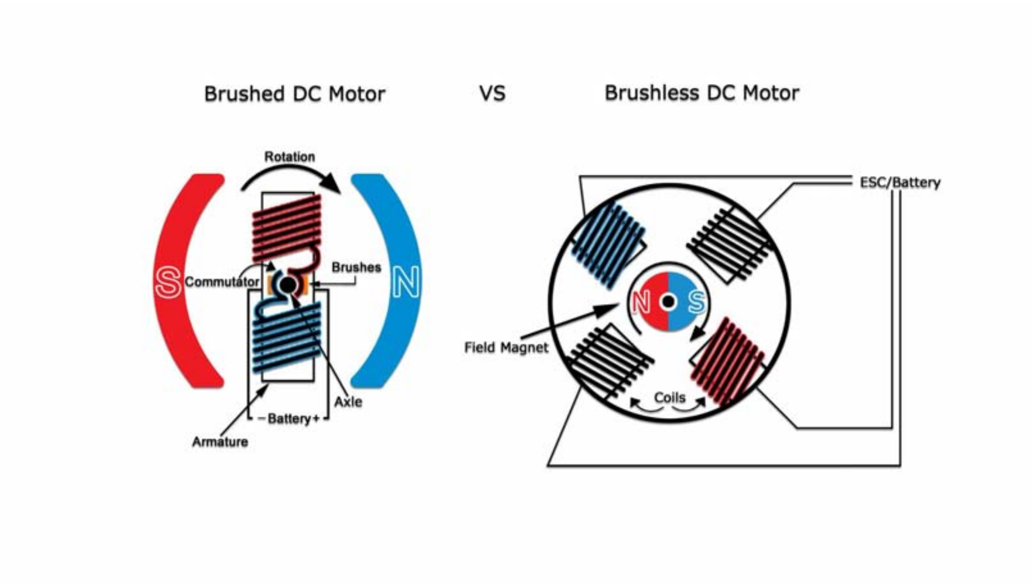

Figure 2.16: Quick and easy picture of main differences between brushed and brushless DC motor. `https://www.youtube.com/watch?v=RsqHr2cpp4M`.

DC Motor Equations

The main equations that can help in choosing and dimensioning a DC electric motor based on the connected load can be summarized as follows. The output voltage :

$$E_a = k_e \Phi \Omega_m \tag{2.8}$$

where:
E_a : output voltage [V];
k_e : performance motor coefficient;
Φ : electromagnetic flux concern in Gauss' Law [Wb];
Ω_m : rotor velocity [m/s];

As a result of the generation of the electromotive force for the Faraday-Lenz effect, there is also a braking torque. This phenomenon is justified by the fact that the energy supplied to the circuit is dissipated by the resistance and therefore it is expected that the rotor energy will decrease. This happens in the generator, ie when the conversion from electrical to mechanical is done. In the opposite conversion, that is engine operation, the Lorentz's force moves the rotor and the torque produced is of a motive type. The formula for the torque is:

$$\tau_{em} = k_\tau \Phi I_a \tag{2.9}$$

where:
τ_{em} : electromagnetic torque$[Nm^2]$;
k_τ : corrective coefficient associated to the efficiency conversion;
Φ : electromagnetic flux concern in Gauss' Law [Wb];
I_a : current on the rotor[A];

For DC motor in SI units, $k_\tau = k_e$. In the simplified engine circuit it can be stated that:

$$V_a = E_a + R_a I_a \tag{2.10}$$

where:
V_a : Input tension [V];
R_a : Rotor resistance [Ω];

This results in the mechanical characteristic of the motor, that is the definition of the torque as a function of the rotor speed. From the combination of the three previous equations you get:

$$\tau_{em} = k\Phi \frac{V_a}{R_a} - \frac{(k\Phi)^2 \Omega_m}{R_a} \tag{2.11}$$

which represent the equation of a straight line with negative angular coefficient.

2.3.4 AC Motor Equations

The AC motor differs from the DC type motor for the type of source adopted, that is, an alternating current generator. The concatenated flux between the rotor and stator is timed with the source for which the electromotive force will be:

$$e(t) = \frac{d\lambda}{dt} \tag{2.12}$$

where e is the electromotive force and λ the concatenated electromagnetic flux.

$$e_a(t) = -w\Lambda sen(wt) \tag{2.13}$$

where : w is the electric pulsation, directly dependant to frequency and Λ is the concatenated flux amplitude. Refers to the two-phase electric AC motor

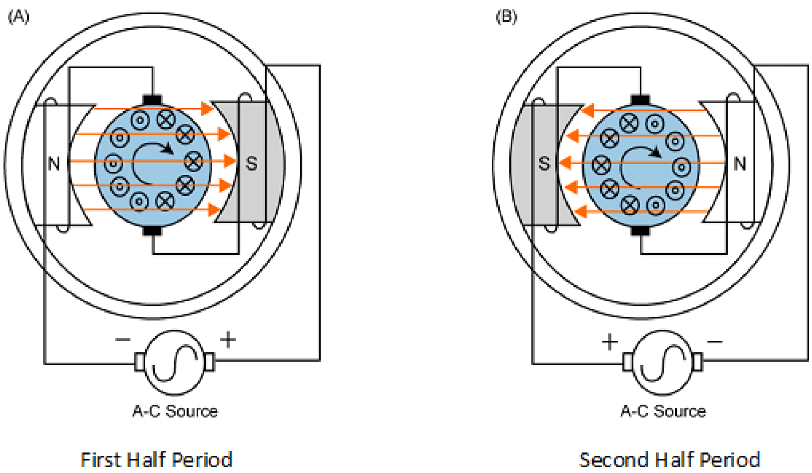

Figure 2.17: Basic principal function of AC motor [58].

in figure 2.17, the electromotive force amplitude is equal to $E = w\Lambda$. the main hypothesis to reach these results is constant velocity. If it is chosen an alternating current aligned in phase to the tension, the electric power will be:

$$P_a = e_a(t) \cdot i_a(t) \tag{2.14}$$

$$P_A = \frac{w \cdot \Lambda \cdot I}{2} \tag{2.15}$$

$$\tau_{em} = 0.5 \cdot \Lambda \cdot I \tag{2.16}$$

Between ω and ω_m which represent respectively the electric pulsation and the motor round-per-minute, exist a relation of direct proportionality that is:

$$\omega = p \cdot \omega_m \tag{2.17}$$

If the alternating current is not in phase with tension, the result is the production of less power than the case with current and tension in phase:

$$P = 0.5 \cdot \omega \cdot I \cdot cos(\phi) \tag{2.18}$$

where ϕ is the phase gap between current and tension. The electromagnetic torque will be:

$$\tau_{em} = 0.5 \cdot p \cdot \Lambda \cdot I \cdot cos(\phi) \tag{2.19}$$

The direct conclusion is that more polarity correspond to more deliverable power. How ever remain the problem that power is strictly variable with the source. The solution become from the combination of more than one phase, ie three phases displaced of 120 degree and we obtain:

$$P_A(t) = e_A(t) \cdot i_A(t) + e_B(t) \cdot i_B(t) + -e_C(t) \cdot i_C(t) \tag{2.20}$$

and the total average power is:

$$P = 0.5 \cdot \omega \cdot \Lambda \cdot I \cdot 3\cos(\phi) \tag{2.21}$$

and the electromagnetic torque:

$$\tau_{em} = \frac{3}{2} \cdot p \cdot \Lambda \cdot I \cdot cos(\phi) \tag{2.22}$$

The main advantages of this configuration is that the power and torque variation is zero and mainly that we obtain three times more elaborated power with minor electric cables occupied volume. This is the best compromise solution between advantage and disadvantage, between deliverable power and performance respect to mass and volume. For this project will be choose the AC brushless motor type, for the advantages previously denoted. It is not a out of way choice, indeed also for real solar aircraft this solution meets requirements. In addition the gear boxes will be remove and use the direct drive motors to provide power directly to the propeller. This alternatives reduce losses from mechanical dray as well as increase efficiency and propulsion system reliability.

Chapter 3

Aerodynamic and Structural Conceptual Design

In this chapter will present the first results of the feasibility study related to the conceptual development of the electric motorglider presented roughly in the introduction chapters. It will treat constraints and requirements, focusing on the capabilities the aircraft has to meet. At the end of the chapter, you will have the means to start an in-depth study of this aircraft configuration. In particular, they will be developed:

- initial weight estimation with different approaches;
- definition of the aerodynamic profile that best meets the requirements;
- first step validation of glider performance.

3.1 Design : Requirements and Approach

Design is a discipline diffused in many areas, from automotive to home products and also aviation. Very often the design scope is confused with the graphic draw of the product but the designer tasks are far from this. The draw is the end result of a process that primarily involves the intellectual and creative abilities of a design team that is not exclusive and driven only by an aesthetic principle, but must create the geometric description of a thing to be built[39]. The designer possesses creative ability and knowledge of the main physical and mathematical laws that allow him to assert his idea to the most advanced steps of development. The design process is established right in the early stages of developing a new product, for example in aviation, it is a new aircraft. It is in the preliminary phase, to which this thesis refers to, that the figure of the designer finds its environment. This route starts when the specifications for a new aircraft are requested by the customer. These technical specifications include performances, requirements and constraints that must be taken into account throughout the development path. Typically, the product creation process affects all departments and rarely happens in a cascade way but is a constant and iterative loop as shown in the Figure 3.1. From the previous chapters it has been seen how the history of electric aviation is present but poor compared to that of general aviation and only data related to past projects would not yield satisfactory results. For this reason, has been given to the author the opportunity to span the choices, if justified, of requirements, constraints and dimensional approach, in addition to three main requirements:

1. wingspan from 8 to 12 meters;
2. rising speed 2 m/s;

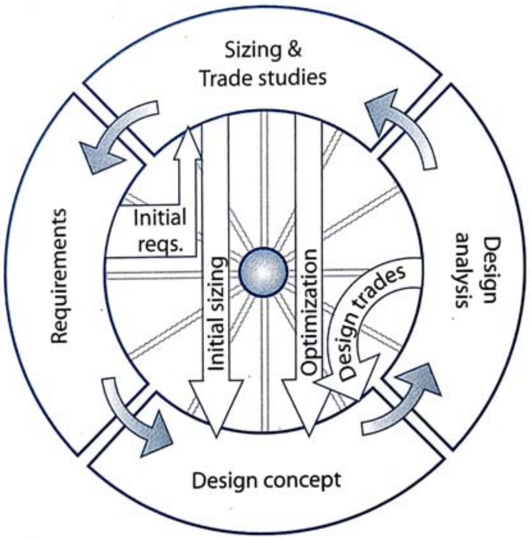

Figure 3.1: The Design Wheel [39].

3. maximum weight 200 kg;

The initial requirements have been advanced by Professor Sambin, who has full interest in continuing and expanding the *Merlo* project. The maximum wing length derive from the available laboratory area. While the mass and performance requirements are linked to the *Merlo* project. First of all, this project refers to a specific aircraft category that is glider and in particular motorglider. This narrows the circle of airplane categories, providing also requirements in an indirectly way, demanding in the history of modern aviation. From this simple indication it is possible to find the direction to follow in the search for the main qualities that a glider must possess, both in terms of geometry, structure and aerodynamics. As it is easy to guess, the approach chosen for this project focuses on historical research and statistical evaluation of the aircraft properties already built and marketed. In fact, this technique is the most widespread in aeronautical design inside a private company. Typically, designers have an internal library of factory projects from which it is possible to extract informations needed for initial estimates. The preliminary phase of the development and sizing of a motor-powered electric propulsion required a study of traditional sailplanes and motorglider in order to obtain key design parameters and, above all, validated by the experimentation and sale of the product. This is the chosen way for this project, in order to be more coherent with aeronautical industries internal dynamics, as guessed from [39],[34] and [23].

3.1.1 Glider Airworthiness: Rules for a Safety Project

With the term Airworthiness, we refer to normative and design rules developed through the history and based on real projects, that established if an aircraft could or not fly. The entire performances are contained on the *Flight Envelope Diagram*, explained at the end of this chapter. In order to create the flight envelope diagram and to obtain some basic settings, we refer to the regulations regarding ultra-light aircraft design. There are several collections of rules issued over time, including, in Italy, the **RAI**, issued in 1942, which provides basic information on the maximum loads on aircraft ,as to make prototypes of structure. In the United States, the CAA is currently present; in France, Germany and United Kingdom the normative **BCAR-E** is simple and easy to implement, suitable for the amateur builder. For the acrobatic sailing category, the BCAR-E regulation provides a load factor of +6 with a safety coefficient of 1.5. In this paper, for carrying out loads and performance estimates, it was chosen to adopt the BCAR-E regulation, which is the forerunner of JAR22 and OSTIV regulations. Please note that the design criteria provided for in this regulation are still valid and applicable to gliders that do not exceed 726 kg. A more detailed explanation will be provided in the appropriate paragraph. Currently in Italy, an airplane is defined as ultra-light if it complies with the criteria laid down in the pillar law of 25 March 1985, No. 106, which governs the recreational or sporting flight whose implementation law is **D.P.R. 5 August 1988, no 404**.[23][34] The aircraft must meet the following constraints:

- maximum take-off mass of 300 kg
- stall speed not exceeding 65 km/h;

At this point, the reader known the inferior and superior limit for the motorglider realization, the limit stall speed from which it is possible to derive some important information, presented on following paragraphs.

3.1.2 Force Balance for in-Flight Glider

An aircraft in flight is subject to different forces and moments, which are a consequence of pressure distributions and shear forces. As far as the flight phase is concerned, the main forces affecting the aircraft and visible on Figure 3.2 are:

- **Lift (L)**, perpendicular to the flight direction;
- **Drag (D)**, parallel to the flight direction;

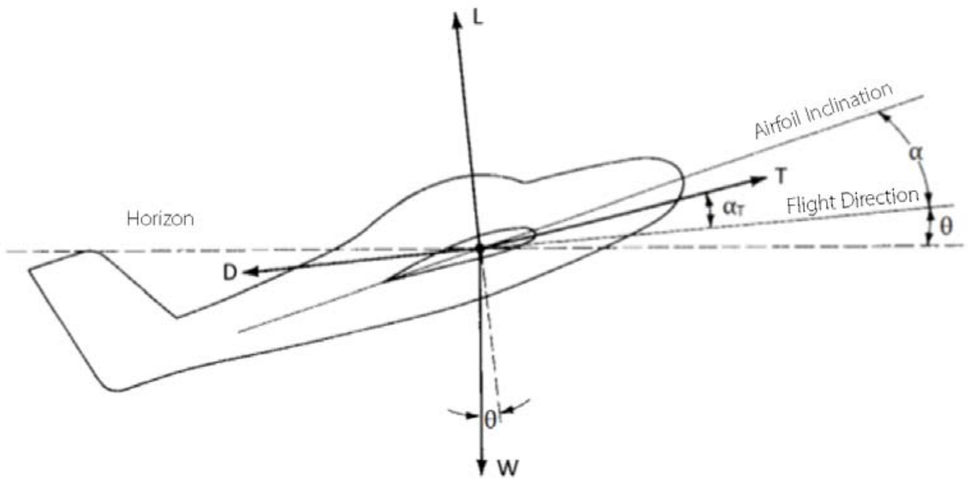

Figure 3.2: Forces acting on in-flight aircraft[40].

- **Weight** of the aircraft, which acts vertically downwards, turning to the centre of the Earth;
- **Thrust** exerted by the propulsion system, which can typically be inclined at a certain α_T angle with respect to the direction of advancement of the aircraft.

These quantities allow us to make initial evaluations of the characteristics that the aircraft have to comply with flight requirements or vice versa known performance, obtaining aircraft behaviour in different flight configurations to be compared then with the requirements. The *Flight Mechanics* elementary equation, are based on the Newton's Law. In particular the equilibrium forces relation with the main hypothesis of **steady flight** and **Incompressible flow**, that means we are studying the aircraft behaviour as take a photograph in a specific instant and assume this behaviour every time that we meet the same parameters, is:

$$ma = Tcos\alpha_T - D - Wsen\theta \tag{3.1}$$

$$ma_c = Tsen\alpha_T + L - Wcos\theta \tag{3.2}$$

First equation refers to flight direction, while the second to the orthogonal flight direction[40]. The flight configurations of interest are:

1. take-off

2. climb
3. cruise
4. dive
5. landing

These configurations will be evaluated in chapter 5: *The Self-Sufficient Electric Solution*, in which knowing the performance will be derived the first attempted flying powers, useful for sizing the engine. For a major part of mission time, the aircraft will be on levelled flight, phase called cruise. In this condition the airplane maintains the same altitude with no acceleration. The force balance equations are reduced to:

$$T cos\alpha_T - D = 0 \tag{3.3}$$

$$T sen\alpha_T + L - W = 0 \tag{3.4}$$

To conclude, the angle α_T can be assumed equal to zero. In this way we obtain the *Force Balance Equation for Cruise Flight*:

$$T = D \tag{3.5}$$

$$W = L \tag{3.6}$$

3.1.3 L/D Efficiency Parameter

From the force balance equations it is possible to define some fundamental parameters for the preliminary size of the aircraft. These include aerodynamic efficiency L/D, a non-dimensional term which define the best flight condition where *Lift* is maximized than *Drag* that is minimized. The required Thrust is directly related to the weight and the efficiency of flight through the equations:

$$\frac{W}{T} = \frac{L}{D} \tag{3.7}$$

from which:

$$T = \frac{W}{L/D} \tag{3.8}$$

equal to

$$T = \frac{W}{C_L/C_D} \tag{3.9}$$

The procedure for identifying the variation of the required Thrust according to speed is as follows:

1. Choose a speed V_∞, knowing the weight, the wing surface and atmospheric variable, it is possible to calculate C_L required for this flight configuration:
$$C_L = \frac{W}{0.5\rho V_\infty^2 S} \tag{3.10}$$

2. Knowing C_L, observe the corresponding C_D on the profile polar graph, adjust with finite wing equation;

3. Calculate the required thrust.

The following diagram is then obtained: It is noted in Figure 3.3 that the

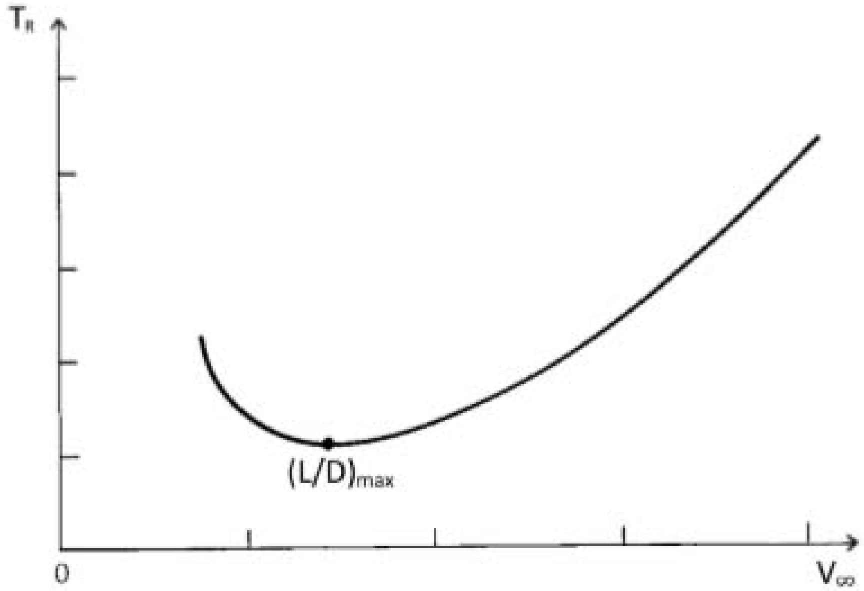

Figure 3.3: Required Thrust to V_∞ diagram [40].

required thrust is minimum at a certain velocity value at which the maximum aerodynamic efficiency is achieved. The wing is exploited the best of its potential, maximizing the lift produced against a drag minimization. The efficiency parameter is also function of the angle of attack. The equations that will allow us to evaluate the maximum efficiency condition can be summarized below and will be widely used in the following paragraphs.

$$C_{L_{maxL/D}} = \sqrt{C_{D_{min}} \cdot \pi \cdot e \cdot AR} \tag{3.11}$$

Where e is the *Oswald coefficient*, will be depth later.

$$\frac{L}{D} = \frac{1}{2 \cdot \sqrt{\frac{C_{D_{min}}}{\pi \cdot e \cdot AR}}} \tag{3.12}$$

$$V_{L/D_{MAX}} = \sqrt{\frac{2 \cdot W_0}{\rho_\infty \cdot S} \sqrt{\frac{1}{C_{D_{MIN}} \cdot \pi \cdot AR \cdot e}}} \tag{3.13}$$

3.2 Preliminary Weight Estimation

Sizing is one of the most critical and important evaluation in aircraft design and it define the size of the aircraft. In particular its weight have to perform best characteristics and meet the requirements. In this process, the main parameter is the mass and consequently inertia and centre of mass. The aircraft mass is a fundamental variable, because it deeply influences the technical development. In a modern aircraft the main and always present requirement is to design a light machine because that means less power to reach same objectives. The moments of inertia are also important for stability and manoeuvrability.
One of the first designer tasks is to find a list of aircraft similar to what the customer commissioned in terms of performance and category. Weight prediction approaches are two: *statistical* and *analytical*. The most adopted approach is the statistical that consists in the creation of a database of aircraft belonging to the same category and similar in technical aspects to what it is intended to achieve. The analytical approach, on the other hand, provides for fixing some parameters that are believed to have a major influence on the empty weight, typically structural. Then theoretical relationships that allow these parameters to be linked, are identified. In any case, both roads make extensive use of the experience gained by the designers team. There are three methods to estimate the empty weight:

1. **estimation based on aircraft configuration**: it is not sufficiently accurate to use as base on future calculations;

2. **parametric and statistical analysis**: it is the most used in the preliminary phase and uses database of aircraft containing information such as empty weight, maximum speed, stall, efficiency, wing load;

3. **dimensional detail analysis**: you need to know in detail all the components that will involve the project. Knowing the volume, it is

multiplied by the specific weight to get the weight of the part. This technique is useful if minor modifications to an aircraft must be made, in which the constituent parts list is detailed.

For the definition of the first attempt mass, the statistical method was adopted by an aircraft database specifically created and available in Appendix A. In addition to this, reference was made to [18] to compare derivative equations later on. The database that was compiled is based primarily on the free resources available by [42] and presents a list of tens of thousands of gliders and motorgliders produced in history. Data were collected for about 170 aircraft between "acrobatic", "open-class", 15 and 18 meters, large and small prototypes. The aircraft in the appendix were built from the 70s onwards, when technological advances and new industrial techniques as well as the use of new materials have allowed to create new, more powerful geometries.
At the same time, first calculation was performed with the formulas described by[39] and presented below.

$$W_0 = W_{crew} + W_{payload} + W_{fuel} + W_{empty} \tag{3.14}$$

where: W_0 : is the maximum weight
W_{empty} : refers to all components which define the vehicle less payload, fuel and persons.
To simplify the calculation, both fuel and empty weigths can be expressed as fractions of the total weight:

$$W_0 = \frac{W_{crew} + W_{payload}}{1 - \frac{W_{fuel}}{W_0} - \frac{W_{empty}}{W_0}} \tag{3.15}$$

W_0 can be determined if W_f/W_0 and W_e/W_0 can be estimated. Knowing that W_{fuel} and $W_{payload}$ for a solar motorglider can be set to zero, we obtain:

$$W_0 = \frac{W_{crew}}{1 - \frac{W_{empty}}{W_0}} \tag{3.16}$$

At this point, using Reymar's formulas and data on Figure 3.5, was obtained a first guess value for W_0 by iteration starting from W_0 guess value of 100 kg. It is necessary to remember that the equation :

$$\frac{W_e}{W_0} = AW_0^c K \tag{3.17}$$

does not involve such geometric parameters or anything else, but it is a power law interpolation of data developed by Reymar [39]. First calculations re-

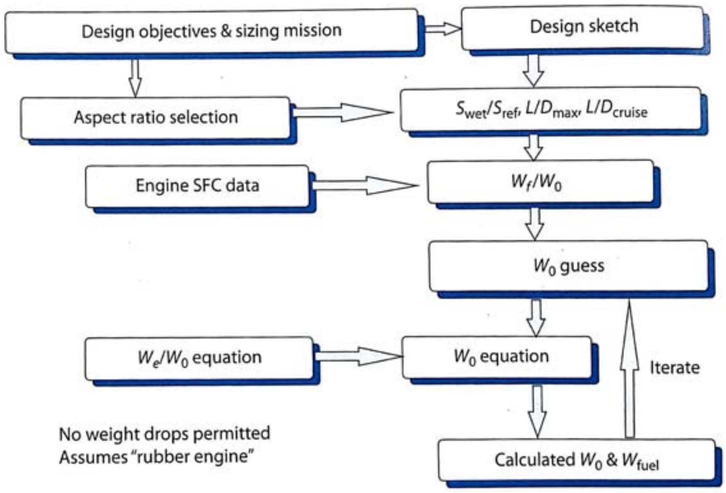

Figure 3.4: First order design method [39].

$W_e/W_0 = AW_0^C K_{vs}$	A	{A-metric}	C
Sailplane—unpowered	0.86	{0.83}	−0.05
Sailplane—powered	0.91	{0.88}	−0.05
Homebuilt—metal/wood	1.19	{1.11}	−0.09
Homebuilt—composite	1.15	{1.07}	−0.09
General aviation—single engine	2.36	{2.05}	−0.18
General aviation—twin engine	1.51	{1.4}	−0.10
Agricultural aircraft	0.74	{0.72}	−0.03
Twin turboprop	0.96	{0.92}	−0.05
Flying boat	1.09	{1.05}	−0.05
Jet trainer	1.59	{1.47}	−0.10
Jet fighter	2.34	{2.11}	−0.13
Military cargo/bomber	0.93	{0.88}	−0.07
Jet transport	1.02	{0.97}	−0.06
UAV—Tac Recce & UCAV	1.67	{1.53}	−0.16
UAV—high altitude	2.75	{2.48}	−0.18
UAV—small	0.97	{0.86}	−0.06

K_{vs} = variable sweep constant = 1.04 if variable sweep = 1.00 if fixed sweep

Figure 3.5: Empty weight fraction versus W_0 [39].

Glider	W_{crew}	W_0	W_e/W_0
	65	180	0.640078
	85	230	0.63245

Motorglider	W_{crew}	W_0	W_e/W_0
	65	200	0.6751
	85	255	0.666978

Table 3.1: Reymar's equation results for total weight and empty weight fraction estimation.

ported in Table 3.1.

A first important observation that can be conducted is linked, in addition to the different mass that distinguishes glider and motorglider, to the different value of empty mass fraction. This is due to the fact that a motorglider must sustain its glider-structure and also an extra load, due to the presence of the engine, propeller, tank, engine structure, stiffening. That is why the empty mass fraction of the motorglider is superior to the glider.
In order to obtain a better estimate of the first attempt mass, the data contained in the previously cited database have been thoroughly investigated. In particular, graphs have been developed for gliders, motorgliders and the entire database in terms of geometric and mass parameters as can be seen in Figures 3.6,3.7,3.8,3.9.

The graphs have been developed by studying the equations that minimize the *average square error deviation* through functions already implemented in **Excel**®[1]. There are linear, polynomial and power interpolation equations, along with parameter R^2, which defines how much close are equations in the representation of compiled values. These equations are necessary to estimate the design parameters of an aircraft which, although belonging to the class of gliders, has a very modest wingspan, below the usual 15 meters.
From the tables shown in Figure 3.11 and 3.12 and obtained from the graphs 3.6,3.7,3.8,3.9, it was possible to choose additional relevant parameters and allow you to evaluate the reciprocal tendency of the most important variables such as weight, wingspan, aspect ratio to the variation of the aircraft category or between their. Please note that each marker in the chart refers

[1]for more information on how **Excel** can define a tendency line, visit `https://support.office.com/it-it/article/Equazioni-per-il-calcolo-delle-linee-di-tendenza-12cfdaa5-0652-436f-839c-0561e8620ba5`

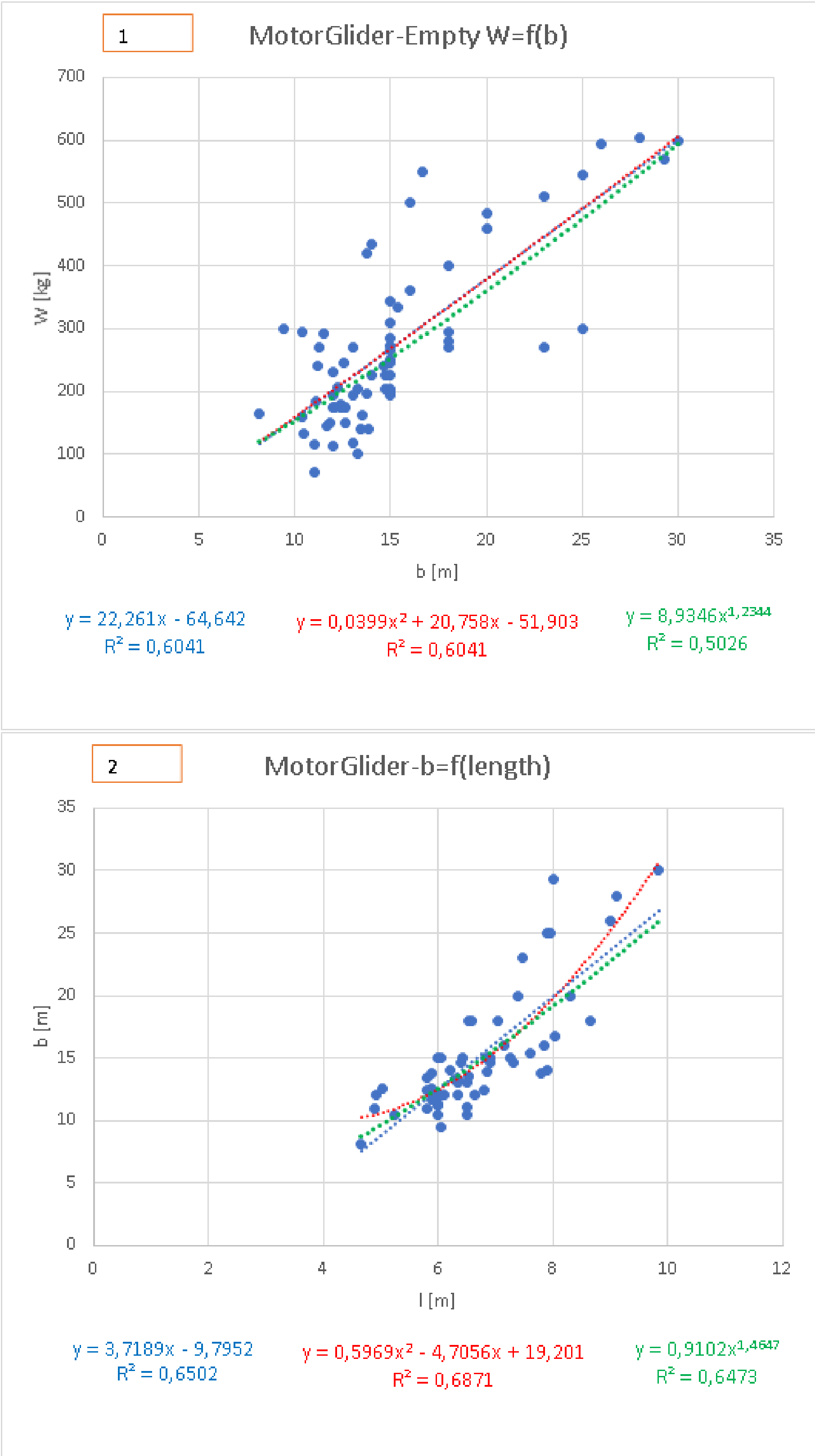

Figure 3.6: *empty weight* in [kg] expressed as a function of wingspan b on the top; Wingspan as a function of aircraft's length. Both for only Motorglider.

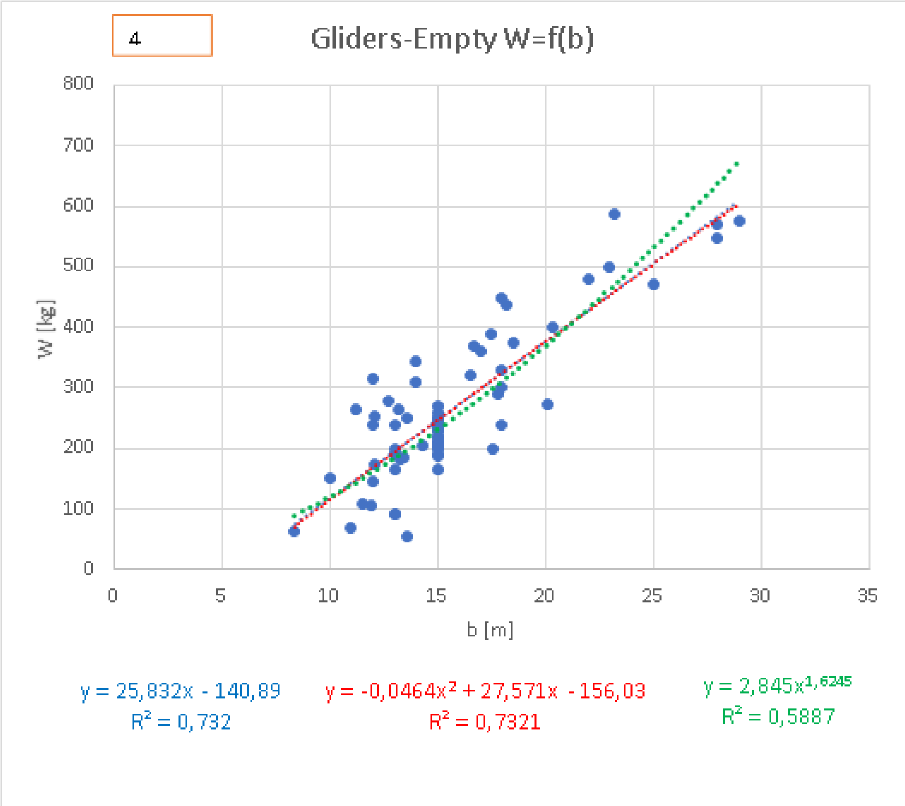

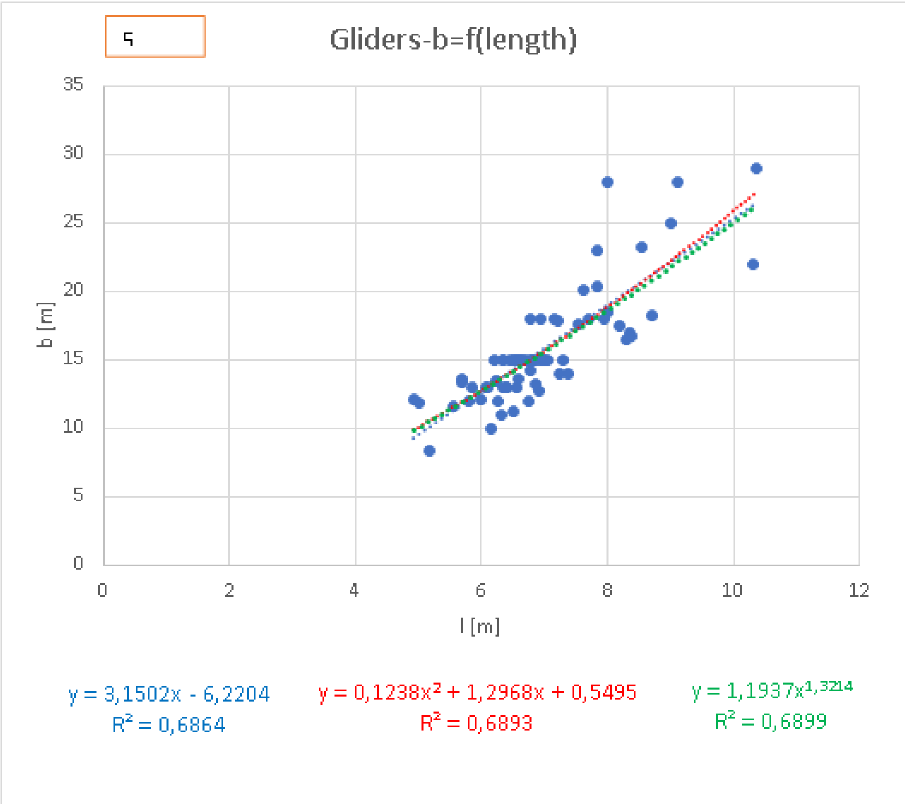

Figure 3.7: *empty weight* in [kg] expressed as a function of wingspan b on the top; Wingspan as a function of aircraft's length. Both for only Glider.

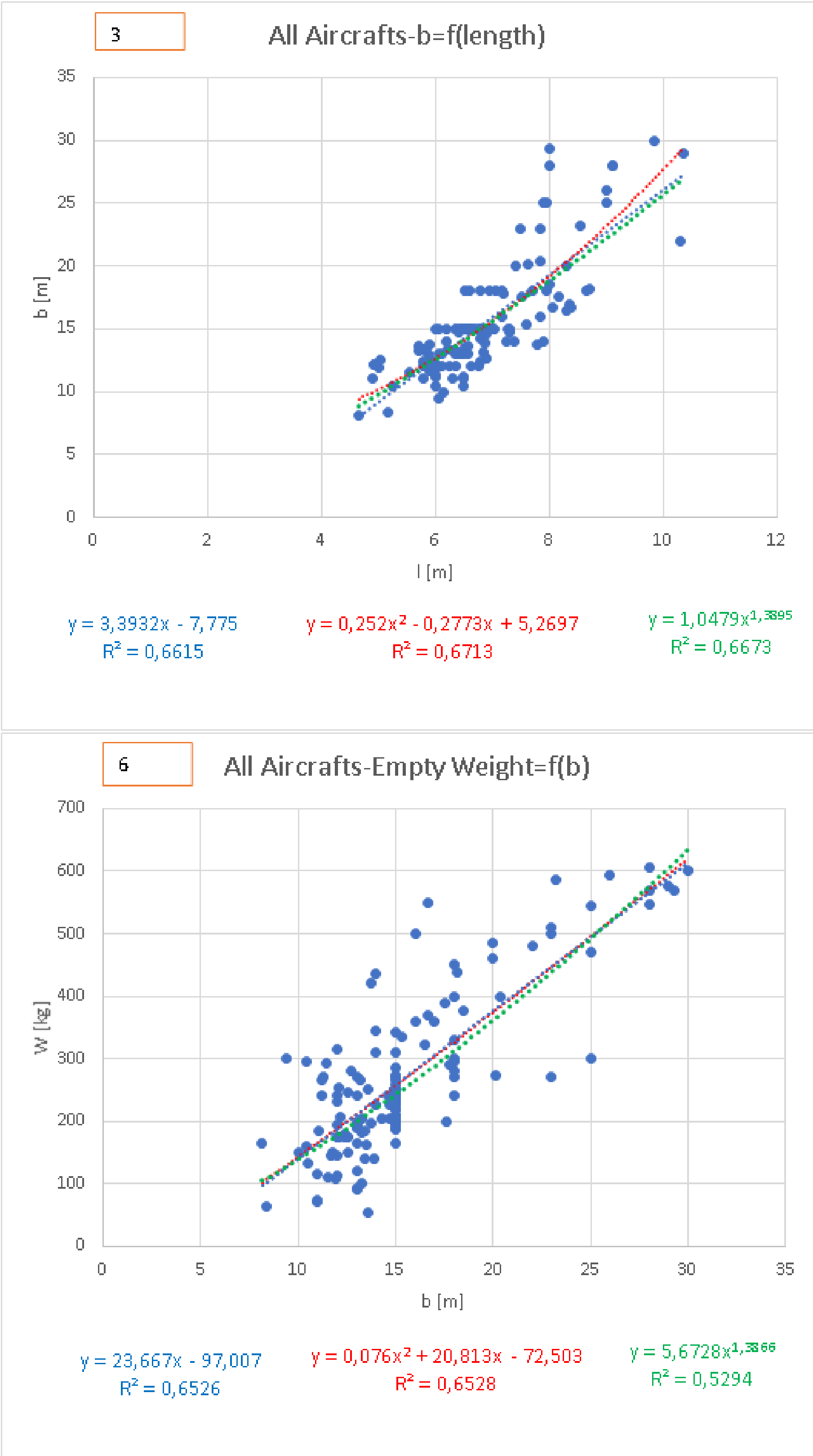

Figure 3.8: Wingspan as a function of aircraft's length on the top; *empty weight* in [kg] expressed as a function of wingspan b. Both for all aircraft.

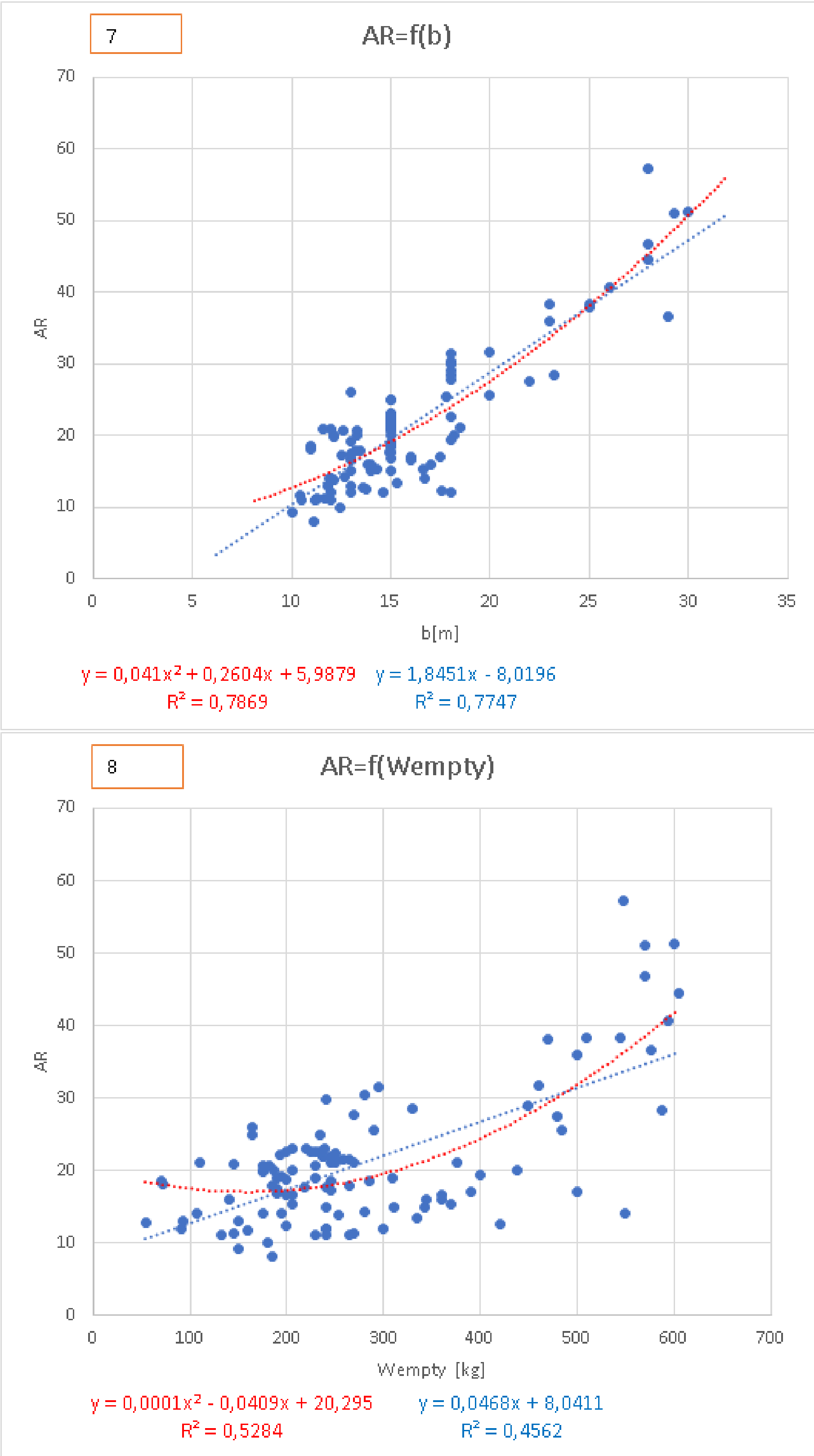

Figure 3.9: Wing Aspect ratio as a function of wingspan [m] on the top and empty weight[kg] for only motorglider.

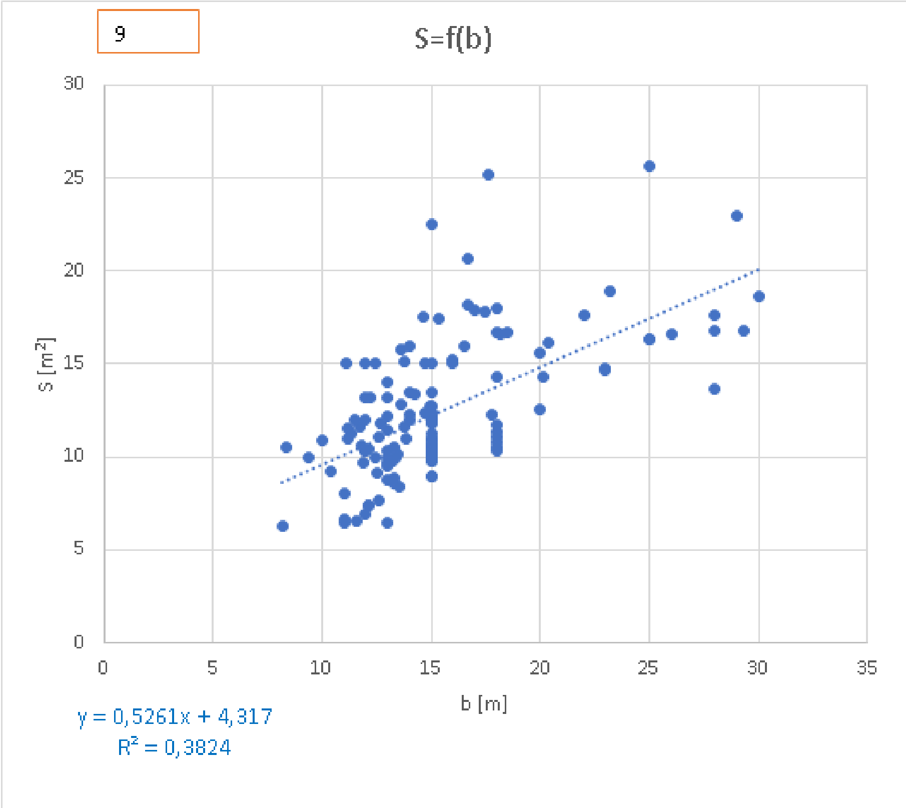

Figure 3.10: Wing surface[m^2] as a function of wingspan [m] for only motor-glider.

to the technical specifications of a truly crafted glider or motorglider. Before defining the selection of project variables, consider the following considerations:

- from the chart labelled with number 1, it can be noted that the empty weight of the motorglider as well as the gliders in graph 4 increases as the wingspan increases with a law of linear interpolating curve (the best to interpolate the data , as indicated by parameter R^2); The most simple justification is possible to associate to the fact that at the profile having equal 1m chord, increasing the mass to be lifted, the wing surface which is equal with these assumptions to the wingspan, must necessarily increase.

- Graphs 2 and 5 show the wingspan as a function of the length. The fuselage length in the direction of the motion is essentially related to stability and mass requirements. In this case the interpolation laws that most closely approximate to represent the data are the linear and the polynomial ones.

- In graphs with numbers 3 and 6, on the other hand, are reported and dated all aircraft and their trend curves for the relationship between weight in relation to the wing opening and wingspan according to the length.

- To conclude from Figures 7, 8 and 9 we extracted the interpolation equations of aspect ratio and surface as a function of wing aperture and empty weight for the first and wing aperture for the second.

At this point, you know about the trends of the data and it is possible to investigate the configuration of the solar-powered motorglider by identifying the best compromise of variables that would meet all the requirements. In

	S $[m^2]$	b $[m]$	AR	$W_{empty}[kg]$
Glider	12.5	15.667	21.034	263
Motorglider	12.37	15.155	21.3	272.71

Table 3.2: Average value of main geometric and mass parameters belonged to the created database and available in appendix A.

table 3.2 are presented the average values of the most important quantities relative to the created database.

In order to continue with dimensioning and design processes of the solar powered glider, it was necessary to set some useful parameters. Following what happens in technical centres operating in the aircraft sector, we chose to set the *Aspect Ratio* value to 20. This choice is justified by the fact that gliders have AR from 20 to 30. Thanks to the graphs 7 and 8, it has been found that AR grows up with wingspan and mass. Being the minimum historical wingspan values and knowing the average values extrapolated from the database, the choice of 20 has been reached. Along with the aspect ratio value, the fuselage length and the wingspan value were also selected. To do this it was necessary to apply the database interpolation curves adopted by using a prediction method for lower values than the minimum values of data in the database. This information is collected in the Figures 3.11 and 3.12. As regards the wingspan, we remember that the dimensional constraints applied to it, permit values varying from 8 to 12 meters. Within this range, the value of 12 meters was chosen as the first attempt to study this configuration. The choice is justified by the following observations:

W_{empty} Estimation using Statistic Equations

Equation 6

linear — Variable

b [m]	W_{empty} [kg]	W0 (crew 65)	W0 (crew 85)
8	92.329	157.329	177.329
9	115.996	180.996	200.996
10	139.663	204.663	224.663
11	163.33	228.33	248.33
12	186.997	251.997	271.997
13	210.664	275.664	295.664

polynomial — Variable

b	W_{empty} [kg]	W0 (crew 65)	W0 (crew 85)
8	98.865	163.865	183.865
9	120.97	185.97	205.97
10	143.227	208.227	228.227
11	165.636	230.636	250.636
12	188.197	253.197	273.197
13	210.91	275.91	295.91

power law — Variable

b	W_{empty} [kg]	W0 (crew 65)	W0 (crew 85)
8	101.3962861	166.3962861	186.3962861
9	119.3851023	184.3851023	204.3851023
10	138.164819	203.164819	223.164819
11	157.6857941	222.6857941	242.6857941
12	177.9058332	242.9058332	262.9058332
13	198.7885311	263.7885311	283.7885311

Equation 1

linear — Variable

b	W_{empty} [kg]	W0 (crew 65)	W0 (crew 85)
8	113.446	178.446	198.446
9	135.707	200.707	220.707
10	157.968	222.968	242.968
11	180.229	245.229	265.229
12	202.49	267.49	287.49
13	224.751	289.751	309.751

polynomial — Variable

b	W_{empty} [kg]	W0 (crew 65)	W0 (crew 85)
8	116.7146	181.7146	201.7146
9	138.1509	203.1509	223.1509
10	159.667	224.667	244.667
11	181.2629	246.2629	266.2629
12	202.9386	267.9386	287.9386
13	224.6941	289.6941	309.6941

power law — Variable

b	W_{empty} [kg]	W0 (crew 65)	W0 (crew 85)
8	116.37224	181.37224	201.37224
9	134.5835772	199.5835772	219.5835772
10	153.2763373	218.2763373	238.2763373
11	172.4130936	237.4130936	257.4130936
12	191.9625207	256.9625207	276.9625207
13	211.8979661	276.8979661	296.8979661

Equation 4

linear — Variable

b	W_{empty} [kg]	W0 (crew 65)	W0 (crew 85)
8	65.766	130.766	150.766
9	91.598	156.598	176.598
10	117.43	182.43	202.43
11	143.262	208.262	228.262
12	169.094	234.094	254.094
13	194.926	259.926	279.926

polynomial

b	W_{empty} [kg]	W0 (crew 65)	W0 (crew 85)
8	61.5684	126.5684	146.5684
9	88.3506	153.3506	173.3506
10	115.04	180.04	200.04
11	141.6366	206.6366	226.6366
12	168.1404	233.1404	253.1404
13	194.5514	259.5514	279.5514

power law

b	W_{empty} [kg]	W0 (crew 65)	W0 (crew 85)
8	83.3972931	148.3972931	168.3972931
9	100.9832229	165.9832229	185.9832229
10	119.8346111	184.8346111	204.8346111
11	139.9022463	204.9022463	224.9022463
12	161.1432821	226.1432821	246.1432821
13	183.5199349	248.5199349	268.5199349

Stender Equation — *Gliders and MotorGliders*

b	W_{empty} [kg]
8	116.6809202
9	135.109142
10	154.0468463
11	173.4549526
12	193.3007161
13	213.5562496

Noth Equation — *Gliders and MotorGliders*

b	W_{empty} [kg]
8	164.9146128
9	230.6979994
10	311.4961451
11	408.7161786
12	523.7442014
13	657.9474841

Rectangular wing hypothesys, means that S=b*1, unit chord

Figure 3.11: Evaluation through interpolation equation of main design parameters.

Lenght and Aspect Ratio Estimation

Equation 3

	Variable	
linear	l [m]	b [m]
	4	5.7978
	5	9.191
	6	12.5842
	7	15.9774
	8	19.3706
	9	22.7638
	10	26.157
polynomial	l [m]	b [m]
	4	8.1925
	5	10.1832
	6	12.6779
	7	15.6766
	8	19.1793
	9	23.186
	10	27.6967
power law	l [m]	b [m]
	4	7.192538551
	5	9.80705614
	6	12.63458562
	7	15.65249476
	8	18.84357833
	9	22.19421594
	10	25.69329719

Equation 8

	Variable	
linear	Wempty [kg]	AR
	100	12.7211
	125	13.8911
	150	15.0611
	175	16.2311
	200	17.4011
	225	18.5711
	250	19.7411
	275	20.9111
	300	22.0811
polynomial	Wempty [kg]	
	100	17.205
	125	16.745
	150	16.41
	175	16.2
	200	16.115
	225	16.155
	250	16.32
	275	16.61
	300	17.025

Equation 7

	Variable	
linear	b [m]	AR
	5	1.2059
	6	3.051
	7	4.8961
	8	6.7412
	9	8.5863
	10	10.4314
	11	12.2765
	12	14.1216
	13	15.9667
polynomial	b [m]	
	5	8.3149
	6	9.0263
	7	9.8197
	8	10.6951
	9	11.6525
	10	12.6919
	11	13.8133
	12	15.0167
	13	16.3021

Figure 3.12: Evaluation through interpolation equation of main design parameters.

1. it is the smallest value with which sailplane and motorglider have ever been built. This is a historical concern and there are some examples in the database such as the *Radab Windex*. Consequently, having real and commercialized project testimonies as a comparison samples, the following calculations will reflect reality in a more faithful way than a prototype of glider with people. This consideration should be evaluated in order to be able to market the product.

2. higher wingspan value within the range 8-12 meters, allows to maximize the wing surface at the same aspect ratio and this has important consequences both in aerodynamic and energetic fields. In fact, having larger surfaces used to increase the lift capacity, it is possible to reduce the wing load (assuming that the project weight value has been set) and also have more space to be covered by photovoltaic panels for solar energy acquisition.

Fixed the *aspect ratio* and *wingspan* parameters, the empty mass value and pilot derived from the data in database and referring to aircraft were investigated. There was a value around 200 kg, precisely 192 kg for motorglider. while for gliders, the mass associated with a wingspan equal to 12 meters is equal to 160 kg. An important gap and especially linked to the additional weight of engine, propeller, tank and more. These values were compared with the Reymar's equation, which estimates a motorglider weight of 255 kg for motorglider with an 85 kg pilot, while with reference to the database, 255 kg is associated to a 65 kg pilot. The values of the aircraft list built for this project are more trustworthy. With reference to [18], we used the weight estimation equation in the preliminary design phase, associated to Stender[2][16] and modified by McCready for the realization of its solar aircraft prototype called *Solar Challenger*.

$$W_{airframe} = A(nSb^3)^B \tag{3.18}$$

Where A = 0.31 and B = 0.311 in Imperial Units. Once converted in metric units and using the aspect ratio definition $AR = b^2/S$, we can rewrite:

$$W_{airframe} = 8.763n^{0.311}S^{0.778}AR^{0.467} \tag{3.19}$$

Now, decompose AR to obtain an equation which independent variables are S and b:

$$W_{airframe} = 8.763n^{0.311}S^{0.311}b^{0.934} \tag{3.20}$$

[2]Developed in 1969, is based on statistical sailplanes data

This model was widely adopted by Bailey[43], Colozza [44], Irving[15] and Rizzo[45]. With this equation, it was possible to obtain a good interpolation of the data entered in the database, as can be seen in Figures 3.13. The graph is logarithmic type as reported in [18]. This equation was then numerically implemented in a worksheet to obtain the corresponding mass value for a 12-meter wingspan aircraft. The results are shown in Figure 3.11. To finish the mass estimation, Noth's equation was also used, which can always be seen in a logarithmic graph in Figures 3.14. However, Noth's equation does not represent well the data contained in the database, it tends to overstate reality. This may be due to the fact that the database to which Noth refers also includes scale models, drones, UAVs.

W_0 [kg]	AR	b [m]
255	20	12

Table 3.3: Chosen value for predicting aerodynamic performance.

Numbers in Table 3.3, will represent the values of the basic parameters for the evaluation of aerodynamic performance. Subsequently, the weight of the energy infrastructure must belong into the difference between the glider and the motorglider weight estimation, around 40 kg, in which the weight of the engine, propeller, photovoltaic panels and accumulators will fall. This concept will be taken up in Chapter 5.

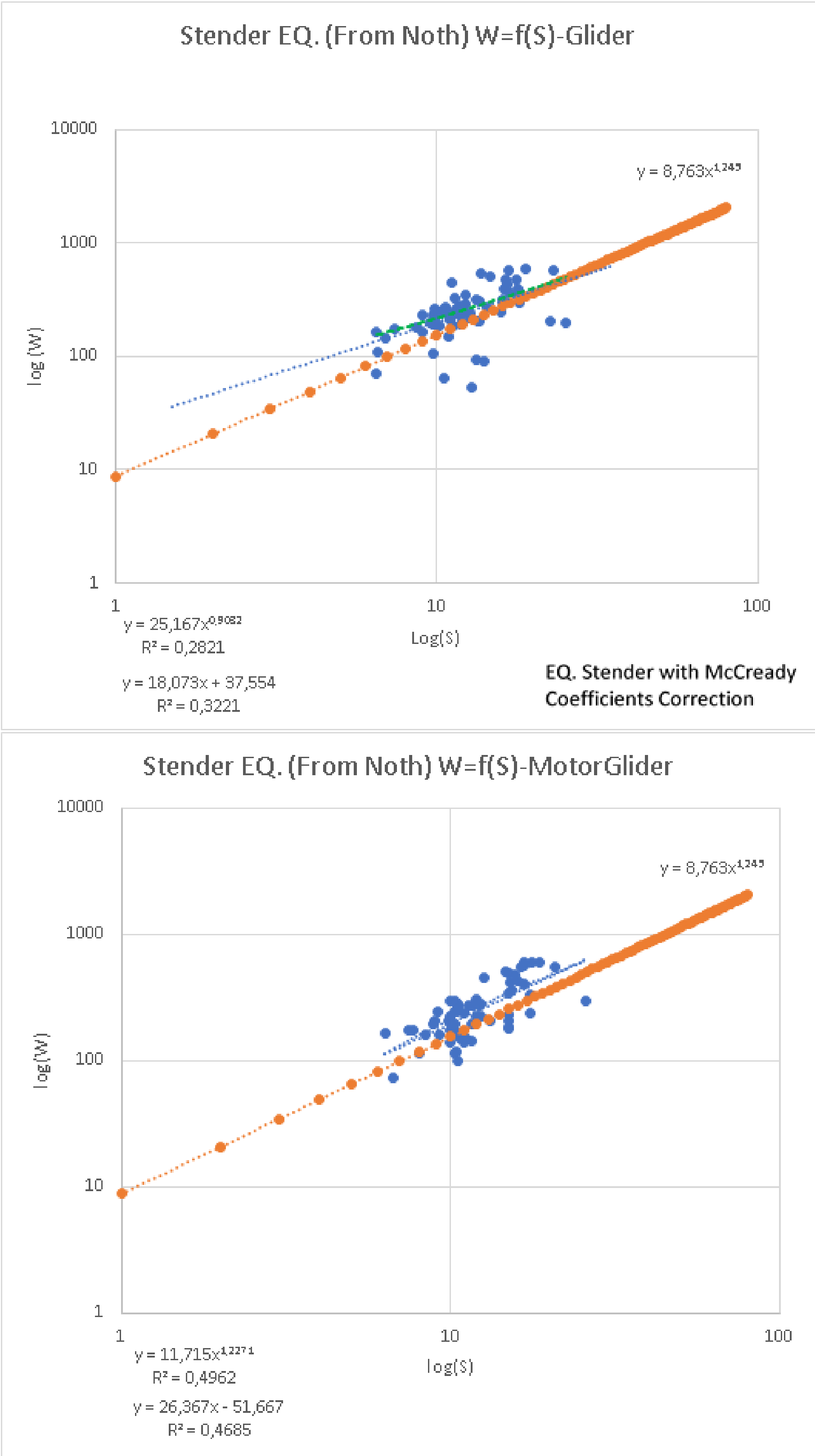

Figure 3.13: Stender equation[16] and database data in logarithmic graphs which variable is S $[m^2]$ and dependant parameter is W [kg]. It is clear the good alignment between data and Stender's equation.

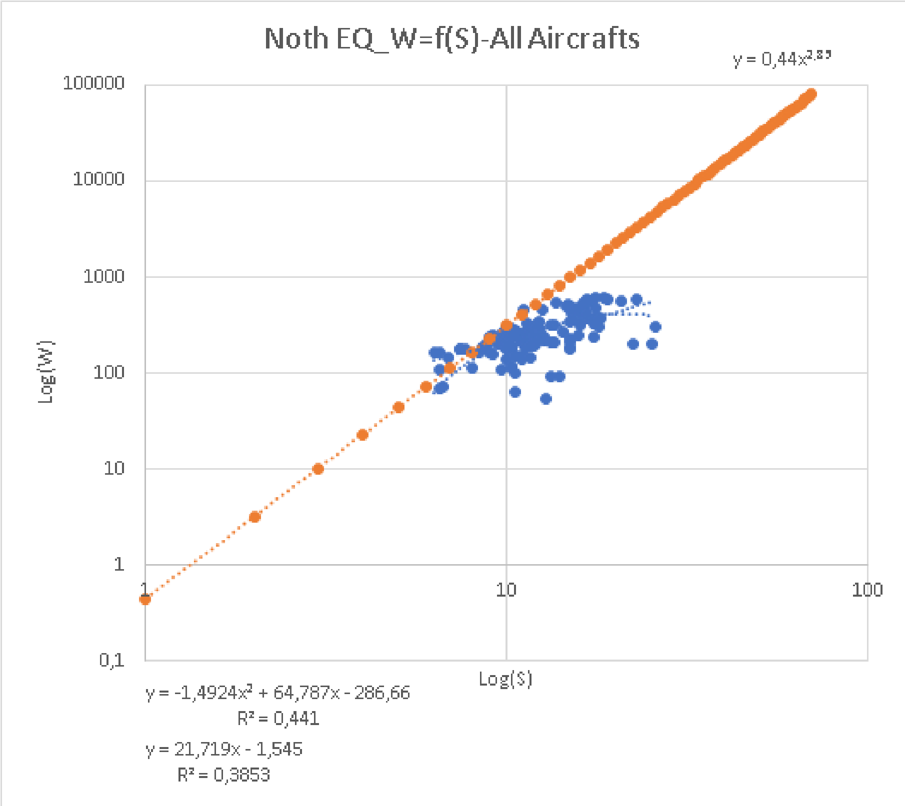

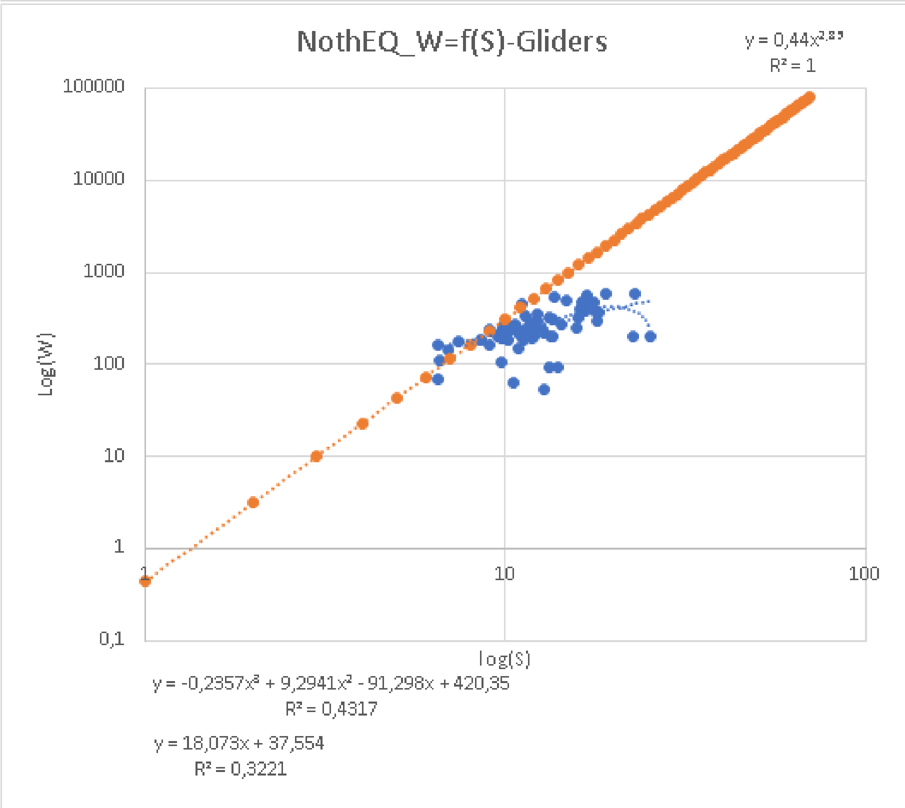

Figure 3.14: Noth equation[18] and database data in logarithmic graphs which variable is S [m^2] and dependant parameter is W [kg]. Noth's equation overstate glider's weight data containing in database.

3.3 Preliminary Airfoil Design

The origin of the Lift is attributed to the difference in pressure between the upper and lower surfaces of the wing. This happens when an air stream flows around the aircraft. At low speeds and therefore low Mach values, it is possible to assume the incompressible fluid hypothesis on which most of the previously presented and following equations are based. The flow that invest the profile is divided and particles have to move quicker on the upper surface than on the lower. The velocity gradient that is generated, produces a change of pressure acting on the wing surface which is expressed by the lift force. For these reasons, the airfoil to be used is of fundamental importance in the aircraft realization. In metaphorical terms, wings are the heart of the airplane, but management is entrusted to a computer or human pilot. Indeed the airfoil influences performance, stability, stall speed. Thanks to the centenary knowledge of the fluid behaviour on aerodynamic profiles, it is possible to make a selection according to the aeronautical category that project belongs. From the introductory chapters we have understood the general aerodynamics of a plane and a glider. A glider is a high-aerodynamic machine that fully utilizes the potential-kinetic energy conversion to generate speeds from altitude and hence to fly. In most of the commercial glider, the requirements that an airfoil has to respect are:

- high efficiency
- elevated lift
- low drag
- high power factor

To these requirements, two more were added, following the design of a solar autonomous aircraft [14],[18],[26], finding the best compromise, precisely:

- larger laminar behaviour
- Reynolds operation from 100'000 to 1E6
- performing at low speeds
- uniform behaviour while varying Reynolds

With these requirements, an extensive survey was carried out on the most commonly used airfoil in aeronautics and included in the database, as well as [18],[26].

3.3.1 Introduction: Main Airfoil Parameters

The airfoil represents the elemental unit that forms the wing and thanks to its particular geometry that it is possible to produce lift. You can observe it virtually by cutting with a plan, parallel to the plan of symmetry, the wing. The main components can be summarized as follows: **leading edge**: the origin point of airfoil coordinates and where the current separation occurs; **trailing edge**: point at the end of the airfoil where airfoil finish and the reconnection of the flows are observed;**The chord** line that joins the leading edge with the trailing edge along the horizontal reference axis;**Camber line**: refers to curvature of the airfoil, determines the lift for zero angle of attack;**Thickness**: Distances between upper and lower surface of the profile;

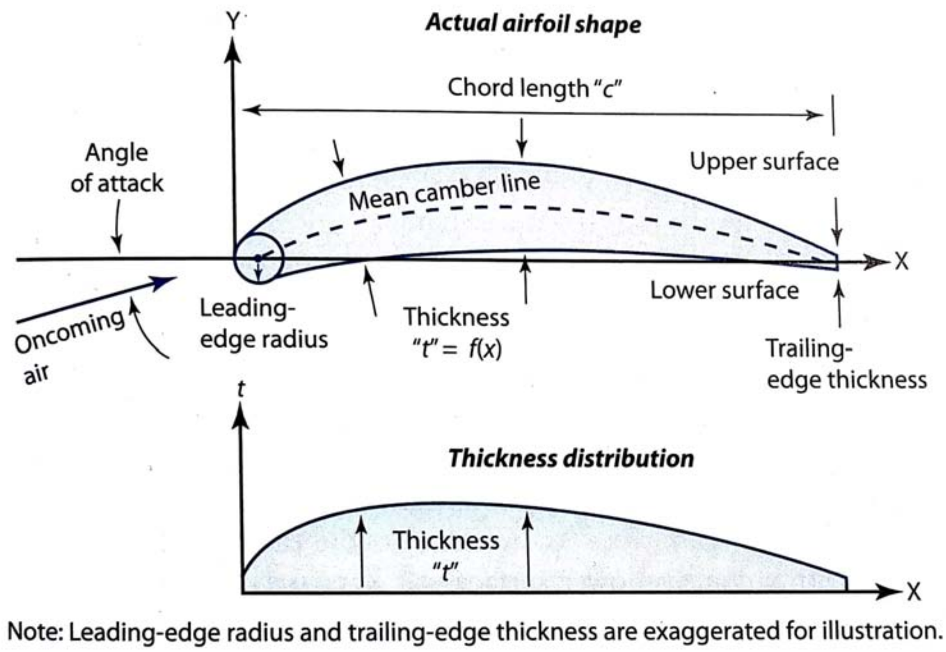

Figure 3.15: the airfoil geometry and principal features [39].

From a first analysis of the airfoil with which we plan to build an aircraft wing, we can extract some interesting properties such as the preliminary and approximate individuation of the stall angle. This concept can be graphically understood with reference to the images related to the polar curve paragraph. In any case, the stall phenomenon, from an aerodynamic point of view, begins when fluid flows are no longer able to adhere to the profile. This happens to the upper surface. Please refer to the image in Chapter 2, Figure 2.6.

3.3.2 Aerodynamic Considerations on Finite Wings

The airfoil is used to form the wing which has finite length, unlike the first aerodynamic theories which hypotheses considered an infinite length wing. This discrepancy between the theoretical world and the real world has led to the introduction of new parameters such as *induced drag* and *downwash* phenomenon as consequences of the finite wing dimension. The previously selected aspect ratio is a non-dimensional key parameter for identifying wing geometry and performance, at least preliminarily. It is defined as:

$$AR = \frac{b^2}{S} \tag{3.21}$$

The induced drag depends on the aspect ratio value. For supersonic or military aircraft it is very small while it can reach 20-30 times higher values for highly efficient aircraft. In particular a high AR value, meaning a long and thin wing, will be associated with a very low induced drag value and therefore the fundamental contribution of the drag will be the airfoil drag. In a wing that can be first approximated as a three-dimensional airfoil, the gradient of pressure between the upper and lower surface tends particle to move to the extremities, this because the particles in addition to floating the surfaces in the direction of motion, also move along the direction of the three-dimensional development of the wing, that is, out of the plan of typical fluid motion. The motion along this direction is precisely due to the existence of a pressure difference between the two surfaces forming the wing, together with the absence of an infinite wing. The low pressure area recalls the particles present in the area below the low pressure wing causing the so-called extremis vortices. The air suction action also causes a twist that propagate towards the joint and causes a change of the fluid incidence. The wing will see a current at the *effective angle* given by the difference between the *geometric angle* and the *induced angle*.

Equal to the wingspan, a wing with a high aspect ratio has the wing tip more distant from the fuselage than a wing with a lower aspect ratio. Then as a percentage, the wing portion affected by this reduction of the Lift due to tip vortices is reduced, and there is less Lift loss for greater aspect ratios.

Changing the aspect ratio corresponds to decreasing the stall angle of the airfoil. This is the reason why along the wing, at the tip tends to increase the aspect ratio so that the stall angle is greater, and then maintain aerodynamic control.

Paradoxically, the lift generation in a finite wing is responsible for the formation of a further contribution in the drag, which is the induced drag, of the end vortexes referring to the phenomenon of downwash and a lowering of the lift curve. Due to the formation of vortexes, which absorb energy from fluid motion, an energy counterbalancing promoted by a propulsion system is required. Also the downwash phenomenon locally deviates the flow that will encounter the wing at a lower angle than the geometric, the effective angle. This causes the decrease in the lift curve.

3.3.3 List and Properties of Chosen Airfoils

For the choice of the aerodynamic profile to be adopted, a first selection was made taking into account those profiles families generally used by industrial constructors and which in particular meet the requirements for low Reynolds and the maintenance of laminarity of the flow. Thanks to **Profili2**®software, it was possible to process the list of profiles that are included in this selection. There are several family of profiles, from the *NACA* 4 series to the *GOE* family and *Wortmann*. As far as the fuselage is concerned, a NACA 6 series profile is selected, minimizing fuselage interference and parasitic drag, maintaining laminarities up to 35-40 percent of their length [34][39]. This information will be of great use for the graphical representation of the developed configuration. A common peculiarity to these profiles is that they are fairly thick and have good curvature, with the exception of the FX-71-L-150 which is symmetrical but used in certain applications. These particular geometries are well suited to gliders that require high aerodynamic performance at low speed. Refer to the figure 3.16 showing the environment of flow conditions in which gliders are typically dimensioned. The airfoil belonging

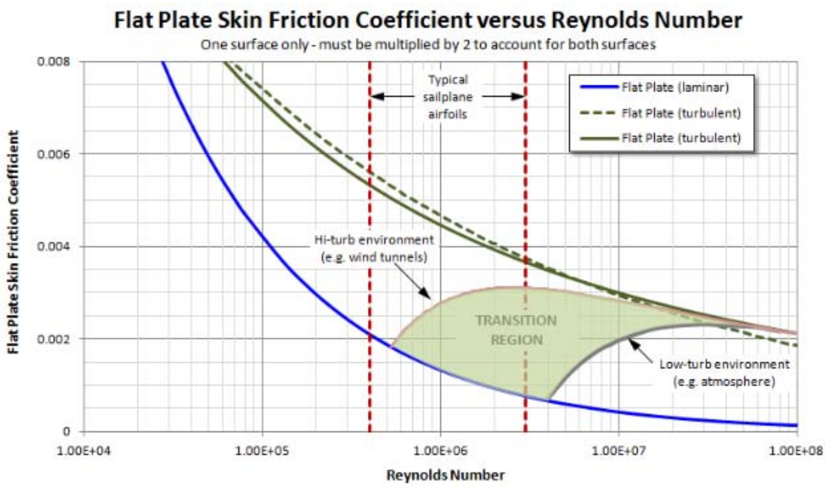

Figure 3.16: Typical sailplane operating condition, in terms of Reynolds number.

to the Wortmann family often appear in the aircraft database, in particular

for aircraft built from the 70's onwards. They are primarily intended for sailplane use and other low Reynolds number applications. They are laminar flow sections, medium to high cambered. High pitching moment but this is not a disadvantage on sailplane, where tail lengths are long. Great airfoil, able to preserve laminar region and reduce drag[47].
Thanks to **Profili2**®, that is the updated visual interface of the well known *XfoiL code*, the selected airfoil was investigated.

NASA NLF1015
Spessore max 14.99% al 40.3% della corda
Camber max 4.70% al 61.1% della corda
Mach = 0.0000 - NCrit = 11.00

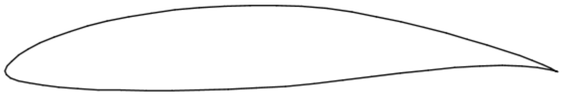

FX 61-147
Spessore max 14.77% al 33.9% della corda
Camber max 3.18% al 33.9% della corda
Mach = 0.0000 - NCrit = 11.00

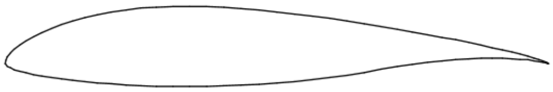

GOE 501
Spessore max 12.80% al 30.0% della corda
Camber max 6.30% al 50.0% della corda
Mach = 0.0000 - NCrit = 11.00

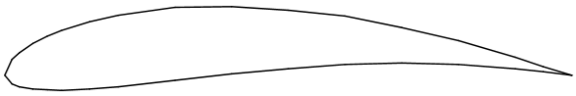

E214 (11,1%)
Spessore max 11.08% al 31.4% della corda
Camber max 4.03% al 52.4% della corda
Mach = 0.0000 - NCrit = 11.00

E387
Spessore max 8.88% al 28.8% della corda
Camber max 3.83% al 39.2% della corda
Mach = 0.0000 - NCrit = 11.00

FX 63-137 13,7% smoothed
Spessore max 13.72% al 29.9% della corda
Camber max 5.94% al 52.8% della corda
Mach = 0.0000 - NCrit = 11.00

FX 60-126-1
Spessore max 12.60% al 27.9% della corda
Camber max 3.96% al 56.5% della corda
Mach = 0.0000 - NCrit = 11.00

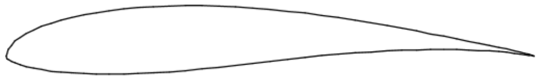

FX 61-184
Spessore max 18.37% al 37.1% della corda
Camber max 3.09% al 62.9% della corda
Mach = 0.0000 - NCrit = 11.00

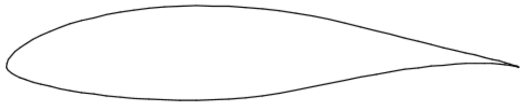

NACA4415
Spessore max 15.00% al 30.0% della corda
Camber max 4.00% al 40.0% della corda
Mach = 0.0000 - NCrit = 11.00

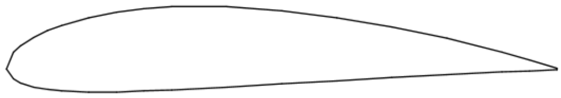

GOE 493
Spessore max 15.08% al 33.7% della corda
Camber max 3.36% al 52.6% della corda
Mach = 0.0000 - NCrit = 11.00

FX 63-120
Spessore max 12.01% al 30.8% della corda
Camber max 5.24% al 50.0% della corda
Mach = 0.0000 - NCrit = 11.00

FX 71-L-150-20
Spessore max 15.00% al 33.9% della corda
Camber max 0.00% al 0.0% della corda
Mach = 0.0000 - NCrit = 11.00

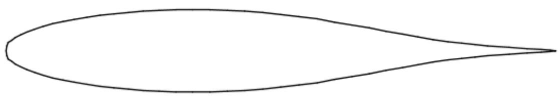

The *Xfoil* Code XFOIL is an interactive program for the design and analysis of subsonic isolated airfoils. It can performs:

- Viscous (or inviscid) analysis of an existing airfoil
- Airfoil design
- Drag polar calculation with fixed or varying Reynolds and/or Mach number
- Plotting of geometry, pressure distributions, and polars

The inviscid formulation of XFOIL is a simple linear-vorticity stream function panel method. A finite trailing edge base thickness is modelled with a source panel. The equations are closed with an explicit Kutta condition. A Karman-tsien compressibility correction is incorporated, allowing good compressible prediction all the way to sonic conditions. The theoretical foundation of the karma-Tsien correction breaks down in supersonic flow, and as a result accuracy rapidly degrades as the transonic regime is entered.
For the viscous formulation, the bounday layers and wake are described with a two-equation lagged dissipation integral BL formulation and an envelope e^n transition criterion, both taken from the transonic analysis/design ISES code. The entire viscous solution is strongly interacted with the incompressible potential flow via the surface transpiration model. This permits proper calculation of limited separation region. The drag is determined from the wake momentum thickness far downstream. A special treatment is used for a blunt trailing edge which fairly accurately accounts for base drag.[48]

3.3.4 The Airfoil Polar Graph

The polar curve of an airfoil, synthesizes the aerodynamic feature, reporting the drag and lift coefficient, indeed C_l and C_d, depending on the angle of attack. Thanks to the **Profili2**®software, it was possible to investigate airfoil behaviour in different fluid environments, described by the Reynolds Number. With these graphs, available in Appendix B, it was possible to address the first considerations and identify airfoils that best meet the requirements previously defined.

All profiles are highly efficient, and only the evaluation of the efficiency value is not a valid discriminant for the airfoil selection. Therefore, it is necessary to go deeper, while increasing the credibility of XfoiL results. The final choice will be a compromised on all the specifics. Below are the considerations for each profile or family: the profile *E214* has a discrete behaviour for Reynolds over 250000 achieving efficiency values and flight power greater than 150 for Re = 2E6. When approaching the stall, XfoiL outlines a stable behaviour, in spite of the *E387* profile which has a drastic change near the stall, as well as efficiency and power are affected by sensitive variations while varying Reynolds. *Wortmann FX 61-147* shows good properties, both for the maximum Cl value, efficiency, power, and uniformity of performance as the Reynolds vary. *Wortmann FX 61-184* has a thickness of about 25 percent higher than the previous one. This affects the drag. The benefit in terms of lift is not so far from Wortmann FX 61-147. *Wortmann FX 63-120* is similar from the point of view of performance at FX 61-147, especially at low Reynolds. It remains a potential profile for a future configuration. *Wortmann FX 63-137* is one of the most desirable airfoils for high-lift low Re models. The high-lift capability and mild-stall characteristics are among its key attributes. It has a good behaviour at Re = 200k and above, especially in terms of power and efficiency. The lift is very high thanks to the high curvature. The stall of the FX 63-137 is an example of a "slow" trailingedge stall which produces a plateau in the $C_l - \alpha$ curve past the point of stall initiation[53]. The *Wortmann FX 71-L-150-20* is a symmetrical profile with a thickness of 15 per cent of the chord. does not have good properties as the profiles previously described. The *NACA 4415* is very stable and guarantees, according to XfoiL, a very high stall angle with gradual behaviour. Among the airfoil displayed is what shows the best uniformity of Cl at the Reynolds variation. However, power and efficiency values are standard. *Goe 493* does not have a high curvature. This has the advantage of producing low leading edge twisting moments but has the disadvantage of producing low Cl values. XfoiL also determines a not so homogeneous behaviour for these profiles. The *Goe 501*, on the other hand, has a high curvature, which would make the flight unstable. The behaviour is not well described by XfoiL.

The choice of the airfoil was twice. The main reason is to research both into constructive practice and requirements that have been set. In fact, as previously stated, the lift decrease along the wing until it reaches zero at the wing extremis. It is known that camber plays a major role in determining lift capacity. At the same angle, increasing the airfoil curvature you reach higher lift values but the stall angle decreases. If the curvature is reduced by going towards the end without a built twist, there will be an aerodynamic twist, because the angle of aerodynamic attack changes when the curvature changes. To have an elliptical distribution of lift, which is obtained with an elliptical wing shape but difficult to obtain in practice, the wing should be twisted positively. However, this would cause an early stall at the end because the curvature is smaller, bringing the aircraft into an extremely unstable configuration of the "screw", from which it is difficult to escape. So if aerodynamic twist is counterbalanced by an equal geometric twist in the opposite direction you get a good compromise. In practice, in order to keep the coefficient of lift from the root to the end almost constant, a more curved end profile of the root is adopted[34]. For this reason, two profiles belonging to the same family were chosen: Wortmann, ie FX 61-147 and 63-137. Comparing the two polar curves, the approximate value of the zero aerodynamic angle could be highlighted, from which to process the negative wing geometric twist angle. From comparisons figures, it is noted that the value is about 2.5 degrees, which makes it possible to rotate the root profile of 1.5 degrees clockwise while the end of the wing of 1 degree counter-clockwise.

Another configuration that could be studied is to use the same profile from the root to the end, with a negative twist and tapering the whole wing. This reduces the construction complexity. The Wortmann FX 63-137 due to its curvature, however, would not allow the best use of the surface for energy acquisition. This will then be developed in Chapter 5. With the chosen configuration, the extremity airfoil produces a higher lift value, given the same incidence angle. The airfoil and wing configuration chosen , according to [34], would allow better stall stability which would be more gradual. Also, the airfoil 63-137 shows a tendency to stall next, according to XfoiL at FX 61-147, although it is much curved.

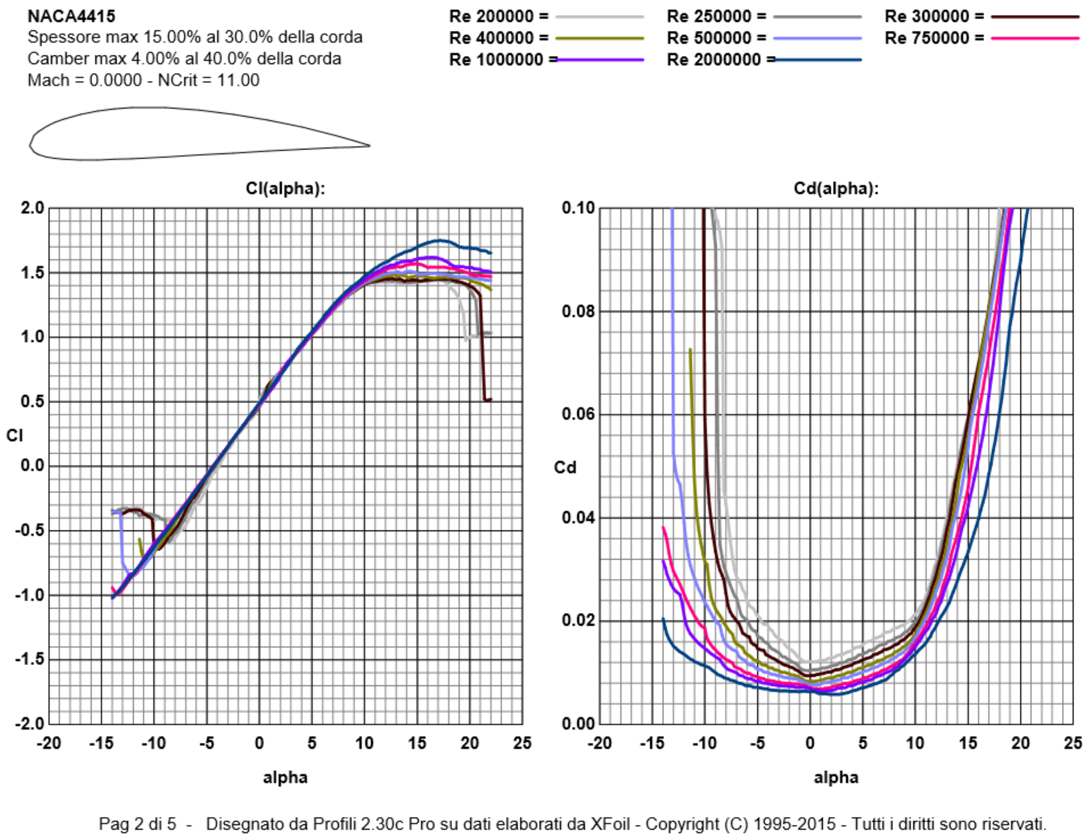

Figure 3.17: Polar graphs example, relative to NACA 44415 airfoil.

Re = 750000
Mach = 0.0000
NCrit = 11.00

FX 61-147 =

FX 63-137 13,7% smoothed =

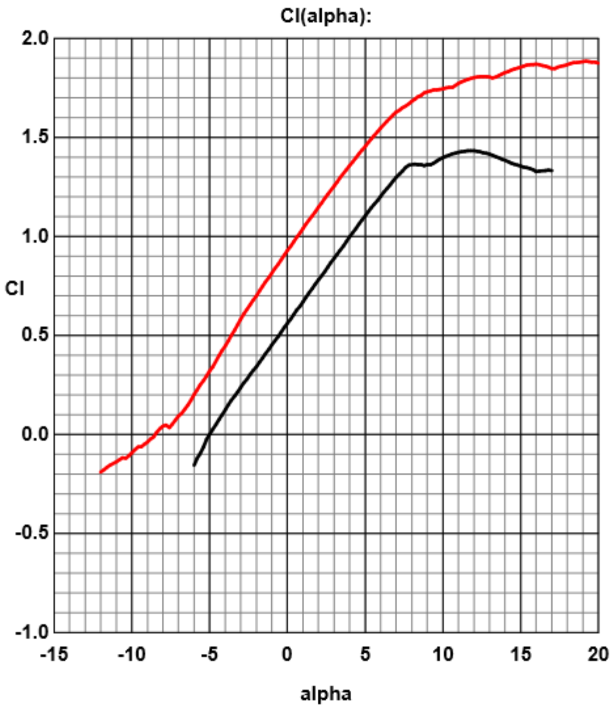

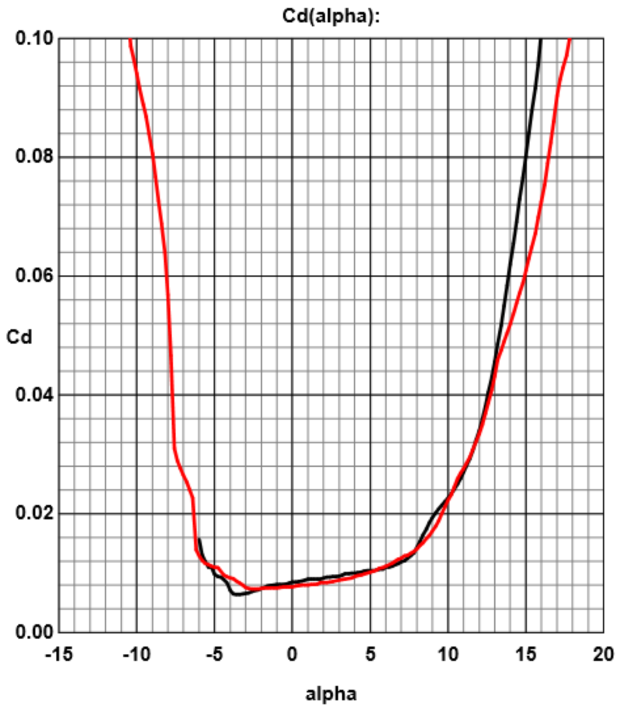

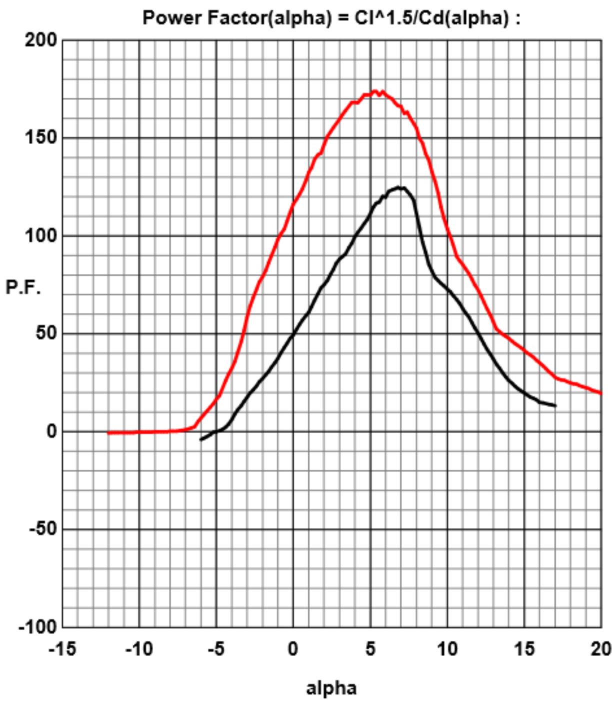

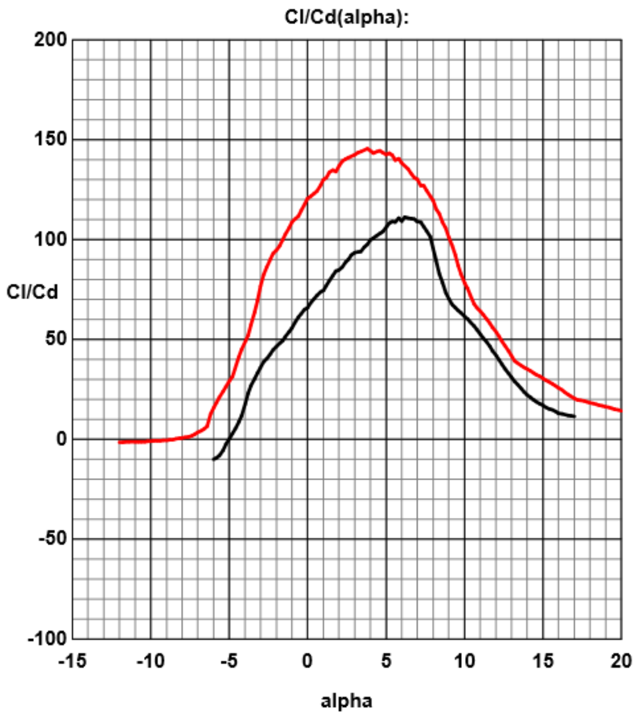

3.3.5 Wing Geometry

For the choice of the wing shape, the suggests of Prof. Pajno was used [34], an expert in sailplane design and studies. In particular, it was chosen to make a double tapered wing with a global factor of 0.3. The choice of double tapering was made to limit the construction's complexity to the advantage of a decrease in mass compared to a wing with an equal chord length from the root to the end. Factor 0.3 was chosen to have a small enough tip to maximize mass distribution based on the structural behaviour of the part. The value of the first quarter of the wing (x1) was chosen at 0.5. In particular, the graph shown in figure 3.18 is used, which collects a set of data processed by the University of Delft and which would result in a wing shape that minimizes interference with fuselage and induced drag. The root chord length value was assigned to 800 mm, based on a series of sample aircraft of similar geometry and having quoted draws. The graph was used to set a root chord value of 1 meter and then was scaled with a factor of 0.8. The wing, as can be seen from figure 3.19, does not have a simple trapezoid but the incoming edge is swept by an angle called *swept angle* while the output edge of each tapered profile is aligned. This is a reverse wing configuration. This particular form is the perfect compromise between aerodynamic and constructive demands, which tends to approach the elliptical shape [34]. At this point, knowing the first attempt wing shape, it is possible to store it and go further. In particular we proceed to find the aerodynamic centre that in first approximation we can define at one quarter of the chord on the mean aerodynamic profile. For this purpose was used two difference method, both belonging to Reymar[39], one analytic and one by draw. For what about the analytic way, was define two other subway, developed to encounter the particular wing geometry. The main Reymar's method equation, define the mean aerodynamic chord length, of a trapezoidal wing, to be:

$$\tilde{C} = \frac{2}{3} C_{root} \frac{1 + \lambda + \lambda^2}{1 + \lambda} \tag{3.22}$$

where λ is the taper ratio.
However the wing shape, could be defined as a composed of two trapezoidal wing, with different taper ratio. For this reason and because there are not explications on how to do in this situation, two others way was investigated.The first one considered a $\tilde{\lambda}$ as the mean taper ratio. We have:

$$\lambda_1 = \frac{0.696}{0.8} = 0.87 \tag{3.23}$$

$$\lambda_2 = \frac{0.24}{0.696} = 0.3448 \tag{3.24}$$

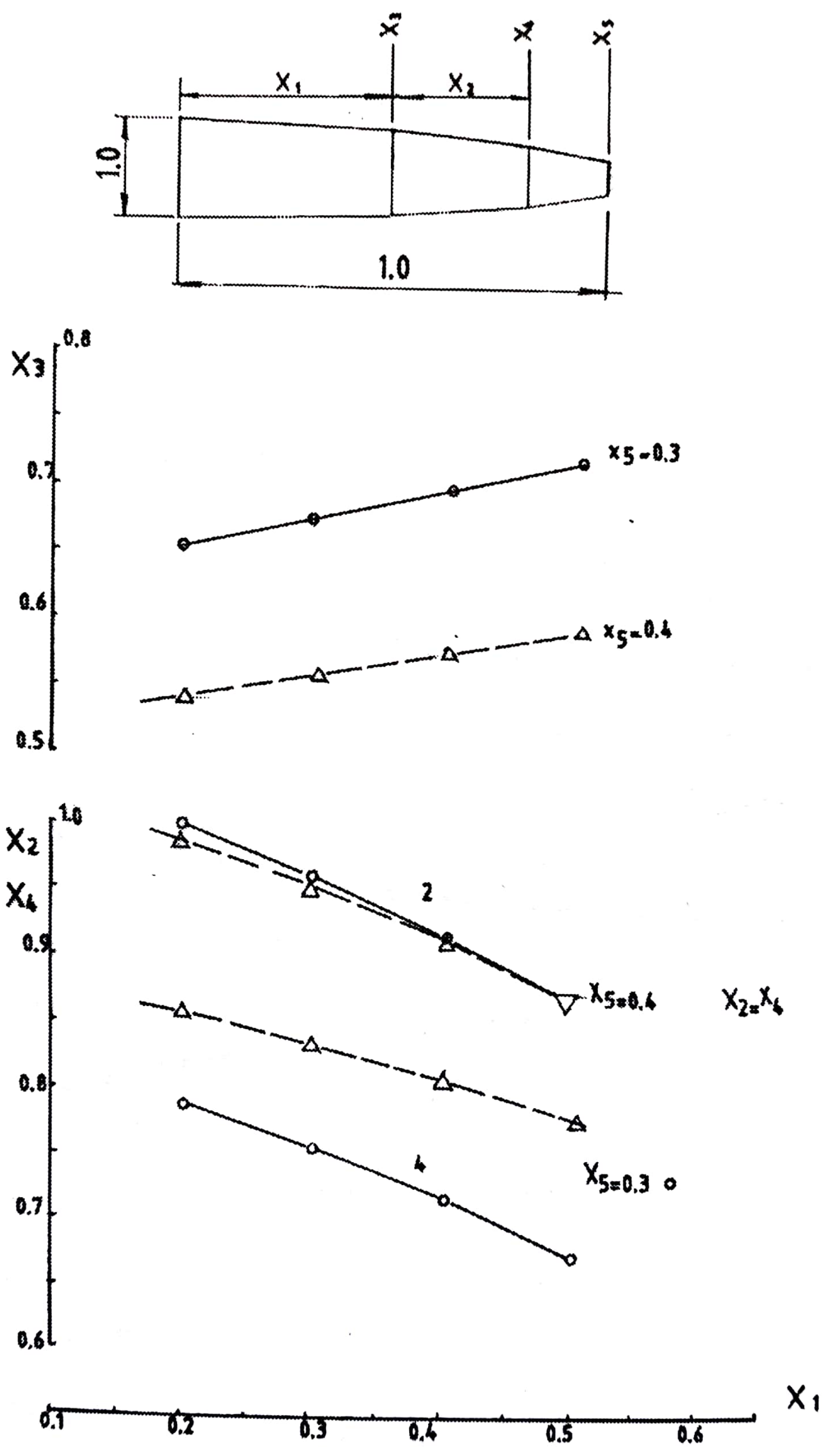

Figure 3.18: Graphs developed thanks to Delft University which help to perform best wing shape with minor induced drag.

So the $\tilde{\lambda}$ is equal to 0.6074. The corresponding mean aerodynamic chord length, using equation 3.22, is 0.656. This value does not coincide with the graphical method, exposed in figure 3.19. A second direction was chosen: Considering the main aerodynamic chord of each half-wing section.

$$\tilde{C_1} = f(\lambda_1) = 749.205mm \tag{3.25}$$

$$\tilde{C_2} = f(\lambda_2) = 505.02mm \tag{3.26}$$

and doing the arithmetic average we obtain:

$$C_{\tilde{AVG}} = \frac{\tilde{C_1} + \tilde{C_2}}{2} = 627.112mm \tag{3.27}$$

that is equal to graphical method. Indeed these formulation have the same conceptual background with the graphical method, instead the first one hasn't.

The wing surface computed by **SolidWorks**®is equal to:

$$A = 7.26m^2 \tag{3.28}$$

Using additional graphs in Figure 3.20a,3.20b,3.20c, developed by Delft University, the Oswald coefficient was calculated. The *Oswald Coefficient* is a correction factor that represents the change in drag with lift of a three-dimensional wing or airplane, as compared with an ideal wing having the same aspect ratio and an elliptical lift distribution[39]. Knowing the global taper ratio, ie 0.3, and the Aspect ratio, ie 20 corrected to 19.5, from graphs 3.20b we obtained that $1/e_{Rr} = 1.05$. This number have to be modified to taking into account the fuselage interference 3.20c. Assuming a streamlined fuselage to reduce the *wetted area* [49] and reading the graph 3.20c, we obtained for AR=20 the value of 1.5. This value has to be multiplied by master fuselage section to wing surface fraction and we have the parameter $1/e_{fus}$. The last correction regarding the wing position:

$$n = \frac{K_e}{\frac{1}{e_{Rr}} + \frac{1}{e_{fus}}} \tag{3.29}$$

and the result is :

$$n = e_{TOT} = 0.8247 \tag{3.30}$$

K_e is a empirical corrective coefficient refers to wing position. In this case, upper wing was choose and a value of $K_e = 0.9$ is established[34].
This terms will be very useful soon, when will be explained the lift curve correction.

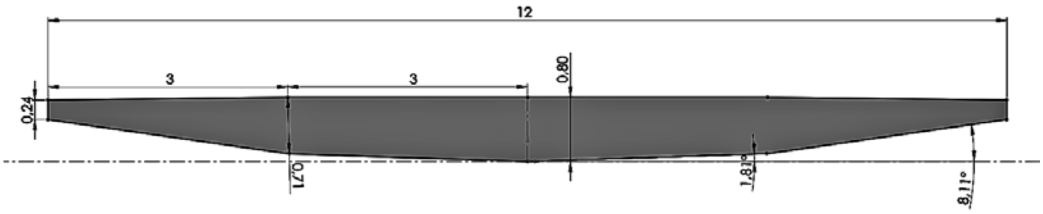

(a) The wing shape geometry with quoted dimension in meter.

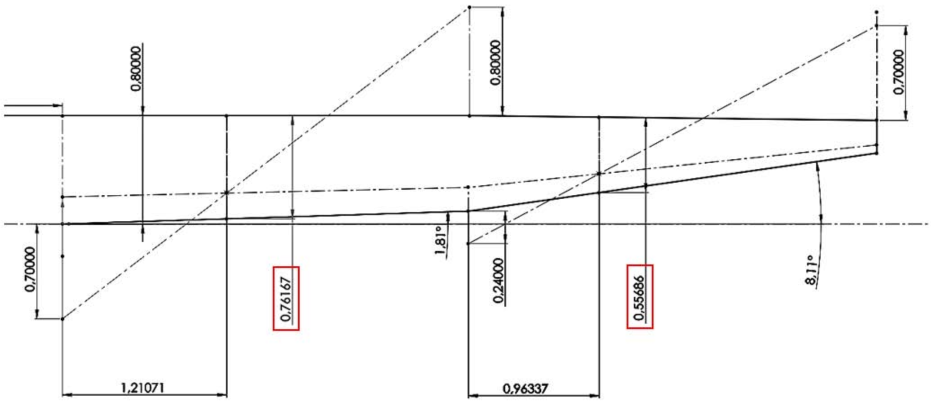

(b) Calculation of the aerodynamic mean chord lenght using Reymar's graphical method [39].

Figure 3.19: Wing geometry designed in **SolidWorks**®with quoted measure and mean aerodynamic chord length evaluation.

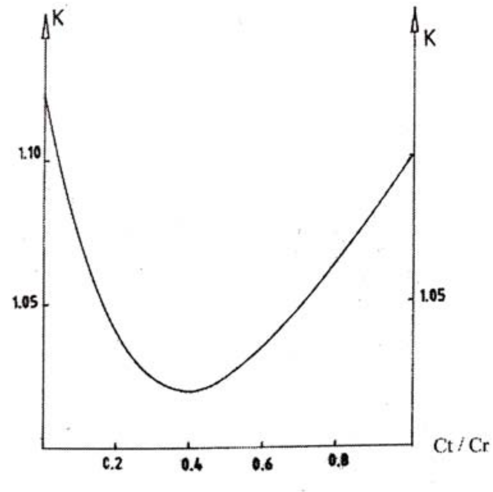

(a) Oswald Coefficient correction with graphic data[34].

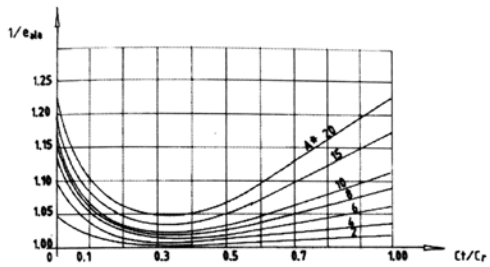

(b) Oswald coefficient correction as a function of Aspect ratio and taper[34].

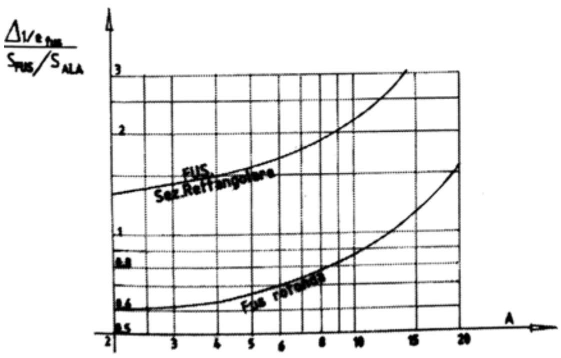

(c) Oswald coefficient correction due to fuselage presence[34].

3.3.6 Tail Dimensioning and Design

In order to estimate the tail size of first attempt, some aspects of flight mechanics were made. The tail plan is responsible along with vertical stabilizer and rudder of providing adequate stability to the aircraft during flight. Its main function however is to introduce the glider, according to the will of the pilot, in nose up, dive or general descent. The tail plan then controls the levelling of the aircraft and the pitch. Assuming to be in level flight conditions, with a $C_{l_{Wing}}$ of 1 and $C_{l_{Tail}}$ produced at the tail plan of 0.5, was made a balance of moments. The author is aware of the strong hypotheses introduce, but they are fundamental for an initial estimate of the size of the vehicle and not alien to aeronautical practice. The first step to be taken was to identify the centre of gravity of the aircraft. Being an imaginary geometric place in which the whole mass is thought to be concentrated and therefore also said *centre of mass*, it was necessary to evaluate its position with a physical strategy. In fact, the geometry of the structure and its weight, interior components and electronics are not yet known, but there is an estimate of the total aircraft weight. **Solidworks**®were used to obtain a first estimation of the centre mass position , which is now definable as a volumetric centre. In fact, the 3D draw that will be shown later, represents the aircraft as a solid body. A density of 1000 kg/m^3 was set for each part, from the fuselage to the stabilizer, and the centre of gravity was required. It is not so far from reality to think that where more volume lies in an airplane, it also lives more mass. In the constructive reality, the distinct component is typically known, so it is possible to refine this calculation. Finally, we evaluate a prototype that is hooked and left suspended. Reference to 3.20, and imposing the condition of

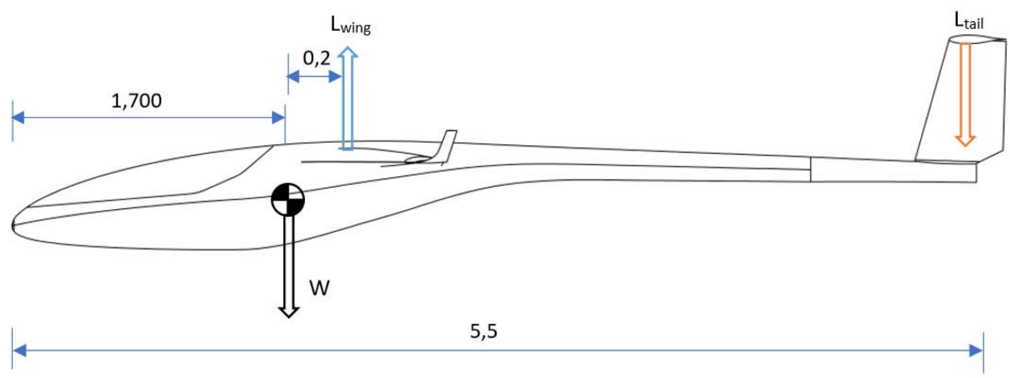

Figure 3.20: Conceptual and qualitative force distribution on a sailplane;Dimension in meters.

zero momentum, it is obtained a first tail length value of :

$$L \cdot 0.2 - L_{tail} \cdot 3.8 = 0 \tag{3.31}$$

$$S_{tail} = \frac{S \cdot C_{L_{wing}} \cdot 0.2}{C_{L_{tail}} \cdot 3.8} = 0.7642m^2 \tag{3.32}$$

$$l_{tail} = \frac{S_{tail}}{chord_{tail}} = \frac{0.7642}{0.325} = 2.35m \tag{3.33}$$

Typically the tail airfoil is a biconvex symmetric category. For this reason was chosen the HQ 1.0-8. The same study-process adopted for wing airfoil was used for tail airfoil. On the draft, to reproduce the condition at which it is dimensioned for, the airfoil is twisted by 2 degrees counter clockwise to create negative lift.

3.3.7 Correction of Aerodynamic Parameters

The polar curves previously calculated by **Profili2®**, are correct as long as the infinite wing hypothesis is maintained in reality. Logically, this can not be done and it is necessary to re-evaluate calculations for a finite wing geometry. As explained above, the relaxation of the infinite wing hypothesis results in a change of slope in the lifting curve with increased Drag. That is, we see a decrease in the angular coefficient of the curve Cl = f (alpha). Using formulas drawn from [34] and [39],we extract values of Cl that could be obtained under real conditions. We anticipate the concept for which these calculations, based on semi-empirical formulas and/or graphical experimental data estimates, do not take into account a number of factors such as fuselage intersection, presence of ailerons, local variations of Reynolds, transient phenomena , surface treatment and so on. This is a correction made on a series of theoretical data by using formulas elaborated by other people's experiences and here adjusted.
Now will be present the hand-calculation phases and at the end a table in which there will be the data corrections. This corrections, as the evaluation of different performance was previously done on selected airfoil, will interest Reynolds number varying from 100 000 to 1E6 and for each profile.

1. First of all is necessary to evaluate the C_l = f(α) angular coefficient of theoretical data a_0, made by **Profili2®**. We read tables supplied by the software from which the graphs in appendix B are processed. In particular, the C_l data corresponds to the angles present in the positive zero zone. This is because in this area it can be stated, with good approximation, the linear behaviour of the lift when vary the angle of incidence.

2. The precedent value, that is really close to 2π but not at all, will be inserted on the formula:

$$a = \frac{2\pi AR}{pAR + 2} \tag{3.34}$$

   where p is

$$p = \frac{wingsemiperimeter}{wingspan} = \frac{12,25}{12} = 1.02083 \tag{3.35}$$

   this will be do for each airfoil : FX 61-147 and FX 63-137.

3. A weighing average on the wings surface of the values a_1(refers to FX 61-147) and a_2(refers to FX 63-137) is performed, particularly in profile

FX 61-147 competing to the first tapered wing portion, while at 63-137 the second tapered wing portion. Area values are: $4.49m^2$ and $2.81m^2$. The obtained values will be used to re-calculate Cl according to the formula:

$$Cl = a_{AVG} \cdot (\alpha - \alpha_{0_{AVG}}) \tag{3.36}$$

4. Calculating α_0 of both airfoil, varying the Reynolds number. In particular for Re= 100k, 400k, 750k, 1E6.

5. A weighing average on the wings surface of the values α_{0_1} and α_{0_2} is performed, obtaining for each of the precedent Reynolds value the term $\alpha_{0_{AVG}}$ to insert in the precedent formula.

6. Evaluate the induced angle with formula:

$$\alpha_i = \frac{Cl}{\pi ARe} \tag{3.37}$$

7. Calculate the effective angle as $\alpha - \alpha_i$

8. Obtained the correction of C_D estimation, adding the contribution of induced Drag.

$$C_D = C_{d_0} + \frac{C_L^2}{\pi eAR} \tag{3.38}$$

9. Used the same expression above to evaluate the tail contribution.

10. Calculate the parameter $C_{l\alpha_A}$ called *the Lift Gradient Coefficient* for each profile, varying the reynolds Number.This will be useful for evaluating the contribution of glider and tail

$$C_{l\alpha_A} = \frac{2\pi AR}{2 + \sqrt{AR^2 + 4}} \tag{3.39}$$

11. A weighing average on the wings surface of the values $C_{l\alpha_{A1}}$ and $C_{l\alpha_{A2}}$ is performed.

12. Calculate the term Y_{fus}

$$Y_{fus} = 1 - 0.25\left(\frac{d}{b}\right)^2 + 0.025\left(\frac{d}{b}\right) \tag{3.40}$$

13. Multiply Y_{fus} for $C_{l\alpha_A}$, obtaining $Cl_{glider+us}$

14. Obtain the Total Cl of the glider:

$$Cl_{glider} = \left[Cl_{glider+fus} - Cl_{io} \cdot \frac{S_{Tail}}{S_{ref}} + \frac{q_0}{q}\frac{S_0}{S}\left(1 - \frac{d\alpha_i}{d\alpha}\right)\right] \cdot cos(\Delta_{0.25c}) \tag{3.41}$$

where S_{ref} correspond to S_{Wing}; the term $\frac{d\alpha_i}{d\alpha}$ can be calculate with the expression :

$$\frac{4}{AR+2} \tag{3.42}$$

15. Evaluate $C_{D_{TOT}}$ adding the contribution of tail and fuselage by multiplying each oh them by the fraction $S_{"part"}/S_{ref}$. In particular for the fuselage was followed the Reymar's method for the evaluation of first attempt C_D:

    - Evaluation of the parameter f with the formula :

    $$f = \frac{l_{fus}}{d_{AVG}} = 22.1774 \tag{3.43}$$

    d_{AVG} was calculate from 5 section of lofted fuselage, that will be later explained.

    - calculate:

    $$FF = \left(1 + \frac{60}{f^3} + \frac{f}{400}\right) = 1.06094 \tag{3.44}$$

    - the fuselage wetted surface evaluated thanks to **Solidworks**®is equal to 5.08841 m^2
    - $C_{D_{fus}}$ is equal to:

    $$C_{D_{fus}} = C_{f_{fus}} \cdot FF \cdot \frac{S_{wet}}{S_{ref}} = 0.001393 \tag{3.45}$$

16. The process concludes with the calculation of entire glider C_D:

$$C_D = C_{d_0} + \frac{C_L^2}{\pi e AR} + \left(C_{d_{0_{tail}}} + \frac{C_{l_{io}}^2}{\pi e_{tail} AR_{tail}}\right)\frac{S_{tail}}{S_{ref}} + C_{D_{fus}} \tag{3.46}$$

Using this procedure, it is possible to obtain values that seems to be realistic, indeed they are decreased respect to the original value. How ever the effective and almost doubtless aerodynamic values, can come only from experimental test, on model or prototypes. Having no resources to make a model or prototype, we tried to describe the fluid behaviour around the model using CFD software, as outlined in Chapter 4. For a better comprehension of data concerned on the correction paragraphs, it is necessary to evidence that : the Aspect Ratio of tail plan was 7.23; the term p equal to 1.1383. The study of the airfoil properties and their correction have been carried out at multiple Reynolds values, not only at the ground level. The reasons are twice, for an exhaustive description of the performance and for identifying the operating range of the aircraft. The Reynolds number previously described can be simplified by associating it with the combination of speed and altitude that define the atmospheric environment of the study. For example, referring to the mean aerodynamic chord length (ie 0.627 m) as the characteristic length, a Reynolds value of 100,000 corresponds to be 22,000 meter on ground at 25 m/s or 15,000 meter at 6 m / s; a value of 400000 corresponds to an altitude of 5000 meters at 15 m / s; at 750000 we have 2500 meter at 22 m / s and finally 1E6 is 1500 meters at 27 m / s or at ground level at 24 m / s. A simple and immediate consideration, can be done on the $C_{L_{wing}}$ value respect to $C_{L_{glider}}$ value. It is evident that the contribution on lift produced from the entire glider is not so important. This value was obtained considering the tail plan geometry(AR, S_{Tail}) and functionality but not its twisted orientation. The minus sign in equation 3.41, derived from the tail plan main function as it is to give authority control on glider movement to the pilot and in static condition to be levelled. The tail plan have to create a negative lift, indeed it works at negative $C_{l_{Tail}}$ to provide the required balanced moment against the lift moment. A better evaluation of the complete $C_{L_{Glider}}$ value have to be execute using other mean, for example CFD programs.

3.4 The Flight Envelope Diagram

The flight envelope diagram is a graphical representation of the performance that the aircraft in general must satisfy to meet specifications and constraints. Specifically, this is a 2D Cartesian diagram that reports the load factor according to the velocity corresponding to the variation of Cl. In order to obtain the flight envelope diagram of the motorglider dimensioned in this project, reference was made to [20][21][34][39] and performance was reproduced in different atmospheric conditions. The rules that was considered are referred to BCAR-E protocol. Description on first paragraph of this chapter. Two methods were used with reference to [34] and [39] which will be discussed below. For each method, the BCAR-E rules for acrobatic glider was used. Example and normative parameters on Figure 3.21:

The first method, associated to designer Daniel Reymar [39], starts considering a decreased value of maximum Cl averaged from the maximum Cl

Re = 100 000		Re = 400 000		Re = 750 000		Re = 1E6	
Airfoil		Airfoil		Airfoil		Airfoil	
FX 61-147	FX 63-137	FX 61-147	FX 63-137	FX 61-147	FX 63-137	FX 61-147	FX 63-137
α [°] Cl	α [°] Cl	α [°] Cl	α [°] Cl	α [°] Cl	α [°] Cl	α [°] Cl	α [°] Cl
0 0.4577	0 0.3945	0 0.5259	0 0.9108	0 0.5599	0 0.9224	0 0.57	0 0.926
3 0.7737	3 0.6674	3 0.8533	3 1.2359	3 0.889	3 1.2494	3 0.9	3 1.2554
a_0 [1/rad]	a_0 [1/rad]	a_0 [1/rad]	a_0 [1/rad]	a_0 [1/rad]	a_0 [1/rad]	a_0 [1/rad]	a_0 [1/rad]
6.0356	5.206	6.25334	6.20941	6.28581	6.2457	6.303	6.29154
a_1 [1/rad]	a_2 [1/rad]	a_1 [1/rad]	a_2 [1/rad]	a_1 [1/rad]	a_2 [1/rad]	a_1 [1/rad]	a_2 [1/rad]
5.37265	4.63417	5.56647	5.52737	5.59537	5.55967	5.61068	5.60047
a_{AVG} [1/rad]		a_{AVG} [1/rad]		a_{AVG} [1/rad]		a_{AVG} [1/rad]	
5.0906		**5.55142**		**5.58163**		**5.60675**	
$Cl_{\alpha 1}$	$Cl_{\alpha 2}$	$Cl_{\alpha 1}$	$Cl_{\alpha 2}$	$Cl_{\alpha 1}$	$Cl_{\alpha 2}$	$Cl_{\alpha 1}$	$Cl_{\alpha 2}$
5.44823	4.69936	5.64478	5.60512	5.67409	5.63789	5.6896	5.67926
$Cl_{\alpha AVG}$		$Cl_{\alpha AVG}$		$Cl_{\alpha AVG}$		$Cl_{\alpha AVG}$	
5.15996		5.62951		5.66015		5.68562	
C_{d0}	C_{d0}	C_{d0}	C_{d0}	C_{d0}	C_{d0}	C_{d0}	C_{d0}
0.03	0.03	0.01	0.07	0.008	0.036	0.009	0.06
C_{d0AVG}		C_{d0AVG}		C_{d0AVG}		C_{d0AVG}	
0.03		**0.033278**		**0.018882**		**0.02878**	
Cl_{Glider}		Cl_{Glider}		Cl_{Glider}		Cl_{Glider}	
10.0202		**10.491**		**10.63278**		**10.5462**	
α_0 [°]	α_0 [°]	α_0 [°]	α_0 [°]	α_0 [°]	α_0 [°]	α_0 [°]	α_0 [°]
-1.7	-2	-4.6	-8	-5	-8.4	-5	-8.5
α_{0AVG} [°]		α_{0AVG} [°]		α_{0AVG} [°]		α_{0AVG} [°]	
-1.815		**-5.908**		**-6.308**		**-6.347**	

Re = 100 000	Re = 400 000	Re = 750 000	Re = 1E6
Airfoil	Airfoil	Airfoil	Airfoil
HQ 1,0-8	HQ 1,0-8	HQ 1,0-8	HQ 1,0-8
α [°] Cl	α [°] Cl	α [°] Cl	α [°] Cl
1 0.0232	1 0.2549	0 0.1377	0 0.1383
5 0.68	3 0.4855	3 0.4743	3 0.4696
a_0 [1/rad]	a_0 [1/rad]	a_0 [1/rad]	a_0 [1/rad]
9.23676	6.60669	6.42906	6.32783
a_1 [1/rad]	a_1 [1/rad]	a_1 [1/rad]	a_1 [1/rad]
6.52809	4.66929	4.54375	4.4722
a_{AVG} [1/rad]	a_{AVG} [1/rad]	a_{AVG} [1/rad]	a_{AVG} [1/rad]
6.52809	**4.66929**	**4.54375**	**4.4722**
Cl_α	Cl_α	Cl_α	Cl_α
7.02853	5.02723	4.89207	4.81504
$Cl_{\alpha AVG}$	$Cl_{\alpha AVG}$	$Cl_{\alpha AVG}$	$Cl_{\alpha AVG}$
7.02853	5.02723	4.89207	4.81504
C_{d0}	C_{d0}	C_{d0}	C_{d0}
0.0138	0.0061	0.0049	0.0044
C_{d0AVG}	C_{d0AVG}	C_{d0AVG}	C_{d0AVG}
0.0138	**0.0061**	**0.0049**	**0.0044**
α_0 [°]	α_0 [°]	α_0 [°]	α_0 [°]
0	0	0	0

Table 3.4: Table relative to the correction process of wing and tail airfoil main parameters[34].

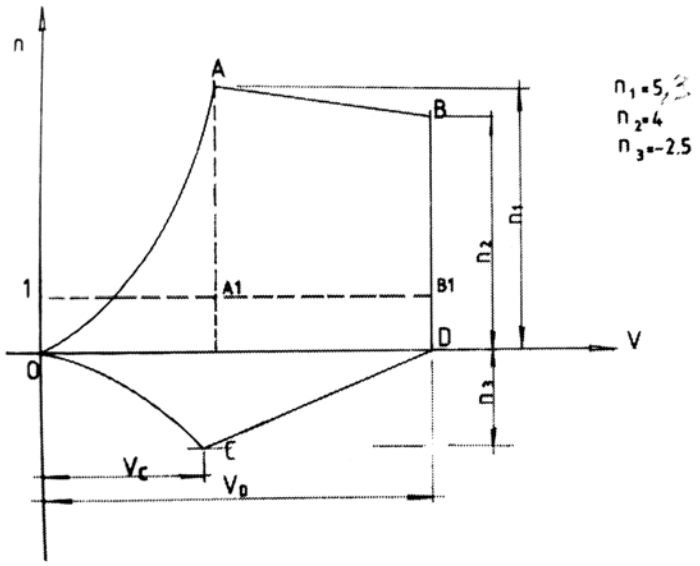

Figure 3.21: Flight Envelope Diagram example and load factor limit for acrobatic glider[34].

airfoil values, reported as:

$$Cl_{MAX} = 0.9\frac{Cl_{Root} + Cl_{tip}}{2}cos(\Delta_{0.25c}) \tag{3.47}$$

where $\Delta_{0.25c}$ referring to the swept angle of all airfoil at a quarter of their chord. with this equation, Reymar try to have a first attempt value of decreased C_L due to finite wing condition. The swept angle value was obtained thanks to **SolidWorks**®and using equation[39]:

$$tan(\Delta_{0.25c_1}) = tan(\Delta_{LE_1}) - \frac{1-\lambda_1}{AR_1(1+\lambda_1} = 1.3137degree \tag{3.48}$$

$$tan(\Delta_{0.25c_2}) = tan(\Delta_{LE_2}) - \frac{1-\lambda_2}{AR_2(1+\lambda_2} = 5.965degree \tag{3.49}$$

Knowing the swept angle of the two section tapered wing, was applied the Equation 1. AR_1 is equal to 8.021 and AR_2 to 12.82.
Thanks to the elaborated data from **Profili2**®the $Cl_{MAX_{AVG}}$ values of the first and second parts of the wing and a weighing average on the surface were obtained to take into account the different distribution of aerodynamic properties. In particular, knowing the $C_{l_{root}}$, was considered the $C_{l_{tip}}$ less 2.5 degree respect to the $C_{l_{root}}$, for twisting effect. In Figure 3.22 are collected the Flight envelope diagram referring to Reymar's method. For the second

one method, referred to Prof. Pajno [34], was used the corrected value of C_l and C_d as previously presented. Results in Figure 3.23. Also a complete Glider performance study was achieved and results are stored on Figure 3.24.

Both methods used the same calculation steps:

1. The n-value, is imposed from 0 to 5 and the $C_{l_{MAX}}$ value is known(precisely for Pajno's method, was choose the C_l and C_L values around 12 degree angle of attack, where the linear tendency start to change);

2. using the equation:
$$V = \sqrt{\frac{2 \cdot n \cdot W}{\rho \cdot C_{l_{MAX}} \cdot S}} \tag{3.50}$$
it is possible to obtain velocity for each value of the load factor;

3. The stall speed is obtained when n=1;

4. The **A** condition, correspond to the limit load factor (5) value at maximum C_l

5. The **B** condition, similar to the **A** condition, refers to a load factor value of 4 and a limit speed of 75 m/s. This parameter is obtained from [34] and equal to :
$$V_B = V_D = 9\frac{W}{S} + 78 knots = 9 \cdot 35.124 \cdot 0.2084 + 78 = 142.741 knots = 73 m/s \tag{3.51}$$
rounded to 75 m/s;

6. The negative section of the flight envelope diagram is obtained as the positive section, imposing the n value variation and C_l value, that is -0.8 this way, indeed the glider has to preserve performance with a maximum negative lift of -0.8 (smallest number)

7. The A1 and B1 condition, permits to evaluate the lift coefficient value for fly in that precise atmospheric condition with the maximum velocity obtained in A condition and imposed from airworthinesses.

This procedure was adopted for all graphs presented in here and obviously both evaluation methods, changing only the reference $C_{L_{MAX}}$ value. The numbers relative to flight envelope graphs are reported on Appendix C.

From the charts and diagrams of the flight envelope emerges as at Re = 100k, the BCAR-E rules is not respected. This results in lowering of the altitude range in which the vehicle is properly operated. Comparing the

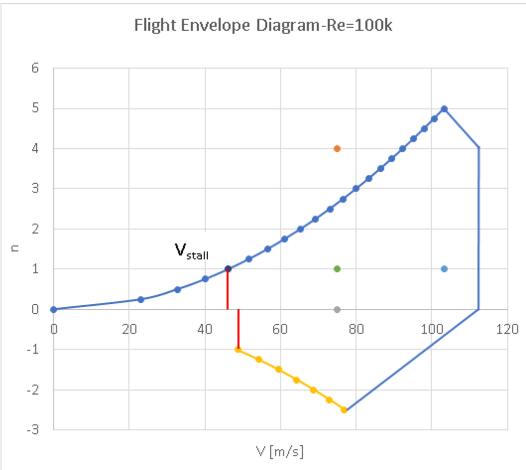

(a) Re = 100k.

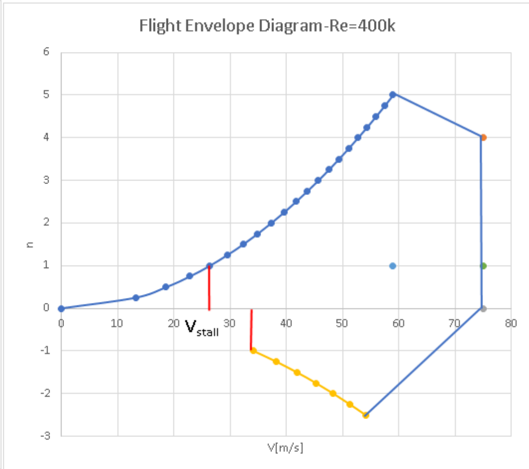

(b) Re = 400k.

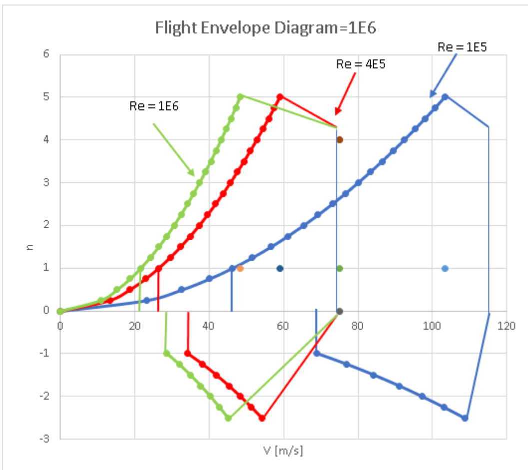

(c) Re = 1E6.

Figure 3.22: Reymar's method [39] for *Flight Envelope Diagram* estimation.

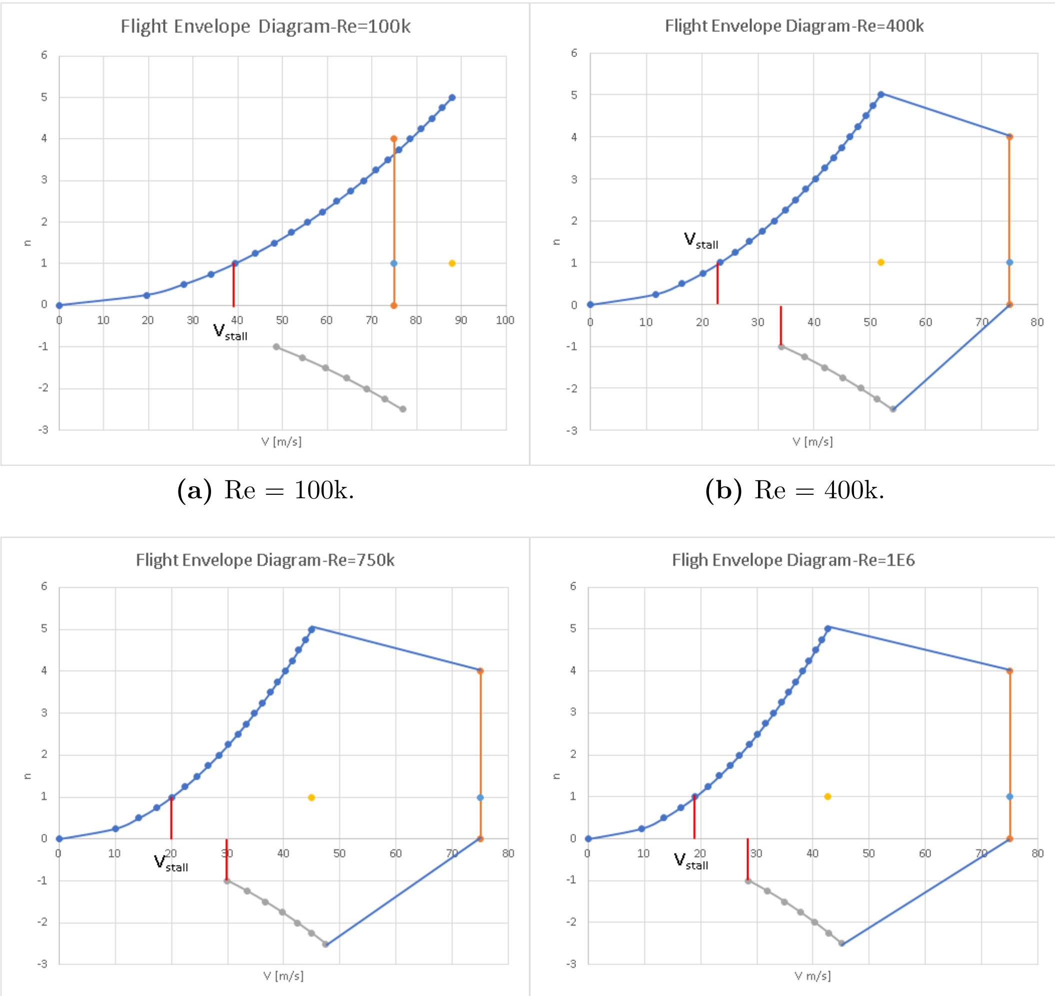

(a) Re = 100k.

(b) Re = 400k.

(c) Re = 750k.

(d) Re = 1E6.

Figure 3.23: *Flight Envelope Diagram* using Pajno's Method [34] referenced to wing only.

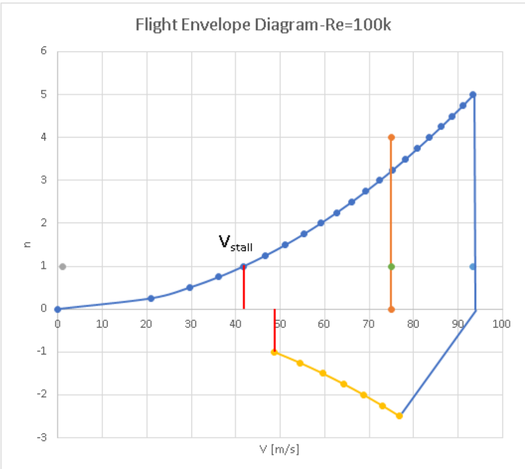

(a) Re = 100k.

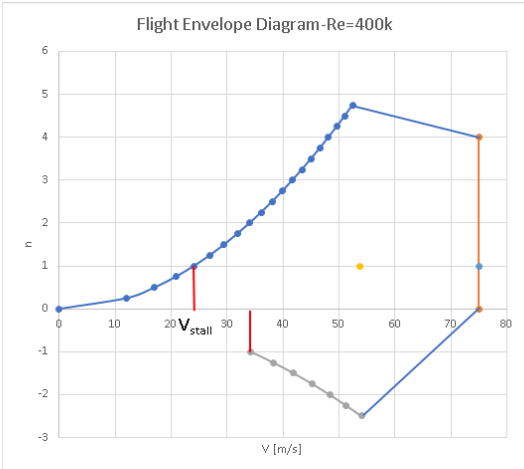

(b) Re = 400k.

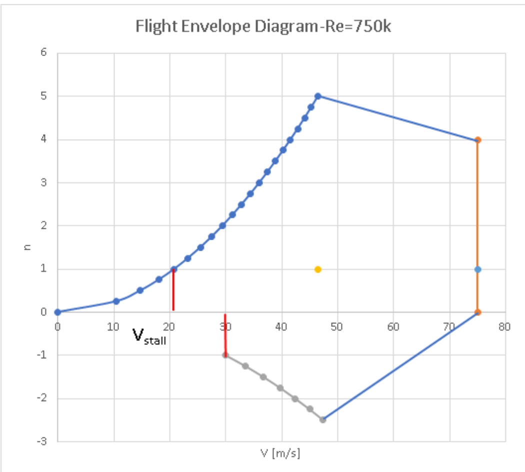

(c) Re = 750k.

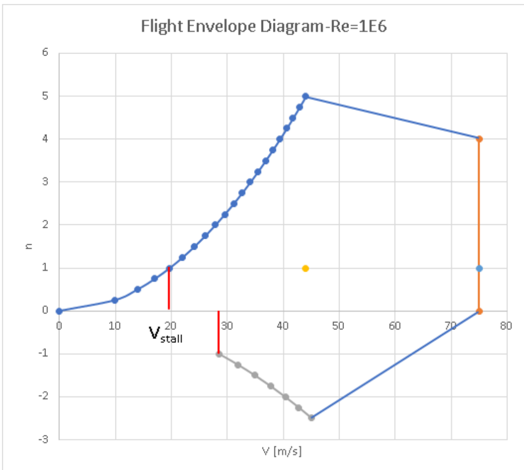

(d) Re = 1E6.

Figure 3.24: *Flight Envelope Diagram* using Pajno's Method [34] referenced to complete Glider.

flight envelope for wings and gliders only, the difference is very slight and due to the not significant lowering of the lift glider coefficient. One special rule that every ultralight aircraft has to respect, is the Stall velocity of 65 km/h, 18m/s. Considering equation 3.50, the stall condition was calculated with this parameters:

- ρ = 1.225 kg/m^3
  n=1
  W=2500 N
  S= 7.26
  V_{stall} = 18 m/s
  The resultant C_l is equal to 1.735

From data obtained thanks to Prof. Pajno[34], this requirements is reached on the ground, indeed the stall velocity at 1500 m is little higher due to the air density decrement. While, Reymar's method, gives for Re=1E6 a $C_{L_{MAX}}$ value that is lower and equal to 1.39. The stall velocity is higher and with his evaluation method it is not possible to respect the Stall rule. How ever, we could consider the aerodynamic action of a flap extracted. The required $C_{L_{MAX}}$ is obtained if the first taper wing part has a flap oriented at 17.5 degree. This information was elaborated with **Profili2**®. For the entire glider, the specification respect is equal to wing considerations indeed there's a change of 10% on $C_{L_{Wing}}$ respect to glider. It is recalled that for the analysis of the flight envelope, both for the Pajno method and the Reymar method, we used the massive limit values of C_l to the corresponding value which in each profile is obtained at 12.5 degrees. The flight envelope was represented based on XfoiL's graphs attesting the end of the linear slope on C_l curve around 12 degrees. However, following the study of the finite wing, as mentioned in the previous paragraphs, there is a lowering of the C_l curve followed by an elongation of the stall at slightly higher angles.

3.4.1 Spiral Flight Performance

Spiral flight is the most well-known flight configuration with glider. Volovelistic technique involves the teaching of the fundamental rules for the gusts recognition so as to achieve a climb or if it is intended to descend, a downhill. The direction of motion integrated in time, form a spiral. The spiral geometry in ideal flight conditions is determined by the speed and the angle at which it is approached. Thus, a study of the performance of the motorglider was performed in these terms, identifying the vertical velocity knowing the lift coefficient, drag, bank angle and horizontal velocity using the **Excel**®calculation engine. Subsequently, the graphs called "*glider polar*" were explained with the results obtained. The equations of Prof. Pajno have been used[34].

$$V_x = \sqrt{\frac{2 \cdot \rho \cdot W}{C_l \cdot S}} \tag{3.52}$$

$$V_z = \sqrt{\frac{2 \cdot C_d^2 \cdot W}{\rho \cdot C_l^3 \cdot S}} \tag{3.53}$$

Each point of the polar corresponds to a certain Cl. The energy dissipated in the motion of the glider must be in balance with the loss of potential energy:

$$D \cdot V = W \cdot V_z \tag{3.54}$$

From this expression it is apparent that the descent speed V_z must be multiplied by the factor $n^{\frac{3}{2}}$ If we call the inclination angle ϕ, the equilibrium must be:

$$n = sec\phi \tag{3.55}$$

Turning speeds are related to flying speeds hovered by relationships:

$$V_{x\phi} = V_x sec\phi^{\frac{1}{2}} \tag{3.56}$$

$$V_{z\phi} = V_z sec\phi^{\frac{3}{2}} \tag{3.57}$$

Also if we call the spiral radius r, it is linked to the velocity V_ϕ and to the bank angle ϕ with the relation:

$$r = \frac{V_{x\phi}^2}{tan(\phi) \cdot g} \tag{3.58}$$

From these equation, was possible to reproduce the characteristic polar velocity graph referring to $C_{l_{wing}}$ in Figure 3.25 and $C_{l_{glider}}$ in Figure 3.26. Also the Spiral radius performed at different velocity and bank angle 3.27(this last case, only Re =1E6 condition was studied) was obtained. You can see an example of Spiral flight graph in Figure 3.27 From the comparisons, it has been possible to understand that the fuselage influences is negligible, as it does not improve lift, but influences drag. Comparing the graphs related to the spiral performance with the characteristics of wings and the performance of the whole glider, it is noted that the mild variation in the Cl value of the overall aircraft results in a small increase in the descent speed not so significant to arouse particular doubts. It is noted that the increase in the bank angle translates into an increase in the rate of fall, as the lift is not directed against gravity but rather balancing the centrifugal force to carry out the circular motion. For this reason, high bank angle manoeuvres, which

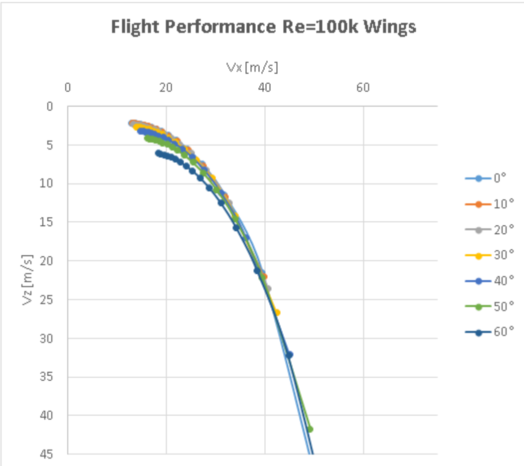

(a) Polar velocity graph-wing-Re=100k.

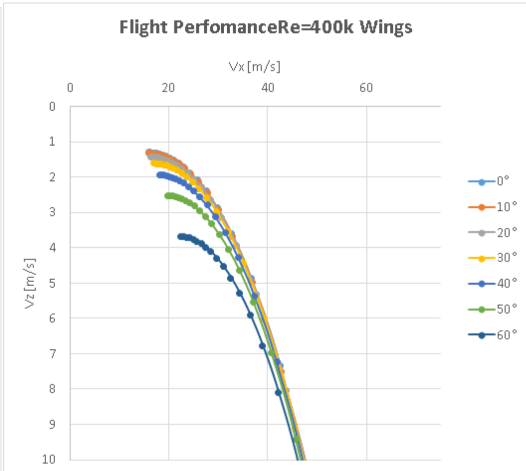

(b) Polar velocity graph-wing-Re=400k.

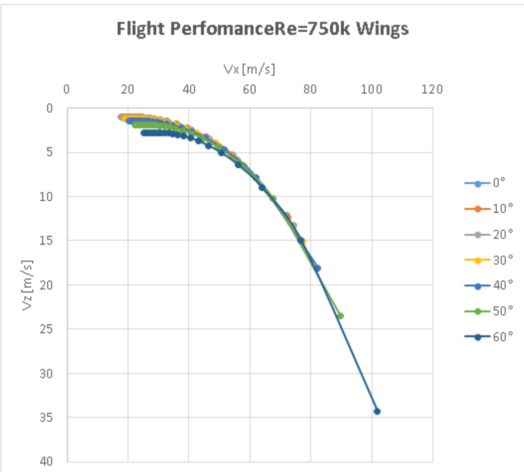

(c) Polar velocity graph-wing-Re=750k.

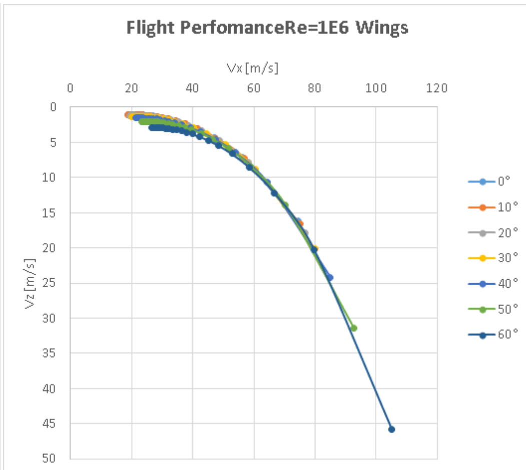

(d) Polar velocity graph-wing-Re=1E6.

Figure 3.25: Polar velocity graphs at different Reynolds Number referred only to $C_{L_{Wing}}$.

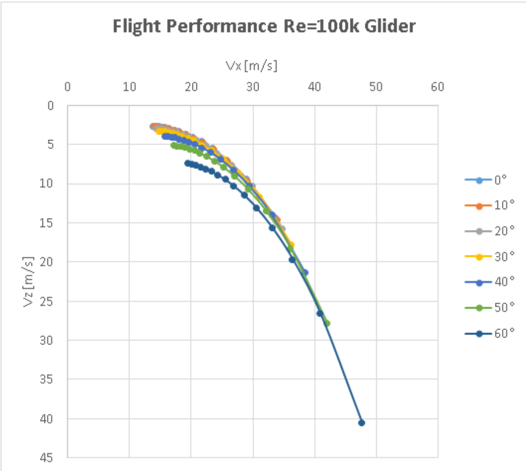

(a) Polar velocity graph-Glider-Re=100k.

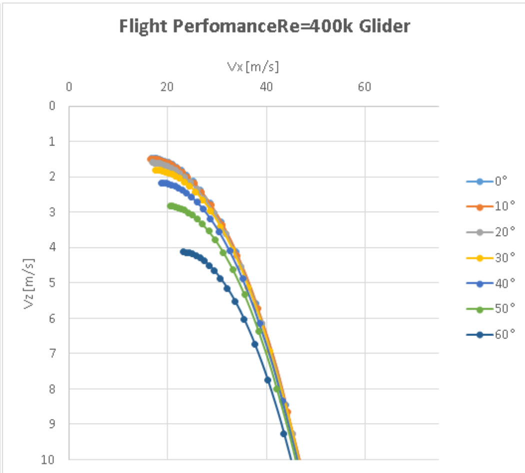

(b) Polar velocity graph-Glider-Re=400k.

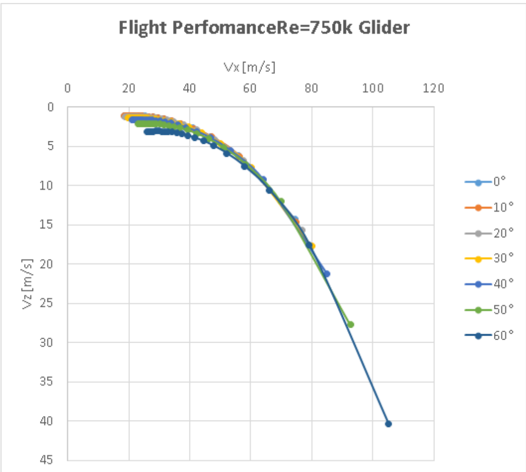

(c) Polar velocity graph-Glider-Re=750k.

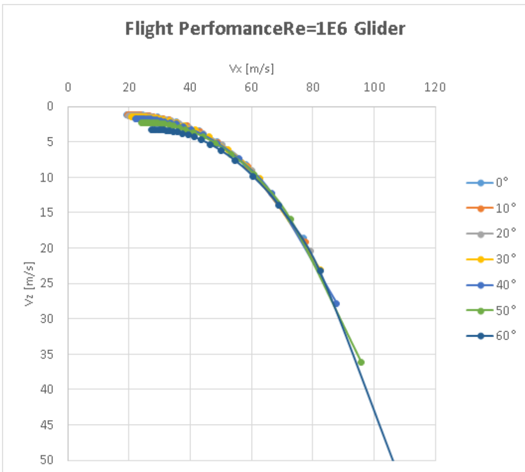

(d) Polar velocity graph-Glider-Re=1E6.

Figure 3.26: Polar velocity graphs at different Reynolds Number referred only to $C_{L_{Glider}}$.

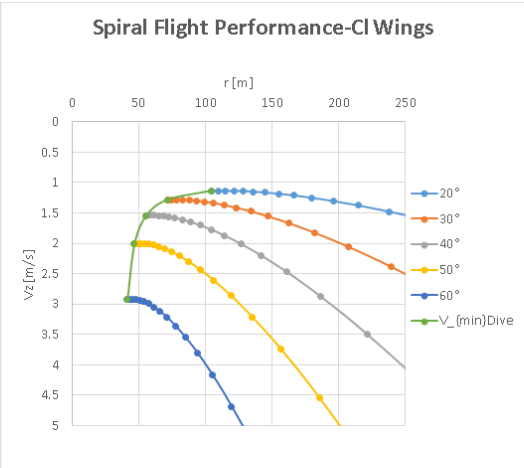

(a) Spiral Fligth Performance $C_{l_{Wing}}$- Re=1E6.

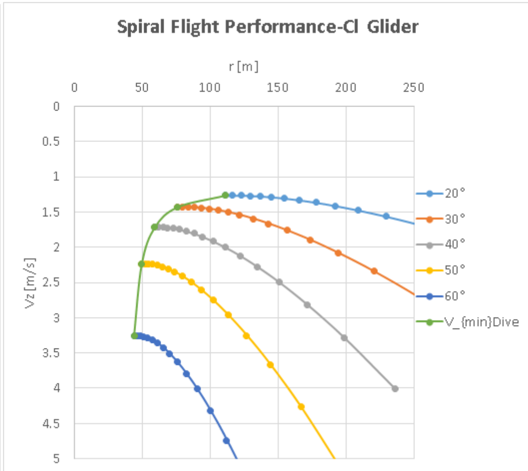

(b) Spiral Fligth Performance $C_{l_{Glider}}$- Re=1E6.

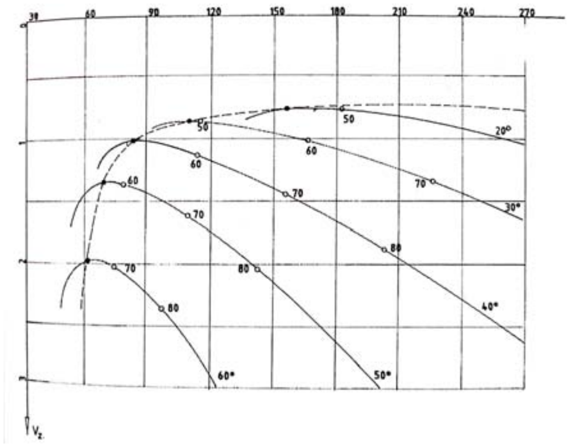

(c) Example of Spiral Flight perfomance [34].

Figure 3.27: Spiral Flight Performance evaluated with $C_{L_{Wing}}$ and $C_{L_{Glider}}$ to characterize the dive velocity as a function of spiral radios.

are considered acrobatic, must be realized at high altitudes, indeed the terrain is reached faster and also increases the stalling speed. The atmospheric conditions are relevant, because reducing altitude, we increase density and so losses, lift capacity at same speed. As you can see, there is a general reduction on velocity field. This could be read as a security requirement : having a low vertical speed, permits more controllable system in the descent phase, where the aircraft is typically very close to terrain.
Collected data on Spiral flight performance are stored in Appendix C.

3.4.2 Climbing Flight Performance

The evaluation of the ascending performance is important as it allow us to evaluate the goodness of the project. In this case, a study of this performance field was also conducted based on the hypothesis that the reference air mass thermal profile is parabolic and the intensity of the vertical velocity of the thermal varies according to the law:

$$V_z = V_{z0} \cdot \left[1 - \left(\frac{r}{R}\right)\right] \tag{3.59}$$

Where V_{z0} correspond to the airmass velocity for r=0; R is the maximum radius of the thermal air mass. if r is too big, this representation is no more valid. it is reasonable to assume the following values for the characterization of the thermal air mass:

$$V_z = 2.3 \cdot \left[1 - \left(\frac{r}{300}\right)\right] \tag{3.60}$$

Using this equation and precedent value obtained during the *Spiral flight* study, it is possible to determine the ascending velocity of the glider. Specifically, the difference between vertical thermal velocity of the air mass and the minim dive velocity, give an estimation of the ascending value. Results on Figure 3.28, 3.29. For example at 30 degree bank angle the ascending velocity is evaluable on the orange curve, equal to 0.595 m/s and 0.78 m/s, respectively for entire glider and only wings. It is possible to observe that for α = 15 degree and below 60 degree of bank angle, both glider nd only wing evaluation show a positive ascending value when immersed on an ascending natural thermal flow. While for an high bank angle value, as 60 degree, it is impossible to rise in altitude. How ever C_L referred to α = 15 degree, is an improbable value to reach without stall incoming. For this reason, also C_L value corresponding to α = 3-5-8 degree was studied. The final conclusion is that for 3 AoA degree, the provided C_L is not sufficient to absorb thermal energy and convert it in an ascending trajectory, while for 5 and 8 degree this is quite possible. Indeed the bank angle at which we can recognize the best ascending configuration is 30 degree.

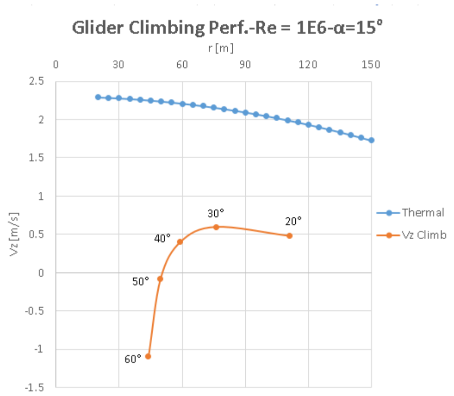

(a) Climbing perfomance based on Glider corrected values for Re=1E6, α=15 degree.

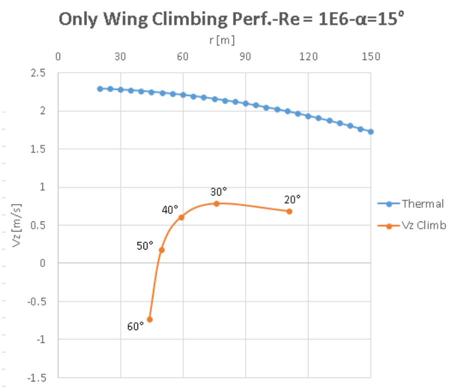

(b) Climbing perfomance based on only wing corrected values for Re=1E6, α=15 degree.

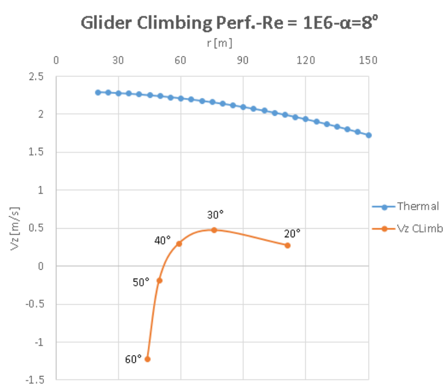

(c) Climbing perfomance based on Glider corrected values for Re=1E6, α=8 degree.

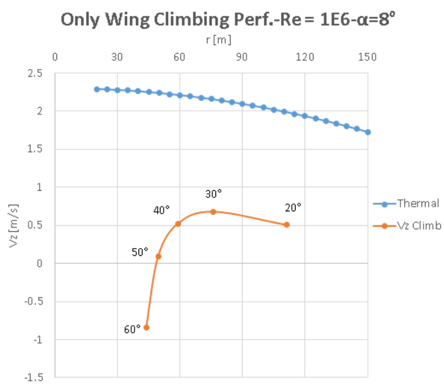

(d) Climbing perfomance based on only wing corrected values for Re=1E6, α=8 degree.

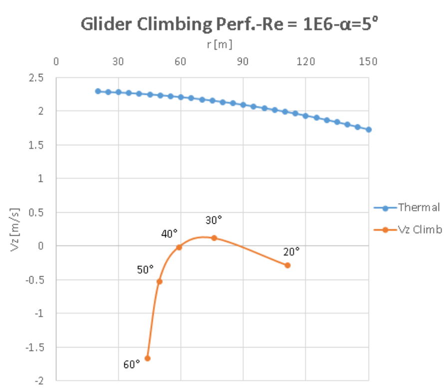

(e) Climbing perfomance based on Glider corrected values for Re=1E6, α=5 degree.

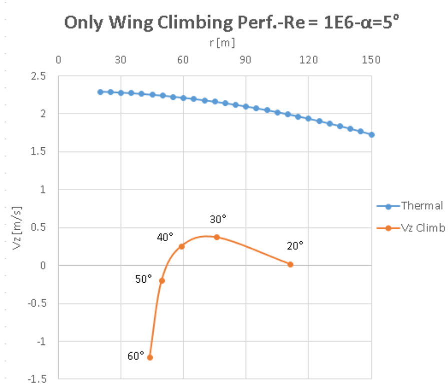

(f) Climbing perfomance based on only wing corrected values for Re=1E6, α=5 degree.

Figure 3.28: Evaluation of glider compared with only wing climb performance, Re=1E6.

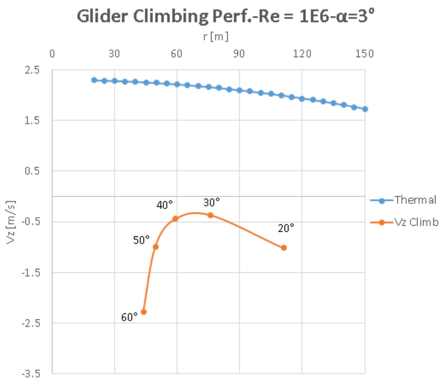

(a) Climbing perfomance based on Glider corrected values for Re=1E6, α=3 degree.

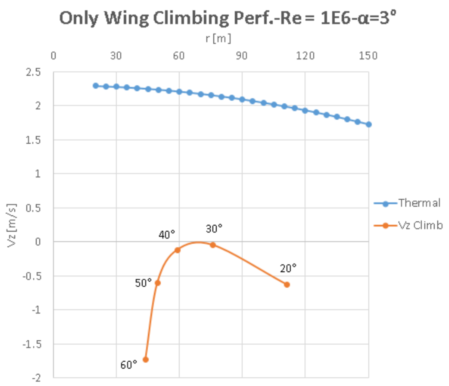

(b) Climbing perfomance based on only wing corrected values for Re=1E6,, α=3 degree.

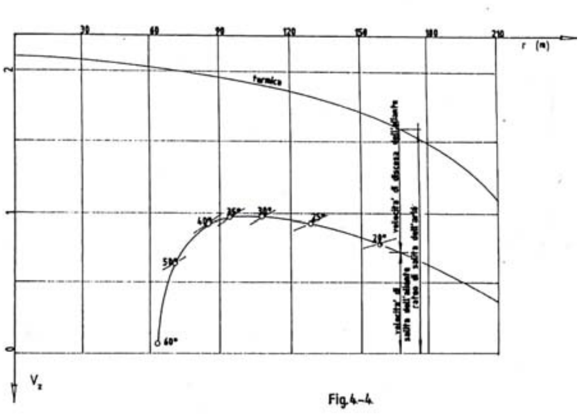

(c) Example graph on climbing perfomance [34]

Figure 3.29: Evaluation of glider compared with only wing climb performance, Re=1E6.

3.4.3 Maximum Efficiency Velocity $V_{L/D_{BEST}}$

The maximum aerodynamic efficiency speed corresponds to the speed value that makes possible to use all the wing potential. This assists in setting up a flight configuration where the L / D ratio is the maximum. A direct consequence is the definition of the maximum aperture cone that allows to reach the maximum distance before landing. This parameter, in addition to providing information on the performance of the aircraft, also meets a safety criterion. In adversity, the pilot can set the maximum speed to land safely. From an aerodynamic point of view, the highest efficiency condition is achieved when the C_d value is minimal. Therefore, a **Matlab**®script was created that allows you to evaluate this condition for a given dimension value and speed range. Graphs have been created that show the optimal value between induced drag and parasitic drag and the maximum L/D value when changing speed. The complete code is available on Appendix C. This code use the *Functions* : `atmoscoesa` and `correctairspeed`. `atmoscoesa` implements the mathematical representation of the 1976 Committee on Extension to the Standard Atmosphere (COESA) United States standard lower atmospheric values for absolute temperature, pressure, density, and speed of sound for the input geopotential altitude. Below 32000 meters, the U.S. Standard Atmosphere is identical with the Standard Atmosphere of the International Civil Aviation Organization (ICAO). `correctairspeed` Calculate equivalent airspeed (EAS), calibrated airspeed (CAS) or true airspeed (TAS) from one of the other two airspeeds. Based on assumption of compressible, isentropic (subsonic flow), dry air with constant specific heat ratio (gamma). What results from the calculations is that the maximum efficiency of the dimensioned motorglider it is around 20. At first approximation, say that for each 1 meter lost, it can travel 20 meter horizontally. This efficiency value is in agreement with aircraft that have similar wingspan in the database. Moreover, the maximum efficiency rate varies from a minimum of 23 to about 26 m/s. Considering that the stall speed is around 17 m/s, there is a fair gap between the two sizes.

3.4.4 *Lofting* the Solar Powered Motorglider

At the same time as the sizing phase proceed, was provided a shape and a geometry to the aircraft, taking into account all the values, assumptions and constraints that were handled. The tool used is **SolidWorks**®and in particular the *LOFT* function that allows interpolation of adjacent sections through a guide curve constraint. The fuselage was designed from a NACA 6 series airfoil, which minimizes parasitic resistance and interference with

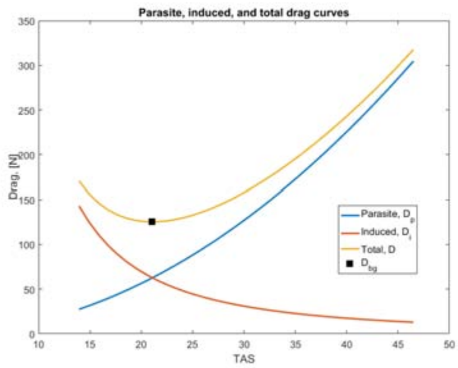

(a) Re=1E6-TAS:15-50m/s-$C_{d_{Glider}}$=0.03173-h=1500m.

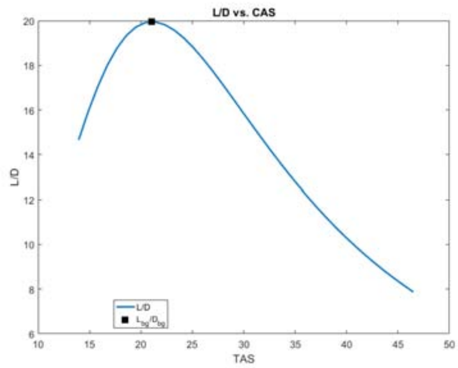

(b) Re=1E6-TAS:15-50m/s-$C_{d_{Glider}}$=0.03173-h=1500m.

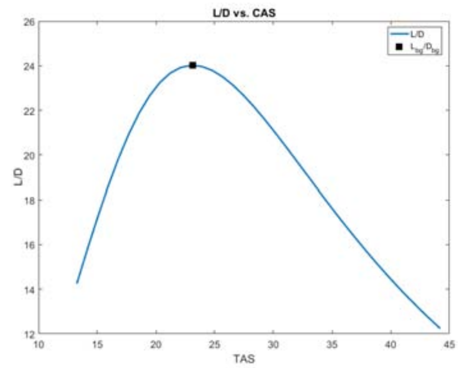

(c) Re=750k-TAS:15-50m/s-$C_{d_{Glider}}$=0.02189-h=2500m.

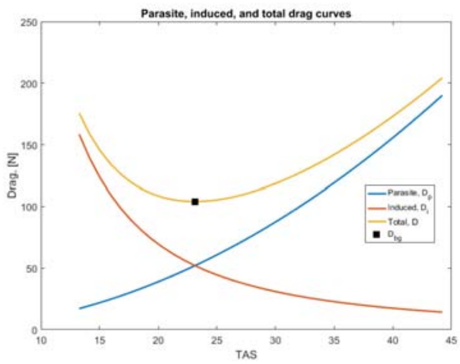

(d) Re=750k-TAS:15-50m/s-$C_{d_{Glider}}$=0.02189-h=2500m.

Figure 3.30: Evaluation of Best L/D evaluating first the induced and parasite drag composition, second the distribution of L/D against TAS; The C_d value use is associated to that of the glider.

wings[34]. The winglets are wing extremities, added in order to reduce the flow vortices and slightly increase the slope curve as they cause an increase in AR. They extract energy pulling it out from vortexes that would otherwise be produced in the absence of winglets. Also there is a saving in terms of resistance. The winglet design was not dealt with in detail, but the formulas provided by [34] have been used, Figure 3.31. Their actual usefulness will be further explored with the CFD method. The vertical stabilizer has a length of 0.7 m and it belonging to T type category. This is a fairly common choice in modern glider. One important consideration to be faced is deflection and check whether the stall current invades the tail plan. The essential reason why the horizontal stabilizer is positioned high is tied both to minimizing the wet surface of the fuselage, as well as to the design issue, and to avoid affecting the deflection effect of the air stream promoted by wings. According to [39], however, it is also necessary to evaluate if the tail plan is outside the vortices produced during stall, so that the tail plan remains authoritarian. Reference is made to the image 3.31 , extracted from [39]. Below are presented some images post-processed thanks to **SolidWorks®**. The dimension of every part are listed in Appendix C.

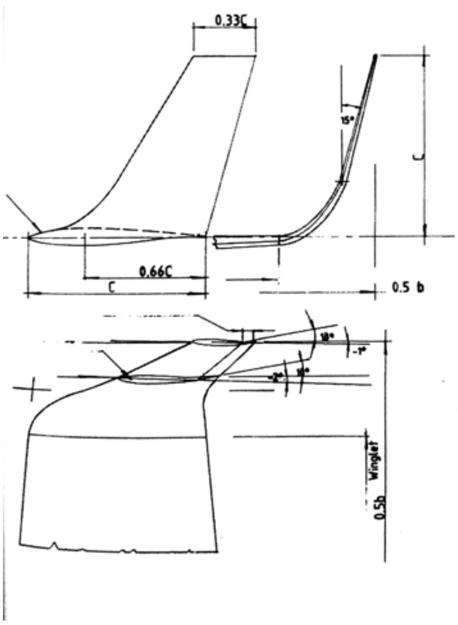

(a) Winglets dimension for design[34].

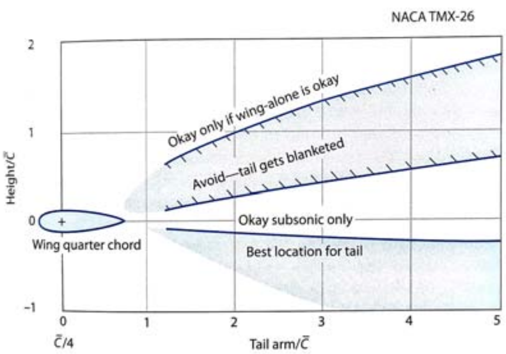

(b) Aft tail positioning [39].

Figure 3.31: Useful suggestion provide by [34] and [39] on the tail plan position and winglets design.

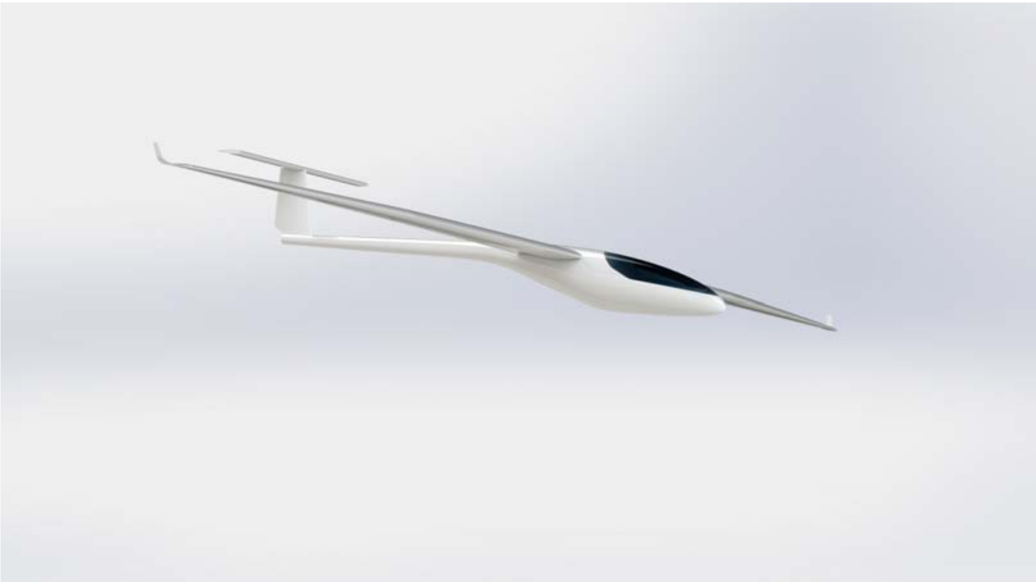

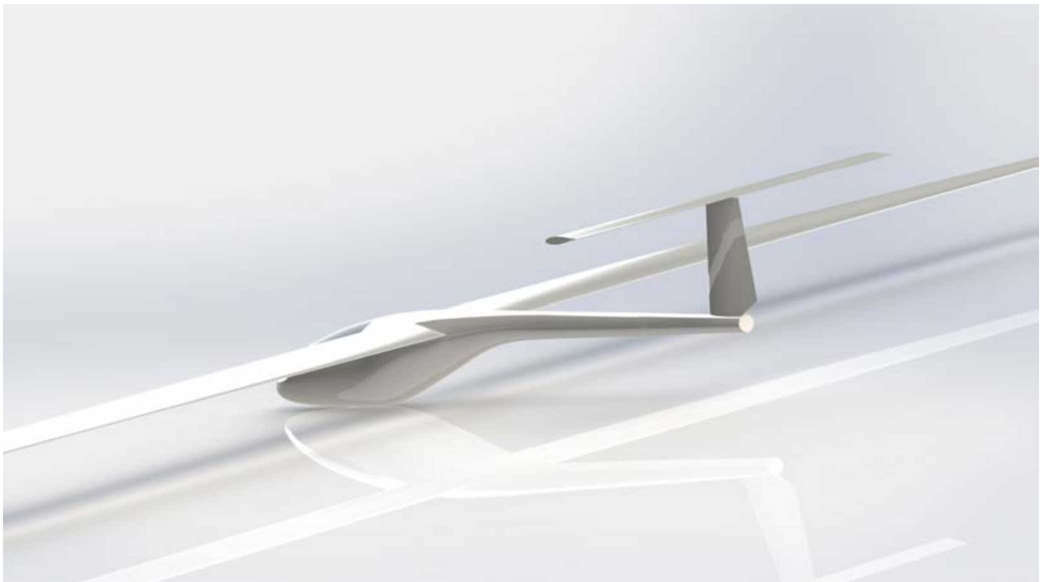

Chapter 4

Computational Fluid Dynamics Simulations

This chapter discusses issues related to 2d and 3d fluid dynamics analysis, focusing on the results and the main settings while trying to provide a more general framework for equations with relevant references. In particular, most of the available material and knowledge is referred to [50].

4.1 Introduction to Computational Fluid Dynamics

The *Computational Fluid Dynamics* is a numerical problem solving strategy for fluid dynamics problems, external or internal, which is realized in a finite and discrete fluid volumetric domain. As with *Finite Element Method* (FEM) analysis, equations are applied element by element. In practice this happens thanks to the use of computers that allow now to reach near real results (if correct analysis is set), relaxing some basic hypotheses that allow hand calculation. The procedure with which simulation is performed can be summarized with the image 4.1. The tool that will be used in this elaboration is **ANSYS**®and can be thought as the black box and many times the "*black box*" expression appears in the use of a software. This means that the user does not understand what lies within the black box and does not even informs about the consequences of setting one or the other option. CFD software is now very powerful but not smart. That is, we have to be careful with it to return a valid result. So do not understand the tool, you run the risk of insert junk and obtain other junk. The **User Inputs** regard to

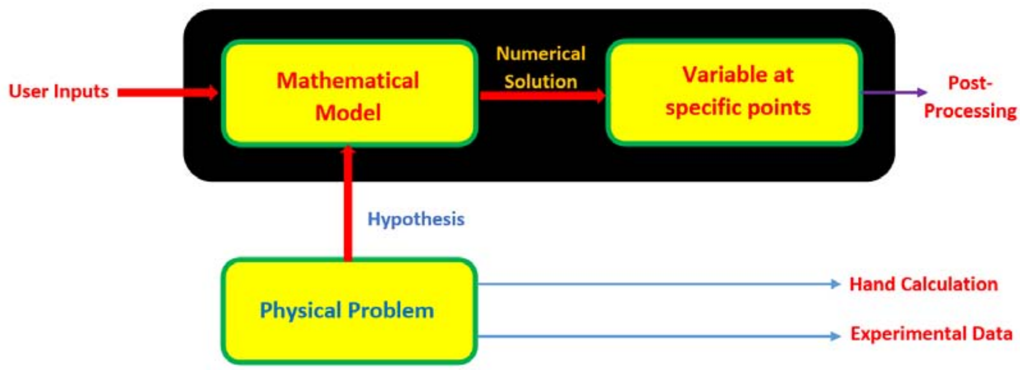

Figure 4.1: Summarize scheme of correct analysis procedure.

the geometry and boundary conditions of the problem; **Physical Problem** mean the type of problem that we are going to solve within the software;

Mathematical Model refers to the algorithm that we want to use, hypothesis and solution implication; **Numerical Solution** is the solution-step, in which the solver operates to obtain results and **Post-Processing** linked to **Variables at some Points** permits the results evaluation and verification of model set-up.

4.2 Governing Equation

Fluid dynamics is based on 3 key laws:

1. Conservation of mass
2. Conservation of moment
3. Conservation of energy

These equations can be expressed in *differential* form if applied to a single fluid particle that moves in the fluid domain or in *integral* form if applied to the entire domain. The two formulations are equivalent. The set of conservation equations are however non-linear and coupled, and the problems for which there is unique solution are irrelevant and based on very restrictive hypotheses. The CFD technique allows to solve these equations in a computational way by providing approximate solutions. Governing equations are converted into *algebraic* equations and solved by numerical methods. The **ANSYS**®solver is called **FLUENT**, which adopts the finite volume method. The underlying principle is to take the entire fluid domain into small elements or volumes, so the set of equations is applied to each of them. The mathematical model that is solved is:

$$\bigtriangledown \cdot \vec{V} = 0 \tag{4.1}$$

$$\rho(\vec{V} \cdot \bigtriangledown)\vec{V} = - \bigtriangledown p + \mu \bigtriangledown^2 \cdot \vec{V} \tag{4.2}$$

where : $\vec{V}$ is the velocity vector;
p is the pressure module; the unknowns are $\vec{V}$ dependant to x and y if two dimensional problem or x,y,z if three-dimensional problem, and p as a function of coordinate system variable as velocity. The Finite Volume Method, used the integral form of the equation of mass conservation and momentum to solve a fluid-dynamic problem. The equations are typically written in the *Eulerian reference system*, where the behaviour of a tiny particle is observed. Following all the particles that make up the fluid would not be possible. The Lagrange reference system is useful if the reference is a big ball but not in

these case. The strategy is to move from focusing on a particle, to the observation of points which characterize the volume control discretizazion, that is to say that:

$$V(x_0, y_0, t_0) = V_0 \tag{4.3}$$

ie when the particle is in position x0 y0 at time t0 will have the speed v0. This is obviously an abstraction because a point does not have a motion field. This is the Eulerian reference. Now if all the particles passing through that point have those characteristics, it can be said that there is no temporal dependence. It is said that the flow is *stationary*. Obviously the particle can change speed in the evolution time of its motion, but the field of motion obtained in the domain will not change over time.

The system of algebraic equations derived from the initial ones previously cited, refers to integral rather than differential equations. In this passage it is good to consider that an error is introduced, as they are approximating symbolic equations in finite equations. Moreover, the algebraic equations are not linear and this can be observed from the integral form:

$$\int_S \rho\vec{V} \cdot (\vec{V} \cdot \vec{n}) dS = -\int_S p\vec{n} dS + F_{viscous} \tag{4.4}$$

The first term, so the left term, is not linear because there's the product of two unknown terms. To solve this non-linearity one has to proceed linearising and solving iteratively. Discretisation error can be reduced by re-dimensioning the element size. In particular, it can be shown that the error is proportional to the square of the element size. However, this requirement goes against the resources calculation in hardware terms and thus of analysis time. The exact solution would be to get zero element size and an analysis that takes an infinite time. For a better comprehension of the resultant equation set, see Figure 4.2.

The *Navier-Stokes equations* is the name of momentum equation that in **FLUENT** are modified, considering the *Reynold's average*. It is a mathematical strategy based on real observation to approximate the turbulence tendency of particles as an average and it is based on the assumption that

$$u = u_{AVG} + u' \tag{4.5}$$

where u' is the fluctuation of the variable u. If we do the average of the precedent equation, we obtain that u'_{AVG} is equal to zero. This have to be extended also to v and w. If we substitute the assumption on motion field variables to the Continuity equation, we obtain the same previous form but it is called *The Reynold's Average Continuity Equation.* This is extended also to the momentum equation. How ever, **FLUENT** gives the possibility

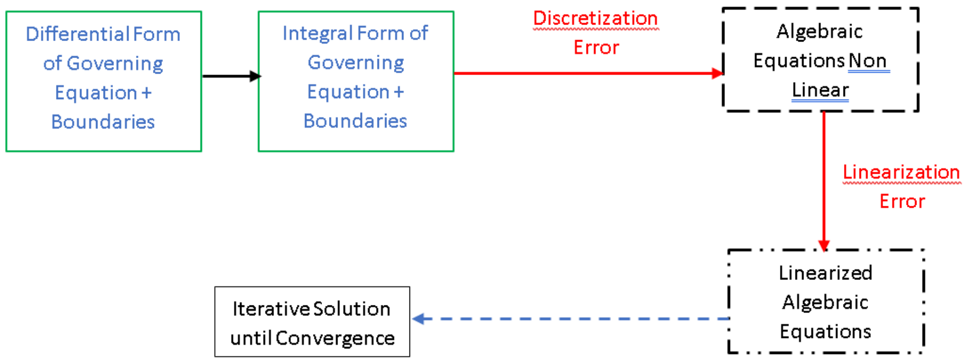

Figure 4.2: Solved set equation process in FLUENT [50].

to choose from a set of possible case studies. By selecting one of them, the equation set is imposed but it is necessary to know the hypotheses that in particular are:

1. Permanent condition
2. Incompressibility fluid
3. Newtonian fluid

The objectives of this group of analysis are essentially:

1. the study of the three-dimensional glider created, by commercial use CFD software and used in the aeronautical industry ;
2. Validation of data obtained through simple calculations or algorithms based on simplified hypotheses;
3. study of Cl and Cd values for three-dimensional aircraft;
4. Qualitative analysis of fuselage-wing interference;
5. Qualitative Flow analysis around geometry;

All this by changing the boundary conditions in terms of Reynolds number and angle of attack.

4.3 Pre-Processing

In this analysis phase, the geometry is imported or created in the CFD software. In ANSYS this happen on the sub program *MECHANICAL APDL*. Then the fluid domain is identified and the object in it. In this project, 2D and 3D geometries were created in **Solidworks**®and later imported into **ANSYS**®. In this context, the geometry was subtracted from the fluid volume, obtaining a cavity, whose surfaces are labelled with the term *wall* [1].To walls the *NO SLIP* condition was applied, since the stream velocity at the boundaries is equal to zero. To conclude, in the geometry phase, the boundary condition areas for 3D analysis and contours for 2D analysis have been selected, typically: *Farfield1* labelled those fluid input surfaces to the domain to which an incoming speed condition was imposed; *Farfield2*, on the other hand, represents the fluid outlet surfaces to which a pressure output condition was set and equal to zero. A very important issue in order to maximize the accuracy of the solution is the size of the fluid volume, as can be seen in the images. Ideally, the size should tend to infinity. However, having no tools for discretizing such a large domain, it has been chosen a compromise dimensions and accepted the consequences. The geometry chosen for the 2D fluid control volume is the union between a circle and a square [50] and you can see a reference image in Figure 4.3. Radius R10 is equal to 25m, the edge H11 is equal to 50m. While for the three-dimensional study, a parallelepiped geometric fluid domain was chosen to simplify later stages. The second important step in the pre-processing phase is *discretization.* As for the two-dimensional simulators, the mesh used, has a series of manual arrangements in order to obtain a parametrized discretization based on the distance from the centred airfoil. In particular, the final result was obtained after a series of attempts by evaluating the element parameters: *element quality, skewness, orthogonal quality* as discriminants. *Spheres of influence* have been created with decreasing sliding dimensions having radius equal to 10m, 5m, 1.5m for FX 61-147 and 5m, 2m, 1.2m for FX 63-137 , while the profile has undergone a forced sizing process on the sides and also the *inflaction* option was imposed in order to compute as much as possible the particle layers that are moving around the profile. Some images of the meshes used are reported in the figure. Regarding the three-dimensional discretization, however, the automatic fluent mode with fine-sizing request was used. Below on Table 4.1 is presented the number of elements and nodes of each set template. On Figures 4.5 ,4.6, 4.7 are reported the statistics graphics on main parameters that have been considered to obtain a good representation

[1]With this label, FLUENT know that fluid can't pass through it

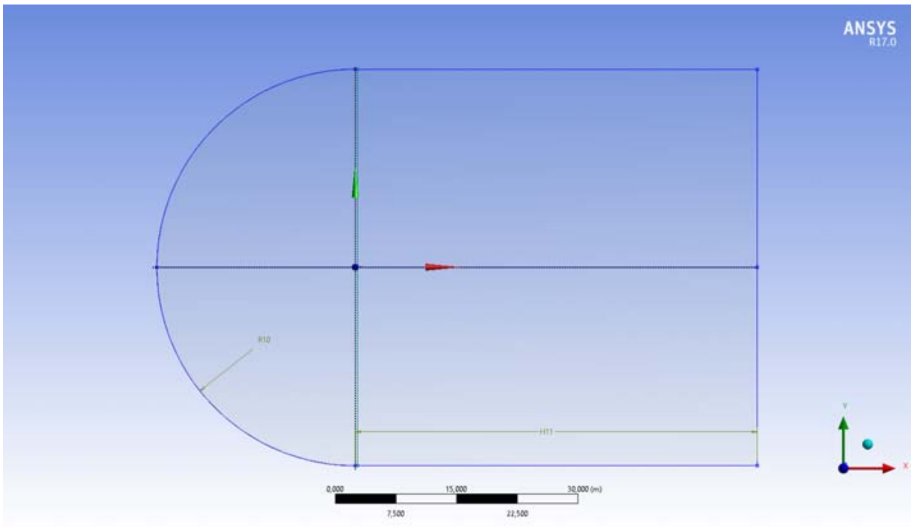

Figure 4.3: Control fluid volume dimension.

	FX 61-147	FX 63-137	Glider
Elements	141837	69023	2575971
Nodes	141901	70137	457309

Table 4.1: Number of Nodes and Elements for the two set of 2D simulation for both airfoil and for the 3D simulation.

Element Quality	MIN	0
	MAX	0.99988
	AVG	0.9325
Skewness	MIN	1.31E-10
	MAX	0.90691
	AVG	6.36E-2
Orthogonal Quality	MIN	0.17687
	MAX	1
	AVG	0.9879

Table 4.2: 2D Mesh statistics on FX 61-147 airfoil.

Element Quality	MIN	7.38E-2
	MAX	0.99947
	AVG	0.91183
Skewness	MIN	1.03E-9
	MAX	0.0.94747
	AVG	9.75E-2
Orthogonal Quality	MIN	8.34E-2
	MAX	1
	AVG	0.98254

Table 4.3: 2D Mesh statistics on FX 63-137 airfoil.

of fluid volume. In particular for the parameter *Element quality*, the perfect mesh has a value of 1; for the parameter *Skewness* that consider element's deformation, the perfect mesh would have a value of 0; the parameter *Orthogonal Quality* for an ideal mesh is equal to 1. This last term represent a very critical parameter that can include also the element skewness. Indeed to calculate the orthogonal quality, FLUENT elaborate the gap between the vector from the cell centroid to the centroid of each of the adjacent cells, and the vector from the cell centroid to each of the faces.

4.4 Solution Set-Up

The setup phase takes place within the graphical interface of the Fluent solver. Up to now no problem-solving method has been set. The software does not know the boundary conditions and even the equations it needs to use. It has been chosen to work with the *K-ω SST* algorithm because it is able to approximate fluid separation, fluid-surface interaction, and the

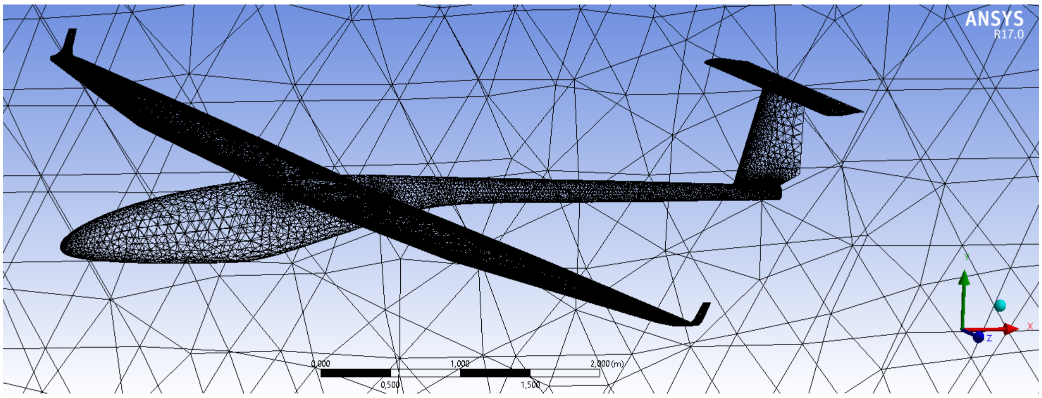

(a) 3D mesh on glider model.

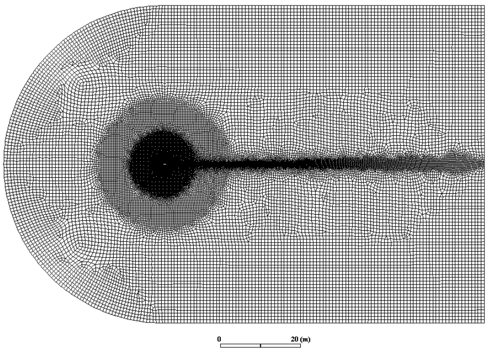

(b) 2D mesh on FX 61-147.

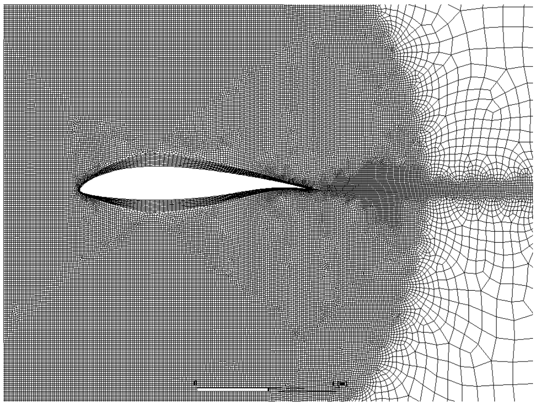

(c) 2D mesh on FX 61-147.

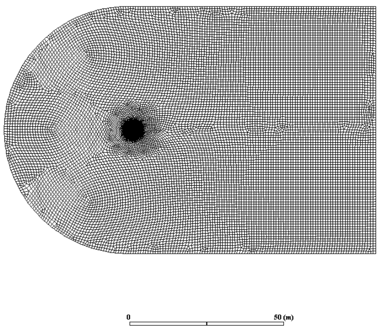

(d) 2D mesh on FX 63-137.

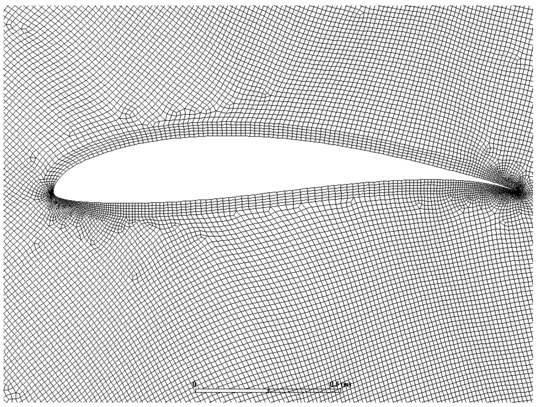

(e) 2D mesh on FX 63-137.

Figure 4.4: Different type of mesh on different models, from 2D airfoil to 3D Glider.

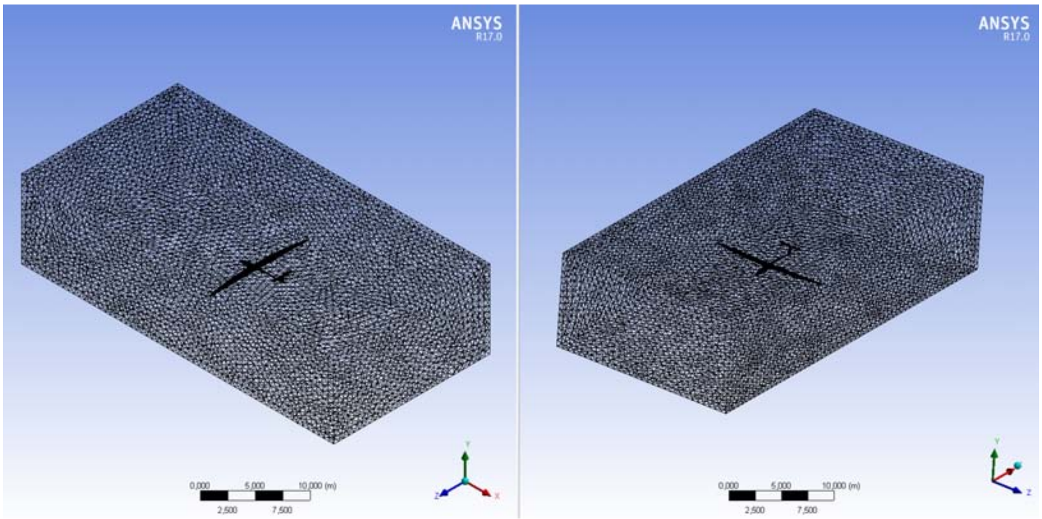

(a) 3D glider model mesh.

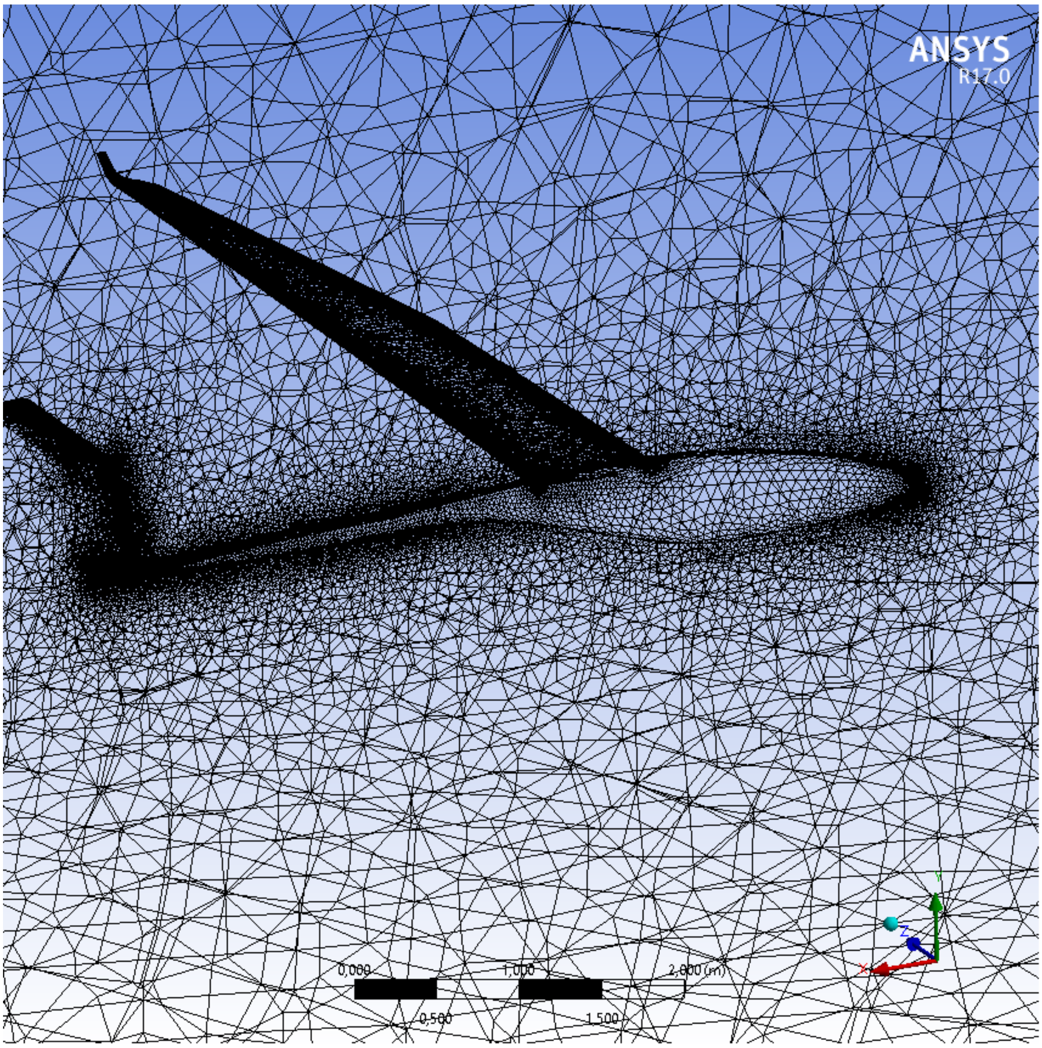

(b) 3D glider model mesh.

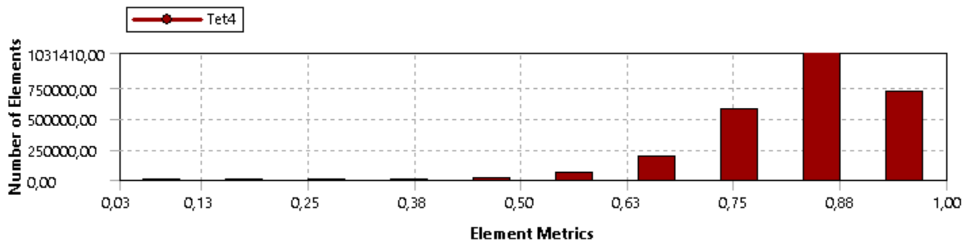

(a) 3D mesh statistics : Element Quality.

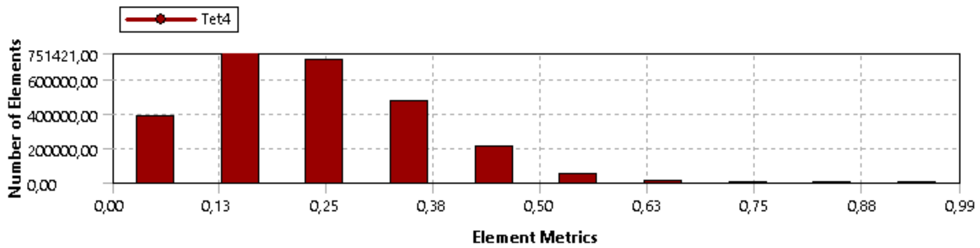

(b) 3D mesh statistics : Skewness.

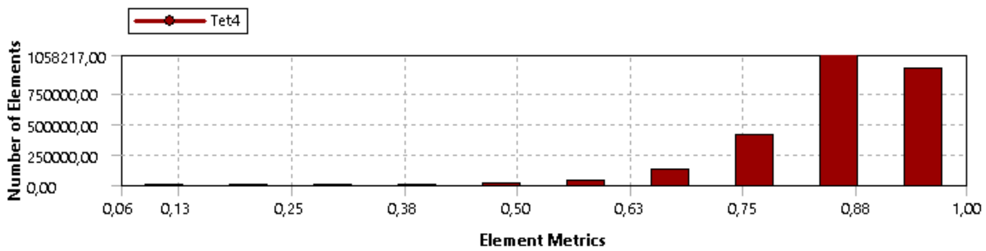

(c) 3D mesh statistics : Orthogonal Quality.

Figure 4.5: 3D mesh parameters describing discretization quality onEntire Glider.

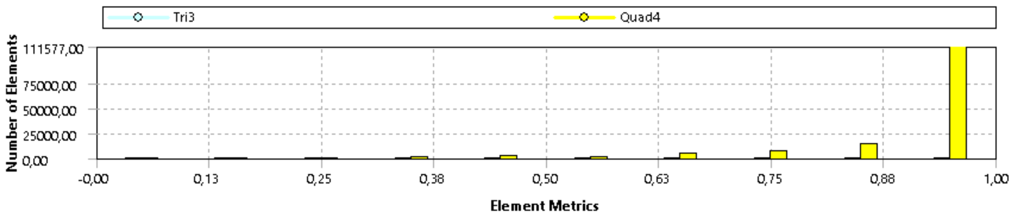

(a) 2D mesh statistics FX 61-147 : Element Quality.

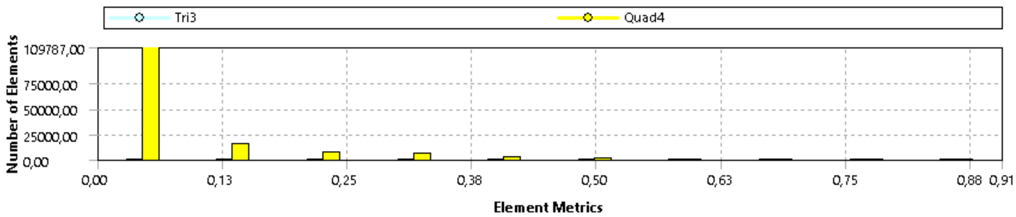

(b) 2D mesh statistics FX 61-147 : Skewness.

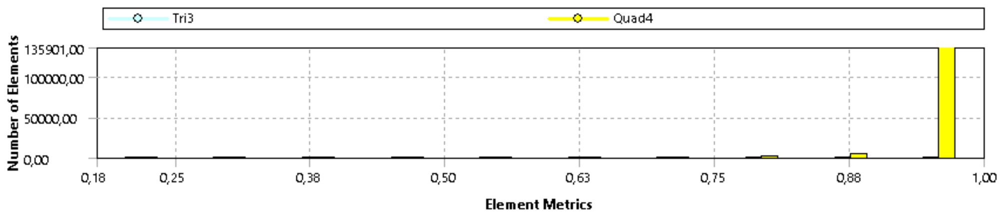

(c) 3D mesh statistics FX 61-147 : Orthogonal Quality.

Figure 4.6: 2D mesh parameters describing discretization quality on FX 61-147

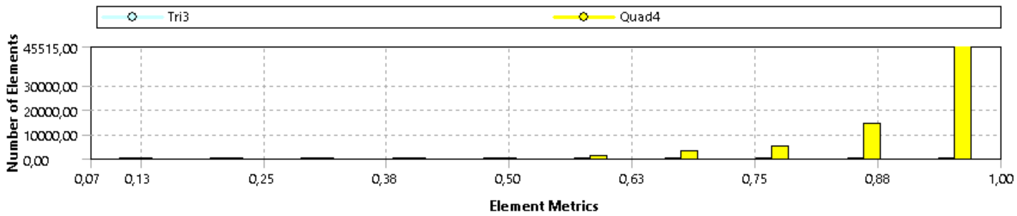

(a) 2D mesh statistics FX 63-137 : Element Quality.

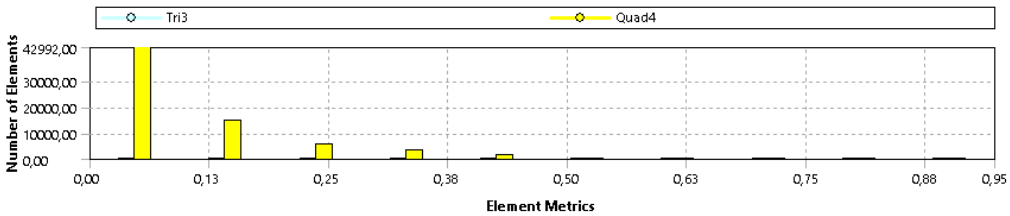

(b) 2D mesh statistics FX 61-147 : Skewness.

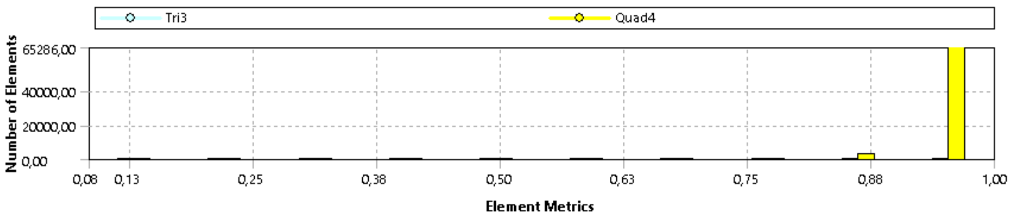

(c) 3D mesh statistics FX 61-147 : Orthogonal Quality.

Figure 4.7: 2D mesh parameters describing discretization quality on FX 63-137.

	Density [kg/m^3]	Velocity [m/s]	Viscosity[$Pa \cdot s$]	Altitude [m]
Re=750k	0.957	13.5	1.71	2500
Re=1E6	1.058	17	1.74	1500

Table 4.4: Set Up environment conditions(ρ,velocity and viscosity) evaluated with characteristic length of 1 m to obtain Re=1E6 and Re=750k.

detection of Cl and Cd values best suited for subsonic applications.

A two-dimensional study was initiated, focussed on validating the data provided by **Profili2**®and pushed to the assessment of fluid separation, thanks to the code potentiality. This was done for both profiles, FX 61-147 and FX 63-137, under the conditions of Reynolds 1E6 and 750k, to which density values, flow rates, characteristic length and dynamic viscosity on Table 4.4 were complied with. The attack angle was varied from -2 to 12.5 for each study group. The "monitors" of the lift and drag non-dimensional have been inserted, recalling that:

$$C_{l_x} = f(-sen\alpha) \tag{4.6}$$

$$C_{l_y} = f(cos\alpha) \tag{4.7}$$

$$C_{d_x} = f(cos\alpha) \tag{4.8}$$

$$C_{d_y} = f(sen\alpha) \tag{4.9}$$

Was set a number of iterations equal to 1000 for the airfoil analysis and 350 for the entire aircraft analysis. Airfoil analyses reached convergence around 600 iterations with residuals below 1e-6. While complete aircraft analyses, such as airfoil analysis, converge around 300 iterations but residuals tend to stabilize at higher values.

4.5 Post-Processing : Results

In the post-processing phase, the results are analysed and the final considerations are made.

4.5.1 Airfoil CFD Results

For each set of analyses, it was observed that in the fluid domain and for each cell away from the interference geometry, the velocity value is equals to the initial one. This is a sanity check of the solution and the respect of the boundary condition. However, a negative consideration must be advanced,

and in particular on mesh set-up. It is noted that mesh is not able to describe boundary layer in the most appropriate way, Figure 4.16. It would be necessary to increase the number of cells across the geometry zone to optimize the analysis of the boundary layer. At the trailing edge, the thickness of the boundary layer is greater, which is consistent with the theory that pressure gradient causes particles to be forced to the lower pressure zone, this results in thickening. For pressure distribution, it is noted that the boundary layer has not influence on it. Is much more marked for velocity distribution. Knowing that the lift is dependent on the pressure distribution, it would be possible to neglect the viscous effect and still obtain good lift approximations.
In Table 4.17 are presented the airfoil C_l and C_d values obtained thanks to **FLUENT**®and shown in a graphical way in 4.18. These results confirm the behaviour of both airfoil. Indeed the FX 63-137 presents a better attitude to produce Lift, while FX 61-147 is quite low. However we have to analyse them in a 3D view, thinking that FX 63-137 is negative twisted and produce a C_l value lower than 1 degrees respect to the Glider orientation, while the FX 61-147 produce a lift higher than 1.5 degree respect to the glider orientation. In this way, as explain before, it is possible to obtain a uniform lift distribution all over the wing. Also flow properties variations, ie change from Re=1e6 to Re=750k, the corresponding C_l value results lower due to lighter density. This can be observed on graphs and tables, even if this change is not so evident.

4.5.2 Complete Wing C_L CFD Results

Following the numerical fluid dynamics analysis of individual airfoil in different external conditions and different angle of attack, a three-dimensional simulation set was performed. The purpose, as mentioned above, is to verify hand-calculations based on the experience of prof. Pajno[34] and simultaneously carry out qualitative considerations about the behaviour of the motorglider when varying flow properties. In particular, analyse the contribution of the winglet to the Lift capacity and Drag values but also to observe qualitatively how the flow behaviour changes in the presence and absence of the wing-tip. Also evaluate wing-fuselage interference; qualitative assessment of turbulence. To do this, was imported the three-dimensional project previously displayed within the **ANSYS**®suite. Once the geometry and control volume, a box of 40x25x10 meters was recognized, the boundaries named *farfield1* and *farfield2* were identified. These will be associated with the boundary conditions that are, respectively, *inlet velocity* and *pressure-outlet*, as for airfoil. **WARNING**: knowing that the volume control box is

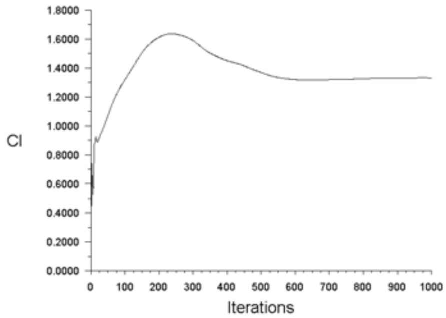

(a) C_l variation graph of FX 61-147 airfoil vs iteration; α=12.5 degree; Re=1E6.

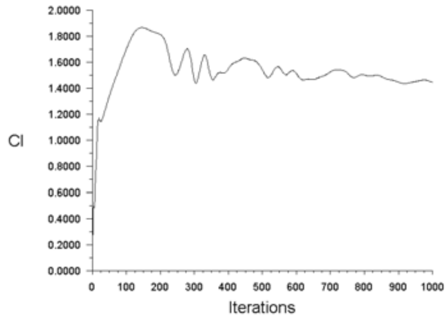

(b) C_l variation graph of FX 63-137 airfoil vs iteration; α=12.5 degree; evident instability due to Stall effects;Re=1E6.

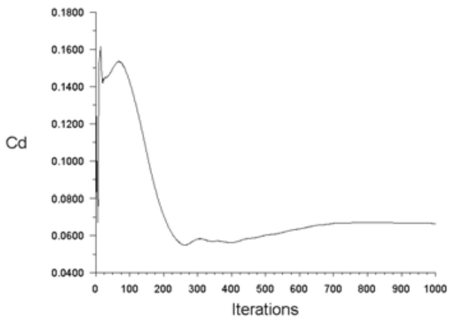

(c) C_d variation graph of FX 61-147 airfoil vs iteration; α=12.5 degree; Re=1E6.

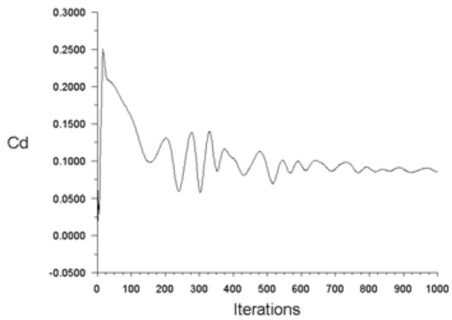

(d) C_d variation graph of FX 63-137 airfoil vs iteration; α=12.5 degree; evident instability due to Stall effects;Re=1E6.

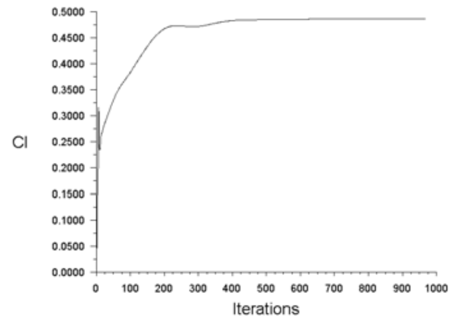

(a) [C_l variation graph of FX 61-147 airfoil vs iteration; α=0 degree; Re=750k.

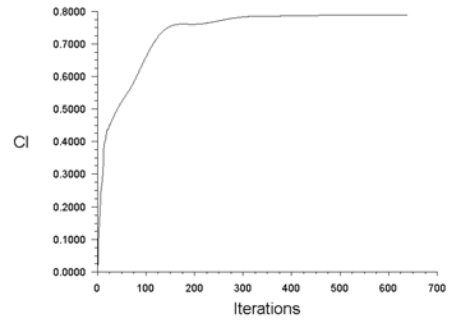

(b) C_l variation graph of FX 63-137 airfoil vs iteration; α=0 degree; Re=750k.

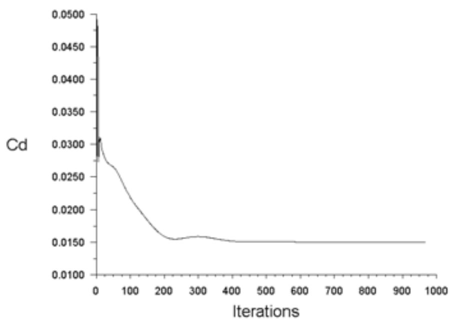

(c) C_d variation graph of FX 61-147 airfoil vs iteration; α=0 degree; Re=750k.

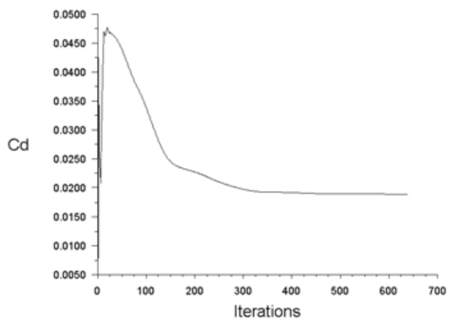

(d) C_d variation graph of FX 63-137 airfoil vs iteration; α=0 degree; Re=750k.

Figure 4.8: C_l and C_d convergence graphs, at different angle of attack, same Reynolds number=1E6

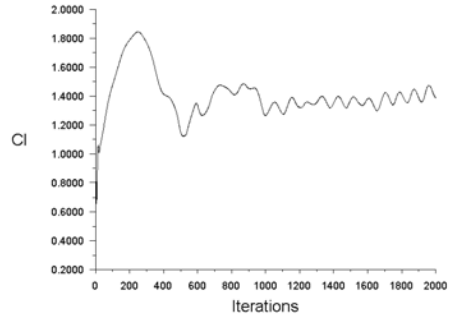

(a) C_l variation graph of FX 61-147 airfoil vs iteration; α=15 degree; evident instability due to Stall effects;Re=750k.

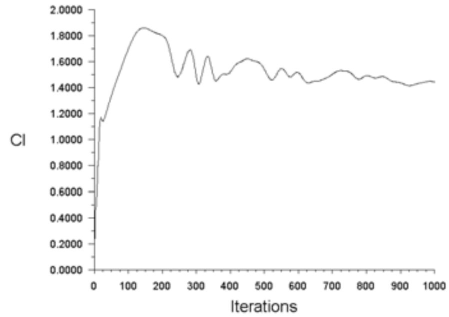

(b) C_l variation graph of FX 63-137 airfoil vs iteration; α=12.5 degree; evident instability due to Stall effects;Re=750k.

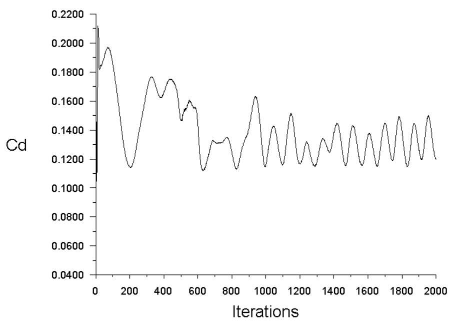

(c) C_d variation graph of FX 61-147 airfoil vs iteration; α=15 degree; evident instability due to Stall effects;Re=750k.

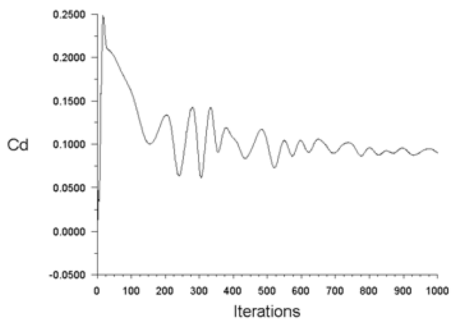

(d) C_d variation graph of FX 63-137 airfoil vs iteration; α=12.5 degree; evident instability due to Stall effects;Re=750k.

Figure 4.9: C_l and C_d convergence graphs, at high AoA: 15 degree for FX 61-147 and 12.5 degree for FX 63-137; same Reynolds number=750k.

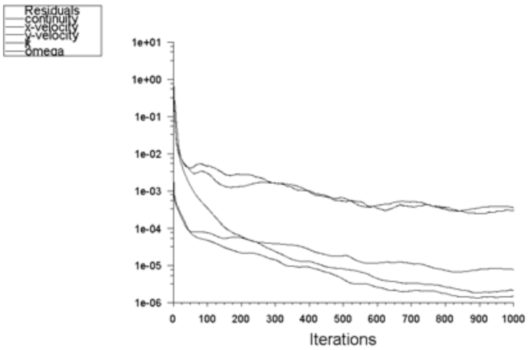

(a) Residuals' graph vs iteration, until reaching convergence below thresold 1e6;Re=1E6 FX 61-147 α=12.5 degree.

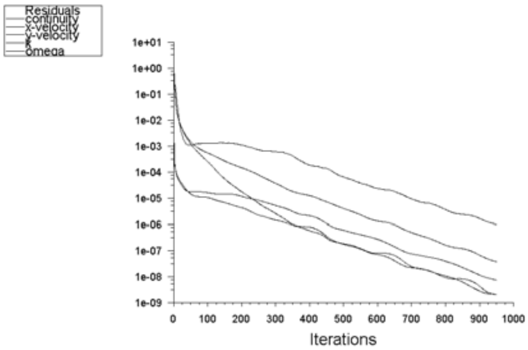

(b) Residuals' graph vs iteration, until reaching convergence below thresold 1e6;Re=1E6 FX 61-147 α=2 degree.

Figure 4.10: Example of difference residuals tendency as a function of simulation parameters.

relatively small, the results will be treated with particular scepticism and for this reason the following analysis will be mostly evaluated qualitatively. The discretization phase was carried out automatically. Finally, in the set-up phase, the mathematical model was set: k-ω SST and boundary conditions. In particular, these simulations were conducted at Re = 1E6, whose combination of parameters is shown in the Table 4.5. This Reynolds value has been chosen respect to the direction of motion with analysis interest in the evaluation of the mean wing C_l. Therefore, the characteristic length used is that of the mean aerodynamic chord, with respect to which the calculations in Chapter 3 have also been carried out. The reference values have been manipulated to comply with the constraints and above all to obtain reasonable value of the C_l and C_d, the area (projection area on a horizontal plan) was set to 7.26 m^2 for wing with winglet and wing without winglet. This is to evaluate the practical use in terms of C_l of the use of winglet whose area projected horizontally is near to zero. The simulations have been initialized with a hybrid method whose peculiarity is, in addition to being automatically based on the setted data, to solve a Laplace Problem across the entire fluid volume to produce a first-attempt velocity and pressure field [54]. The iteration number was varied from 350 to 500, for which all configurations were observed to reach convergence, as shown in images 4.19,4.20. The results over the entire three-dimensional models are shown in figure 4.21 and 4.22. These values agree with the calculation collected since this phase

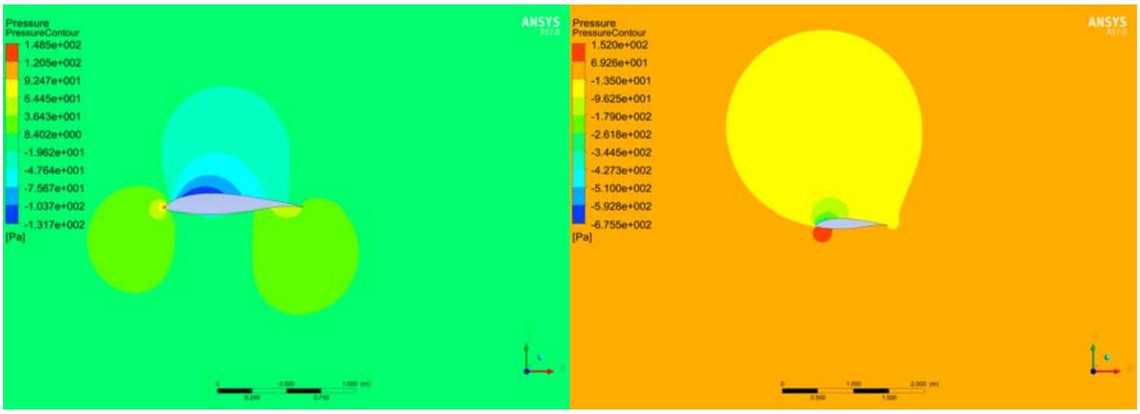

(a) Pressure distribution on FX 61-147;Re=1E6;AoA=0 degree.

(b) Pressure distribution on FX 61-147;Re=1E6;AoA=12.5 degree.

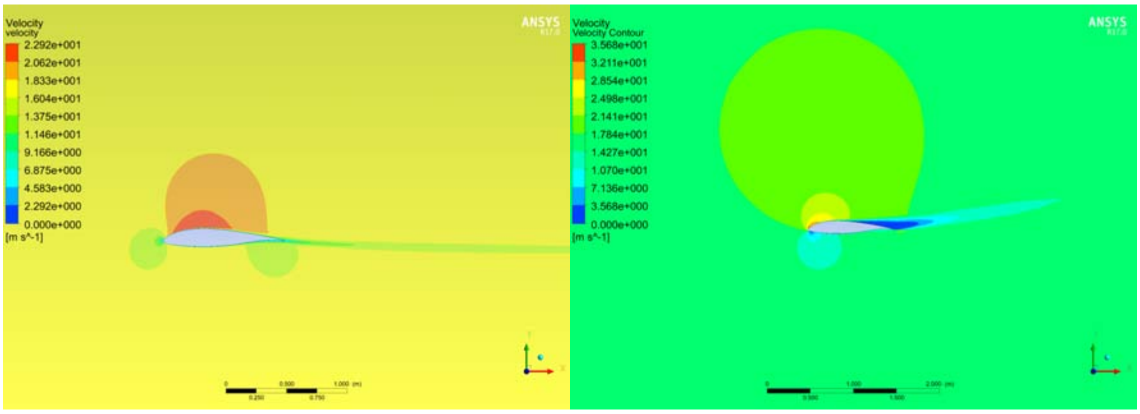

(c) Velocity field distribution on FX 61-147;Re=1E6;AoA=0 degree.

(d) Velocity field distribution on FX 61-147;Re=1E6;AoA=12.5 degree.

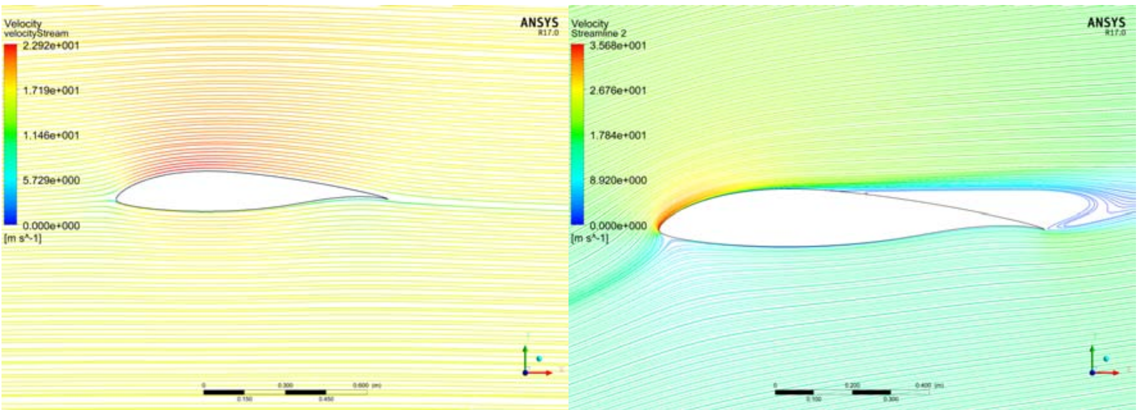

(e) Velocity Streamline distribution on FX 61-147;Re=1E6;AoA=0 degree.

(f) Velocity Streamline distribution on FX 61-147;Re=1E6;AoA=12.5 degree.

Figure 4.11: Post-Process results: Pressure, Velocity field and Velocity stream for FX 61-147 airfoil at AoA=0 and 12.5 degree; Re=1E6.

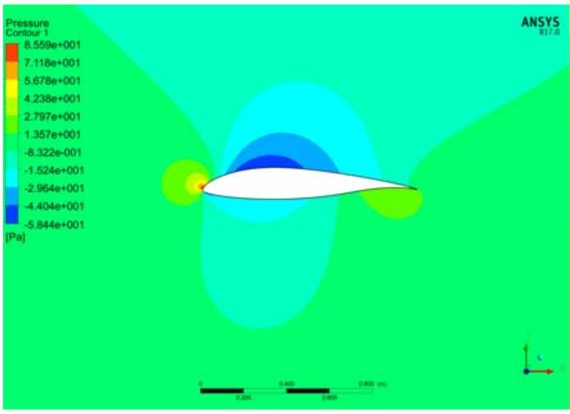

(a) Pressure distribution on FX 61-147;Re=750k;AoA=-2 degree.

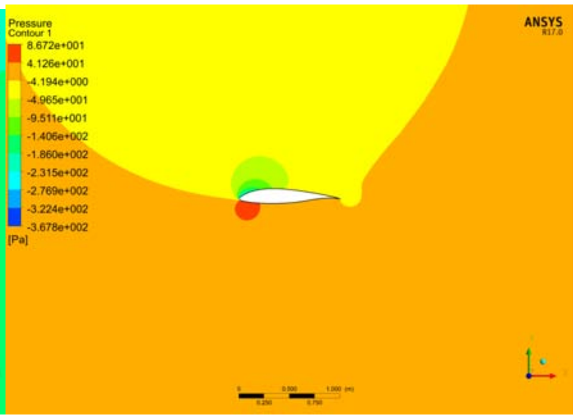

(b) Pressure distribution on FX 61-147;Re=750k;AoA=12.5 degree.

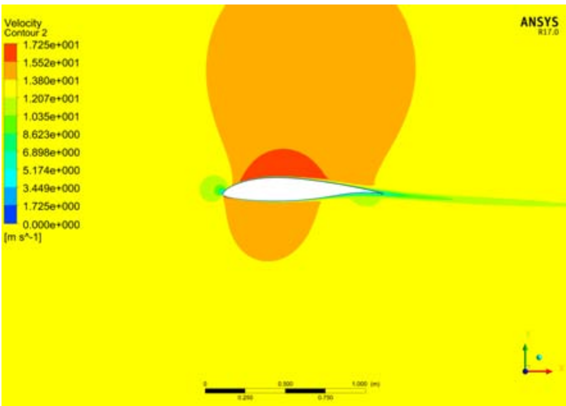

(c) Velocity field distribution on FX 61-147;Re=750k;AoA=-2 degree.

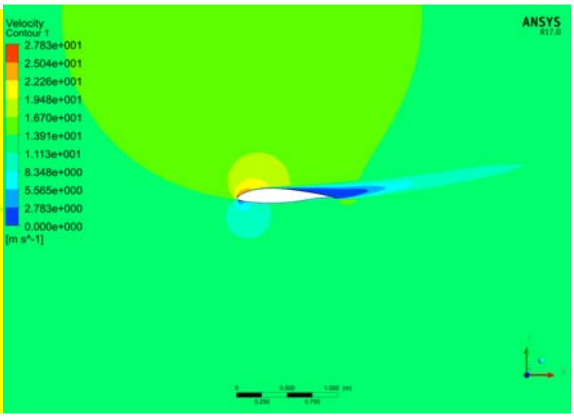

(d) Velocity field distribution on FX 61-147;Re=750k;AoA=12.5 degree.

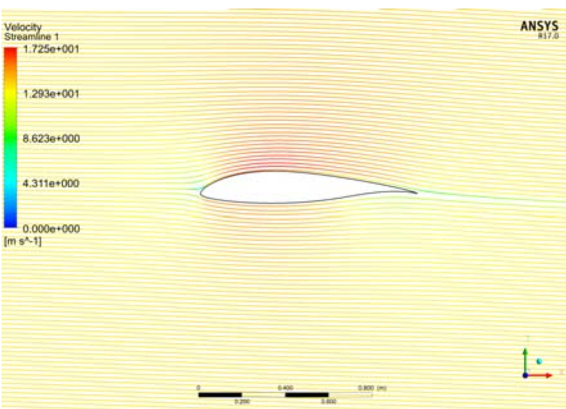

(e) Velocity Streamline distribution on FX 61-147;Re=750k;AoA=-2 degree.

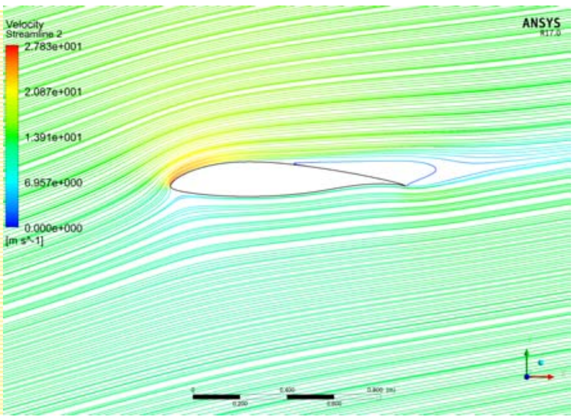

(f) Velocity Streamline distribution on FX 61-147;Re=750k;AoA=12.5 degree.

Figure 4.12: Post-Process results: Pressure, Velocity field and Velocity stream for FX 61-147 airfoil at AoA=-2 and 12.5 degree; Re=750k.

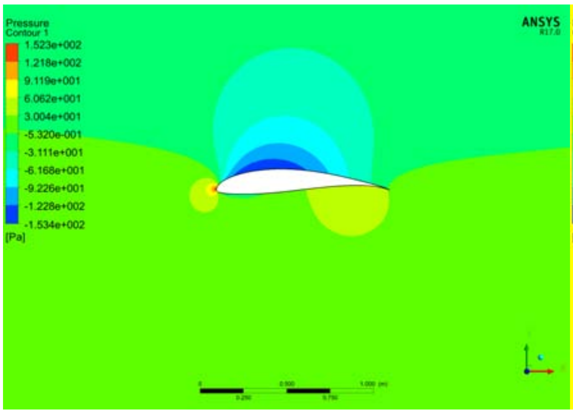

(a) Pressure distribution on FX 63-137;Re=1E6;AoA=0 degree.

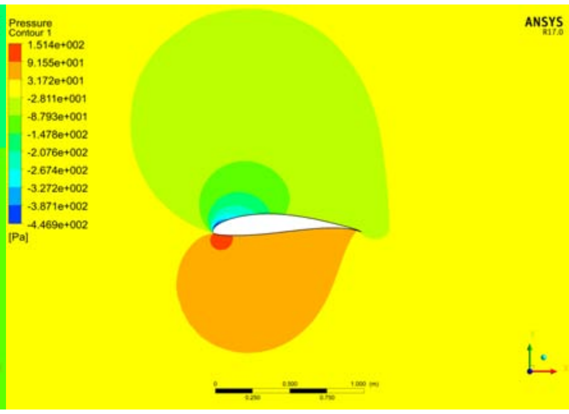

(b) Pressure distribution on FX 63-137;Re=1E6;AoA=12.5 degree.

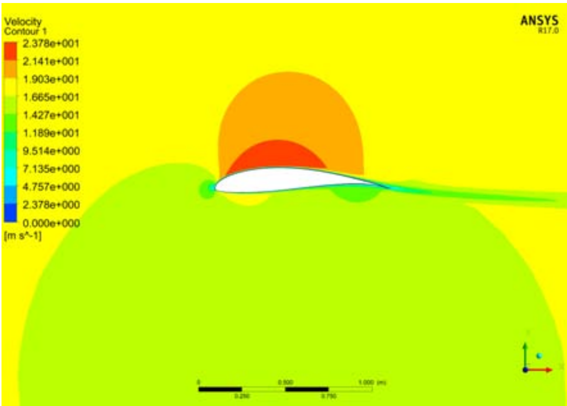

(c) Velocity field distribution on FX 63-137;Re=1E6;AoA=0 degree.

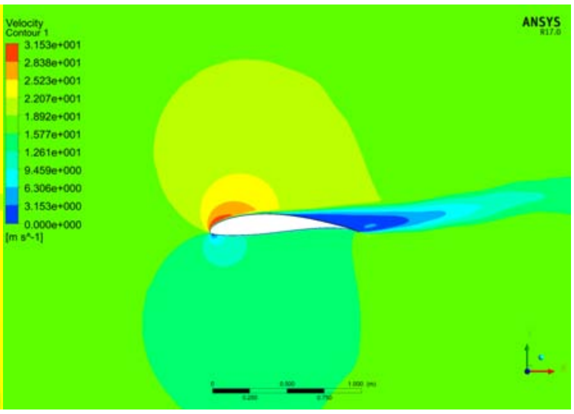

(d) Velocity field distribution on FX 63-137;Re=1E6;AoA=12.5 degree.

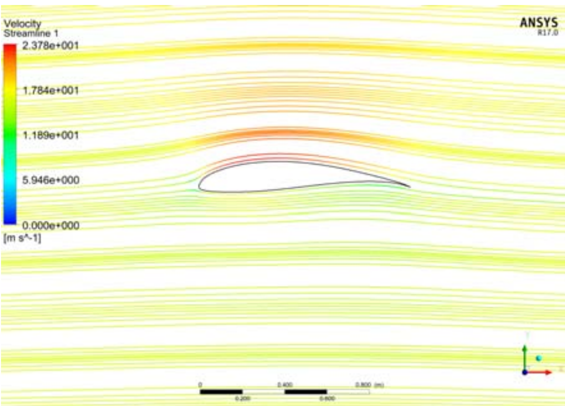

(e) Velocity Streamline distribution on FX 63-137;Re=1E6;AoA=0 degree.

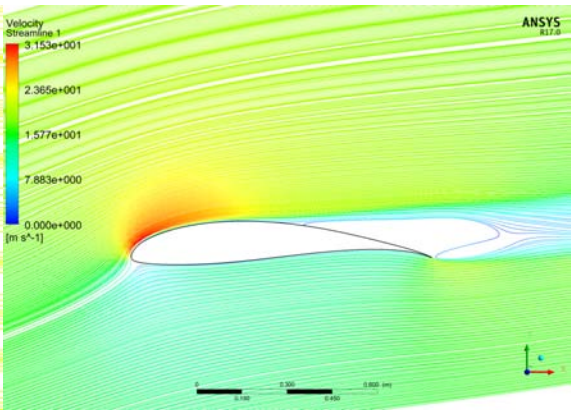

(f) Velocity Streamline distribution on FX 63-137;Re=1E6;AoA=12.5 degree.

Figure 4.13: Post-Process results:Pressure, Velocity field and Velocity stream for FX 63-137 airfoil at AoA=0 and 12.5 degree; Re=1E6.

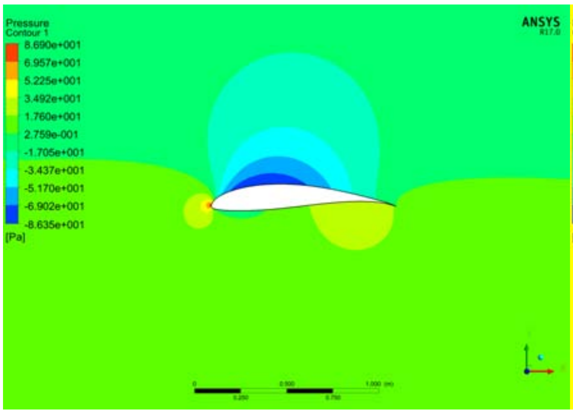

(a) Pressure distribution on FX 63-137;Re=750k;AoA=0 degree.

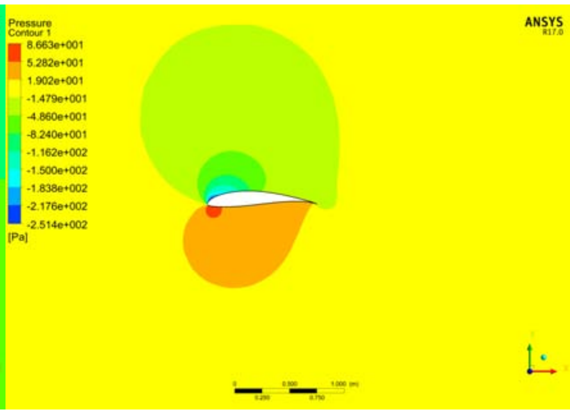

(b) Pressure distribution on FX 63-137;Re=750k;AoA=12.5 degree.

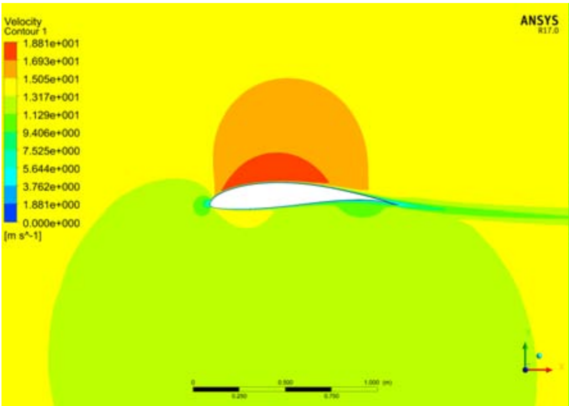

(c) Velocity field distribution on FX 63-137;Re=750k;AoA=0 degree.

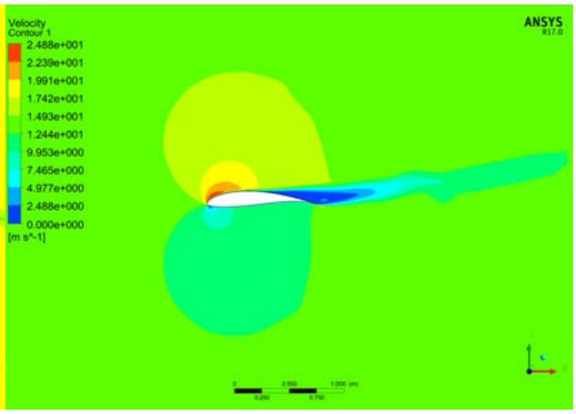

(d) Velocity field distribution on FX 63-137;Re=750k;AoA=12.5 degree.

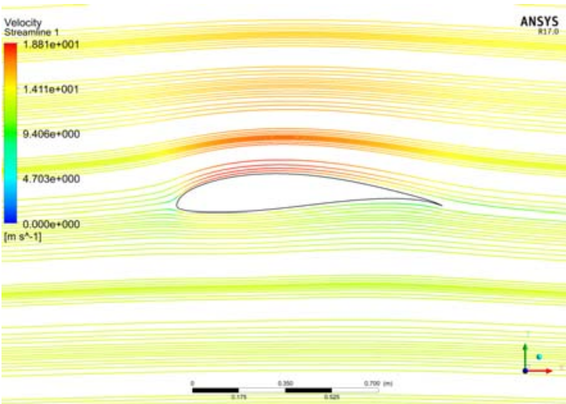

(e) Velocity Streamline distribution on FX 63-137;Re=750k;AoA=0 degree.

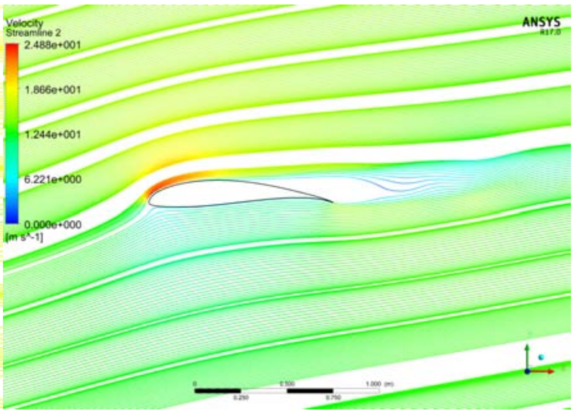

(f) Velocity Streamline distribution on FX 63-137;Re=750k;AoA=12.5 degree.

Figure 4.14: Post-Process results: Pressure, Velocity field and Velocity stream for FX 63-137 airfoil at AoA=0 and 12.5 degree; Re=750k.

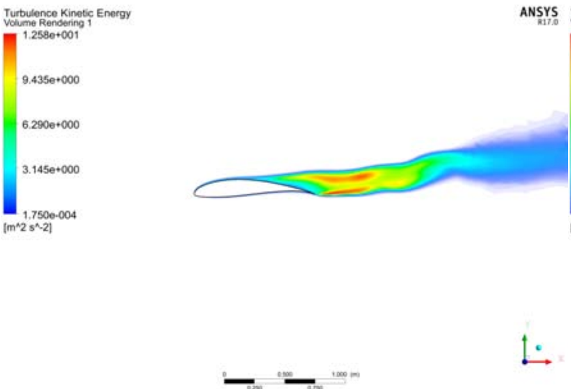

(a) Turbolent Kinetic Energy on FX 63-137 in instable configuration: AoA=12.5 degree; Re=750k.

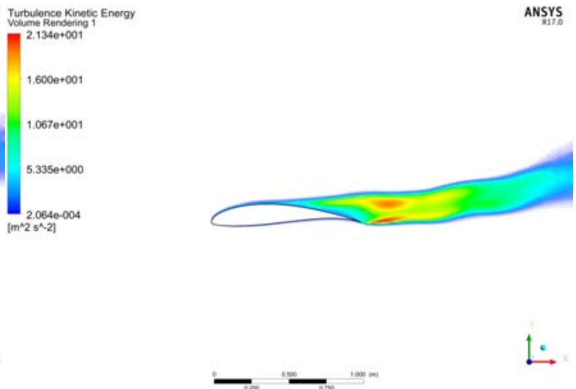

(b) Turbolent Kinetic Energy on FX 63-137 in instable configuration: AoA=12.5 degree; Re=1E6.

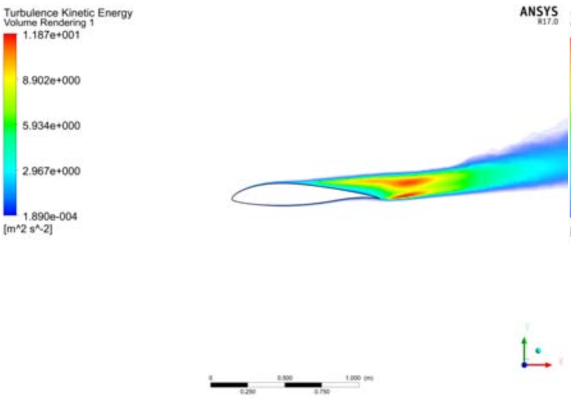

(c) Turbolent Kinetic Energy on FX 61-147 in instable configuration: AoA=12.5 degree; Re=750k.

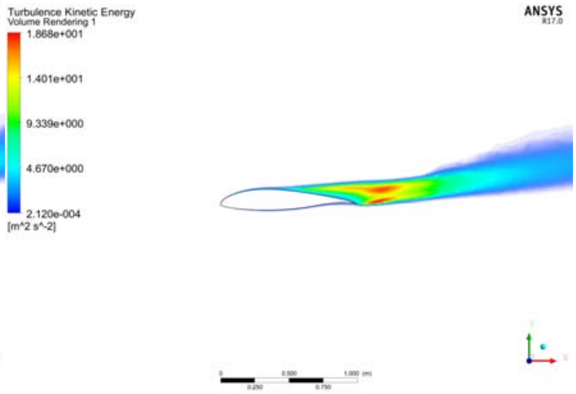

(d) Turbolent Kinetic Energy on FX 61-147 in instable configuration: AoA=12.5 degree; Re=1E6.

Figure 4.15: Post-Process results: Turbolence Kinetic Energy for FX 63-137 and FX 61-147 airfoil at AoA=12.5 degree; Re=1E6 and 750k.

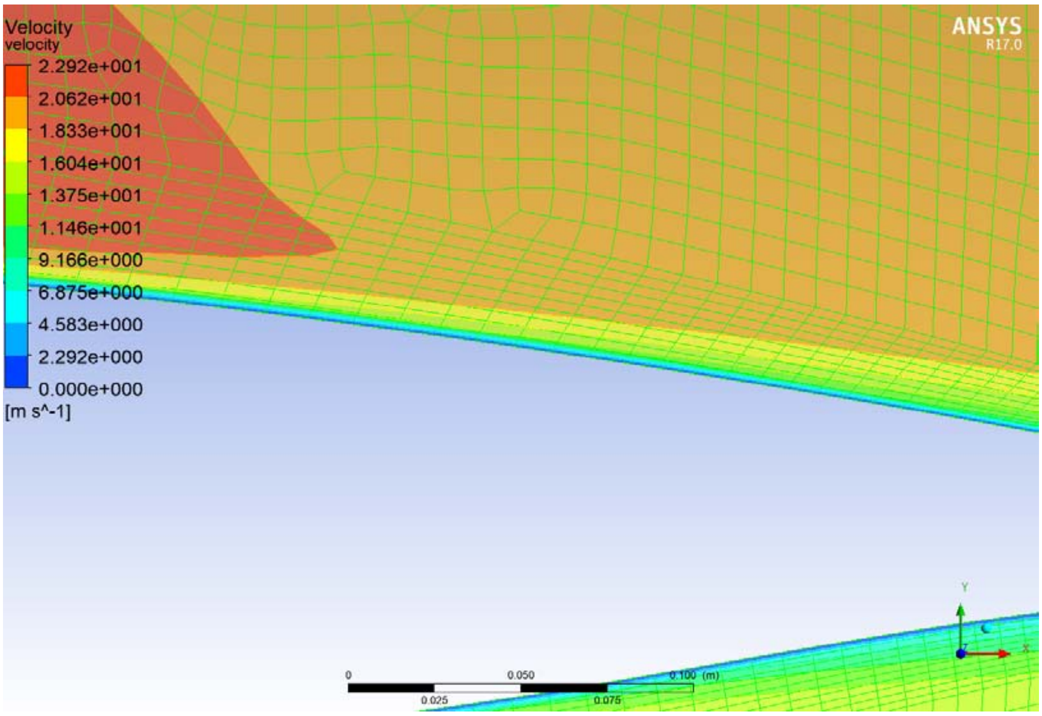

Figure 4.16: Boundary Layer mesh not good approximation. Best compromise between Hardware resources and results quality.

Re=750k							
Environment	v [m/s] = 13.5m/s	h [m] =	2500m	rho [kg/m3] = 0.957		v [Pa*s]=1.71	
Airfoil	FX 61-147			FX 63-137			
	alpha	Cl	Cd	alpha	Cl	Cd	
	-2	2.57E-01	1.47E-02	-2	5.76E-01	1.74E-02	
	0	4.86E-01	1.50E-02	0	7.89E-01	1.89E-02	
	2	7.05E-01	1.61E-02	2	9.83E-01	2.14E-02	
	5	1.01E+00	1.96E-02	5	1.23E+00	2.78E-02	
	8	1.25E+00	2.66E-02	8	1.41E+00	4.07E-02	
	12.5	1.30E+00	7.04E-02	12.5	1.44E+00	9.01E-02	

(a) Airfoil CFD simulation Results at Re=750k when varying AoA.

Re=1E6							
Environment :	v[m/s] = 17m/s	h[m] =	1500	rho [kg/m3] = 1.058		v [Pa*s] = 1.74	
Airfoil	FX 61-147			FX 63-137			
	alpha	Cl	Cd	alpha	Cl	Cd	
	-2	2.69E-01	1.39E-02	-2	5.95E-01	1.65E-02	
	0	4.99E-01	1.42E-02	0	8.09E-01	1.79E-02	
	2	7.19E-01	1.53E-02	2	1.00E+00	2.03E-02	
	5	1.03E+00	1.86E-02	5	1.26E+00	2.64E-02	
	8	1.27E+00	2.52E-02	8	1.44E+00	3.84E-02	
	12.5	1.33E+00	6.66E-02	12.5	1.45E+00	8.51E-02	

(b) Airfoil CFD simulation Results at Re=1E6 when varying AoA.

Figure 4.17: Table containing Airfoil CFD simulation Results at Re=1E6 and Re=750k when varying AoA.

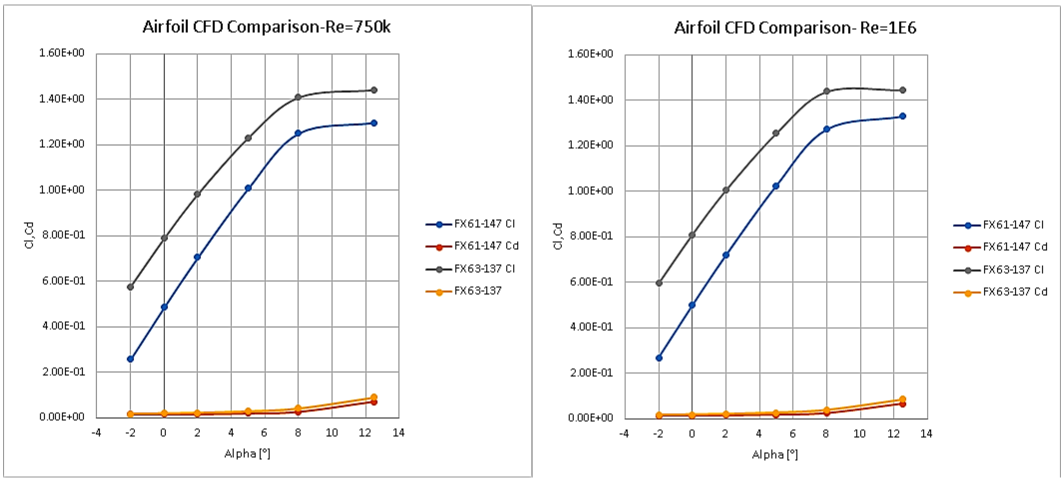

(a) Airfoil CFD simulation Results at Re=750k when varying AoA : C_l and C_d Graph.

(b) Airfoil CFD simulation Results at Re=1E6 when varying AoA : C_l and C_d Graph.

Figure 4.18: C_l and C_d Graph which represents Airfoil CFD simulation Results at Re=750k and 1E6 when varying AoA.

(Chapter 3), and also permit the studies on winglet benefit. Last but not less important, the alignment between hand calculation and CFD results could be explained as the correct set-up problem in ANSYS or as the right validity of empirical formulas used above for the straight line that describe the linear lift coefficient tendency around zero degree. The results in the tables and charts show an interesting performance improvement in terms of C_L in the configuration with winglets than the one in which they are not present. The gap between the two solutions is due to the minimization of the energy vorticity obtained by adding winglets. In the glider without winglet configuration the end vortices are very intense and this means that the vortexes absorb much energy to the flow, decreasing performance. This behaviour agrees with general aerodynamic culture.

Reynolds	V [m/s]	ν $[Pa \cdot s]$	ρ [kg/m^3	l [m]	Altitude [m]
1E6	26	1.74e-5	1.058	0.627	1500

Table 4.5: 3D simulation boundary conditions.

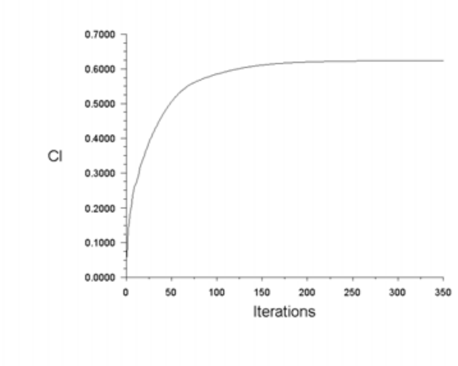

(a) C_l variation graph of 3D model glider with winglet vs iteration; α=0 degree; Re=1E6.

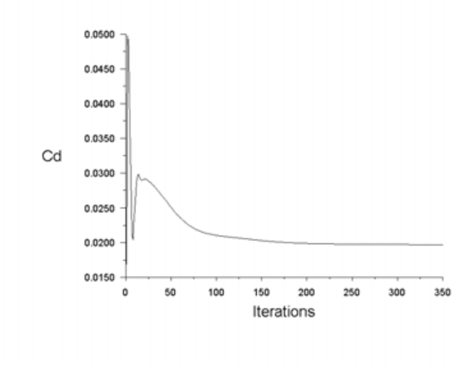

(b) C_d variation graph of 3D model glider with winglet vs iteration; α=0 degree; Re=1E6.

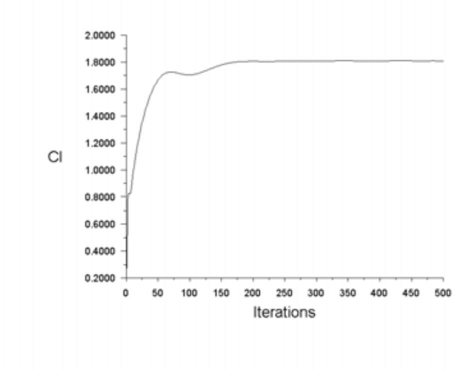

(c) C_l variation graph of 3D model glider with winglet vs iteration; α=15 degree; Re=1E6.

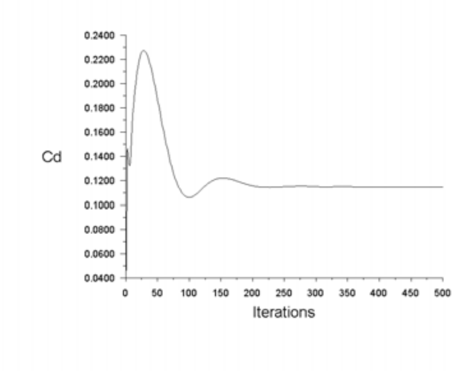

(d) C_d variation graph of 3D model glider with winglet vs iteration; α=15 degree; Re=1E6.

Figure 4.19: C_l and C_d variation graphs vs iteration for 3D glider model with winglet.

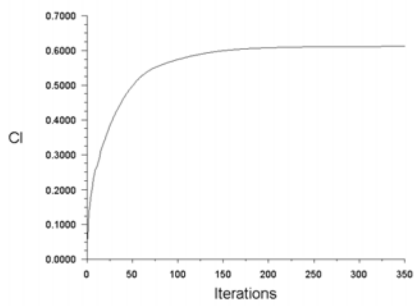

(a) C_l variation graph of 3D model glider without winglet vs iteration; α=0 degree; Re=1E6.

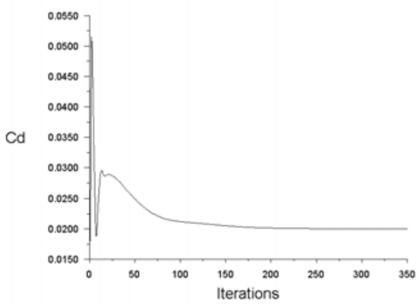

(b) C_d variation graph of 3D model glider without winglet vs iteration; α=0 degree; Re=1E6.

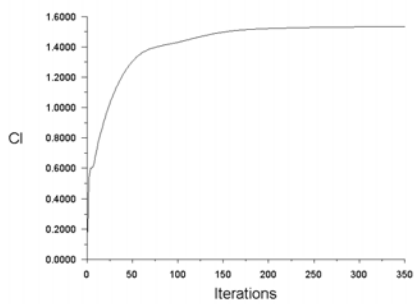

(c) C_l variation graph of 3D model glider without winglet vs iteration; α=10 degree; Re=1E6.

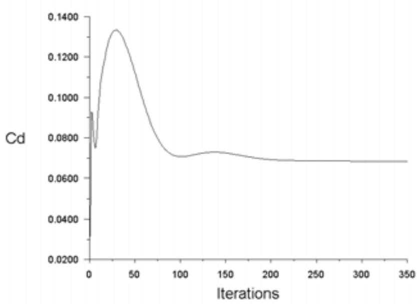

(d) C_d variation graph of 3D model glider without winglet vs iteration; α=10 degree; Re=1E6.

Figure 4.20: C_l and C_d variation graphs vs iteration for 3D glider model without winglet.

Re=1e6									
alpha	iter	continuity	x-velocity	y-velocity	z-velocity	k	omega	Cl	Cd
-3	350	4.72E-05	1.24E-07	5.42E-08	6.24E-08	7.91E-05	2.44E-05	3.11E-01	1.61E-02
0	350	6.12E-05	1.65E-07	7.63E-08	8.52E-08	4.23E-05	7.94E-07	6.24E-01	1.97E-02
2	350	4.37E-05	1.58E-07	6.33E-08	6.43E-08	7.66E-05	3.59E-05	8.35E-01	2.48E-02
5	350	4.72E-05	1.83E-07	7.64E-08	8.47E-08	4.01E-05	5.56E-06	1.14E+00	3.64E-02
8	350	1.04E-04	3.34E-07	1.88E-07	1.84E-07	9.52E-05	2.23E-06	1.41E+00	5.33E-02
10	350	1.62E-04	4.74E-07	3.22E-07	3.02E-07	1.37E-04	2.91E-06	1.56E+00	6.78E-02
15	500	2.59E-04	8.15E-07	6.80E-07	6.22E-07	2.94E-04	4.77E-06	1.81E+00	1.15E-01

(a) CFD results on model glider with winglet at Re=1E6 varying AoA.

Re=1E6									
alpha	iter	continuity	x-velocity	y-velocity	z-velocity	k	omega	Cl	Cd
-2	350	3.48E-05	1.13E-07	4.36E-08	4.50E-08	8.39E-05	3.47E-05	4.01E-01	1.66E-02
0	350	4.54E-05	1.47E-07	6.29E-08	5.97E-08	4.35E-05	7.30E-07	6.12E-01	2.00E-02
2	300	5.80E-05	2.40E-07	1.14E-07	1.15E-07	9.63E-05	4.95E-05	8.18E-01	2.54E-02
5	350	5.85E-05	1.99E-07	9.08E-08	9.97E-08	4.27E-05	5.27E-06	1.12E+00	3.72E-02
8	350	6.48E-05	2.39E-07	1.07E-07	1.08E-07	3.06E-05	8.29E-07	1.38E+00	5.40E-02
10	350	5.96E-05	2.35E-07	1.07E-07	1.12E-07	3.26E-05	9.01E-07	1.53E+00	6.82E-02
15	500	4.29E-05	1.19E-07	6.90E-08	6.62E-08	4.86E-05	1.04E-06	1.79E+00	1.14E-01

(b) CFD results on model glider without winglet at Re=1E6 varying AoA.

Figure 4.21: CFD results at Re= 1E6 on glider with and without winglet.

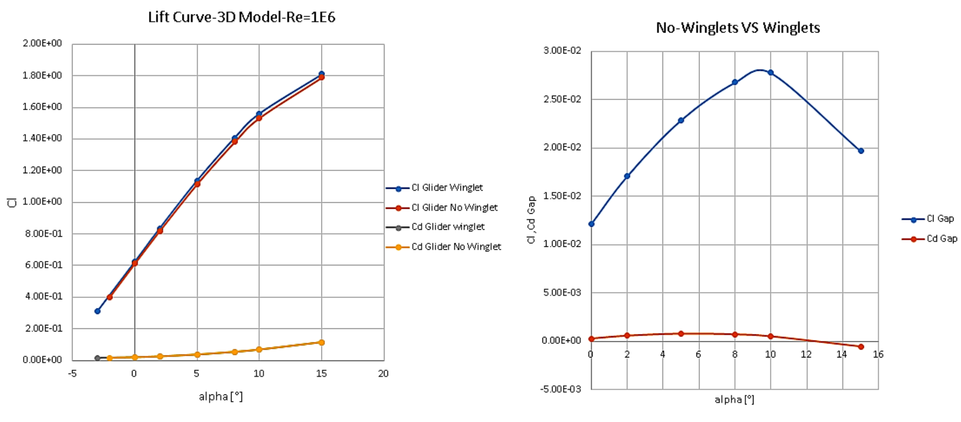

(a) C_l value varying AoA: Glider with Winglet VS Glider without Winglet presented in a graphical way.

(b) Comparison C_l gap between Glider with Winglet VS Glider without Winglet.

Figure 4.22: Difference between C_l values referred to glider with and without winglet.

α[deg]	$C_{L_{Wing}}$	$C_{D_{Wing}}$	$C_{L_{Wing}}$ SIM	$C_{D_{Wing}}$ SIM	% Deviation-Hand Calc.
0	0.620265	0.036395	0.62386	0.019737	0.57959
2	0.815717	0.04195	0.83548	0.024843	2.42284
5	1.108894	0.053119	1.138	0.036415	2.6248
8	1.402071	0.06769	1.4075	0.053319	0.38722
10	1.597522	0.079294	1.5615	0.067757	2.254894
15	2.086151	0.114921	1.8093	0.1147	13.27091

Table 4.6: Comparison between hand calculation performance [34] and simulation results provided by **ANSYS®**;Re=1e6; percentage deviation from hand calculation.

4.5.3 Comparison with Theoretical Results

Following the execution of the simulation series at Re = 1E6 with respect to the average chord length (ie 0.627m), a direct comparison was made between the results obtained by analytical calculations with those obtained numerically. It is good to point out that it would be inappropriate to say that a strategy is better than the other, so that it can be considered as a reference. They are both valid roads that are in agreement on a limited range of possible cases. The FVM method implemented in the CFD, thanks to the k-ω SST algorithm, is able to expand the range of instances where it correctly interprets fluid behaviour. However, the stalling condition is still far from being synthesized with these tools. Precisely with regard to the stall, the empirical-theoretical formulas are not capable of considering its effects. This is evident from the table 4.6, which shows the $C_{L_{Wing}}$ and $C_{D_{Wing}}$ values obtained with the formulas and with simulations. Since it was not considered appropriate to define a better strategy for the other or the one to verify the other, the percentage deviation form of simulation results was compared with the hand calculations. A complete alignment is observed in the range between 0 to 8 degrees, while for $\alpha = 15$ deg AoA there is a clear separation due to the fact that the formulas do not include the stall state.

4.5.4 Glider With and Without Winglet Comparison

In this paragraph, we will look at some of the in-depth considerations on the glider performances with and without winglets. The conclusions that will be recognized, will be supported by images developed through the post-processing software contained in **ANSYS®**. First of all, it is possible to look at the images 4.23, which show the pressure distribution. The low pressure zone increases as the angle of attack increases, that is in accordance with the aerodynamics principles and can be considered a sanity check. Additionally, by increasing the AoA, the low pressure region tends to move towards the inlet edge, with an increasing variation with the remaining upper surface. Just as wings, even the fuselage for how it was designed, contributes to making a difference in pressure between the upper and lower surfaces. At maximum tilting, 15 degrees, high pressure zones are associated, that is in the wedge between the wings, the front and rear fuselage. In this latter area, the affected surface is well defined by the outflow. As for the 4.24 images, which report the distribution of the vector force module, the area most concerned is located at c/4 of the wing and remains almost intact in terms of intensity distribution as increases the angle of attack. The fuselage suffers from an ever-increasing aerodynamic load as the attack angle rises up to 15 degrees in which the wings and fuselage are highlighted. From the 4.25 images, you can observe the particle trajectory. The three images related to the glider with winglet configuration, show the airflow on the entire aircraft at different AoA, from which it is possible to affirm the optimization in the interference between wing and fuselage. High wing location, combined with the fuselage geometry that "accompanies" the flow, allowing better penetration of the fluid field, help to limit wet surface, vortex generation, and overall drag. From the images 4.26, we can observe the advantages of winglets in terms of minimizing the vortex intensity. The images show the fuselage interference of the two glider configurations with and without winglet, for which no specific variation is observed. Subsequent images, on the other hand, are very interesting, indeed they show the flow path with the observer having the same viewing angle of the AoA. In this way we can notice the contribution of adding winglets. The two images were obtained with the same initial flow parameters (speed, density, etc.) at the same angle of inclination. Ignoring the numbers for which accuracy is not guaranteed, the difference in flow behaviour is immediate. The glider without winglet configuration shows an intense swirling motion at the wing tip. This is partially dampened in the configuration with winglet.

With these simulations, it was possible to evaluate fluid behaviour on a real-size virtual model, finding its overall aerodynamics properties, identifying the negative and positive aspects of the configuration.

4.6 Verification and Validation

The *verification and validation* phase includes in-depth analysis of the settings and environment in which simulations have been conducted, as well as errors consideration. This means the verification that mathematical model

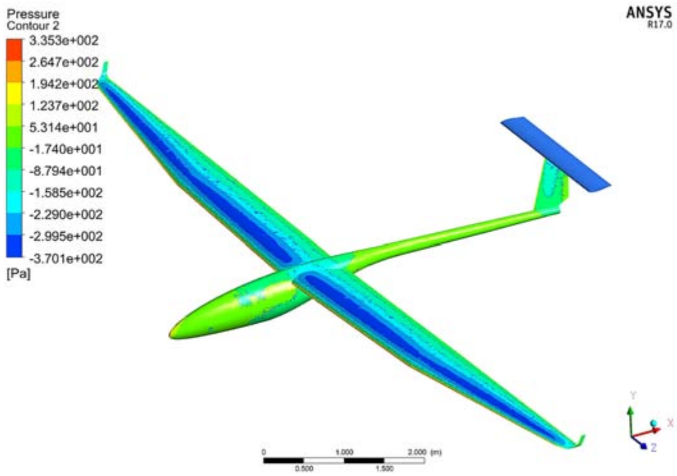

(a) *Pressure Contour* over wings;α= 0 degree.

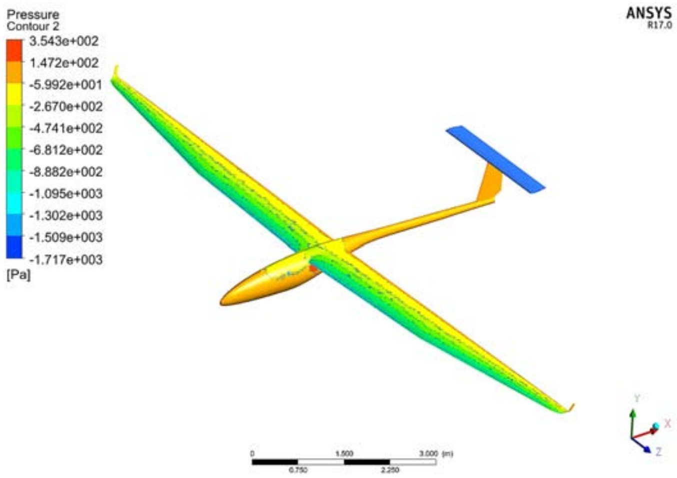

(b) *Pressure Contour* over wings;α= 10 degree.

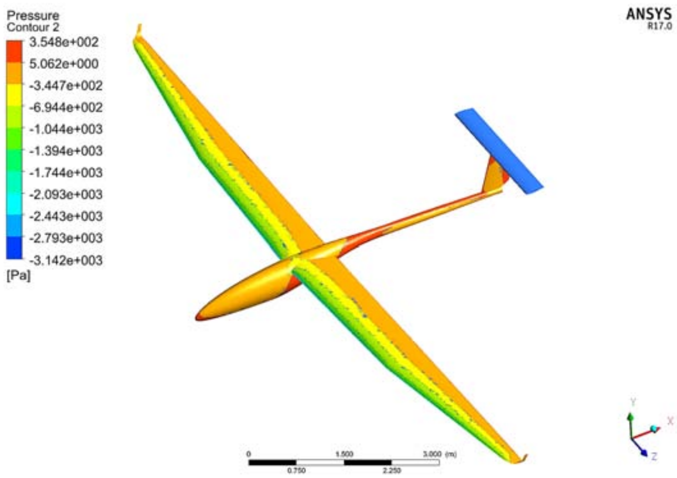

(c) *Pressure Contour* over wings;α= 15 degree.

Figure 4.23: Pressure distribution over fuselage and wings for Glider model with winglet; Re=1E6 along flight direction over wings at 0, 10 and 15 degree.

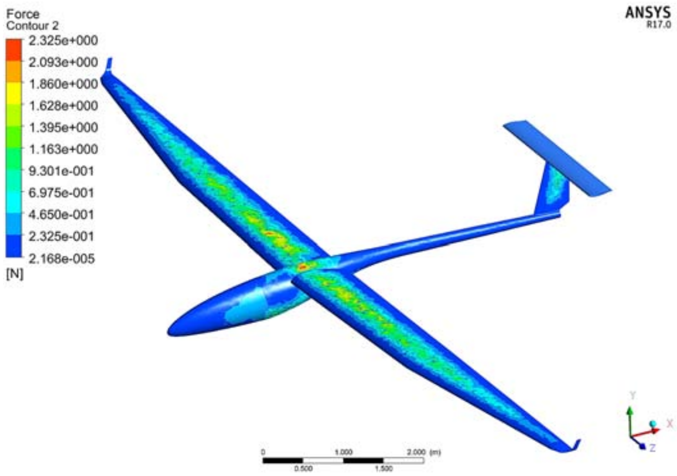

(a) *Force Contour* over wings;α= 0 degree.

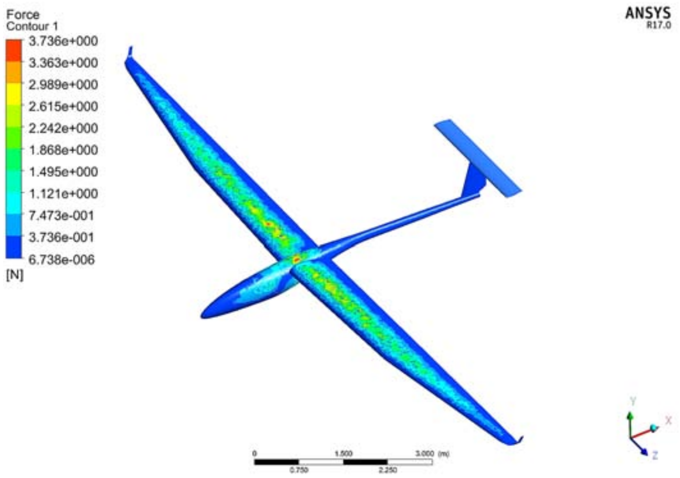

(b) *Force Contour* over wings;α= 10 degree.

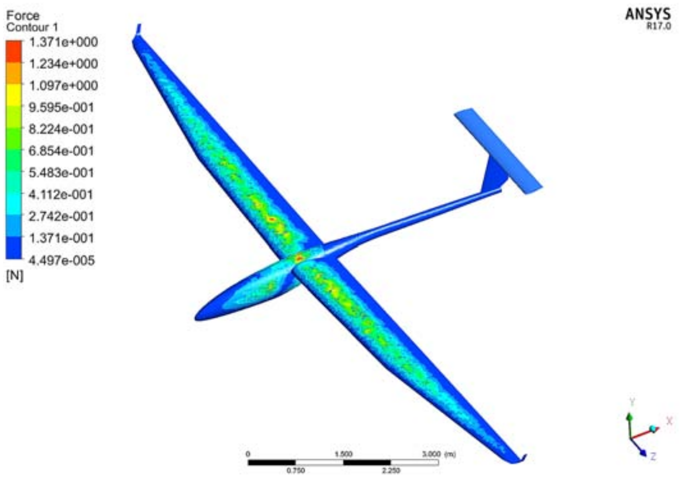

(c) *Force Contour* over wings;α= 15 degree.

Figure 4.24: Force distribution over fuselage and wings for Glider model with winglet; Re=1E6 along flight direction over wings at 0, 10 and 15 degree.

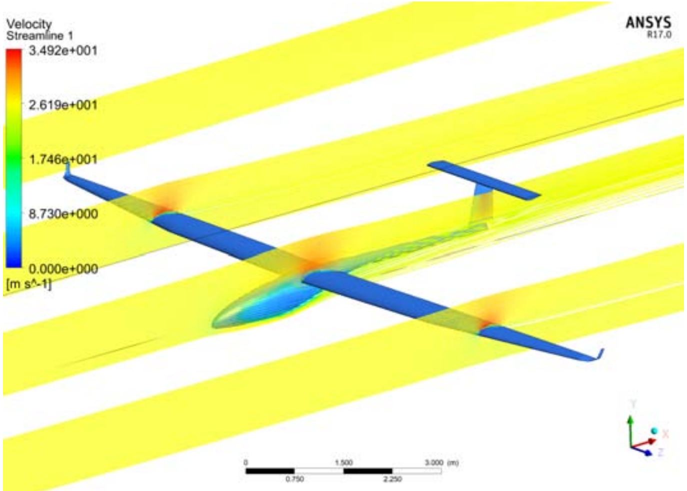

(a) *Velocity Streamline* over wings and fuselage;α= 0 degree.

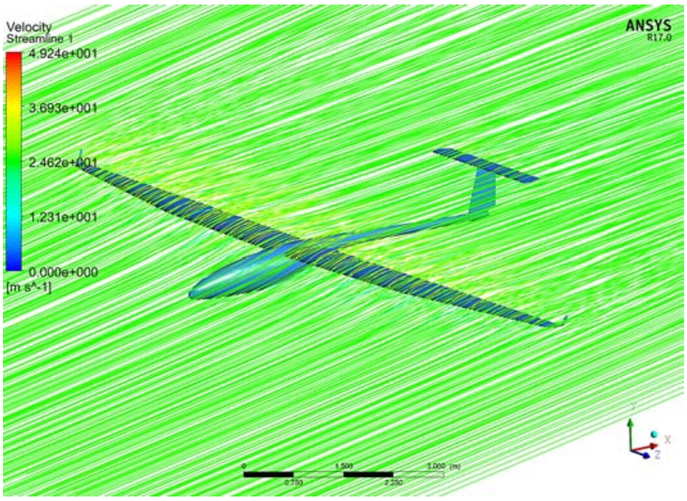

(b) *Velocity Streamline* over wings and fuselage;α= 10 degree.

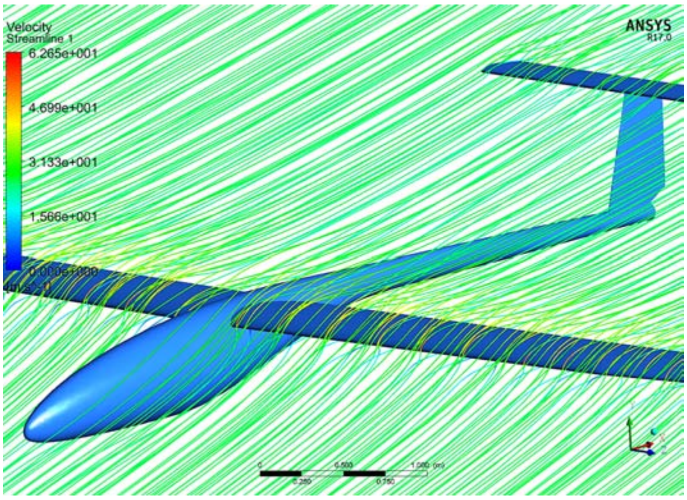

(c) *Velocity Streamline* over wings and fuselage;α= 15 degree.

Figure 4.25: Velocity Streamline over the entire aircraft; Re=1E6 along flight direction over wings at 0, 10 and 15 degree.

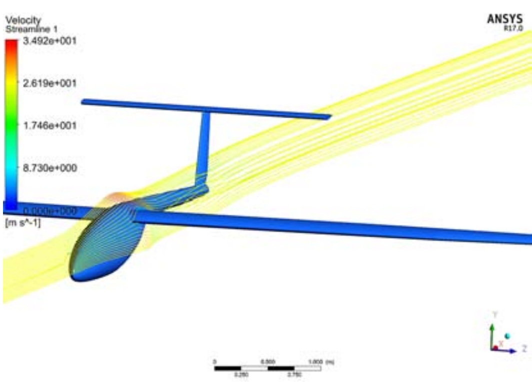

(a) Streamline over fuselage $\alpha = 0$ degree; winglet are not involved.

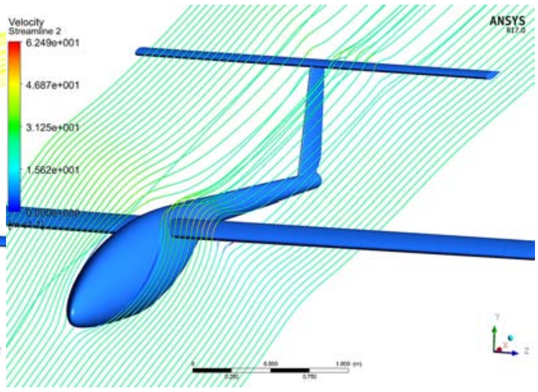

(b) Streamline over fuselage $\alpha = 15$ degree; winglet are not involved.

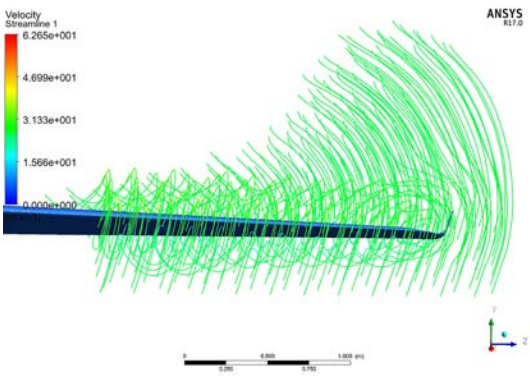

(c) Streamline over wing tips $\alpha = 15$ degree; glider with winglet.

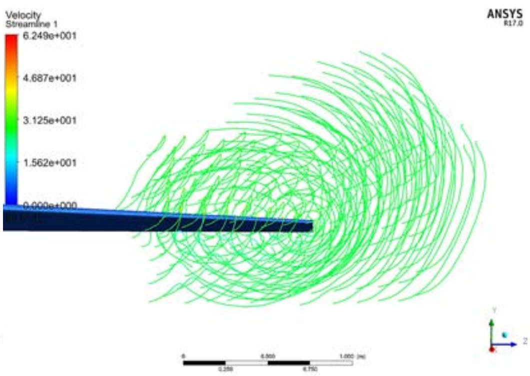

(d) Streamline over wing tips $\alpha = 15$ degree; glider without winglet.

Figure 4.26: Streamline of fluid particles on specific aircraft region to observe vortices and fluid interferences;Re=1E6 comparison between glider with and without winglets.

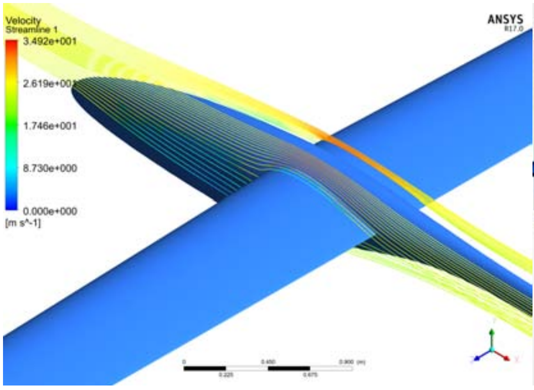

(a) Streamline over fuselage at $\alpha = 0$ degree;Re=1E6; Glider with Winglet.

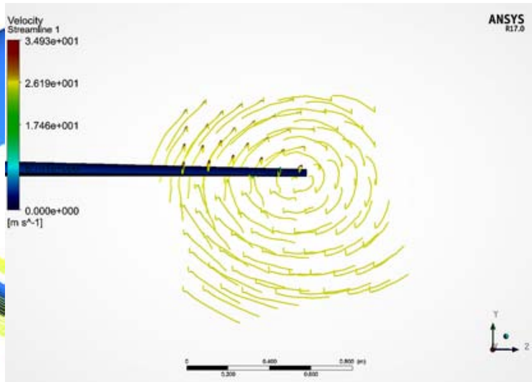

(b) Streamline over wing tip at $\alpha = 2$ degree;Re=1E6; Glider without Winglet.

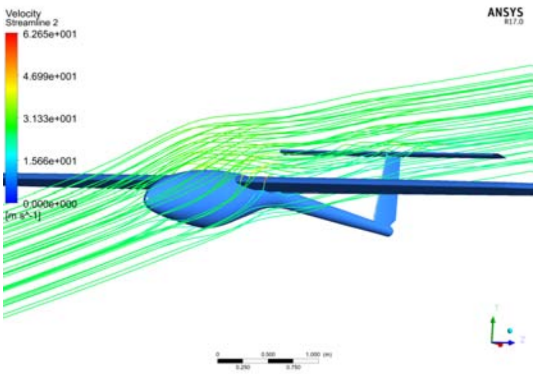

(c) Streamline over fuselage at $\alpha = 15$ degree;Re=1E6; Glider with Winglet.

Figure 4.27: Other post-processing images on wing-fuselage interference and wing-tip vorticity.

was correctly used and it is estimated that the errors introduced by the software are acceptable. A first verification was conducted in the fluid domain, noting that the velocity value is similar to the one initially imposed. A second question that needs to be considered is the software's compliance with the boundary conditions. This evaluation has already been done. However, k and omega values are default. It would be necessary to assess the influence of these factors on the results. Linearisation error is acceptable for airfoil analyses for which all residuals are below the 1e-6 threshold with convergence of the solution, while for the whole aircraft with 350 iterations reaches for part of the residual the value 1e-6 but others stabilize around 1e-3. The discretisation error is unacceptable. It would be necessary to increase the density of the elements near the geometries. All this is a good compromise between the correct solution and the computing resources. About the validation part, this can only be discussed for the analysis group dealing with individual airfoil, as for FX 63-137 there is experimental wind tunnel testing at Re = 300k.

4.6.1 Airfoil C_l Verification

The data validation process obtained using XfoiL and used for preliminary performance estimates was verified by using the document [53], which returns the experimental values of C_l and C_d of the same profile obtained with equal dimensions inside a wind tunnel. In order to be able to accept the FLUENT results, a set of simulations for both profiles was made considering the environmental condition in which the wind tunnel tests were carried out, ie Re = 300k. This value corresponds to a density value of 0.1947 kg/m^3, a viscosity of 1.42 Pa·s and a flow rate of 22 m/s with a characteristic length of 1m. The algorithm employed is the one already mentioned,ie $k - \omega$ SST. In Figure 4.29 are collected the data useless for validation step. In particular for the FX 63-137 airfoil, it is possible to confirm or neglect without doubt the validation test, while for the FX 61-147 airfoil there's no document available on wind tunnel test. From the image 4.29 it is possible to observe that the average error on results obtained from FLUENT is equal to 6.75 %, under the threshold of 10% while XfoiL gives data far away from experimental. Instead we can reasonably affirm that same error will realize with the FX 61-147 airfoil because there's a change in wall geometry but the fluid domain is still the same. For the 3D geometry, it is not possible to do a comparison with experimental or documented data, since the lofted geometry is obviously new. It will be interested to realize a 3D in scale prototype and analyse it in a wind tunnel. At this point the validation step and the entire CFD analysis procedure is concluded.

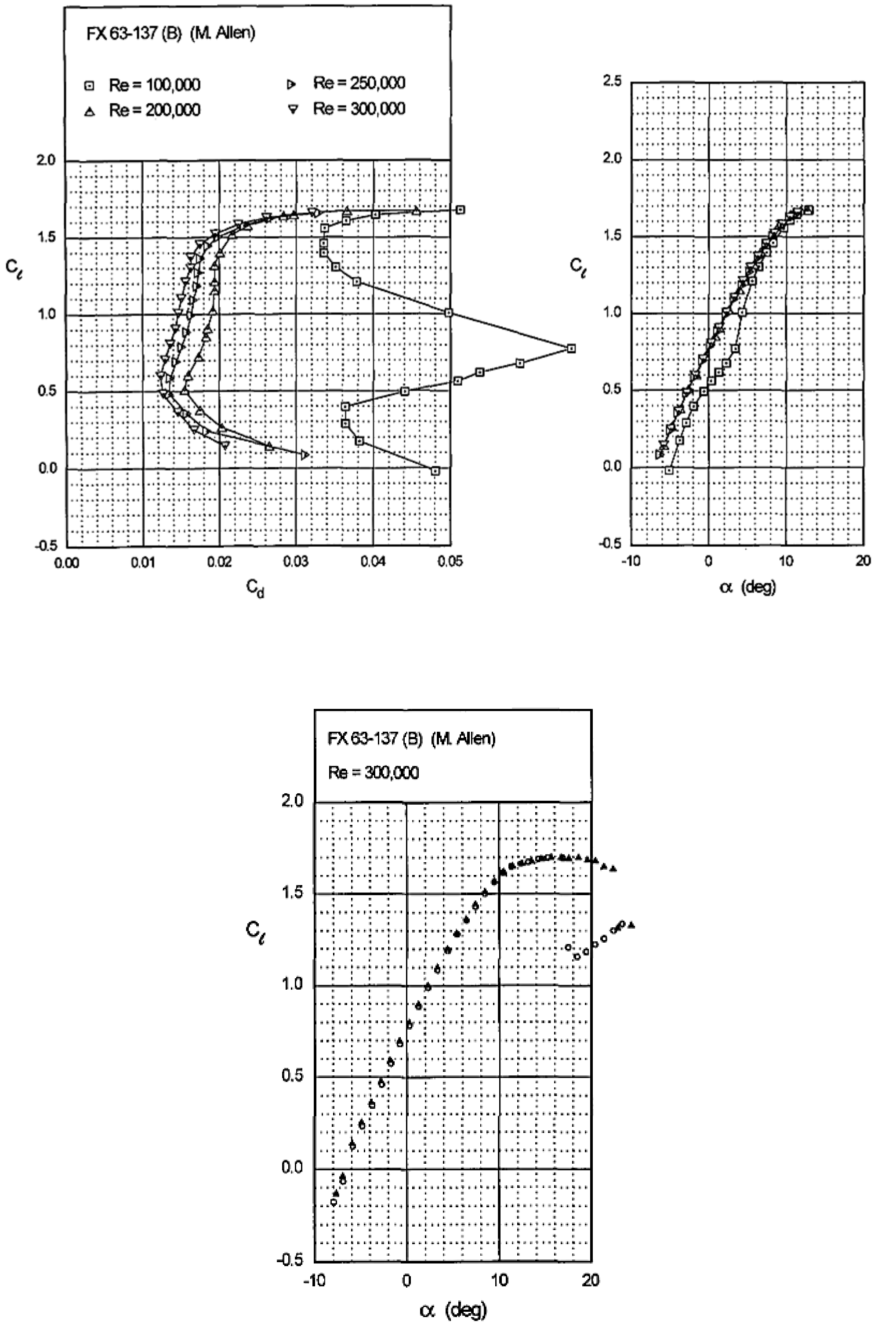

Figure 4.28: Airfoil FX 63-137 experimental data graphs on wind tunnel facilities [53].

Error % Cl Estimation Re=300k

	Alpha	Cl [CFD]	Cl [XfoiL]	Cl [Experiments]	Error %Respect to Experiments	
					CFD	XfoiL
FX 3-137	-2	0.5067	0.673	0.57	11%	14%
	0	0.717	0.9	0.75	4%	20%
	2	0.91125	1.125	0.95	4%	18%
	5	1.1453	1.43	1.25	8%	14%
				0		
					Errore % CFD respect to XfoiL	
FX 61-147	0	0.4383	0.5	/	12%	
	2	0.6527	0.714	/	8%	
	5	0.9474	1.04	/	8%	

Figure 4.29: Value gap between results given from **Profili2**®and **FLUENT**®against the experimental data obtained in a wind tunnel facilities [53].

In Chapter 3 and 4, an in-depth analysis was carried out on the preliminary aircraft aerodynamics, focusing on the correction of performance parameters in order to capture values closer to reality. A 2D-analysis CFD survey for both airfoil at Re = 1e6 and 750k was initiated, an environment in which the wings are located in order to confute or validate XfoiL values. There was a certain convergence of the C_l and C_d values within a range of 10 %. In particular, it is essential to specify how these numeric instruments are very reliable when it comes to modelling fluid behaviour for small angles, while the stall phenomenon can not be fully interpreted. In fact, regarding the C_l limit that the airfoil is able to reach, XfoiL points out that FX 61-147 reaches the stall for angles around 12; while FX 63-137 has the ability to make a stall controlled and stable but around the same angle. This finding is supported by ANSYS 2D analysis. However, if we want to be sure of the airfoil behaviour with a certain margin of safety, we notice that the linear variation of C_l ends around 10 degrees inclination. It can then be concluded that the zone from -2 to 10 degrees is fully described by both Xfoil and ANSYS, while above 10 degrees persists in a shadow area. The three-dimensional survey, however, shows a different behaviour. Although it has set the same solving algorithm for the fluid-dynamic problem, it seems that the so designed motorglider can guarantee a decent stability even at higher inclination angles, for example 15 degrees. This could be theoretically valid, since the introduction of the finite wing involves lower lift curve in favour of a greater stall angle. However, having experimental confirmation of profile behaviour and double verification with XfoiL and Fluent 2D, it is safe to affirm that the models are described with high reliability in fluid behaviour in the linear range of -2 to 8/10 degrees, while for higher α values it will be necessary experimental test on wind tunnel of some kind of prototype.

Chapter 5

The Self-Sufficient Electric Solution

5.1 Introduction

In this chapter we will discuss the preliminary dimensioning of the electric infrastructure consisting of batteries, photovoltaic panels and electric motors. We will not deal with a more detailed description of the elements presented in Chapter 1 but, if necessary, we will go into details as much as possible. This phase follows the methodology used so far. Starting from the requirements that arise from the aerodynamic section, an analysis of the state of the art and the identification of the specifications required for each electrical part are carried out. Then, will be selected a series of industries specialized on electric motor, until the final choice is reached. In this phase, certain assumptions will arise from practical observation that will allow to approach what might be the configuration to build.

5.1.1 Requirements for Energy Devices

The requirements for designing and dimensioning the energy system vary depending on the device we are referring to. However, generic constraints can be identified to ensure the integrity of the entire project. The maximum mass must be contained in the range of 35/40 kg, as specified in Chapter 1. In fact, the mass estimate and all aerodynamic calculations refer to an abstract aircraft but with all the elements present, ie 255 kg including both the structural part, the covering and the endothermic propulsion. However, knowing the gap between the mass estimation of a glider with respect to a motorglider of the same size and the same category, it is possible to impose it as a constraint for the propulsion group. Almost all motorglider are engineered modified gliders that contain engine, propeller, support structure and fuel tank. Another key factor is the occupied volume, a constraint that can be applied to the engine. From the geometry, the tail size is 0.11 meters diameter. This value can be increased by 50% by appropriately modifying the queue structure. As for batteries, they must have a high energy density as a result of weight constraint.

5.2 Estimation of ***Flying Power*** Required

Before proceeding with the investigation of electrical technology that best meets the requirements, it is necessary to identify those requirements. As mentioned above, they derive from the aerodynamic analysis and in particular a fundamental parameter for engine sizing and energy store evaluation is definitely the flying power, mentioned in Chapter 3. The most critical condition expected, is the take-off phase in which the aircraft must be moved from the ground to a required altitude. The data that will be collected from the study of this phase will be used for accumulators sizing. In Chapter 1, Glider requirements were mentioned, in particular the climbing phase had to occur with a climb speed of 2 meters per second. Consider this parameter and set a climb angle of 5 degree. The table shows the initial values.

Vz [m/s]	ρ [kg/m^3	θ[degree]
2	1.225	5

$$V_x = \frac{V_z}{tan(\theta)} \tag{5.1}$$

$$V = \sqrt{V_z^2 + \frac{V_z^2}{tan(\theta)}} \tag{5.2}$$

$$V = V_z \sqrt{1 + \left(\frac{1}{\theta}\right)} \tag{5.3}$$

$$V = V_z \sqrt{1 + \left(\frac{L}{D}\right)} \tag{5.4}$$

With equation 5.2, we obtain a module of the vector velocity equal to 23 m/s. Remembering that the stall velocity is around 17 m/s. The gap between these two values is common sense and is also reflected in ultra-light activity. The transition from equation 5.2 to 5.3 and 5.4 is possible assuming very little angle. Knowing the input parameters, we proceed as follow:

1. Evaluate C_L from equation:

$$C_L = \frac{W \cdot cos(\theta)}{0.5 \cdot \rho \cdot V^2 \cdot S} \tag{5.5}$$

   assuming that the glider is positively oriented to pull up and it has to climb its mass.

2. Knowing the required C_L value, from the converted parameters table, explained in Chapter 3, we derived the corresponding C_D value.

3. calculate the Thrust T [N]

$$T = D + W \cdot sen(\theta) \tag{5.6}$$

$$T = 0.5 \cdot \rho \cdot V^2 \cdot C_d \cdot S + W \cdot sen(\theta) \tag{5.7}$$

4. Calculate the required Power:

$$P[W] = T \cdot V \tag{5.8}$$

An other way to obtain the *Flying Power* is to use the equation:

$$P = \frac{C_L^{\frac{3}{2}}}{C_D} \tag{5.9}$$

but in this form we don't consider the velocity and other environmental properties that help to limit correctly the problem [18]. This is the common procedure, excluding the take off ride that is calculated simply using the Newton's second law. The radical hypothesis used in this method is that we assume the coincidence of the aerodynamic centre with the centre of mass to simplify calculation and obtaining first attempt value. It is not wrong to proceed in this way, indeed the distance between these two reference points is small compared to the entire glider dimensions.

At this point each flight configuration and the respective flight parameters cited above will be reported.

5.2.1 Take-Off Ride

In this Flight configuration the first parameters are presented in Table 5.1. Using the above method, it is possible to define:

V_z [m/s]	θ [deg]	ρ
2	5	1.225

Table 5.1: Take-off ride initial Value.

1. the required lift coefficient to provide flight

$$C_L = 1.05873 \tag{5.10}$$

2. The corresponding drag coefficient extrapolated from glider performance table on Appendix C

$$C_D = 0.05573 \tag{5.11}$$

3. The Thrust evaluated with the equation:

$$T = 0.5 \cdot \rho \cdot V^2 \cdot C_D \cdot S + W \cdot sen(\theta) \tag{5.12}$$

$$T = 348.985N \tag{5.13}$$

4. The Flying Power associated to this flight configuration is:

$$P = T \cdot V = 8026.65W \tag{5.14}$$

5. the take off ride assuming a take off runway of 200 m and starting from V=0 m/s and a constant acceleration:

$$s = 0.5 \cdot a \cdot t^2 \tag{5.15}$$

$$a = \frac{\Delta V}{\Delta t} \tag{5.16}$$

$$s = 0.5 \cdot V \cdot t \tag{5.17}$$

$$t = \frac{200}{0.5 \cdot 23} = 17sec \tag{5.18}$$

$$a = 1.35m/s^2 \tag{5.19}$$

$$F = m \cdot a = 344.25N \tag{5.20}$$

$$P_{decollo} = 5852.25W \tag{5.21}$$

$$P_{TOT} = 13878.9 \approx 15000W \tag{5.22}$$

5.2.2 Levelled Flight with Velocity Increment

Consider an aircraft on levelled flight that needs to increase its speed from 30 to 40 m/s at an altitude of 1500 m. The initial value are shown on Table 5.2

V_z [m/s]	θ [deg]	ρ	V_f [m/s]	V_i [m/s]
0	0	1.058	40	30

Table 5.2: Levelled flight with velocity increment initial value.

1. In this case, the required lift coefficient derived from a force balance system is explained as :

$$C_L = \frac{W}{0.5 \cdot \rho \cdot V^2 \cdot S} = 0.4068 \tag{5.23}$$

2. the associated C_D is

$$C_D = 0.03433 \tag{5.24}$$

3. the thrust to maintain the condition of levelled aircraft is

$$T_{40m/s} = D = 2010.95N \tag{5.25}$$

4. for the flight condition at 30 m/s, the required lift coeficient is

$$C_L = 0.723278 \tag{5.26}$$

5. and the corresponding C_D

$$C_D = 0.04393 \tag{5.27}$$

6. The required power to pass from 30 to 40 m/s is

$$P = \Delta P \cdot \Delta V = 591.098 \approx 1000W \tag{5.28}$$

5.2.3 Increase in Altitude

Consider the dimensioned glider at 1500m in a flight condition with the initial parameters presented below on Table 5.3 :

V_z [m/s]	ρ	V [m/s]	$\rho\ kg/m^3$
1	1.058	30	1.058

Table 5.3: Increase in altitude flight configuration initial value.

1. the corresponding climbing angle is

$$\frac{V_z}{V} = sen(\theta) \tag{5.29}$$

$$\theta = 1.91deg \tag{5.30}$$

2. The required C_L

$$C_L = \frac{W \cdot cos(\theta)}{0.5 \cdot \rho V^2 \cdot S} = 0.722876 \tag{5.31}$$

3. The associated drag coefficient from glider performance table on Appendix C

$$C_D = 0.04393 \tag{5.32}$$

4. The required Thrust

$$T = D + W \cdot sen(\theta) = 238.167N \tag{5.33}$$

5. The required flying power:

$$P = 7055W \tag{5.34}$$

5.2.4 Levelled Flight at $V_{L/D_{MAX}}$

To understand this flight configuration we need to evaluate the maximum efficiency velocity. This term depend on the minimum C_D value:

$$V_{L/D_{MAX}} = \sqrt{\frac{2 \cdot W}{\rho \cdot S} \sqrt{\frac{1}{C_{D_{MIN}} \cdot \pi \cdot AR \cdot e}}} \tag{5.35}$$

Results and initial value are shown on Table 5.4 Typically it is observed that

ρ [kg/m^3]	Altitude [m]	Re	l [m]	$C_{D_{MIN}}$	$V_{L/D_{MAX}}$
1.058	1500	1E6	0.627	0.0317379	23
0.957	2500	750k	0.627	0.0218945	27

Table 5.4: Maximum efficiency velocity and initial value.

$C_{D_{MIN}}$ decreases as ρ decreases and altitude increases. However, on $V_{L/D_{MAX}}$, density variation is more influence than C_D variation.

1. The required C_L at 2500 m for levelled flight is equal to :

$$C_L = 1.05174 \tag{5.36}$$

2. the corresponding C_D

$$C_D = 0.055733 \tag{5.37}$$

3. Required Thrust

$$T = 132.478N \tag{5.38}$$

4. and finally the required Flying Power

$$P = 3465.37W \tag{5.39}$$

5.3 Photovoltaic Panel Choice and Configuration

The device used to recover energy from the primary source, that is solar energy and consequent transformation into electricity is the photovoltaic module. Photovoltaic technology, already described in Chapter 2, has been selected with reference to commercially available energy solutions and therefore immediately obtainable and configurable. The essential requirement for the correct choice of photovoltaic technology can be translated as the optimal compromise between surface available, efficiency and weight. In particular, two technologies were chosen: monocrystalline silicon photovoltaic panel, with a 25 % efficiency and a flexible amorphous silicon photovoltaic panel with optimized efficiency of 15%. The most efficient monocrystalline photovoltaic panels are encapsulated in a structure that binds their movements and are naturally more rigid unlike amorphous plates. They also have minimum dimensions fixed at 10x10 cm. This would make the surface mosaic-process very critical, and even if it was possible to achieve a good coverage, it would be necessary to have modules of a few centimetres between them, resulting in increased Joule losses. If the top surface was coated with monocrystalline modules, given their rigidity, it would risk getting a segmented rather than curvilinear airfoil. This is not acceptable to comply with aerodynamic requirements. From these theoretical and preliminary considerations, it was concluded that it is possible to cover only a fraction of the overall surface area available. This choice is also confirmed by the fact that complete surface coverage, in addition to generating the above-mentioned harmful effects, would also result in critical electronic control management and in an effort to simplify energy absorption. Indeed, the incidence of electromagnetic radiation that we can consider parallel on a small surface compared to Earth, on a curved airfoil such as those adopted, would result in an increase in radiation gradients processed by the photovoltaic panel and consequently of transformed energy with the result that one part of the mass of the panels is not exploited.

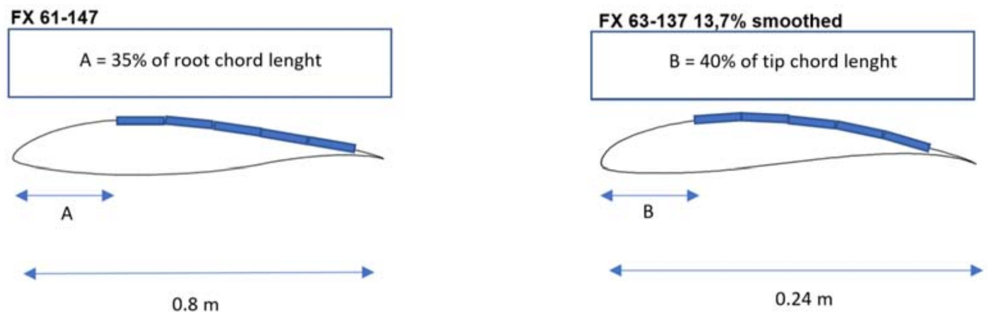

Figure 5.1: Compromise choice based on a surface curve radiance evaluation; minimize losses, maximize energy acquisition[56]; image for qualitative purpose.

For these reasons, it was considered the airfoil exit region as part to be covered, 35% of the chord for FX 61-147 and 40% of the chord for FX 63-137 due to the greater curvature. These values are related to the use of monocrystalline silicon photovoltaic technology as an energy solution. The result is a total available area of 4.67 m^2 for wings, to which part of the tail plan surface is added, resulting to 5 m^2. In the case of adopting amorphous silicon photovoltaic technology, more versatile than monocrystalline but with lower efficiency, the surface that could be covered is almost total: excluding the nose of the airfoil by removing about 10% of the chord, a total surface of $6.53m^2$ is obtained which, together with the tail plane, leads to 7 m^2. The fact that amorphous available area is different from monocrystalline silicon is because the amorphous silicon requirement for the mass is secondary as they are generally lighter than monocrystalline silicon and excluding a few square meters of surface will not favour a noticeably lowering of the mass. With this technology it is therefore preferable to set as the primary objective the maximum solar acquisition due to lower performance. In this way it can become a competitive technology. In Figure 5.2 is shown the selected area for photovoltaic technologies presented above. Practical and historical

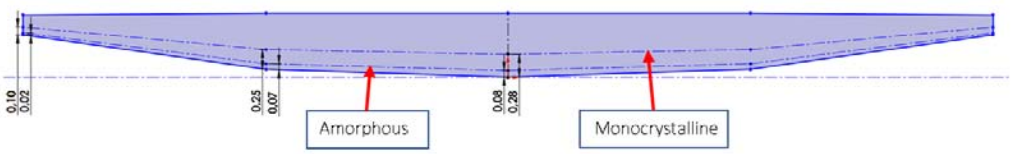

Figure 5.2: Comparison between photovoltaic silicon monocrystalline area respect to photovoltaic silicon amorphous technologies. Dimension in meters.

example are the Solong airplane and NASA project Helios, which mounted solar cells with an efficiency of 20%, silicon monocrystalline technology-based. By contrast, amorphous silicon solar cells with an efficiency of 10 % were used for the Zephyr because thin film solar cell can be bent to fit into the curved wing [26].

5.4 Solar Radiance Evaluation

After defining the two most suitable photovoltaic technologies for this project, it was necessary to identify parameters to which realize a comparison in term of performance. In particular, an energy assessment has been carried out, proceeding as follows:

1. obtaining average monthly solar radiation thanks to the interactive

PVGIS[1] web software, from which was obtained data shown on Figures 5.3, 5.4 and 5.5;

2. approximate calculation of the temporal integer considering a 4-hour interval in the phase of maximum solar radiance;

3. From this last data, was obtained the product with the wing surface selected for each technology;

4. it was then multiplied by the efficiency (η);

5. Finally, the energy values in Watt-hour were obtained in the case of a 1 hour, 2 hours and 3 hours recharge;

The average monthly radiation and the daily radiation intensity trend, have been evaluated for 4 different cities, located at distinct latitudes, from polar to the tropics, and are: Oslo, Padua, Syracuse and Cairo. The values that have been considered refers to the condition of *Global Real Sky*, by which PVGIS provides the trend of radiation on a hypothetical day based on the average of the perturbation phenomena occurring during the selected period. For each of the countries considered, the radiation intensity distribution was evaluated in a hot(July) and cold(December) month, on a reference plan oriented at 0 degree inclination and 0 degree azimuth. This was done in order to obtain an exhaustive analysis of the energy system potential in the underlying hypothesis that the designed motorglider should be marketed. From the images 5.6,5.7, 5.8, 5.9, it can be seen how the solar radiation intensity perceived to the ground changes with the latitude and year period. Also, as can be seen from figure 5.9, the two configurations tend to be equal in terms of acquired energy. Amorphous silicon photovoltaic technology is slightly lower in performance, although it has an higher surface area exposed to solar radiation. Finally, the energy-storage apparatus was designed: sizing batteries. The role of accumulators is to store energy that is fed into them to make it available when required. From the reference [26] it is evident that in the first prototypes of fully solar propulsion aircraft, state of the art of batteries was the bottleneck of the whole project, a feature of performance deficit. Battery technology has evolved since twenty years ago, thanks to the introduction of lithium-ion battery that guarantee high capacity, uniform discharge and high voltage at minimum weight. This technology is widespread in all mobile device, from smartphones to innovative electric cars. Before

[1] *Photovoltaic Geographical Information System* provides a map-based inventory of solar energy resource and assessment of the electricity generation from photovoltaic systems in Europe, Africa, and South-West Asia [54].

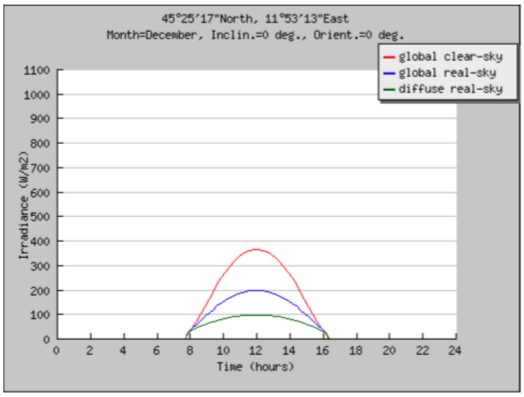

(a) Solar Radiation evaluated in Padova on December.

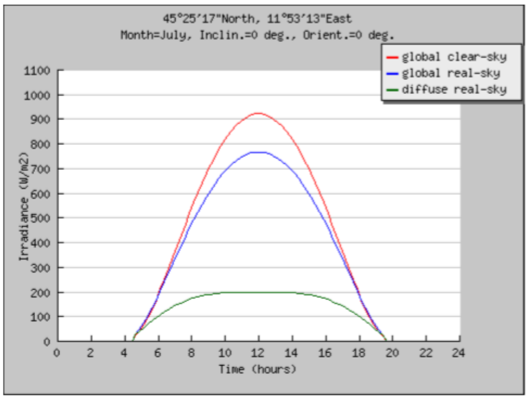

(b) Solar Radiation evaluated in Padova on July.

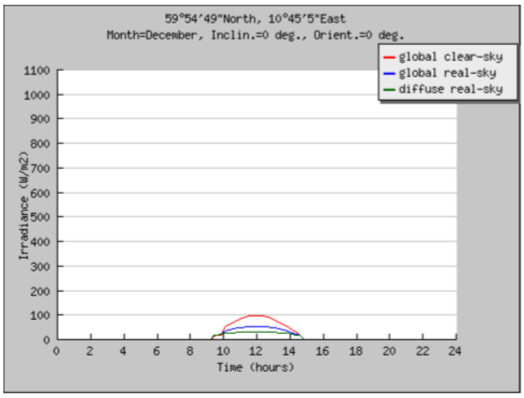

(c) Solar Radiation evaluated in Oslo on December.

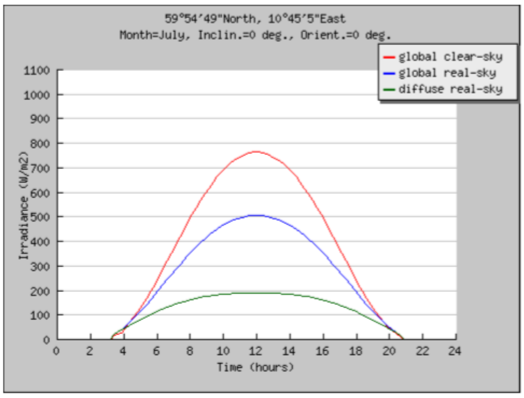

(d) Solar Radiation evaluated in Oslo on July.

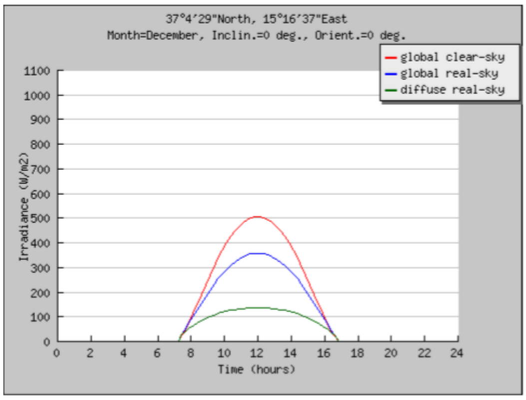

(e) Solar Radiation evaluated in Siracusa on December.

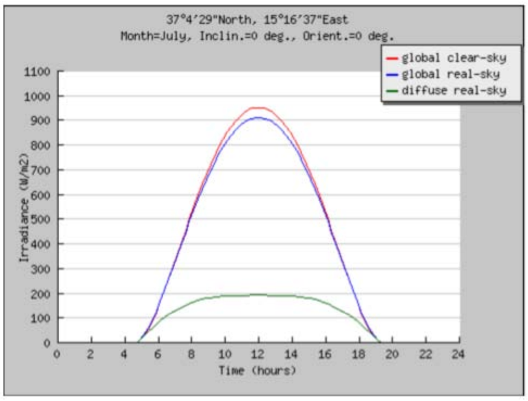

(f) Solar Radiation evaluated in Siracusa on July.

Figure 5.3: Solar radiation evaluated thanks to PVGIS[55] interactive web program for different locations.

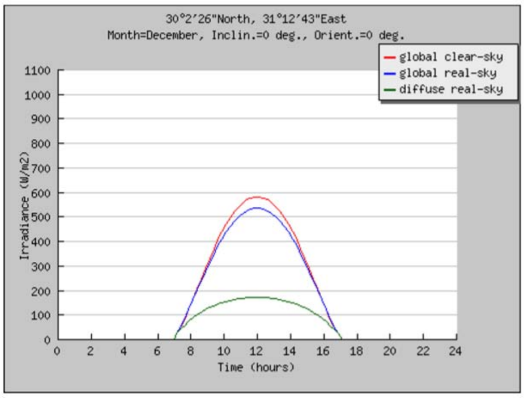

(a) Solar Radiation evaluated in Cairo on December.

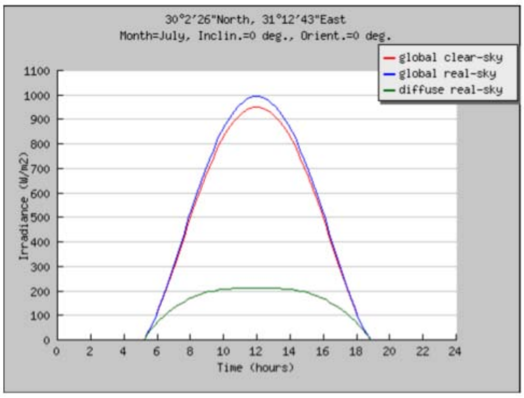

(b) Solar Radiation evaluated in Cairo on July.

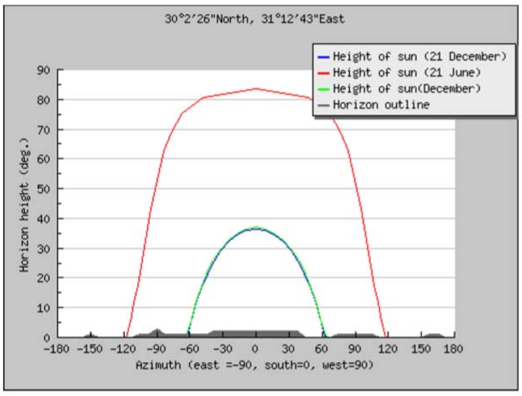

(c) Horizon height in Cairo on december and winter solstice.

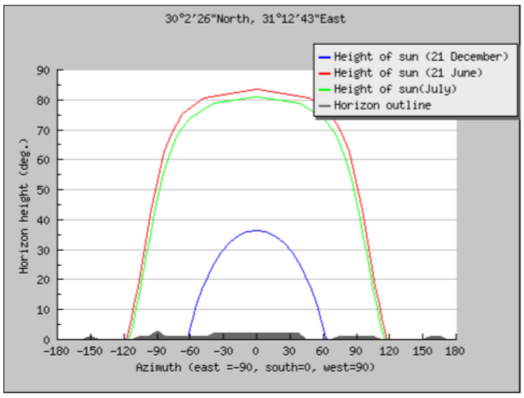

(d) Horizon height in Cairo on July and summer solstice.

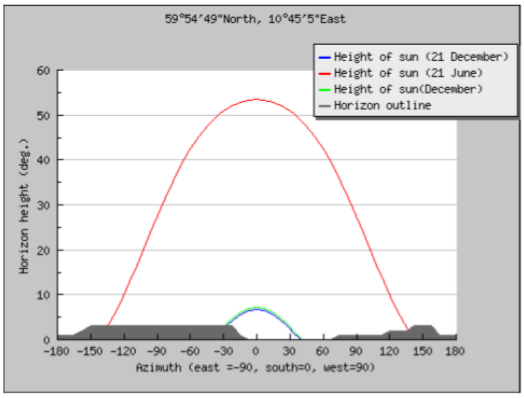

(e) Horizon height in Oslo on december and winter solstice.

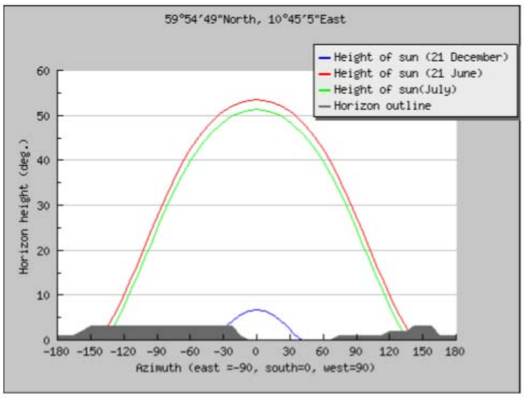

(f) Horizon height in Oslo on July and summer solstice.

Figure 5.4: Solar radiation and horizon height evaluated thanks to PVGIS[55] interactive web program for different locations.

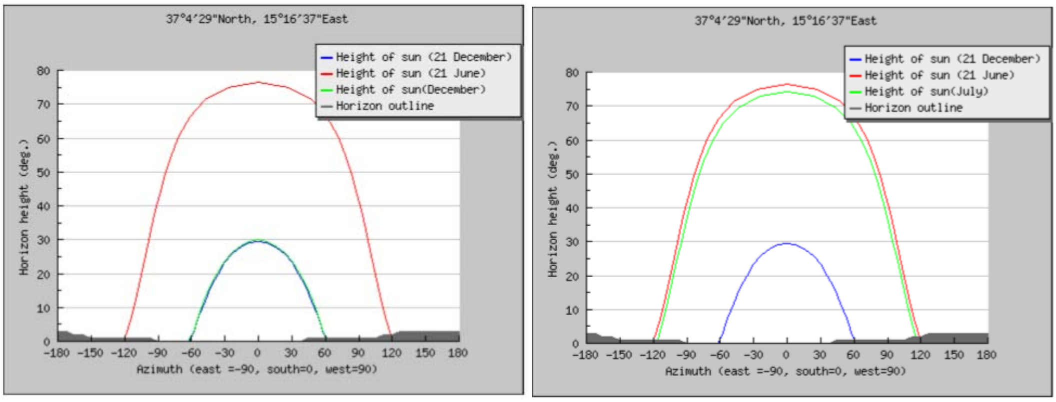

(a) Horizon height in Siracusa on December and winter solstice. **(b)** Horizon height in Siracusa on July and summer solstice.

Figure 5.5: Horizon height on July and December in Siracusa[55].

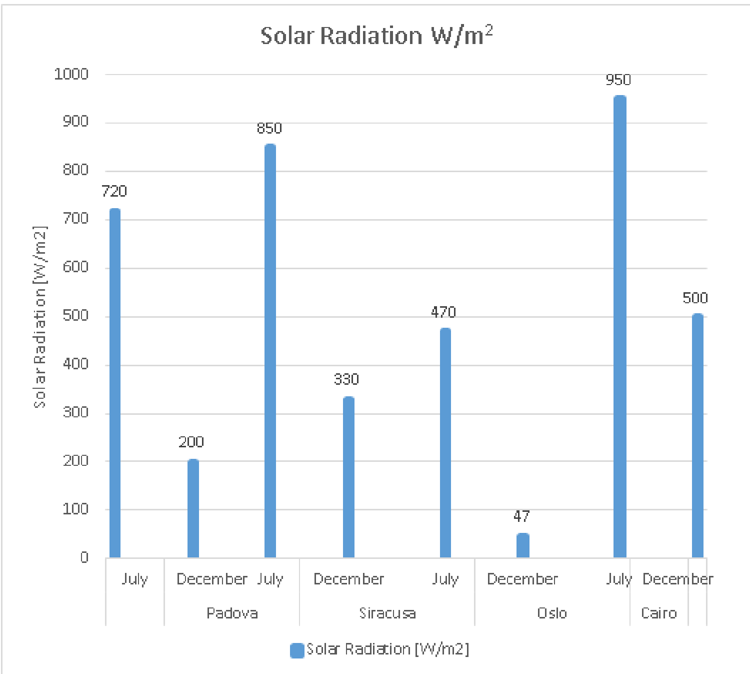

Figure 5.6: Solar Radiation specific energy [W/m^2] for different location at different latitude evaluated thank to PVGIS considering *Global Real Sky*[54].

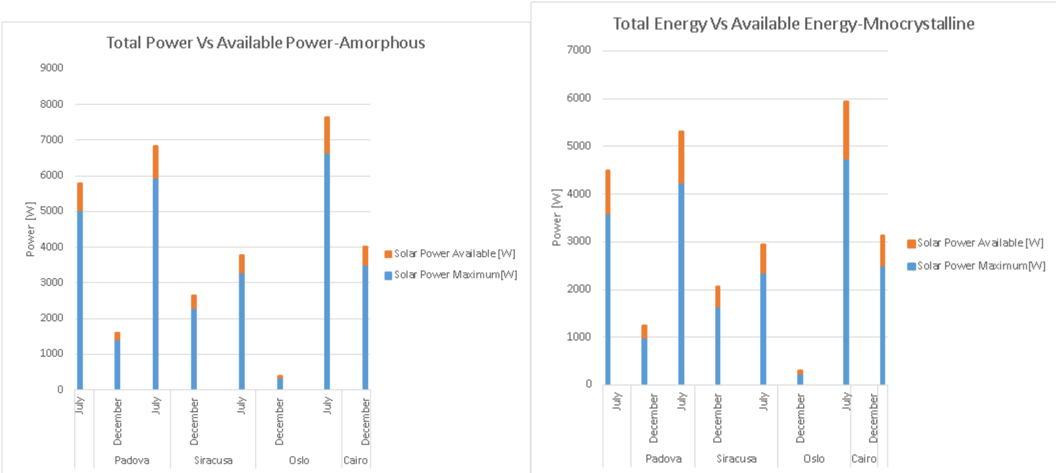

(a) Total vs available energy on selected wing surface for silicon amorphous photovoltaic panel($\eta_{Amorphous} = 15\%$).

(b) Total vs available energy on selected wing surface for silicon monocrystalline photovoltaic panel($\eta_{Monocrustalline} = 25\%$).

Figure 5.7: Comparison between the total and available($\eta_{Monocrustalline} = 25\%$, $\eta_{Amorphous} = 15\%$) energy can be acquired on exposed surface [54].

defining the battery specifications, it is important to look into some important aspects. First, *capacity* is defined as storage energy in the accumulator. It is measured in [Ah] and is the time integral of current supplied by the cell at room temperature until the cell reaches the cut-off voltage; the *specific energy* indicates the energy that can be discharged from the accumulator per unit of mass [Wh/kg]. Capacity is affected by discharge current, temperature, and cut-off voltage. Specifically, as seen from Figures 5.10, capacity is calculated over time intervals. If you plan to fully dissipate the entire battery pack in minor time, then the pull-out capacity decreases and the current intensity is very high. Capacity sensitivity at different discharge regimes is very low for lithium-ion cells. Operating temperature is another factor affecting performance. In particular, for lithium technology, lower temperatures mean lower performance, although generally ohmic losses are lower. In fact, resistivity is also a function of temperature. In any case, the variation in capacity when changing the discharge system has been taken into account in the size of the batteries. The temperature sensitivity of the cell can help you to capture the upper altitude limit operability, surely within the troposphere. From the state of the art on lithium-ion batteries, it was reasonably chosen to consider those that have a specific energy of 250 Wh/kg. The battery dimensioning was performed in the worst condition, that is, where the highest power is required. This is the take-off phase. According to estimates previ-

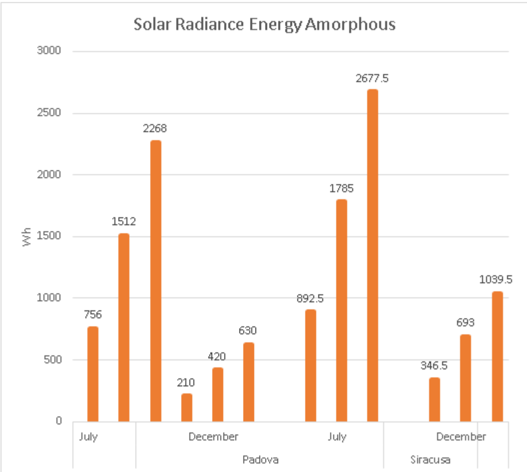

(a) Solar Radiance energy acquired from amorphous silicon photovoltaic panel.

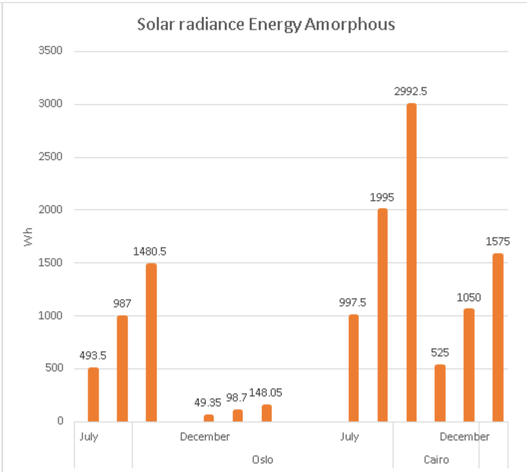

(b) Solar Radiance energy acquired from amorphous silicon photovoltaic panel.

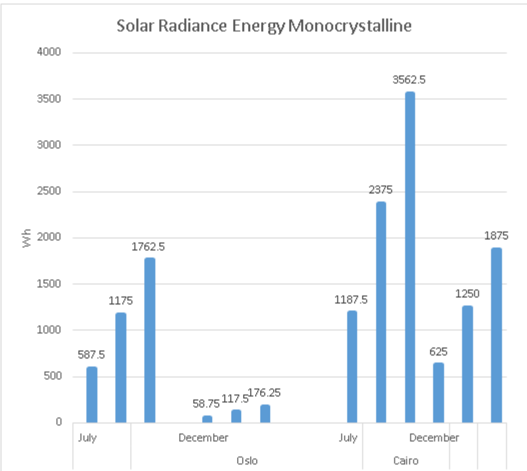

(c) Solar Radiance energy acquired from monocrystalline silicon photovoltaic panel.

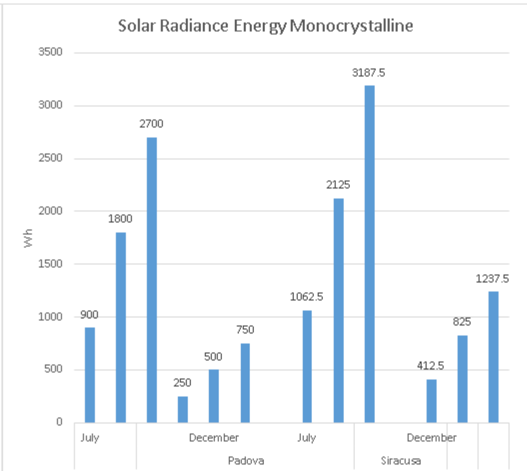

(d) Solar Radiance energy acquired from monocrystalline silicon photovoltaic panel.

Figure 5.8: Energy can be acquired in different location on silicon monocrystalline and amorphous technology-based photovoltaic panel[54].

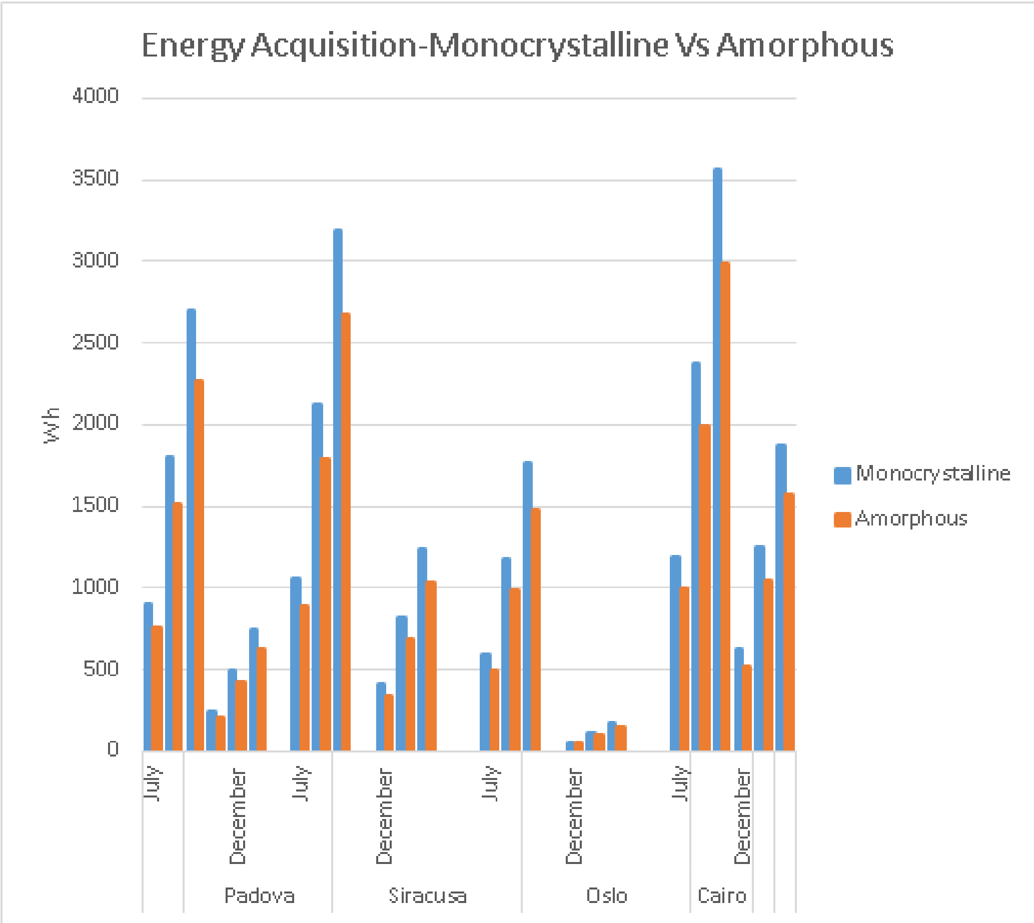

Figure 5.9: Direct comparison between energy acquired from monocrystalline and amorphous silicon technology-based photovoltaic panel[54].

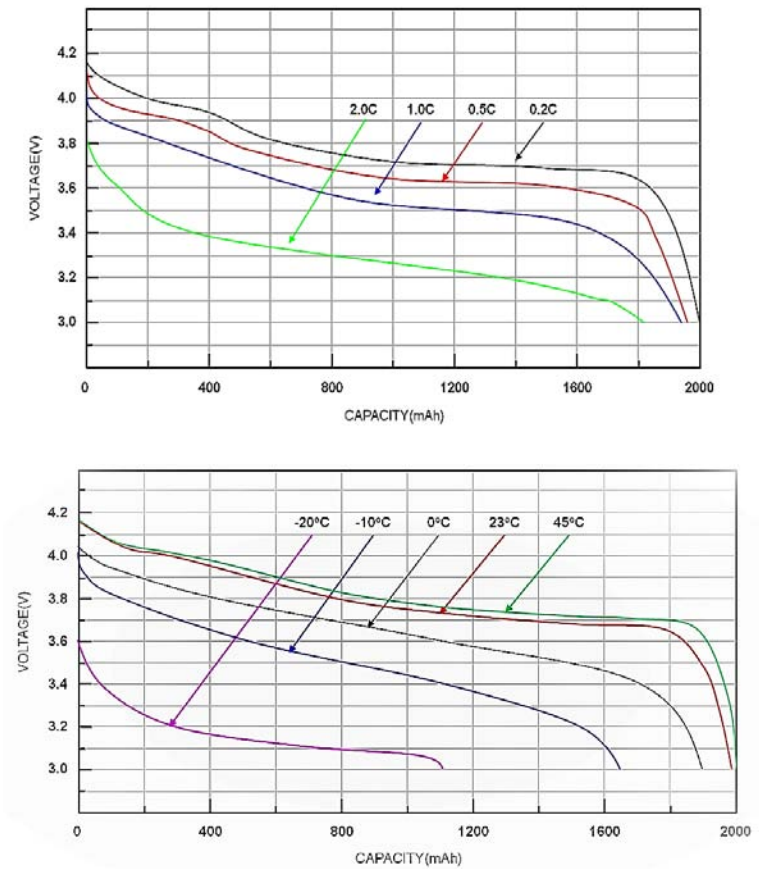

Figure 5.10: Li-Ion cell performance variation, depending on time discharge and temperature[58].

ously made, the required take-off power is approximately 15 kW. Assuming that the ascending phase is reasonably attested to around 5 minutes, ie 300 seconds, we get the total energy:

$$E = 15000 \cdot 300 = 4500000Ws \tag{5.40}$$

$$E = 1250Wh \tag{5.41}$$

The energy density value 250 Wh/kg have to be modified to consider the time discharge influence(10% lost) and also to preserve the battery wellness(20% loss). The final value is around 180 Wh/kg. Also the total energy required for the take-off has to be varied, indeed a battery can't develop its entire capacity. A 25 % energy reserve was considered. If an energy amount of 1250 Wh is required, means that we need to recharge batteries until 1700 Wh energy amount is reached. With 180 Wh/kg batteries, the total required mass is around:

$$W_{Battery} = \frac{EnergyRequired}{EnergyDensity} = \frac{1700}{180} = 9.4kg \approx 10kg \tag{5.42}$$

The previous Figure 5.9 is now updated (5.11) to evaluate which are the conditions where we are sure to recharge the vehicle and which the energy is not sufficient. From figure 5.11 it is possible to observe that every winter

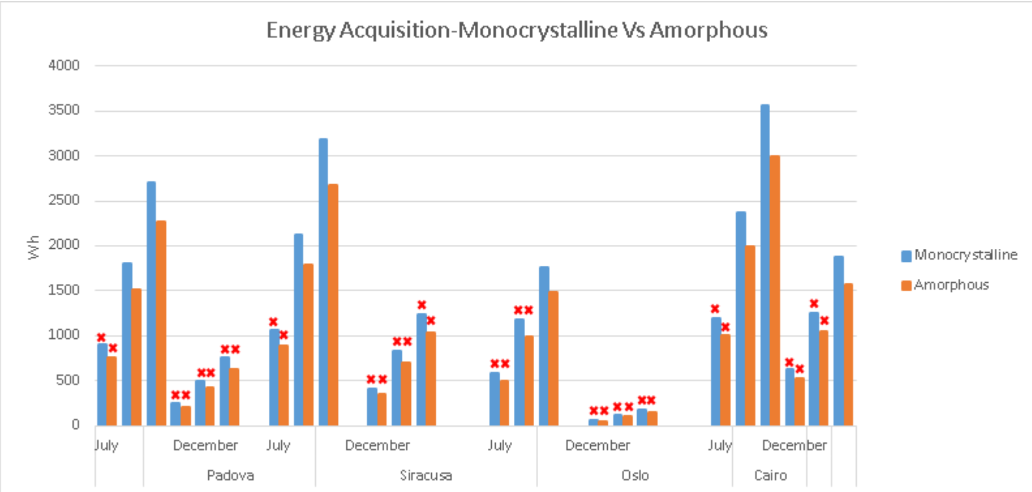

Figure 5.11: Define rechargeable temporal limits based on energy required for take-off.

from Polar to tropics it is impossible to reach 1700 Wh based on the defined radiance value, except in Cairo in December, 3 hours is sufficient for both technologies. In Oslo it is impossible for monocrystalline as for amorphous to reach the required energy in a 3 hours limit time. In 2 hours we can develop the required energy for take off in Padua and Syracuse in summer. In Oslo we need almost 3 hours in summer to complete the charge phase.

Assume to be in flight with batteries complete charge at 1700 Wh and 1250 Wh delivered energy. This can happen if the glider is driven by other airplane or during a 2-3 hours flight with perfect ”seeing” condition. With this energy storage, we analyse the other flight configurations:

1. 7 kW power required for altitude acquisition. The permitted time flight is approximately:

$$t = \frac{1250}{7000} \approx 11'(min) \tag{5.43}$$

2. 3 kW power required for levelled flight in best L/D condition

$$t = \frac{1250}{7000} \approx 25'(min) \tag{5.44}$$

5.4.1 Photovoltaic Panel Mass Estimation

For the estimation of the mass of photovoltaic equipment, values from the datasheet of several manufacturers will be used which will be proposed and analysed below. In particular, the photovoltaic panel density value was obtained and then applied to the surface made available for energy absorption.

On Table 5.5 and 5.6 are reported different types of photovoltaic technology

Prod.	Type	Dim. [mm]	Weight [kg]
Terasol GSC 150	Flex	1375x670x1.5	2.81
Solbian SP78	Flex	855x546x2	1.1
SoloPower SP1	CIGS	2187x400x2	2.1
MR Watt	Rigid	156x156x0.25	13E3
MR Watt	Rigid	125x125x0.25	10E-3
MR Watt	Rigid	52x156x0.25	5E-3

Table 5.5: Comparison between commercial flexible and rigid photovoltaic alternatives

that are marketed. The difference in terms of mass between rigid and flexible is clear but also the efficiency variation. The calculation of rigid panel type mass considered the same thickness of flexible structure. Indeed rigid panel dimension are referred to a single cell with no covering elements. Typically,

Prod.	ρ [kg/m^3]	S [m^2]	Mass [kg]	η
Terasol GSC 150	1671	7	17.5	16.4 %
Solbian SP78	1178	7	16	15 %
SoloPower SP1	1200	7	16	11 %
MR Watt	2136	5	21.36	25 %
MR Watt	2560	5	25.6	25 %
MR Watt	2465	5	24.65	25 %

Table 5.6: Mass estimation based on available surface for energy absorption.

rigid panels request stronger structure and this increases a lot the final mass. However it is necessary to maintain perfectly oriented the cells.

The author suggests to consider for this project the Flexible photovoltaic amorphous technology for the following reasons:

- There are previous works on electric autonomous aircraft that use this type of photovoltaic panel
- Efficiency difference between flexible and rigid monocrystalline has been reduced from 20 years and the amorphous technology will be improve in future while rigid monocrystalline photovoltaic panel are technologically saturated
- more versatile, reaching almost same energy level respect to monocrystalline thanks to the ability to be bent and covering more wing surface
- Less weight thanks to the absence of rigid structure but able to be protect by a plastic cover

5.5 Electric Motor Choice and Configuration

The electric energy converted from photovoltaic panel an then stored on accumulators, is finally transformed into kinetic energy by using propulsion device. The main parts that form the propulsion group are motor, gearbox and propeller. In this work, only requirements and best suitable motor from market will be execute, since the complete sizing will required depth analysis on electric engine functionality, dimensioning of the gearbox and last but not least dimensioning of the propeller that it's a rotate wing. These three terms can be sized perfectly after an iteration process that defines the best compromise parameters. Firstly the engine position was considered. From database and other motorglider project, engine is located frequently on glider nose(5.12: A), on a tractor-propulsion configuration. Rarely was realized an other engine configuration type, called push configuration(5.12: B and C). From the reference [46] we find that pushing configuration has significant advantages from the aerodynamic point of view. In fact, thanks to this configuration, it is possible to reduce the size and consequently the wetted area of the fuselage, while also reducing the drag. Furthermore the clean conditions over the nose will help to maintain laminar conditions over the fuselage profile. Differently from tractor propeller position that makes fuselage flow totally turbulent. Refer to pushing configuration, the motor can be located on top(5.12: B) or on base (5.12: C) of the vertical stabilizer. The first one have motor and propeller positioned on top of the vertical stabilizer. However, this disposition of the propulsion system would involve the action of no negligible bending moments in the joining sections such as the one between the tail plan and the fuselage. Therefore, it would be necessary to increase the diameter of the tail-end or considerably increase the entire fuselage, resulting in a mass increase. The second one considers the pushing propeller on the fuselage end. In this way, the engine torque and propeller push-force is recognized directly along the main resistant structure, that is the longitudinal beam, without secondary effects or any amplification. For these reasons the pushing propeller configuration placed on the fuselage terminal was chosen.

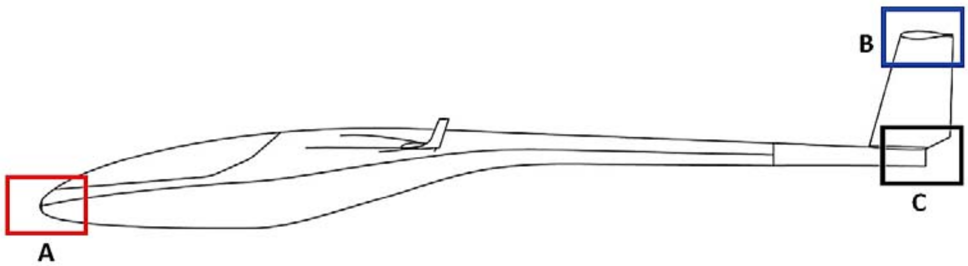

Figure 5.12: Possible location for electric brushless motor.

First of all was necessary to consider the propulsion group requirements to investigate more precisely the commercial solution. For this reason, thanks to [18] a change on power flight parameters was done. Indeed this values refers to the power aircraft have to exert on flow to respect the imposed conditions. The flying power is multiplied for the propeller and motor efficiency, to obtained the power required to the engine. On Table 5.7 shows the final results. An efficiency of 95 % for both propeller and motor is reasonable basing on existing brushless motor and propeller datasheet. The gear box is not considered in this case to limit the fail probability, complexity and reducing power levels. The propeller is inserted directly on motor shaft. Thinking on the motor type, the best choice is the brushless synchronous permanent-magnet electric motor which exhibit great performance, almost no degradation due to contacts, high velocity, little dimensions and mass[26] [18]. Thanks to their performance, a market research was conducted to recognize the best suitable electric motor, basing on the requirements show on Table 5.8 In the brushless motor category there are predominantly two branches: permanent isotropic SPM magnet and anisotropic IPM. The fundamental difference is present in the rotor: in SPM the rotor is a permanent magnet which dimensions permit to have the same properties in every direction you look at, that is isotropic characteristics. On the contrary, the IPM type has a different rotor, which creates an anisotropy of the inductance that increases the torque produced. However, the latter have complications in terms of construction and, as a compromise, SPMs are preferred.

Flight Conf.	Theoric F. P. [W]	η_{motor}	η_{prop}	Required M. P. [W]
Take off	13879.00	0.95	0.95	15301.60
Climb	7055.00	0.95	0.95	7778.00
Levelled L/D_{BEST}	3465.37	0.95	0.95	3820.16

Table 5.7: Evaluation of the ultimate required power from motor, knowing the flight power and assuming reasonably η_{motor} and $\eta_{propeller}$ equal to 0.95%.

Mass Max [kg]	Trasversal Dimensions [m]	Peak Power
10	11x11	15 kW

Table 5.8: Motor requirements and specifications.

Three companies, worldwide present with their products, have been selected. They are : **Lafert**, **NGBe** and **FES**. The latter is a producer of advanced systems for glider propulsion only. In order to make a reasoned choice on the engine to be chosen, it is also necessary to know the round per minute required, so that the propeller can generate the required flying power. This, however, depends on the propeller's performance, which is linked to the propeller design. For this reason, reference was made to an average performance value of 95% for the propeller (optimistic) and then to evaluate the motors presenting the best rotation speed for that application, ie at high rpm. In fact we know that the characteristic torque is inversely proportional to the speed. Therefore, those engines that run low torque but high speeds are required. This is also reflected in the bibliography. However, it should be emphasized that the actual engine choice is essentially based on flying power requirements, according to engine and propeller efficiency, volume and weight. It will be the task of the propulsion team to look for the best propeller profile in order to get the best performance from the entire system.

By comparing the datasheet of the products provided by the first two companies, it was noted that although power, efficiency, and performance requirements were met, we surpassed mass and volume. This is because these companies are concerned with creating electric motors for industrial purposes with different parameters and requirements from the environment in which this project is based. While the FES product, thanks to its experience and the development of aeronautical solutions, offers reliability lowering constructive complexity as it is not necessary to adapt an industrial component for aeronautical use. For these reasons, it is the author's thought to adopt the latter system for the propulsion apparatus. As you can see from Figure 5.13, the parameters are really near respect to these obtained before. With this electric motor solution, the FES producer have created special propeller to mount on the nose and obtained best performance from the electric motor.

(a) Electric brushless Motor, sinchronous permanent magnet.

Maximum torque	75 Nm
Maximum current	200A
Maximum Voltage	116V
Rpm non loaded	45 rpm/V
Rpm non loaded (at 116V DC on Controller)	5300 rpm
Non loaded motor current (at 5300 rpm)	16-18 A
Rpm loaded with FES-DIS-P1-100 propeller (1m diameter)	4500 rpm
Battery current loaded (4500 rpm, 116V) with FES-DIS-P1-102	Up to 200 A
Rotor rink diameter	182mm
Motor length	100mm
Motor weight cca.	8,0 kg
Motor efficiency	82-95 %
Maximum allowed temperature	90 °C
Minimum allowed starting temperature	-20 °C

(b) Performance of the Fes Motor system.

Figure 5.13: The electric brushless motor device, develop to satisfy motorglider requirements.

(a) Propeller develop for best suit the electric motor performance.

Number of propeller blades:	2
Maximum power on a propeller shaft:	23 kW;
Maximum rotational speed:	4500 RPM;
Propeller blade mass excluding attachment bolts:	approximately 260 g each blade;
Diameter of the propeller:	d=1000 (+20,-0) mm;
Service time between periodic controls:	50 hours or 12 months
Service time between special controls:	200 hours
Type of propeller:	tractor;
Sense of rotation:	clockwise looking at direction of flight.
Operating conditions:	the propeller can be operated in any normal environment conditions except hail, sand storm or similar.

(b) Perfomance of the propeller.

Figure 5.14: FES propellers created to obtain best performance from the electric motor.

Chapter 6

Results Summary and Future Developments

The main purpose presented in this thesis refers to the conceptual development and the preliminary dimensioning of a motorglider. This aircraft must be designed to meet the acrobatic requirements of aeronautical regulations and ensure a high level of safety and performance thanks to an innovative electric propulsion system.
The project developed in this thesis, thanks to the contribution of the University of Padua and the AeroLab research group for the advanced design of ultralight aircraft, is the basis for future design studies aimed at the realization of an electric motorglider. The transition from the endothermic to hybrid or fully electric motor is already undergoing advanced development in the automotive sector and is also beginning to affect aeronautical products. This process si driven by the demand to optimize aircraft costs in terms of fuel consumption and maintenance, but also to respond to the irrefutable consumption of fossil fuels, which are going to run out. In this environment, the interest of the University of Padua, Aerospace Engineer faculty, was motivated to start this project. The main purpose is to investigate the major project strategy on glider development, define the constraints and give some input parameters to next researchers generation. The production of a new aircraft is initially carried out by identifying the requirements and constraints provided by the regulations or recognized in the environment where the vehicle will be operational. It is distinguished by military or civil aircraft, then the subcategory to which the aircraft will belong to is selected. In each aeronautical factory, several design teams are involved, each employing a different task and specializing in areas such as safety, combustion, armaments, payloads and so on. The project begins to be real over years as a result of continuous iterations between the groups that make up the entire design chain. This thesis focuses on the preliminary phase of the realization of a new aircraft, focusing the attention of the reader on specific issues, while maintaining a certain level of global generality. From the moment when the first requirements, wing opening and aircraft manoeuvring skills were entrusted, extensive research has been carried out on motorglider produced worldwide, commercial and prototype from the 70s to present days. Indeed, it is precisely in this timeframe that the most innovative projects are recognized and thanks to which an overall design has become a standard for the industry. A conventional historical-statistical approach to design has therefore been chosen, first of all to investigate the history of similar products that have already been established on the market and which have undergone a process of validation of the technical characteristics. A database has been created containing 170 and more aircraft, sailplanes and motorglider, with massive properties and aerodynamic performance. Based on this database it was possible to discern important information such as the ratio between to-

tal mass and wingspan, between length and wingspan, between aspect ratio and aperture, between surface area and weight. This information has been synthesized within graphs from which trend curves have been extracted that minimize the average quadratic deviations of the error, in obtaining that law that best represents tabulated values. The aspect ratio was set at 20, the average value for a conventional glider, followed by a wingspan of 12 meters and a total length of 5 meters. By the limits imposed, these represent the values that should also allow for resistance minimization. With these values, proceeded to estimate the final mass of the aircraft, empty and with pilot. Two methods were used, both statistical but referring to different database. The method of the foremost designer Reymar relates to the use of a power equation based on a database he created; the second refers to the database created ad hoc and present in appendix A. With the first method of iterative nature, a mass value of 255 kg with an 85 kg pilot was estimated while with the second method, the mass value is similar but with 65 kg pilot. It is assumed to be in safety condition assuming that the empty mass is greater than and equal to 190 kg to accommodate a structure that meets the rigidity requirements necessary for performing acrobatic manoeuvres and the propulsive compartment. This is an estimation, a starting value and it is the standard to proceed in the manner just quoted. This value will then be investigated when the material and the final design are available. However, this mass estimate should be of greater value than the final result.
Then the wings, the lift surfaces of the aircraft and the, metaphorically speaking, heart of the plane were made. Following the documents in the bibliography were identified those wing airfoils that satisfy requirements of high efficiency, low drag, high flying power and uniformity of lift as well as stability for low Reynolds number. Two airfoils were chosen: FX 61-147 to the root and FX 63-137 at the end, to ensure high stability near the stall. The performance analysis of these profiles took place as the number of Reynolds changed. In addition, from the study of the lift curves of the individual profiles, made with the XfoiL software implemented in a graphical interface **Profili2**®, the wing was twisted so that the root is clockwise inclined by 1.5 degrees while the end is counter-clockwise twisted of 1 degree, respect to the fuselage. The whole gap, 2.5 degrees, corresponds to the difference between the two airfoil lift curves. The stall phenomenon has been shown in the range of 10 to 13 degrees inclination. Subsequently, was followed the instructions of prof. Pajno, professor of Turin Polytechnic and gliders designer. In particular, reference was made to the University of Delft studies with which Pajno collaborated in order to select the most suitable wing configuration for this project. At the same time, the virtual building process or LOFT of the glider has begun thanks to the **SolidWorks**®software, which consists in the rep-

resentation of external surfaces. The wing so constructed according to the experimental evaluations of prof. Pajno has a double taper and a total area of 7.3 m^2. The tail plan has been identified which guarantees a level flight stability. At first approximation, the surface is 0.76 m^2 with a symmetric biconvex airfoil that develops a $C_{L_{Tail}}$ of 0.5 while the wings develop a $C_{L_{wing}}$ = 1. The T-tail plan was made following Reymar's position indication, by placing it in height so that the turbulent flow at stall condition generated by wings does not invade it. The aerodynamic parameters of XfoiL were then corrected, which are based on infinite wing theory, following the equations of prof. Pajno, modified for practical purposes but derived from Prandtl theory or experimental evaluations. The wings and the whole glider C_L, as well as the correction of the C_D, were obtained. Using the correct values were defined the flight envelope diagrams. Again, two methods have been followed: Reymar considers a modified arithmetic law to take account of the finite wing and its orientation, but still very rough. The second method uses the same calculation steps used for Reymar's method but is based on the correct values obtained by the equations of prof. Pajno. It was therefore possible to verify that the stall rate at Reynolds' highest conditions respects the maximum limit of 65 km/h. However, for security reasons, we need to implement flaps, that help in the landing phase. Following the development of envelope diagrams in accordance with BCAR-E regulations, spiral performance and speed polar curves characterizing the gliders' maneuvers have been obtained.
Note the values of aerodynamic research using semi-empirical formulas and corrected aerodynamic parameters, a fluid-dynamic investigation was started using the **ANSYS**®software: a 2D analysis set for airfoil so that they could evaluate, with algorithms that better interpret turbulence, C_l and C_d adjustments as the attack angle varies. These simulations have been confirmed by experimental tests performed by the Illinois University for low Reynolds profiles. At the same time a 3D survey of the entire virtual glider was also realized, obtaining interesting results for the C_L and C_D values in accordance to them obtained through the formulas. In addition, a series of images were obtained to guide the qualitative assessment of fluid behaviour around the aircraft. Although the three-dimensional model seems to behave good at high angles of attack, there remains a fundamental disparity between the stall limits of 2D and 3D analysis that lead the author to adhere on safety conditions for which the angular interval 10 to 15 degrees, stall zone, have to be explored with experimental evidence. Finally, we have analysed the electrical part, referring to the development of the propulsion infrastructure of the aircraft. A solar radiation survey was carried out in four locations located at different latitudes: Oslo, Padua, Syracuse, Cairo, in order to be

able to fully contemplate the behaviour of the motorglider in a business perspective. Thus, the available amount of surface energy was determined and a comparison of flexible amorphous and rigid monocrystalline technology was performed. It has been chosen the use of amorphous photovoltaic cells that are able to cover a wider surface than rigid monocrystalline and electric motors, the best technology option is linked to the brushless electric motor, which perform high velocity and low mass. The engine was selected based on the flying powers obtained thanks to the knowledge of the correct aerodynamic glider values.

It is concluded that the goals cited at the beginning of this work have been achieved. The necessary constraints and requirements have been obtained to initiate a more in-depth investigation and thus come to a last model that can be experimentally analysed in the form of a prototype. Respecting the requirements, it can be stated that below the 200 kg maximum mass, it is not possible to achieve any aircraft that reflects materials and the company-building constructive engineer. This is justified by the reasons set out in chapters 2 and 3. The 12 meter wingspan has important implications in the induced drag, and based on the database, it is the minimum known value for the gliders that have been constructed and marketed. The remaining requirements have been satisfied with an aerodynamic and propulsion configuration that, at least preliminary, is able to do it.

6.0.1 Future Developments

Concerning future developments, the author hopes that the next issues will focused on aspects that were not considered in this paper, and also in depth investigation on that arguments obtained preliminarily in this work. Future works that have to be done or analysis that have to be realized, are presented below:

1. Survey on flight configurations that are similar to the one evaluated in this work, by altering the airfoil so as to indicate the best compromise combination for the generation of a small but efficient wing. This can only be achieved through an iteration process between the required performance and those that the wing actually produces;

2. Insights into formulas used for aerodynamic parameter correction and specialization with relative validation of the same for low Reynolds environment;

3. Improved performance in turn, from whose evaluations we can extract information to design a better wing;

4. Deepen the CFD analysis by providing high-performance HardWare in order to set up an efficient control volume;
5. Design a mesh that is more regular, possibly manual, in particular with an increase in density element around the airfoil so that it can best shape the boundary layer and its effects;
6. Sizing a first attempt propeller from which to start an iterative process aimed at obtaining the specific requirements for the engine
7. Creation of a propeller extraction mechanism with ground clearance assessment;
8. Dimensioning and realization in a virtual environment, therefore concept, of the internal structure of the entire aircraft. Then based on the distribution of forces and their intensity, define the best materials that achieve a compromise between resistance and mass;
9. When the entire airframe and every single part is in position, the identification of the centre of mass have to be recognized, in order to optimize the tail plan position.
10. Relaxing some strong hypothesis made upon this thesis and solve balance force equilibrium, pressure distribution and lift distribution;
11. Deepening of the glider's flight mechanics to capture the static and dynamic stability in different flight configurations.

Appendix

Appendix A

Database containing sailplanes and motorglider built from 1970 onwards, thanks to which a historical-statistical survey was carried out for the preliminary dimensioning of the motorglider configuration described in the thesis. The following database contains aerodynamic and mass information.

◊		Length[m]	b[m]	W[kg]		Wempty/W0	W/S	Profile	Wing Surface[m^2]	Aspect Ratio	Glide Ratio (L/D)	Model	Year
				empty	Gross								
Glider	from 11,2 to 17,6	6.95	14.95	240	340	0.705882353	26.77165354	NACA 43012A	12.7	17.6	28:1	kometa standard	1960
		6.78	14.27	205	310	0.661290323	23.16890882	NACA23012	13.38	15.22	24:1	Letov LF-107 Lunak	1948
		6.75	12	315	453	0.695364238	34.31818182	FX 71-L-150/20	13.2		27:1	Akaflieg München Mü28	1983
		6.58	13.6	250	350	0.714285714	22.15189873	Göttingen 756	15.8		21:1	DFS Habicht	1936
		6.8	15	238	500	0.476	48.54368932	HQ 21/II	10.3	21.9	40:1	Glaser-Dirks DG-300 Acro	1983
		5.7	13.3	182	280	0.65	32.63403263	FX 66-17 A 182	8.58	20.6	35:1	Glasflügel H-101	1970
		8.18	17.5	390	580	0.672413793	32.58426966	Eppler E 603	17.8	17.1	37:1	Grob G103a Twin II	1980
		6.35	13	190	300	0.633333333	30	S 01	10	16.9	30:1	LCF II	1975
		6.2	15	205	323	0.634674923	23.92592593	NACA 65415	13.5	16.7	34:1	Schempp-Hirth Standard Austria	1959
		8.35	17	360	600	0.6	33.42618384	FX S02-196 / FX 60-126	17.95	16	34:1	Schleicher ASK 21	1979
		6.15	10	150	245	0.612244898	22.47706422	Clark Y	10.9	9.2	25:1	Vogt Lo-100	1952
		7.53	17.6	200	363	0.550964187	14.4047619		25.2	12.3	22:1	Bonomi BS.14 Astore	1935
		6.85	13.2	265	380	0.697368421	38.7755102	PZL NN-8	9.8	17.8	36:1	Allstar SZD-59	1991
		6.25	12	240	357	0.672268908	29.75	Root – NACA 2418, Tip – NACA 2412, Mid – NACA 0012	12	12	20:1	Instytut Szybownictwa IS-4 Jastrząb	1949
		6.91	12.7	280	390	0.717948718	33.05084746	NACA 641412	11.8	14.3	30:1	Marganski Swift S-1	1991
		7.38	14	345	525	0.657142857	42.68292683	NACA 641412	12.3	15.9	28:1	MDM MDM-1 Fox	1993
		7.7	18						14.3	22.7	23:1	SZD-C Żuraw	1952
		7.25	14	311	401	0.775561097	29.7037037	NACA 641412	13.5	15	30:1	SZD-21 Kobuz	1961
		7	15	219	350	0.625714286	27.45098039	Root: Göttingen 549, Tip: M 12	12.75	17.65	28:1	SZD-22 Mucha Standard	1958
		7	15	245	385	0.636363636	31.66118421	Root: NACA 63_3-618, Mid: NACA 63_3-618 (mod.), Tip NACA 4415 (mod.)	12.16	18.58	34:1	SZD-24 Foka	1960
												SZD-32 Foka 5	1966
		8.38	16.67	370	570	0.649122807	31.3876652	NN-8	18.16	15.3	32:1	SZD-50 Puchacz	1979
		6	12.1	254	360	0.705555556	34.48275862	TsAGI R-32-15	10.44	13.8	25:1	Antonov A-13	1958
		6.5	11.2	265	385	0.688311688	33.36221837	Wortmann FX-71-L-150/25	11.54	11	25:1	Celair GA-1 Celstar	1989
		4.92	12.1	175	310	0.564516129	41.83535762	Radab KTH-FFA 17%	7.41	19.75	36:1	Radab Windex	1985
		8.55	23.2	587	820	0.715853659	43.27176781	HQ 41/14,35	18.95	28.4		Akaflieg Berlin B-13	1991
		10.36	29	577	895	0.644692737	38.99782135	Emplanture : Wortmann FX-62-K-153 modifié ; milieu : FX-62-K-131 modifié ; saumon : FX-60-K-126	22.95	36.6	53:1	Akaflieg Braunschweig SB-10 Schirokko	1972
	Over 18	9.1	28	570	850	0.670588235	50.5952381		16.8	46.7	65:1	Binder EB-28	1986
		7.84	20.36	400	644	0.621118012	39.77764052	FX 67K-170/150 (emplanture) et FX 60-126 (saumon)	16.19			Caproni A-21SJ Calif	1973
		7.83	23	500	850	0.588235294	57.82312925	Delft DU 97-127/15	14.7	36		Schempp-Hirth Quintus M	2011
		9	25	470	750	0.626666667	45.98405886	HQ-17	16.31	38	57:1	Schleicher ASH-25	1985
		8	28	548	850	0.644705882	62.04379562		13.7	57.2	70:1	Waibel-Butler Concordia	2012
		5.55	11.55	110	220	0.5	33.63914373		6.54	21	33:1	Brondel ST-11	1982
		5	11.9	107	204	0.524509804	21.03092784	Culver 18%-13%	9.7	14		Maupin Woodstock	1979
	Small	6.3	11	70	188	0.372340426	28.92307692		6.5	18.6		Windward Performance SparrowHawk	2002
		6.85	15	270	540	0.5	50.65666041		10.66	21	40:1	SZD-59 ACRO	1991
		6.95	18	240			0	CA2-134 / 15V2 (s) CAJ1-134 / 18 (esterno)	10.84	29.89	52:1	Akaflieg SB-14	2003
	Performance	6.22	13.44	185	300	0.616666667	29.52755906	NN 18-17	10.16	17.8	33:1	Bielsko B1-PW-5 Smyk	2000
		8.3	16.5	322	512	0.62890625	32		16		33:1	ITA P-1	1996
		6.78	18	330	565	0.584070796	49.60491659		11.39	28.5		Schempp-Hirth Discus 2cT	2004
		6.56	13	240	350	0.685714286	30.64798599	Wortmann FX 67 K 150/17	11.42	15	28:1	Truchet Tr-301 Abyssin	1982
		6.8	15	250	400	0.625	38.0952381	OAP 1-2	10.5	21.4	42:1	Centrair C-101 Pegase	1981
		6.8	15	245	450	0.544444444	43.68932039	HQ21/II	10.3	21.8	41:1	Dirk-Glaser DG-300 Elan	1983
		7.16	18	450	600	0.75	54.05405405		11.1	29	53:1	Jonker JS-1C-18 Evo	2012
		6.98	15	239	465	0.513978495	46.5		10	23	42:1	Kuykendall HP-24 Tetra-15	2012
		6.4	13	200	310	0.64516129	32.63157895		9.5	16.6		Brondel Helium	1985
		6.6	15	210	420	0.5	38.18181818	FX 67-K- 170 FX 60-126	11		38:1	Carman JP-15/38	1979
	Over 1970	5.8	12	145	265	0.547169811	38.4057971	FX 73-CL 1-152	6.9	20.86	32:1	GlasFaser Velino	1992
		6.8	15	245	485	0.505154639	45.28478058	HQ 21	10.71	21.01	41:1	Akaflieg Karlsruhe AK-5 Ardea	1990
		6.5	15	200	310	0.64516129	25.83333333		12	18.8	32:1	Altinger TA-15S Lenticular	1972
		6.6	15	238	544	0.4375	53.70187562		10.13	22	38	Applebay Zuni	1976
		6.73	15	230	350	0.657142857	32.11009174	FX-61-163, FX-60-126	10.9	20.7	35:1	ISF mistral-C	1977
		7.2	17.8	290	410	0.707317073	33.33333333	FX 67-K-170/17	12.3	25.5	43:1	Kervelis BK-7 Lietuva	1972
		6.68	15	220			0	DU 80-176 DU 80-14	9.8	22.96	39:1	Pajno V-1/2 Rondine	2000
		6.45	15	235	450	0.522222222	45	FX-67-K-170,FX-67-K-150	10	22.5	42:1	Pik-20	1976
		6.65	15	250	450	0.555555556	45		10	22.38	39:1	Romagna QR-15 Larus	2014
		6.55	15	230	500	0.46	50	DU84-158	10	22.5	44:1	Schleicher ASW-14	1987
		6.55	15	235	500	0.47	55.55555556	DU89-134/14	9	25	48:1	Schleicher ASW-27	1995
		6.58	15	258	525	0.491428571	50	DU99-147 ; DU99-147 M1 : DU99-147 M2	10.5	21.43	45:1	Schleicher ASW-28	2000
		6.6	15	210					11		38:1	Siren C-38	1981
		6.55	15	230					9.77		44:1	STRA CB-15 Crystal	1986
		5.7	13.6	54	164	0.329268293	12.8125		12.8	12.8	28:1	Ruppert Archeopteryx	2001
		7.04	15	190	310	0.612903226	26.16033755	Wortmann FX-61-163	11.85	19	34:1	Aviamilano A2	1965
		6.49	15	187	310	0.603225806	27.58007117	JACA 63(3)618 vers 63(3)61	11.24	20	35:1	Fibera KK-1 Utu	1964
		5.86	13	165	280	0.589285714	43.07692308		6.5	26	37,5:1	Meier Milomei M-1	1966
		6.35	15	165	300	0.55	33.33333333		9	25	38:1	Morelli M-300	1968
		6.35	15	202	330	0.612121212	14.66666667		22.5		38:1	Schempp-Hirth Standard Cirrus	1969
		8	18.5	376	500	0.752	29.97601918		16.68	21.14	43:1	VSB-62 Vega	1966
		8.71	18.2	438	620	0.706451613	37.39445115	Root : FX 67-K-170, tip : FX 67-K-150	16.58	20	41:1	Akaflieg Berlin B-12	1977
		10.3	22	480	700	0.685714286	39.77272727		17.6	27.5	47:1	Akaflieg München Mü-27	1979
		7.95	18	300	520	0.576923077	28.88888889		18	12	36:1	CERVA CE-75 Sagittaire	1974
		7.62	20.12	272	430	0.63255814	30.04891684		14.31			Lamson L-106 Alcor	1973
		7.3	15	230	350	0.657142857	29.66101695		11.8	19		Neukom S-4 Elfe 15	1977
		6.4	13	93	206	0.451456311	15.60606061		13.2	13	25:1	Advanced Aeromarine Sierra LS	1991
		6.1	13	91	181	0.502762431	12.92857143		14	12	25:1	Bailey-Moyes Tempest	1998
		5.18	8.36	64	157	0.407643312	14.90978158		10.53		16:1	HG-1 Tolpel	1988
		6.07	13	190	280	0.678571429	28.80658436	NACA 4415	9.72	17.4		Jansson-Thor BJ-1B Duster	1971

MotorGlider

5.9	13.74	196	310	0.632258065	26.67814114		11.62		30:1	Alpaero Exel	
4.66	8.16	165	290	0.568965517	46.03174603	Wortmann FX67-K170/17	6.3		16:1	Alpha J-5 Marco	
4.9	11	72.5	163	0.444785276	24.36472347	Wortmann FX-61-184	6.69	18	27:1	AmEagle American Eaglet	
6.5	11.1	185	265	0.698113208	17.66666667		15	8		Avia 50-MP	
6.8	12.43	180	295	0.610169492	19.66666667		15	10		Bonomi BS.22 Alzavola	
6.86	13.87	141	227	0.621145374	20.63636364		11	16	21:1	Carden-Baynes Auxiliary	
6.43	15	225	450	0.5	45		10	22.5	42:1	Eiri-Avion PIK-20	
6.5	10.4	295	472.5	0.624338624					32:1	Phoneix air phoneix	
6.53	13.5	161	350	0.46	41.61712247		8.41			miniLak	
7.9	14	435	626	0.694888179	39.125		16		20:1	Lucas L-6A	2002
8.05	16.68	550	750	0.733333333	36.23188406		20.7	14	25:1	M&D Samburo	1977
6.9	15	343	460	0.745652174	30.66666667		15	15	25:1	Nihon N-70 Cygnos	1970
6	12.2	207	325	0.636923077	24.62121212		13.2			Kocjan Bak	1937
6.1	12	113	213	0.530516432	20.67961165		10.3		18:1	Profe D-8 Moby Dick	1988
6.3	13.3	100	200	0.5	19.04761905	Wing root: SM701, wing tip: Wortmann FX-60-126	10.5		28:1	Profe Banjo	1998
6	11.2	240	350	0.685714286	31.81818182	NACA 23015 at root, NACA 23012 at tip	11	11		Fournier RF-3	1960
6	11.3	270	390	0.692307692	34.51327434		11.3	11.2	20:1	Fournier RF-4	1966
7.8	13.74	420	650	0.646153846	42.98941799	root:NACA 23015, tip:NACA 23012	15.12	12.5	20:1	Fournier RF-5	1968
6.05	9.4	300	445	0.674157303	44.5		10			Fournier RF-7	1970
6.64	12	230	360	0.638888889	24	NACA 43015 root, 43012A from mid span outwards	15	11	24:1	IIL IS-9	1958
7.27	15	285	450	0.633333333	36.49635036		12.33	18.6	41:1	Pipistrel Taurus	2002
7.3	14.7	205	410	0.5	27.33333333	Wortmann FX 63-137	15			Profe D-10 Tucan	1998
4.92	12.1	175	310	0.564516129	41.83535762		7.41	20	36:1	Radab Windex	
5.8	11	115	230	0.5	28.75		8		35:1	SAGITTA	
6.82	15	250	454	0.550660793	43.23809524	root:Wortmann FX-63-131-K; tip:Wortmann FX-60-126	10.5	21	43:1	Schleicher ASW 20	1977
7.6	15.33	335	530	0.632075472	30.33772181		17.47	13.4	22:1	Slingsby Falke	1971
6.05	15	310	440	0.704545455	36.66666667	Wortmann FX-61-184 at root, Wortmann FX-60-126 at tip	12	19	29:1	Sportavia Putzer SFS 31 Milan	1969
5.9	12.6	150	279	0.537634409	25.15779982	Wortmann FX 61-184	11.09			Test TST-1 Alpin	1998
5.8	13.4	141	249	0.56626506	24.9	Wortmann FX 61-184	10		31:1	Test TST-3 Alpin	2000
6.4	14.7	227	449	0.505567929	36.20967742	Wortmann FX 61-184	12.4			Test TST-6 Duo	
6.87	15	205	300	0.683333333	30.45685279		9.85	23	40:1	Test TST-10 Atlas	
7.16	16	500	775	0.64516129	51.66666667		15	17	28:1	Whisper Aircraft	
6.35	13.3	205	315	0.650793651	35.39325843	16% IMD 050	8.9	20	40:1	Alisport Silent 2 Electro	
7.9	25	300	390	0.769230769	15.17509728		25.7		36:1	Icarè 2	
7.48	23	510	850	0.6	57.62711864		14.75	38.26	60:1	Lange Antares 23 E	2011
5.25	10.5	133	250	0.532				11		Martinez Boero-Rovera Puma	
5.8	12.4	175					10		20:1	Test TST-9 junior	2004
6.2	14	225	345	0.652173913	28.75	Mu 14%	12		22:1	Scheibe SF-24 Motorspaz	1960
6	15	200	300	0.666666667	30		10	22.5	40:1	Barel Graal	2000
6.9	14.65	240	440	0.545454545	25.14285714		17.5	12	21:1	PW-3 Backcyl	1988
7.85	16	360	546	0.659340659	35.80327869		15.25	16.6	34:1	PW-6 Twin Piwi	1998
6.35	12	175	290	0.603448276	28.15533981		10.3	14		Alisport Silent Club	1997
6	11.8	150	240	0.625	22.64150943		10.6	13	20:1	Piuma	
6.35	13	195	300	0.65	34.09090909		8.8	19.2	39:1	Alisport Silent 2 A302efi	2006
8.66	18	400	750	0.533333333	44.85645933		16.72	19.38	46,5	Akaflieg DG-1000S Turbine	2011
8	29.3	570	900	0.633333333	53.57142857	HQ 17 and DU 84-132/V3 for winglets	16.8	51	65:1	Binder EB-29	2009
9.84	30	600	850	0.705882353	45.69892473		18.6	51.3	72:1	Eta	2000
6.53	18	295	600	0.491666667	58.13953488		10.32	31.4		Lak-17B FES	2013
7.4	20	460	660	0.696969697	52.38095238		12.6	31.7	56:1	Lange Antares 20 E	2003
8.3	20	485	800	0.60625	51.28205128		15.6	25.6	50:1	Schempp-Hirth Arcus T	2010
6.59	18	280	600	0.466666667	57.14285714		10.5	30.4	52:1	Schleicher ASG-29E	2005
7.05	18	270	525	0.514285714	44.94863014		11.68	27.7	50:1	Schleicher ASH-26E	1993
7.95	25	545	810	0.672839506	49.66278357		16.31	38.32	62:1	Schleicher ASW-22 BE	1986
9.1	28	605	810	0.74691358	45.99659284		17.61	44.5	60:1	Schleicher-Binder ASH-25 MB EB-28	1985
9	26	594	790	0.751898734	47.53309266		16.62	40.67	62:1	Schleicher ASH-25M	1985
5.03	12.55	245	410	0.597560976	44.88232074		9.135	17.25	23:1	Janowsky J-6 Fregata	1993
5.9	11.7	145	235	0.617021277	20.25862069		11.6	11.2	17:1	Piuma Originale	1990
6	10.4	160	250	0.64	27.17391304		9.2	11.7	17:1	Piuma Tourer	2000
6.5	13	270	440	0.613636364	36.06557377		12.2		20:1	Piuma Evoluzione	1999
	23	270	470	0.574468085						Raymond Sunseeker Duo	
	11.47	292	475	0.614736842	39.58333333		12		24:1	Sanstroem Friendship 3	2012
	12	195	300	0.65	29.12621359		10.3	14	30:1	Air Energy AE-1 Silent	
	12.6	175	300	0.583333333	38.96103896		7.7	20.6	34:1	Aviastrotel AC-5M	1998
	13	119	230	0.517391304	22.2007722		10.36		38:1	Pipistrel Apis 13	2003
	15	272	510	0.533333333	48.57142857		10.5		39:1	Masak Scimitar 1	1995
	15	193	281	0.68683274	27.71203156	FX 67-K-170 FX 67-K-150	10.14	22.2		Leister LP15 Nugget	1971
	15	265	495	0.535353535	47.23282443	FX 79-162 / FX 79-133	10.48	21.48	40:1	Fasola NF-3 Beta	1985
	15	245	500	0.49	48.68549172		10.27	21.9		Akaflieg Hannover AFH-24	1980

Appendix B

Airfoil polar graphs containing performance information such as C_l and C_d as a function of AoA α. Also efficiency and power factor terms which provide functionality advise and are fundamental for satisfy selection criteria. This graphs were obtained thanks to **Profili2**®software, which is based on *XfoiL* source code.

E214 (11,1%)
Spessore max 11.08% al 31.4% della corda
Camber max 4.03% al 52.4% della corda
Mach = 0.0000 - NCrit = 11.00

Re 50000 = **Re 70000 =** **Re 100000 =**
Re 200000 = **Re 250000 =** **Re 300000 =**
Re 400000 = **Re 500000 =** **Re 750000 =**
Re 1000000 = **Re 2000000 =**

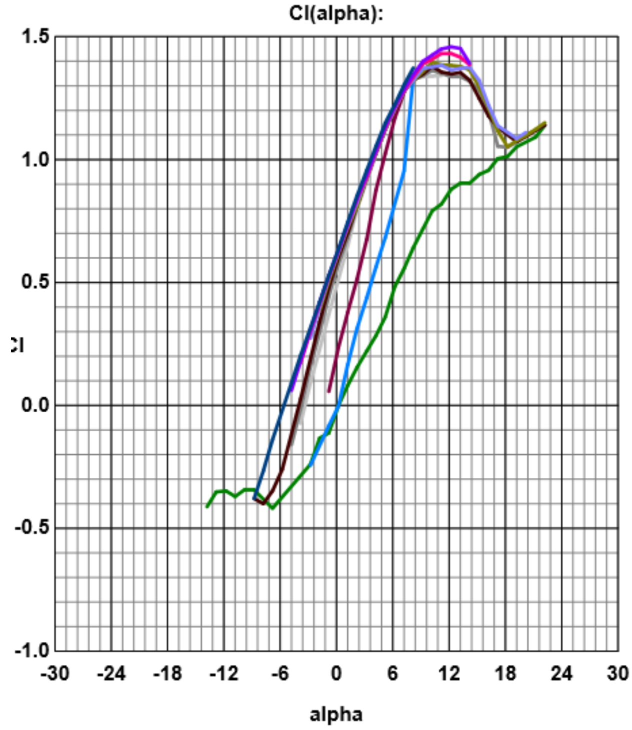

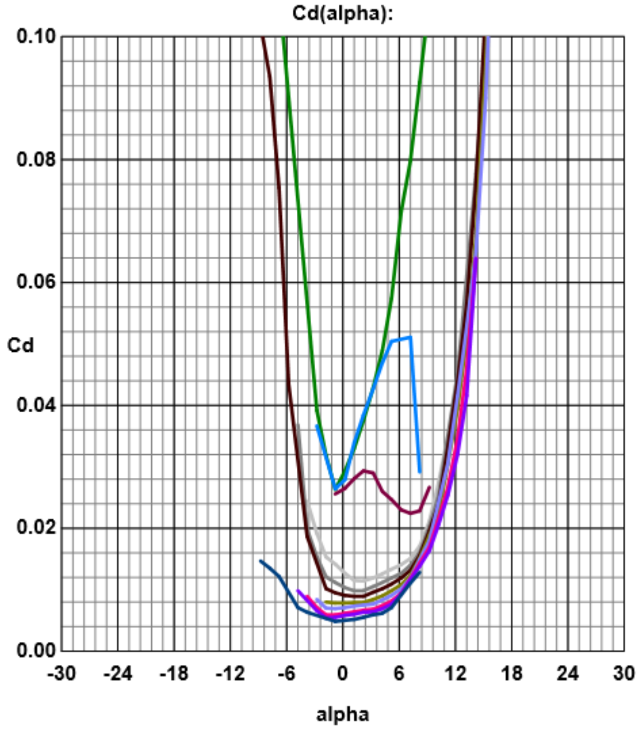

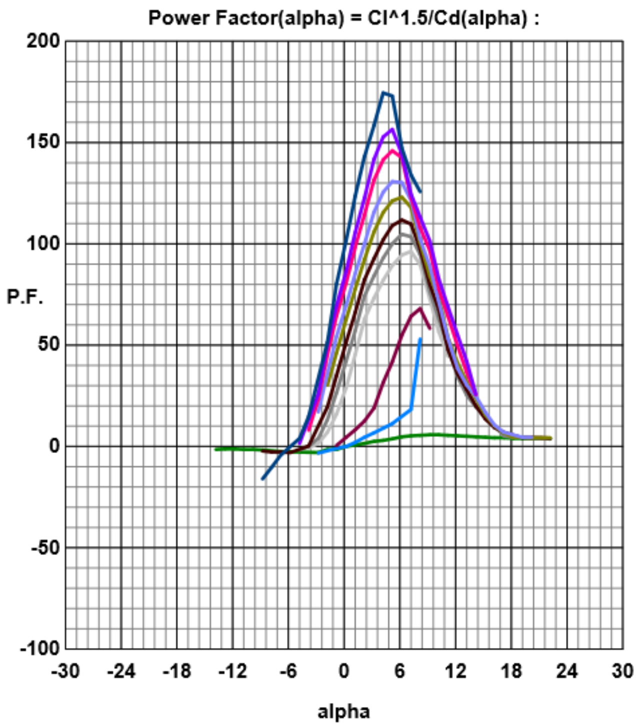

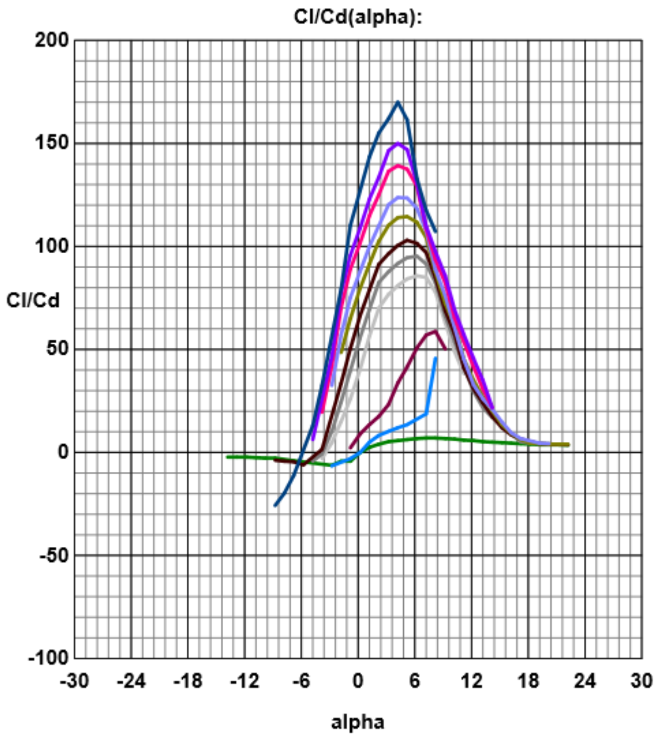

E387
Spessore max 8.88% al 28.8% della corda
Camber max 3.83% al 39.2% della corda
Mach = 0.0000 - NCrit = 11.00

Re 50000 = **Re 70000 =** **Re 100000 =**
Re 200000 = **Re 250000 =** **Re 300000 =**
Re 400000 = **Re 500000 =** **Re 750000 =**
Re 1000000 = **Re 2000000 =**

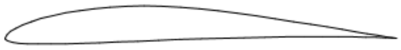

Cl(alpha):

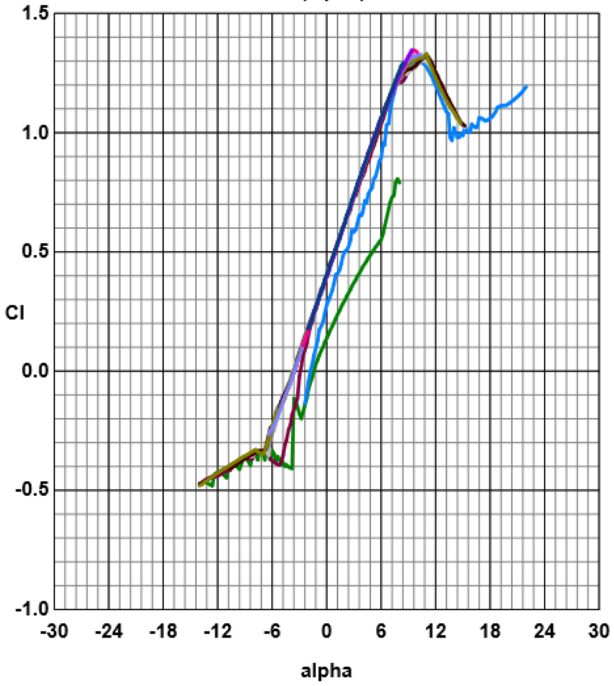

Cd(alpha):

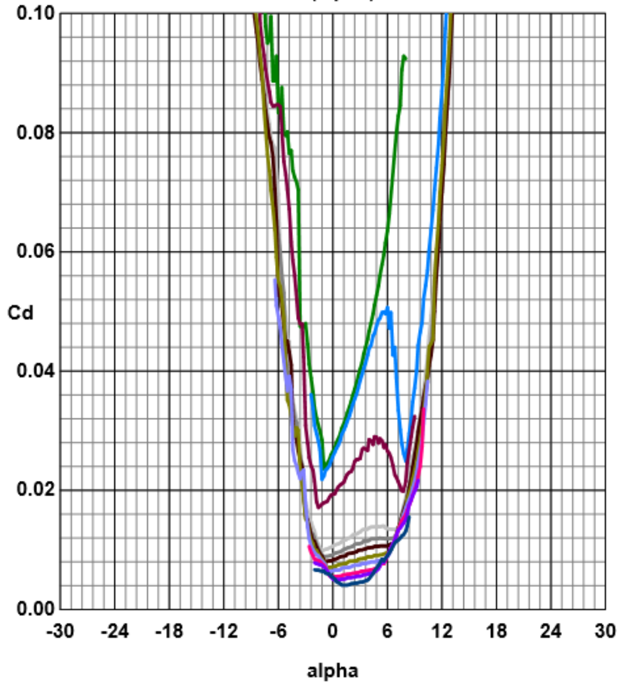

Cl/Cd(alpha):

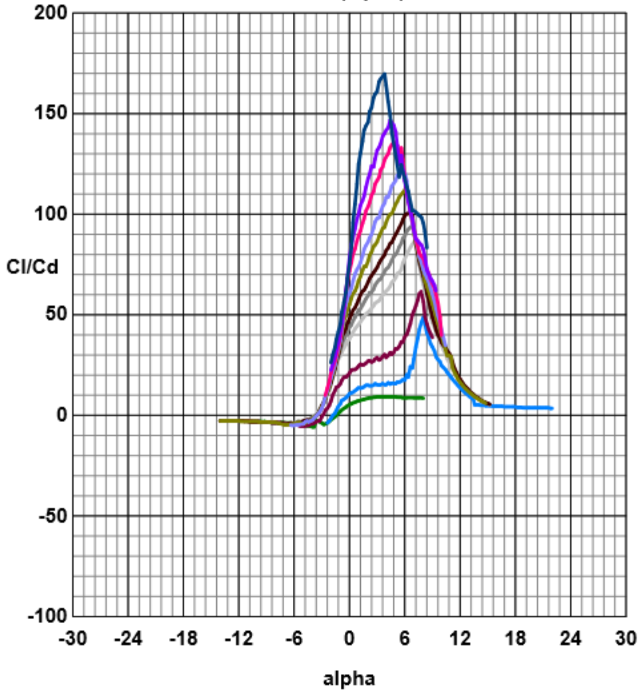

Power Factor(alpha) = Cl^1.5/Cd(alpha) :

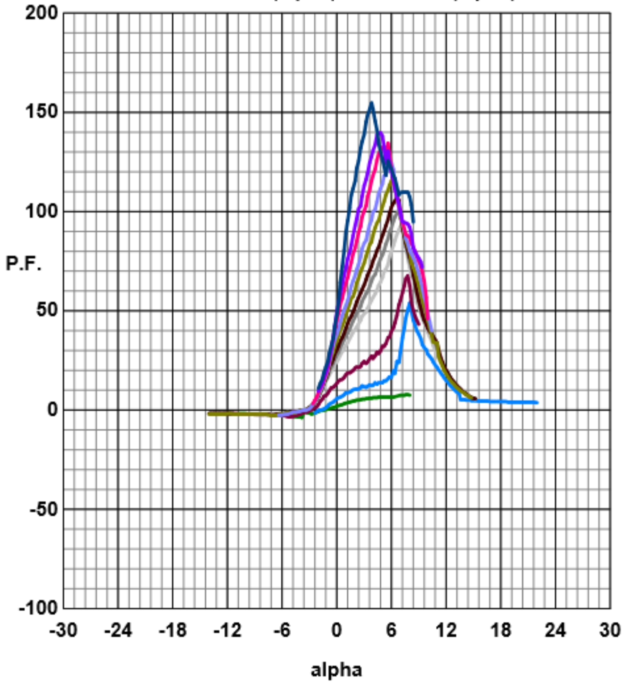

FX 60-126-1
Spessore max 12.60% al 27.9% della corda
Camber max 3.96% al 56.5% della corda
Mach = 0.0000 - NCrit = 11.00

Re 80000 = | Re 100000 = | Re 150000 =
Re 200000 = | Re 250000 = | Re 300000 =
Re 400000 = | Re 500000 = | Re 750000 =
Re 1000000 = | Re 2000000 =

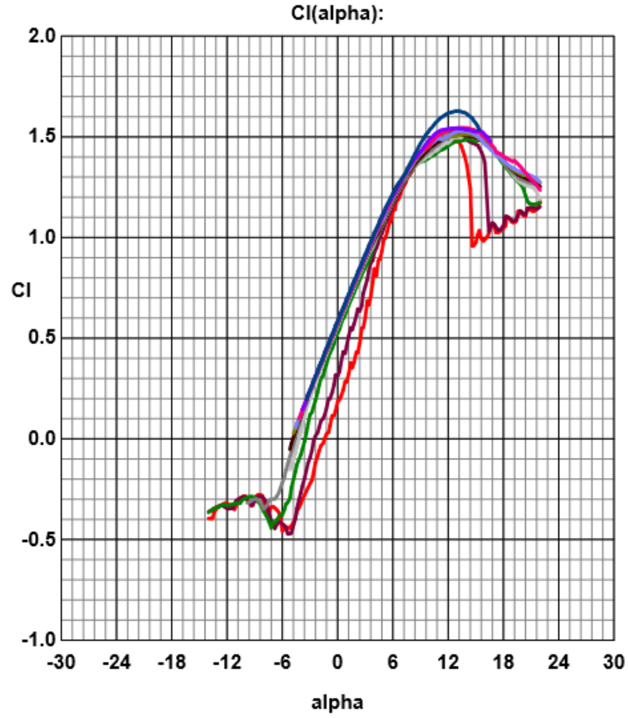

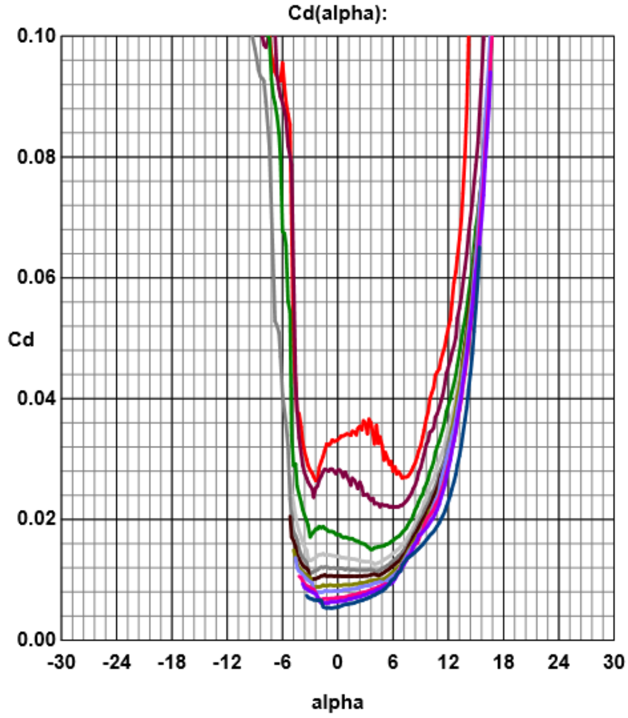

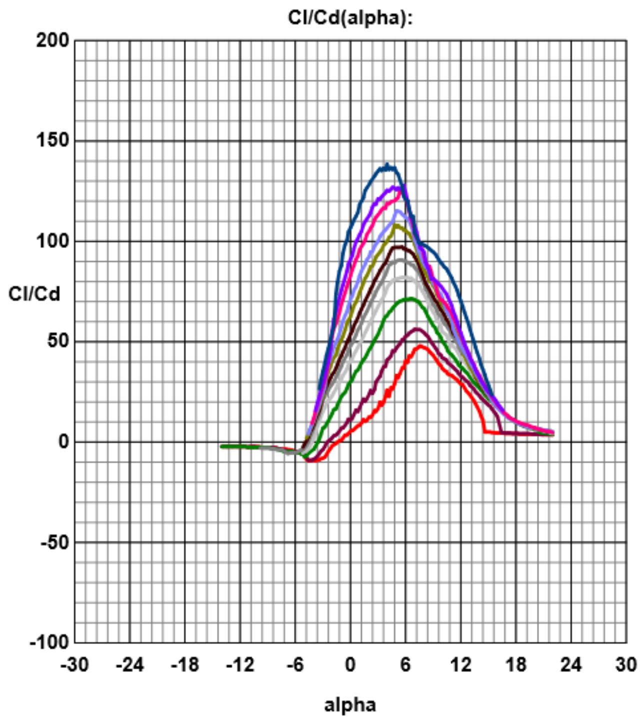

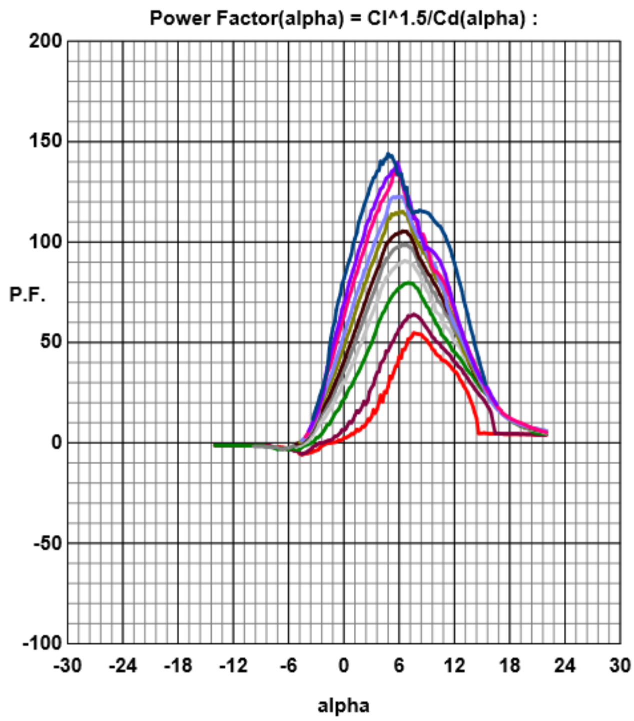

FX 61-147
Spessore max 14.77% al 33.9% della corda
Camber max 3.18% al 33.9% della corda
Mach = 0.0000 - NCrit = 11.00

Re 80000 =
Re 100000 =
Re 150000 =
Re 200000 =
Re 250000 =
Re 300000 =
Re 400000 =
Re 500000 =
Re 750000 =
Re 1000000 =
Re 2000000 =

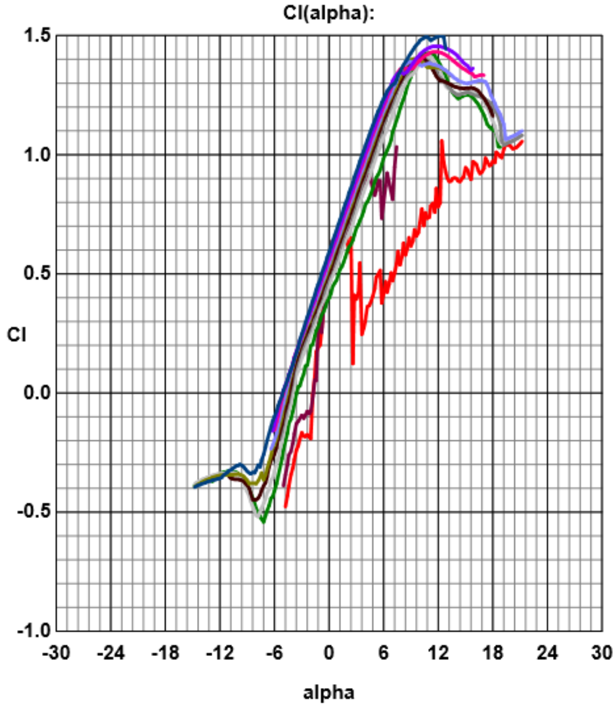

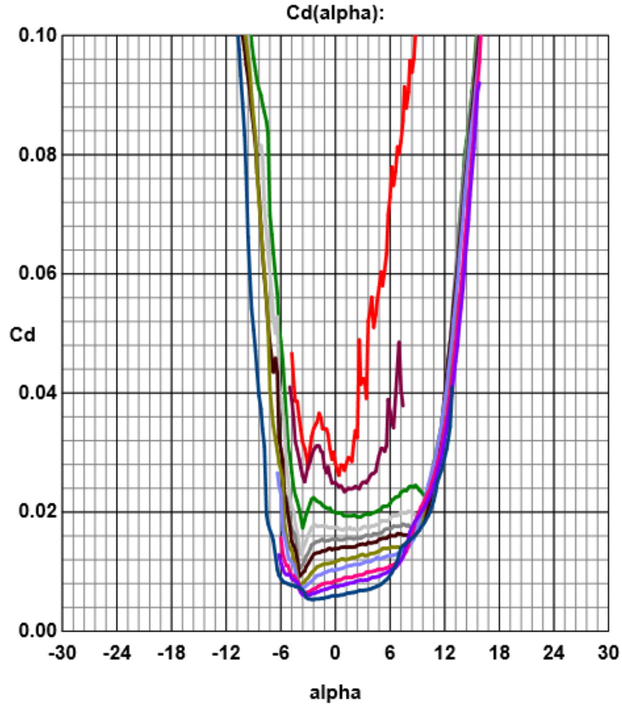

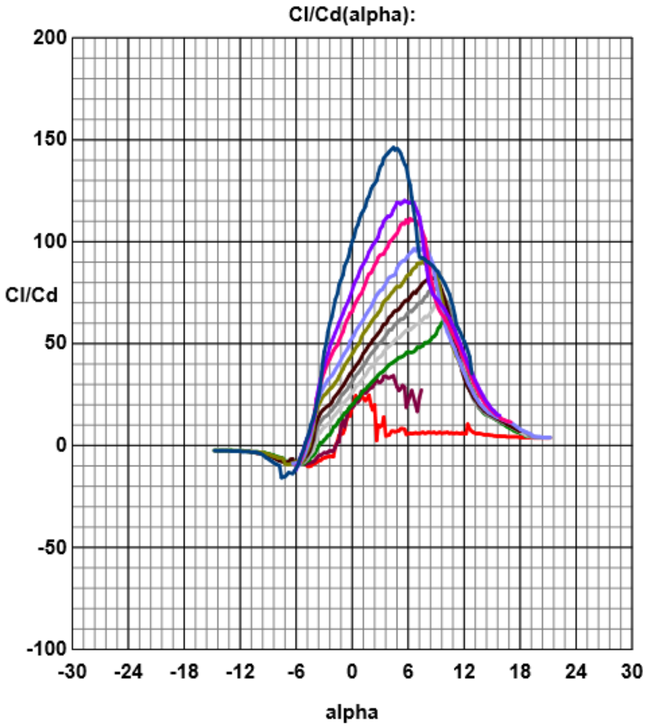

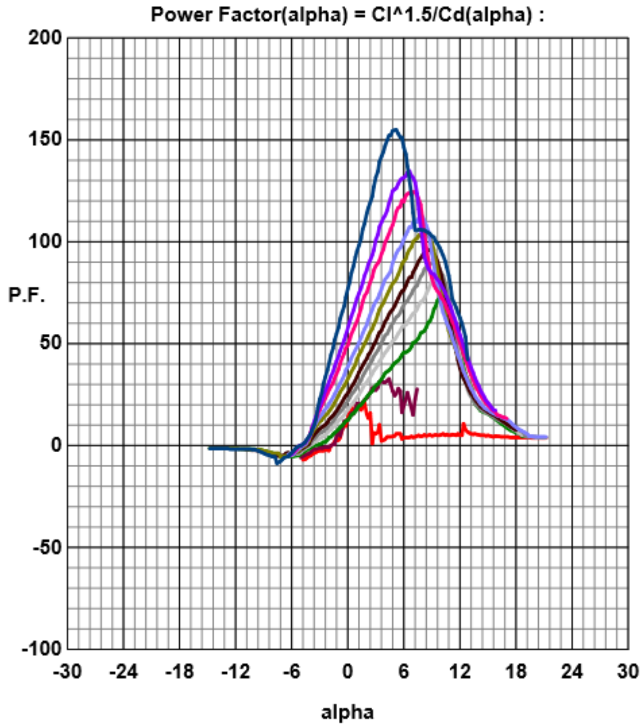

FX 61-184
Spessore max 18.37% al 37.1% della corda
Camber max 3.09% al 62.9% della corda
Mach = 0.0000 - NCrit = 11.00

Re 50000 =
Re 70000 =
Re 100000 =
Re 200000 =
Re 250000 =
Re 300000 =
Re 400000 =
Re 500000 =
Re 750000 =
Re 1000000 =
Re 2000000 =

Cl(alpha):

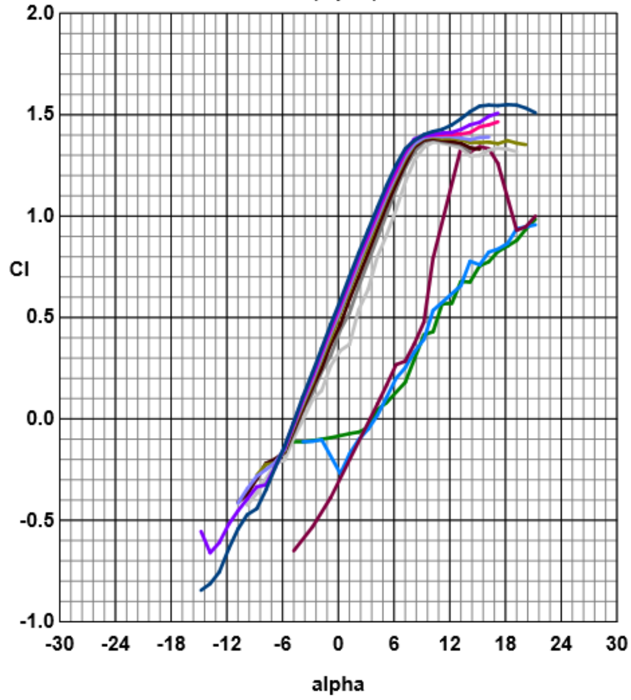

Cd(alpha):

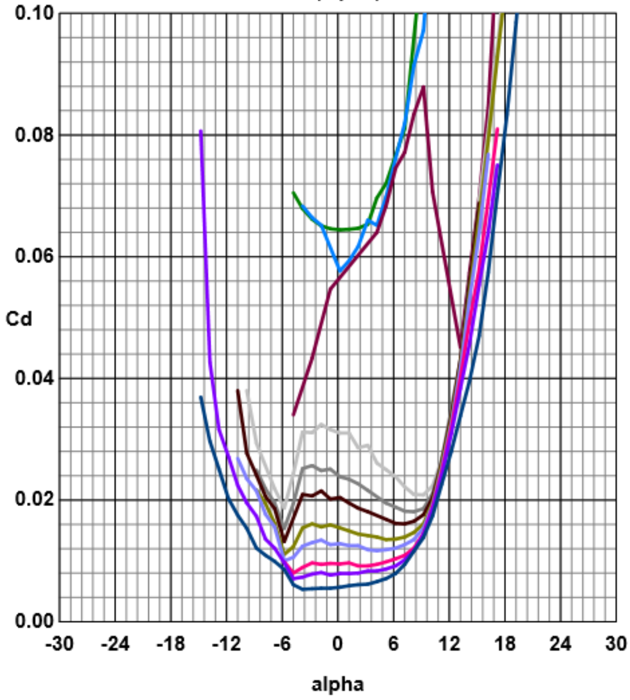

Cl/Cd(alpha):

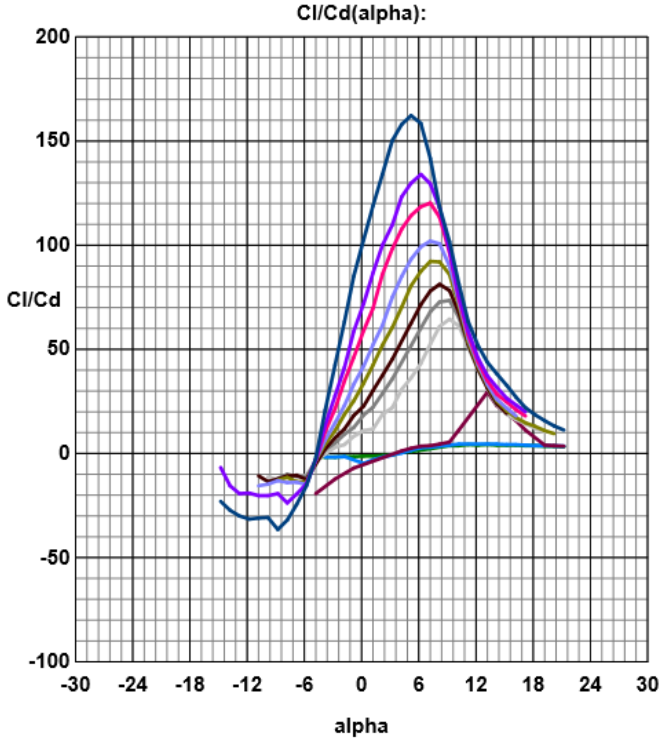

Power Factor(alpha) = Cl^1.5/Cd(alpha) :

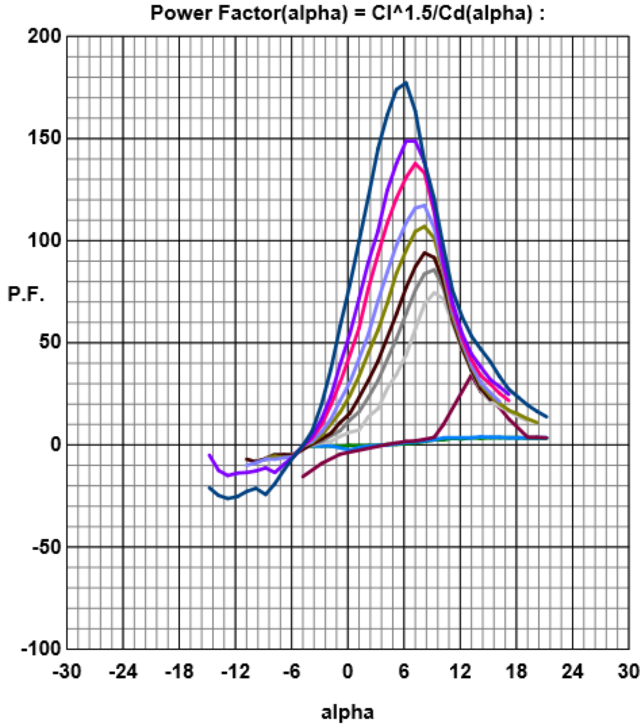

FX 63-120
Spessore max 12.01% al 30.8% della corda
Camber max 5.24% al 50.0% della corda
Mach = 0.0000 - NCrit = 11.00

Re 80000 = — **Re 100000 =** — **Re 150000 =** —
Re 200000 = — **Re 250000 =** — **Re 300000 =** —
Re 400000 = — **Re 500000 =** — **Re 750000 =** —
Re 1000000 = — **Re 2000000 =** —

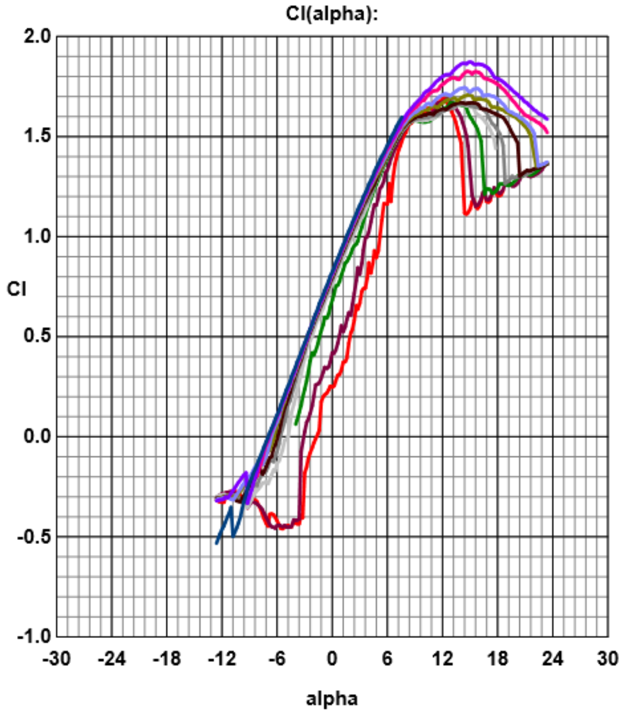

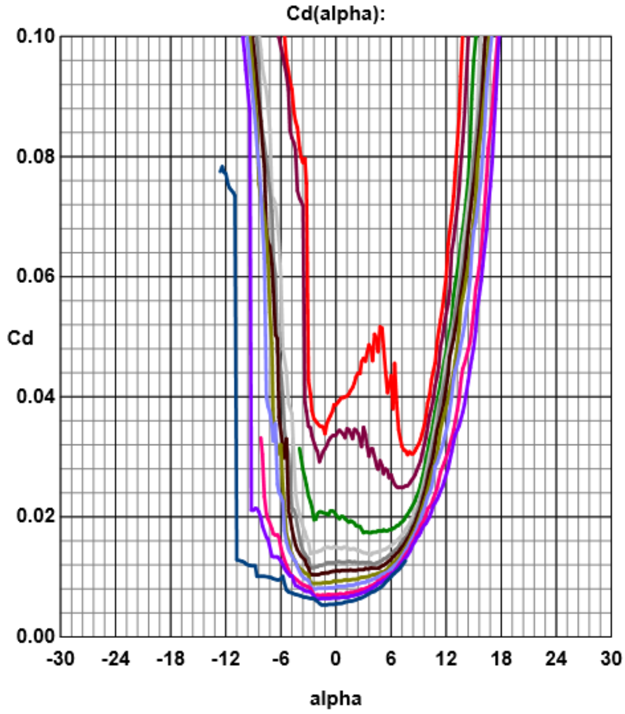

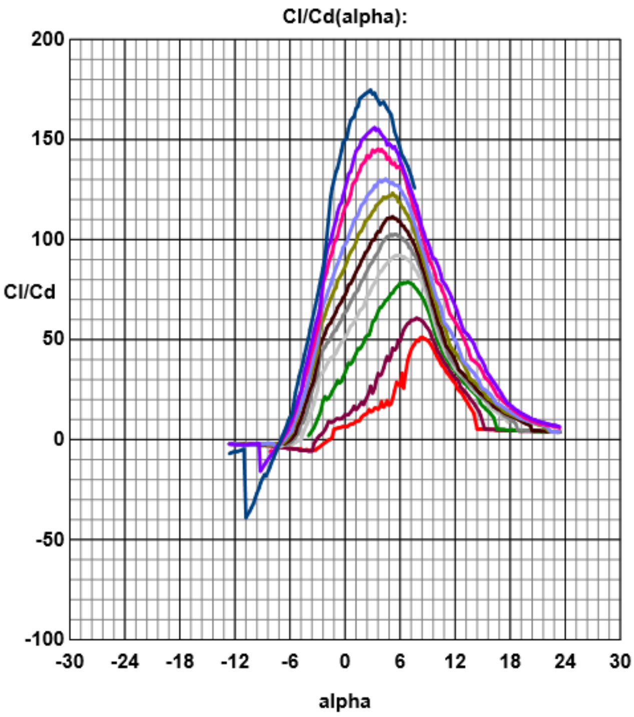

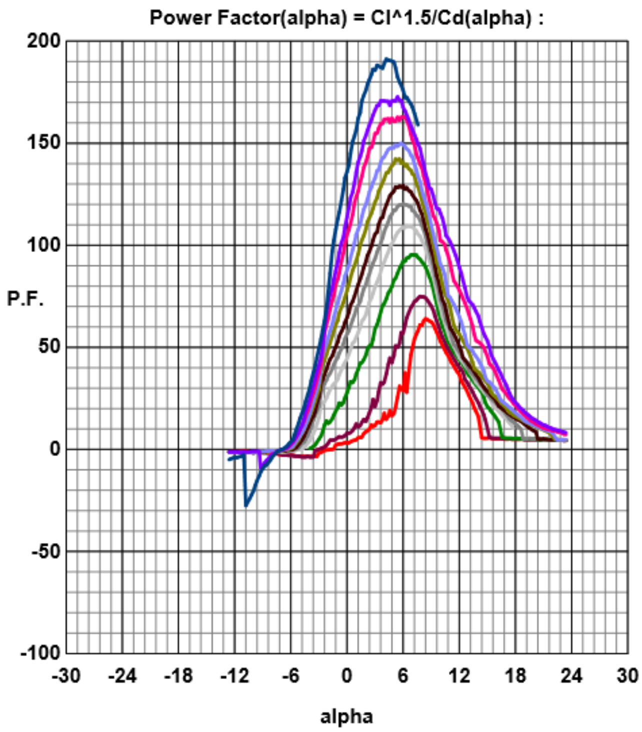

FX 63-137 13,7% smoothed
Spessore max 13.72% al 29.9% della corda
Camber max 5.94% al 52.8% della corda
Mach = 0.0000 - NCrit = 11.00

Re 80000 = **Re 100000 =** **Re 150000 =**
Re 200000 = **Re 250000 =** **Re 300000 =**
Re 400000 = **Re 500000 =** **Re 750000 =**
Re 1000000 = **Re 2000000 =**

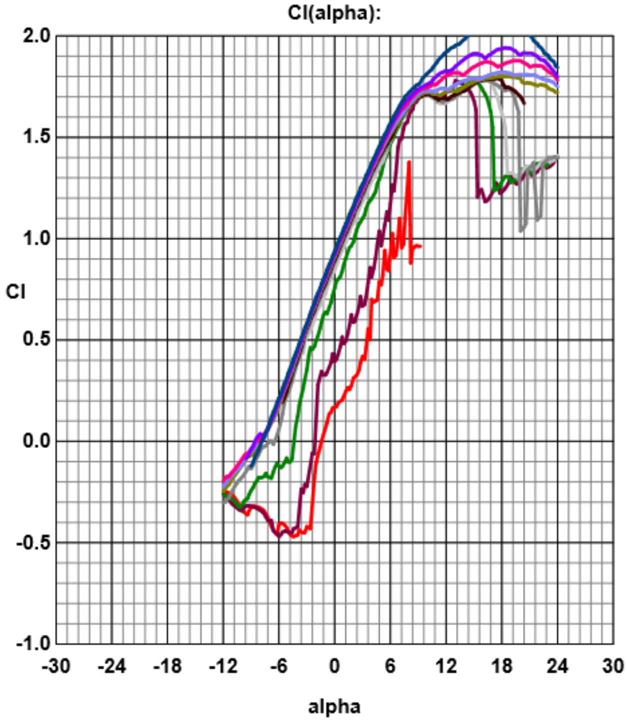

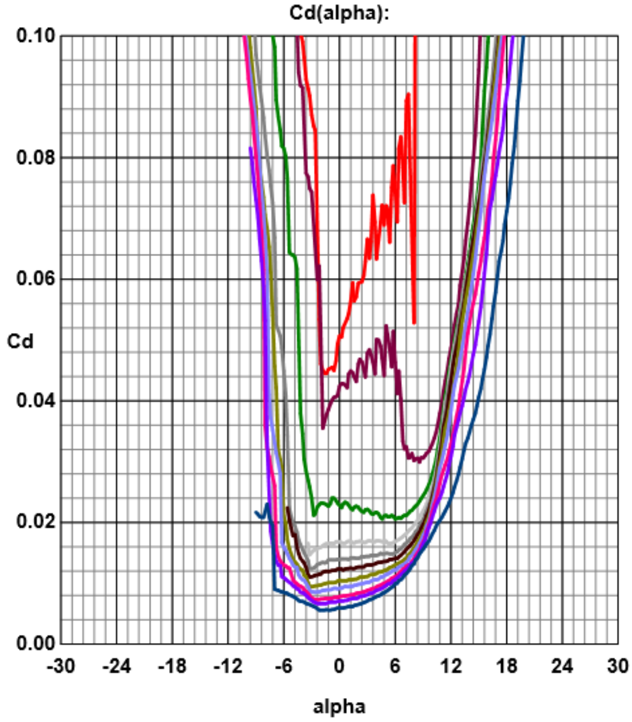

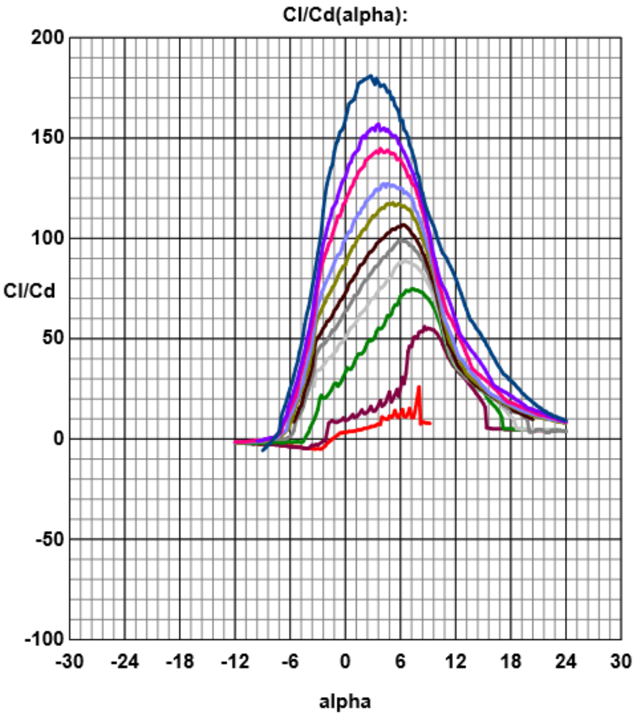

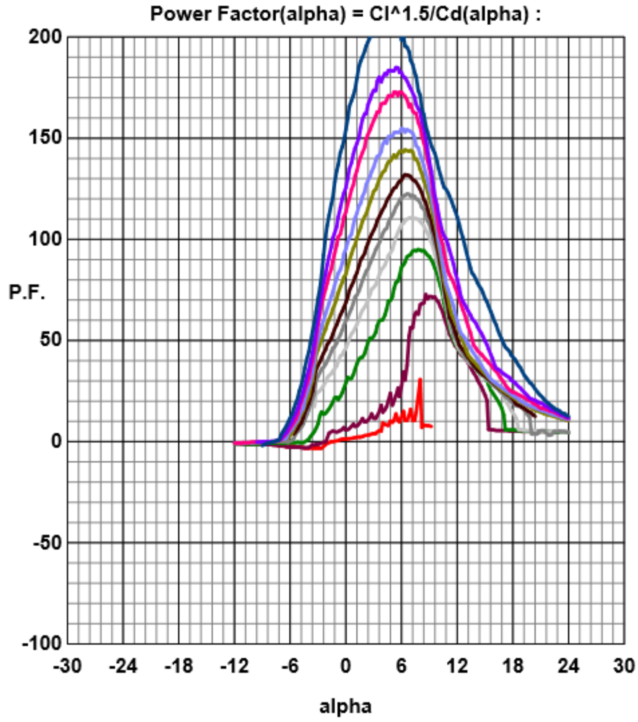

FX 71-L-150-20
Spessore max 15.00% al 33.9% della corda
Camber max 0.00% al 0.0% della corda
Mach = 0.0000 - NCrit = 11.00

Re 80000 =	**Re 100000 =**	**Re 150000 =**
Re 200000 =	**Re 250000 =**	**Re 300000 =**
Re 400000 =	**Re 500000 =**	**Re 750000 =**
Re 1000000 =	**Re 2000000 =**	

Cl(alpha):

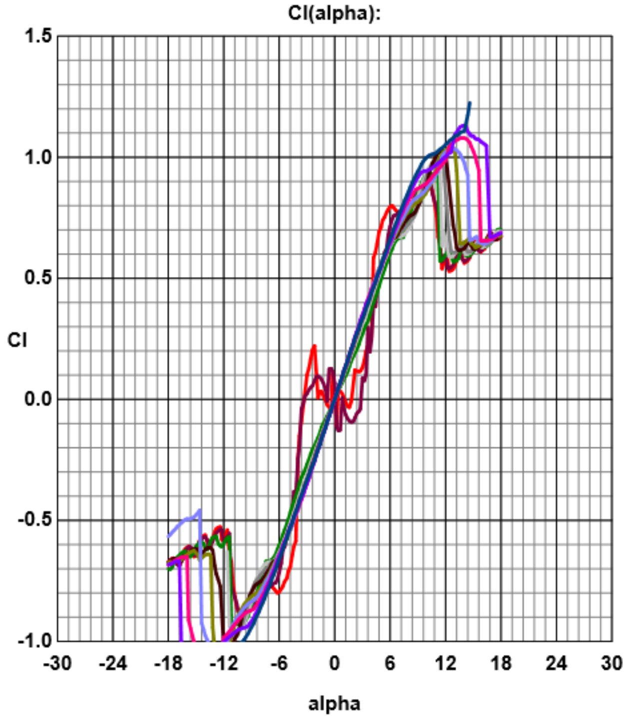

Cd(alpha):

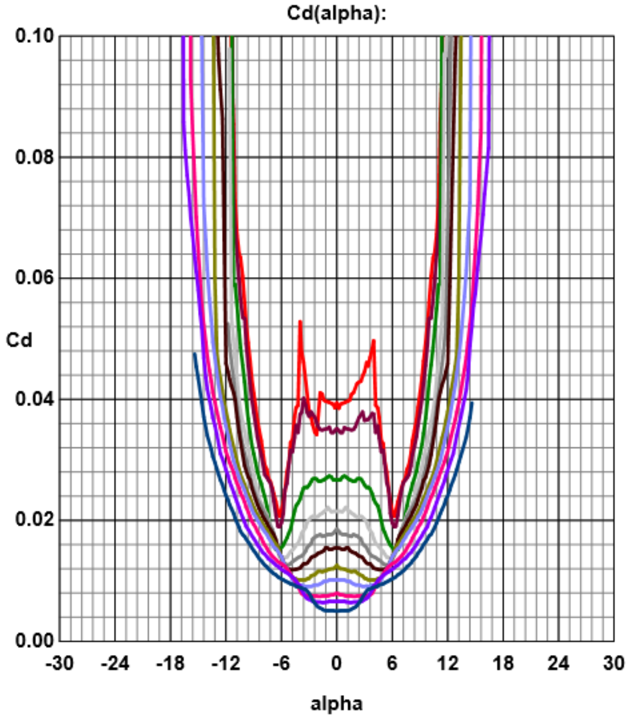

Cl/Cd(alpha):

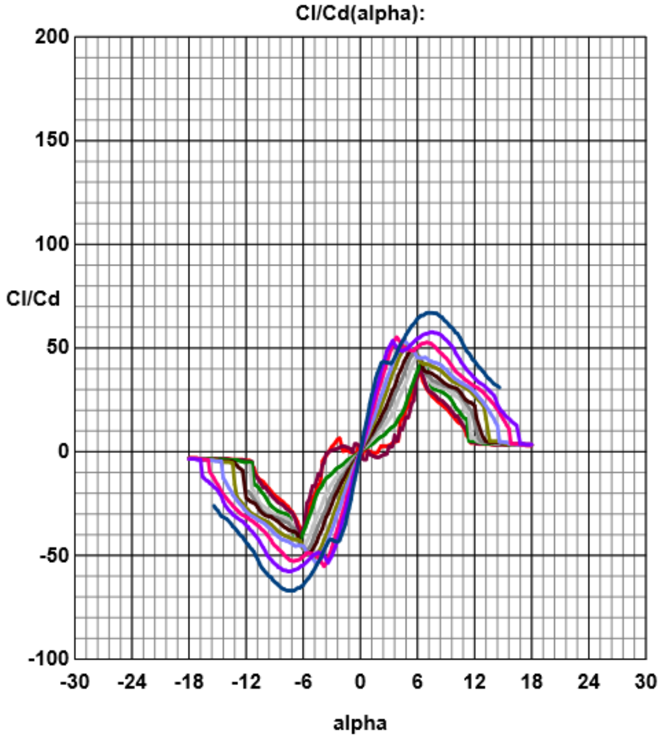

Power Factor(alpha) = Cl^1.5/Cd(alpha) :

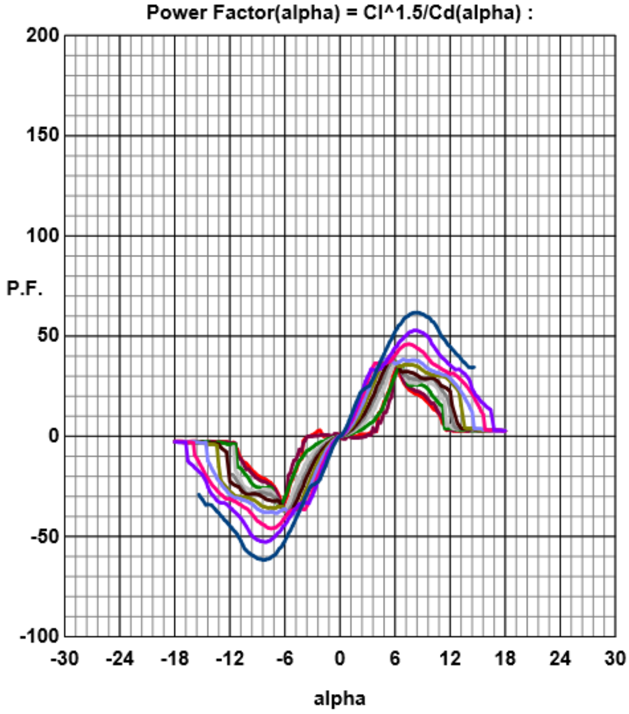

GOE 493
Spessore max 15.08% al 33.7% della corda
Camber max 3.36% al 52.6% della corda
Mach = 0.0000 - NCrit = 11.00

Re 80000 = | Re 100000 = | Re 150000 =
Re 200000 = | Re 250000 = | Re 300000 =
Re 400000 = | Re 500000 = | Re 750000 =
Re 1000000 = | Re 2000000 =

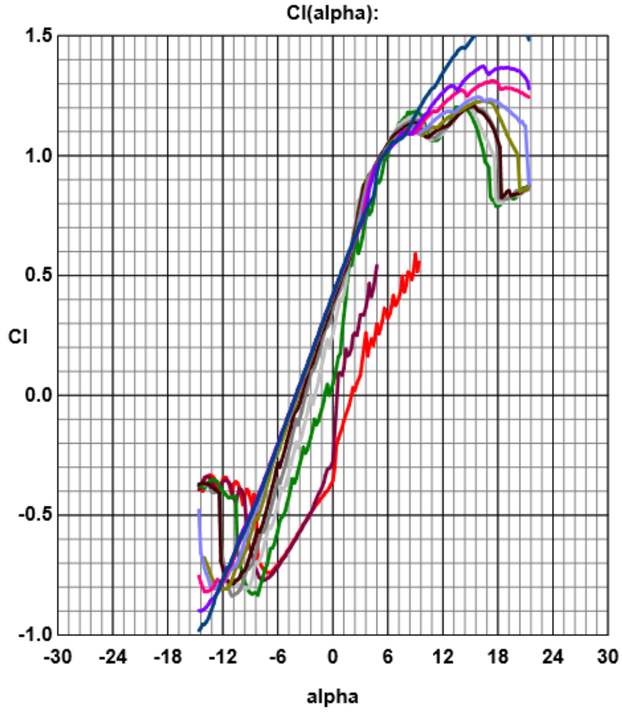

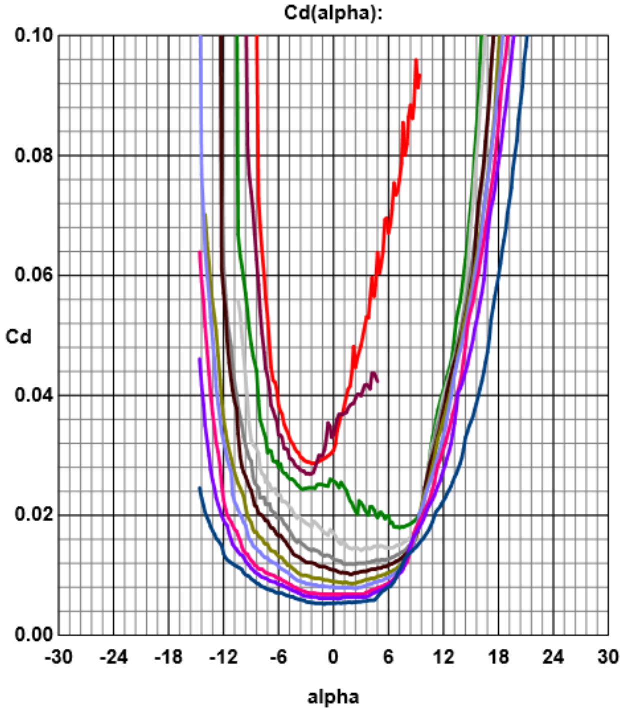

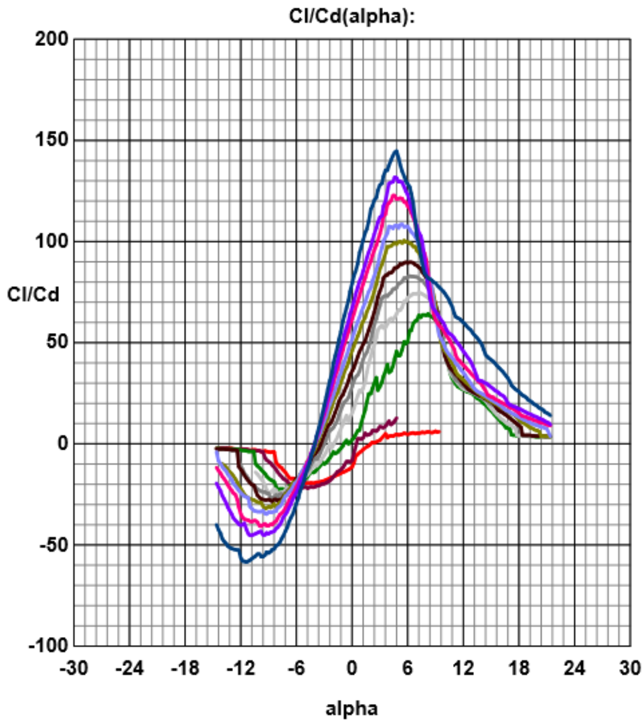

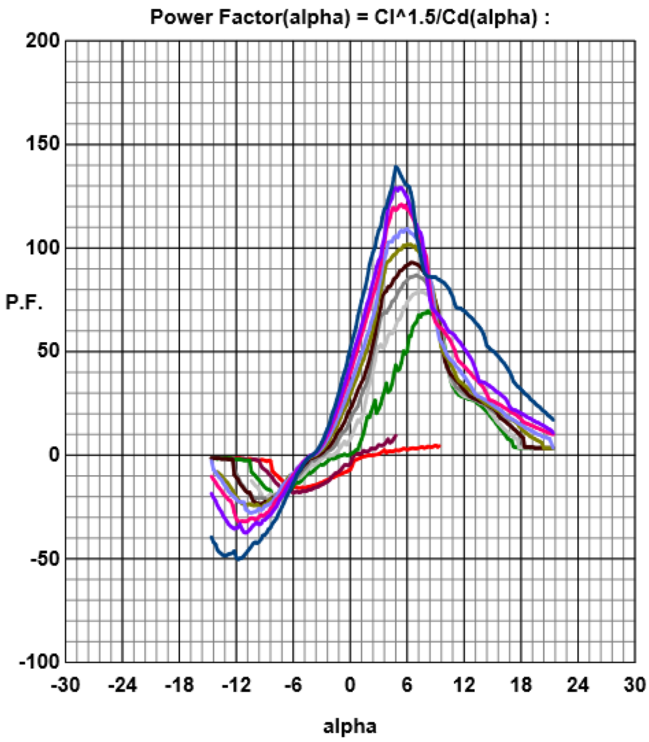

GOE 501
Spessore max 12.80% al 30.0% della corda
Camber max 6.30% al 50.0% della corda
Mach = 0.0000 - NCrit = 11.00

Re 50000 =
Re 70000 =
Re 100000 =
Re 200000 =
Re 250000 =
Re 300000 =
Re 400000 =
Re 500000 =
Re 750000 =
Re 1000000 =
Re 2000000 =

Cl(alpha):

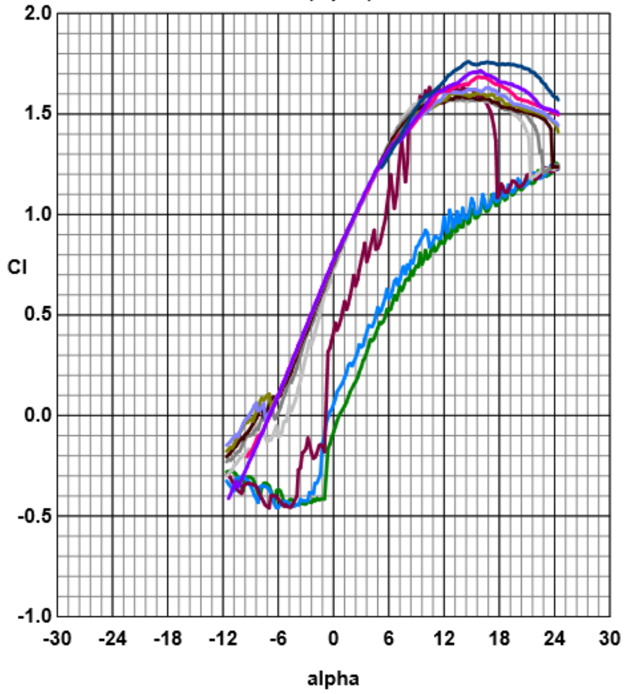

Cd(alpha):

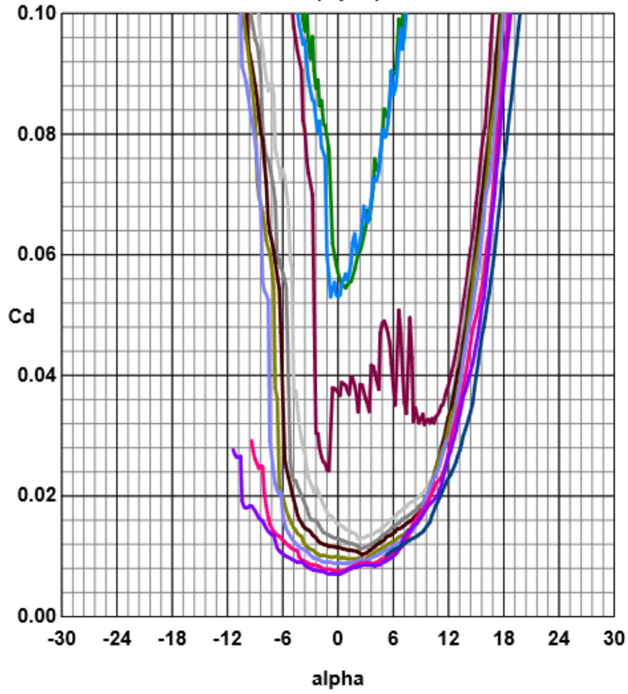

Power Factor(alpha) = Cl^1.5/Cd(alpha) :

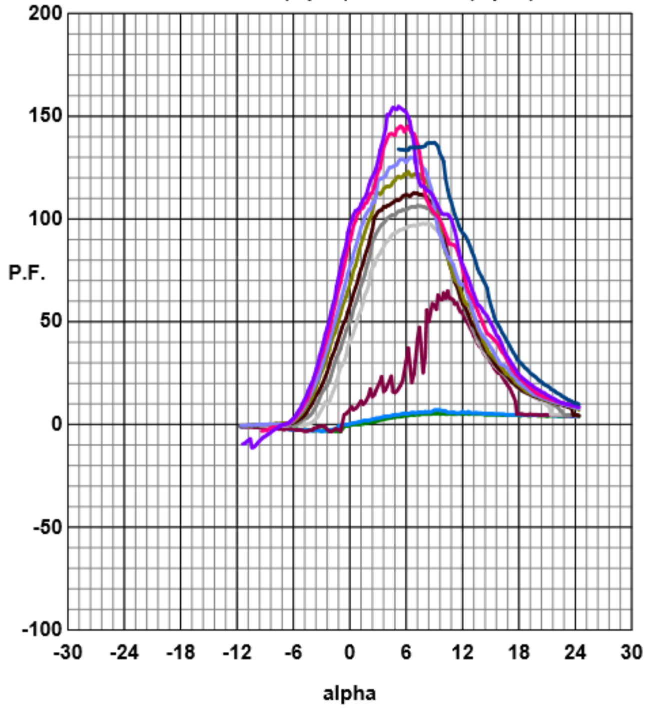

Cl/Cd(alpha):

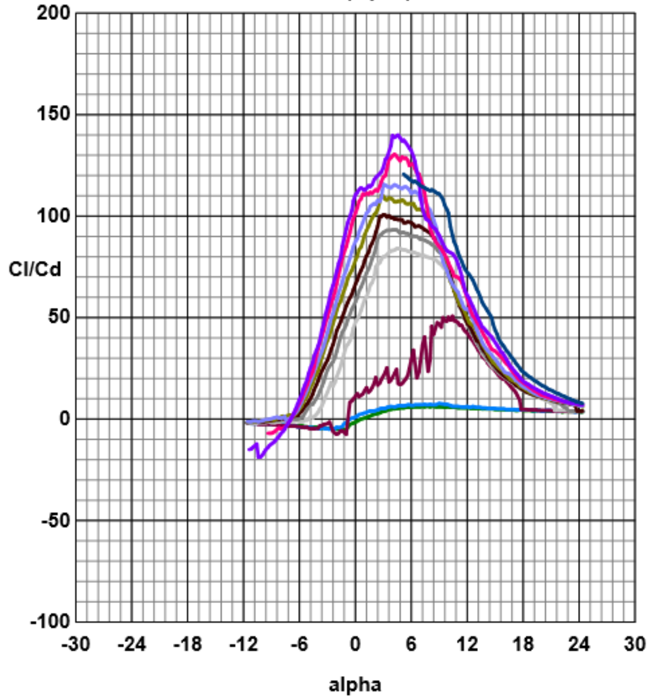

NACA4415
Spessore max 15.00% al 30.0% della corda
Camber max 4.00% al 40.0% della corda
Mach = 0.0000 - NCrit = 11.00

Re 200000 = | Re 250000 = | Re 300000 =
Re 400000 = | Re 500000 = | Re 750000 =
Re 1000000 = | Re 2000000 =

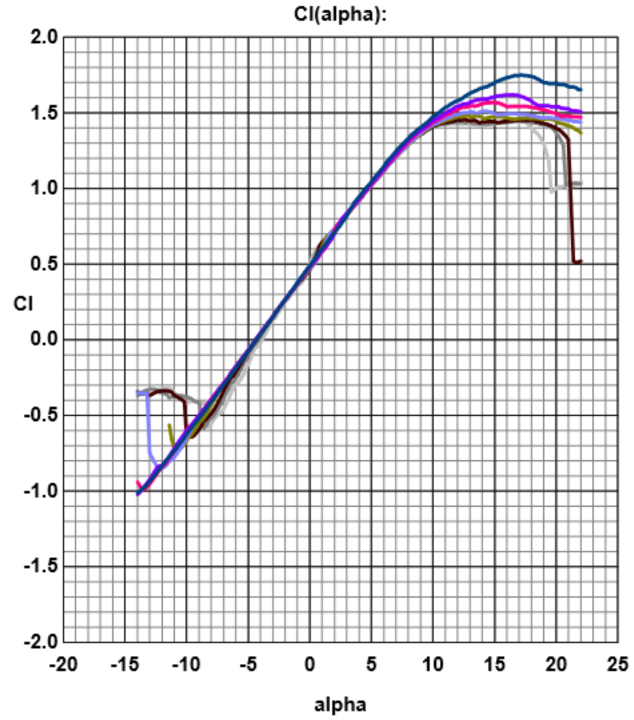

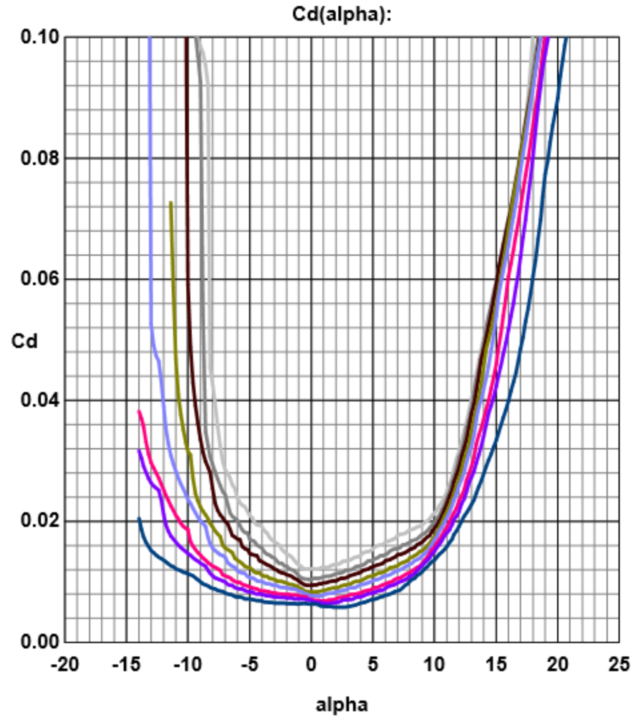

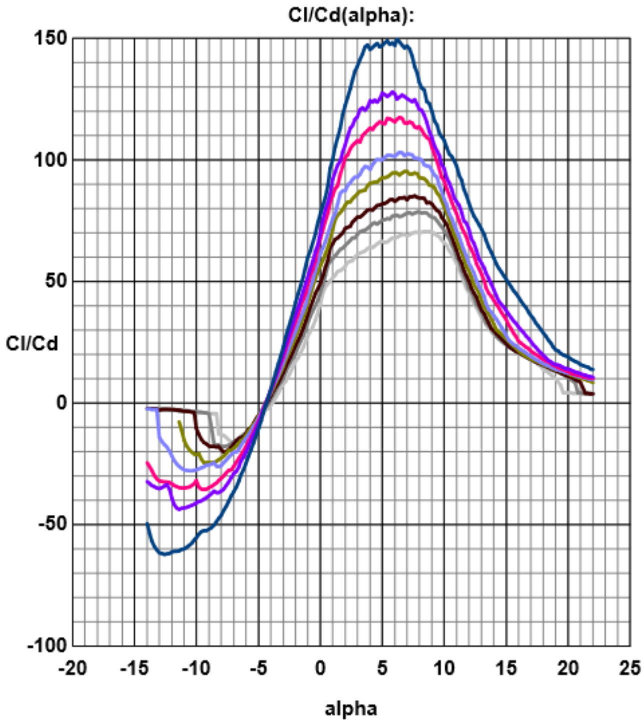

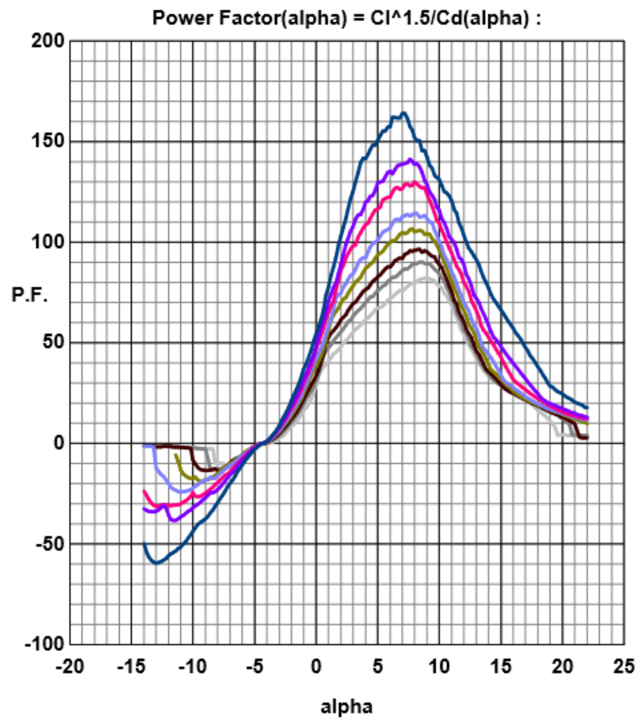

Appendix C

The flight envelope diagram is a graphical representation of the performance that the aircraft in general must satisfy to meet specifications and constraints. Specifically, this is a 2D Cartesian diagram that reports the load factor according to the velocity corresponding to the variation of C_l

Reymar's Method

The first method, associated to designer Daniel Reymar [39], starts considering a decreased value of maximum Cl averaged from the maximum Cl airfoil values, reported as:

$$Cl_{MAX} = 0.9\frac{Cl_{Root} + Cl_{tip}}{2}cos(\Delta_{0.25c}) \tag{1}$$

where $\Delta_{0.25c}$ referring to the swept angle of all airfoil at a quarter of their chord. With this equation, Reymar try to have a first attempt value of decreased C_L due to finite wing condition. Here are reported tables on which graphs on chapter three are based, when varying Reynolds.

Re=100000	rho (10000m)= 0.364	W= 2500 Newton	S = 7.26 m^2
Condition	n	V[m/s]	Cl
	0	0	
	0.25	23.09371385	
	0.5	32.65944333	
	0.75	39.99948572	
Stall	1	46.18742769	
	1.25	51.63911401	
	1.5	56.56781519	
	1.75	61.10022368	
	2	65.31888665	
	2.25	69.28114154	
	2.5	73.02873538	
	2.75	76.59318384	
	3	79.99897143	
	3.25	83.26556941	
	3.5	86.408765	
	3.75	89.44156913	
	4	92.37485538	
	4.25	95.21782147	
	4.5	97.97832998	
	4.75	100.6631649	
A	5	103.278228	0.88692
B	4	75	1.345456
D	0	75	0
	-1	48.63187415	-0.8
	-1.25	54.37208824	-0.8
	-1.5	59.56163845	-0.8
	-1.75	64.33392239	-0.8
	-2	68.77585599	-0.8
	-2.25	72.94781122	-0.8
C	-2.5	76.8937446	-0.8
A1	1	103.278228	0.177384
B1	1	75	0.336364

Re=400000	rho (5000m) = 0.736	W= 2500 Newton	S = 7.26 m^2
Condition	n	V[m/s]	Cl
	0	0	1.34443
	0.25	13.1910295	
	0.5	18.65493282	
	0.75	22.8475333	
stall	1	26.382059	
	1.25	29.49603865	
	1.5	32.31129145	
	1.75	34.90018359	
	2	37.30986564	
	2.25	39.5730885	
	2.5	41.7136979	
	2.75	43.74969545	
	3	45.69506659	
	3.25	47.56093323	
	3.5	49.35631296	
	3.75	51.08863757	
	4	52.764118	
	4.25	54.38800793	
	4.5	55.96479846	
	4.75	57.49836455	
A	5	58.99207731	
B	4	75	0.665416
D	0	75	
	-1	34.20052644	-0.8
	-1.25	38.237351	-0.8
	-1.5	41.88691936	-0.8
	-1.75	45.24304384	-0.8
	-2	48.36684834	-0.8
	-2.25	51.30078967	-0.8
C	-2.5	54.07578037	-0.8
A1	1	58.99207731	0.268886
B1	1	75	0.166354

Re=1000000	rho (1500m) = 1.058	W= 2500 Newton	S = 7.26 m^2
Condition	n	V[m/s]	Cl
	0	0	1.39268
	0.25	10.80981329	
	0.5	15.28738457	
	0.75	18.72314584	
stall	1	21.61962659	
	1.25	24.17147735	
	1.5	26.47852678	
	1.75	28.60007769	
	2	30.57476913	
	2.25	32.42943988	
	2.5	34.18363109	
	2.75	35.85209475	
	3	37.44629169	
	3.25	38.97533611	
	3.5	40.44661776	
	3.75	41.86622686	
	4	43.23925317	
	4.25	44.570002	
	4.5	45.8621537	
	4.75	47.11888374	
A	5	48.3429547	
B	4	75	0.462898
D	0	75	
	-1	28.52521093	-0.8
	-1.25	31.89215535	-0.8
	-1.5	34.93610579	-0.8
	-1.75	37.73530711	-0.8
	-2	40.34074016	-0.8
	-2.25	42.78781639	-0.8
C	-2.5	45.10231864	-0.8
A1	1	48.3429547	0.278536
B1	1	75	0.115724

Modified Pajno's Method with Wing C_L values

This method, referred to Prof. Pajno [34], was used the corrected value of C_l and C_d presented on chapter three and listed on below on **Table of Performance Estimation using [34]**. This group of tables, only $C_{L_{WING}}$ is considered to obtained the flight envelope diagram. Here are reported tables on which graphs on chapter three are based, when varying Reynolds: 100k, 400k, 750k, 1E6.

Re=100000	rho(10000m)=	0.364	W=	2500	Newton	S =	7.26	m^2

Condition	n	V[m/s]	Cl
	0	0	0
	0.25	19.64518	
	0.5	27.78248	
	0.75	34.02645	
stall	1	39.29036	
	1.25	43.92795	
	1.5	48.12066	
	1.75	51.97625	
	2	55.56495	
	2.25	58.93553	
	2.5	62.12351	
	2.75	65.15568	
	3	68.05289	
	3.25	70.8317	
	3.5	73.50552	
	3.75	76.08545	
	4	78.58071	
	4.25	80.99914	
	4.5	83.34743	
	4.75	85.63134	
A	5	87.8559	1.225632
B	4	75	1.345456
D	0	75	0
	-1	48.63187	-0.8
	-1.25	54.37209	-0.8
	-1.5	59.56164	-0.8
	-1.75	64.33392	-0.8
	-2	68.77586	-0.8
	-2.25	72.94781	-0.8
C	-2.5	76.89374	-0.8
A1	1	87.8559	0.245126
B1	1	75	0.336364

Re=400000	rho(5000m)=	0.736	W=	2500	Newton	S =	7.26	m^2

Condition	n	V[m/s]	Cl
	0	0	1.73257
	0.25	11.6199	
	0.5	16.43302	
	0.75	20.12626	
stall	1	23.2398	
	1.25	25.98289	
	1.5	28.46283	
	1.75	30.74337	
	2	32.86604	
	2.25	34.8597	
	2.5	36.74535	
	2.75	38.53885	
	3	40.25251	
	3.25	41.89615	
	3.5	43.47769	
	3.75	45.00368	
	4	46.4796	
	4.25	47.91008	
	4.5	49.29906	
	4.75	50.64997	
A	5	51.96577	
B	4	75	0.665416
D	0	75	
	-1	34.20053	-0.8
	-1.25	38.23735	-0.8
	-1.5	41.88692	-0.8
	-1.75	45.24304	-0.8
	-2	48.36685	-0.8
	-2.25	51.30079	-0.8
C	-2.5	54.07578	-0.8
A1	1	51.96577	0.346514
B1	1	75	0.166354

Re=750000	rho(2500m)=	0.957	W=	2500	Newton	S =	7.26	m^2

Condition	n	V[m/s]	Cl
	0	0	1.780907
	0.25	10.05102	
	0.5	14.21429	
	0.75	17.40888	
stall	1	20.10204	
	1.25	22.47476	
	1.5	24.61987	
	1.75	26.5925	
	2	28.42858	
	2.25	30.15306	
	2.5	31.78411	
	2.75	33.33546	
	3	34.81775	
	3.25	36.23947	
	3.5	37.60747	
	3.75	38.92743	
	4	40.20408	
	4.25	41.44141	
	4.5	42.64286	
	4.75	43.81138	
A	5	44.94952	
B	4	75	0.511751
D	0	75	
	-1	29.99271	-0.8
	-1.25	33.53287	-0.8
	-1.5	36.73342	-0.8
	-1.75	39.67663	-0.8
	-2	42.4161	-0.8
	-2.25	44.98907	-0.8
C	-2.5	47.42264	-0.8
A1	1	44.94952	0.356181
B1	1	75	0.127938

Re=1000000	rho(1500m)=	1.058	W=	2500	Newton	S =	7.26	m^2

Condition	n	V[m/s]	Cl
	0	0	1.792974
	0.25	9.527015	
	0.5	13.47323	
	0.75	16.50127	
stall	1	19.05403	
	1.25	21.30305	
	1.5	23.33633	
	1.75	25.20611	
	2	26.94647	
	2.25	28.58105	
	2.5	30.12707	
	2.75	31.59754	
	3	33.00255	
	3.25	34.35014	
	3.5	35.64683	
	3.75	36.89797	
	4	38.10806	
	4.25	39.28089	
	4.5	40.4197	
	4.75	41.5273	
A	5	42.60611	
B	4	75	0.462898
D	0	75	
	-1	28.52521	-0.8
	-1.25	31.89216	-0.8
	-1.5	34.93611	-0.8
	-1.75	37.73531	-0.8
	-2	40.34074	-0.8
	-2.25	42.78782	-0.8
C	-2.5	45.10232	-0.8
A1	1	42.60611	0.358595
B1	1	75	0.115724

Modified Pajno's Method with Glider C_L values

This group of tables, the entire $C_{L_{GLIDER}}$ is considered to obtained the flight envelope diagram. The difference respect $C_{L_{WING}}$ is about the influence of tail plan and fuselage. Here are reported tables on which graphs on chapter three are based, when varying Reynolds: 100k, 400k, 750k, 1E6.

Re=100000	rho (10000m)=	0.364	W=	2500	Newton	S =	7.26	m^2

Condition	n	V[m/s]	Cl
	0	0	0
	0.25	20.89371	
	0.5	29.54817	
	0.75	36.18897	
stall	1	41.78743	
	1.25	46.71976	
	1.5	51.17894	
	1.75	55.27957	
	2	59.09635	
	2.25	62.68114	
	2.5	66.07172	
	2.75	69.29661	
	3	72.37795	
	3.25	75.33336	
	3.5	78.17712	
	3.75	80.921	
	4	83.57485	
	4.25	86.14699	
	4.5	88.64452	
	4.75	91.07359	
A	5	93.43953	1.08353
B	4	75	1.345456
D	0	75	0
	-1	48.63187	-0.8
	-1.25	54.37209	-0.8
	-1.5	59.56164	-0.8
	-1.75	64.33392	-0.8
	-2	68.77586	-0.8
	-2.25	72.94781	-0.8
C	-2.5	76.89374	-0.8
A1	1	93.43953	0.216706
B1	1	75	0.336364

Re=400000	rho (5000m)=	0.736	W=	2500	Newton	S =	7.26	m^2

Condition	n	V[m/s]	Cl
	0	0	1.616925
	0.25	12.02826	
	0.5	17.01053	
	0.75	20.83356	
stall	1	24.05652	
	1.25	26.89601	
	1.5	29.4631	
	1.75	31.82379	
	2	34.02106	
	2.25	36.08479	
	2.5	38.0367	
	2.75	39.89323	
	3	41.66712	
	3.25	43.36851	
	3.5	45.00563	
	3.75	46.58526	
	4	48.11305	
	4.25	49.59379	
	4.5	51.03159	
	4.75	52.42998	
A	5	53.79202	
B	4	75	0.665416
D	0	75	
	-1	34.20053	-0.8
	-1.25	38.23735	-0.8
	-1.5	41.88692	-0.8
	-1.75	45.24304	-0.8
	-2	48.36685	-0.8
	-2.25	51.30079	-0.8
C	-2.5	54.07578	-0.8
A1	1	53.79202	0.323385
B1	1	75	0.166354

Re=750000	rho (2500m) =	0.957	W=	2500	Newton	S =	7.26	m^2

Condition	n	V[m/s]	Cl
	0	0	1.667361
	0.25	10.38762	
	0.5	14.69031	
	0.75	17.99188	
stall	1	20.77523	
	1.25	23.22741	
	1.5	25.44436	
	1.75	27.48305	
	2	29.38061	
	2.25	31.16285	
	2.5	32.84852	
	2.75	34.45182	
	3	35.98375	
	3.25	37.45308	
	3.5	38.8669	
	3.75	40.23106	
	4	41.55046	
	4.25	42.82923	
	4.5	44.07092	
	4.75	45.27856	
A	5	46.45483	
B	4	75	0.511751
D	0	75	
	-1	29.99271	-0.8
	-1.25	33.53287	-0.8
	-1.5	36.73342	-0.8
	-1.75	39.67663	-0.8
	-2	42.4161	-0.8
	-2.25	44.98907	-0.8
C	-2.5	47.42264	-0.8
A1	1	46.45483	0.333472
B1	1	75	0.127938

Re=1000000	rho (1500m)=	1.058	W=	2500	Newton	S =	7.26	m^2

Condition	n	V[m/s]	Cl
	0	0	1.681658
	0.25	9.83728	
	0.5	13.91201	
	0.75	17.03867	
stall	1	19.67456	
	1.25	21.99683	
	1.5	24.09632	
	1.75	26.027	
	2	27.82403	
	2.25	29.51184	
	2.5	31.10821	
	2.75	32.62657	
	3	34.07734	
	3.25	35.46882	
	3.5	36.80773	
	3.75	38.09962	
	4	39.34912	
	4.25	40.56015	
	4.5	41.73604	
	4.75	42.87971	
A	5	43.99365	
B	4	75	0.462898
D	0	75	
	-1	28.52521	-0.8
	-1.25	31.89216	-0.8
	-1.5	34.93611	-0.8
	-1.75	37.73531	-0.8
	-2	40.34074	-0.8
	-2.25	42.78782	-0.8
C	-2.5	45.10232	-0.8
A1	1	43.99365	0.336332
B1	1	75	0.115724

Table of Performance Estimation using [34]

First 4 tables, refer to the aerodynamic parameters correction process thanks to which we obtain an estimation of a three-dimensional finite wing. Follow spiral flight performance tables. Spiral flight is the most well-known flight configuration with glider. The spiral geometry in ideal flight conditions is determined by the speed and the angle at which it is approached. Thus was identified the vertical velocity knowing the lift coefficient, drag, bank angle and horizontal velocity using the **Excel**®calculation engine. Here are reported group of tables on which performance graphs are based on.

Re=		100000												
alpha [°]	alpha rad	CL_wings	Cd_0	alpha_i	alpha_eff	Cd_wings	a_tail[1/rad]	a_tail[1/°]	Cl_tail	Cd_i_tail	Cd0_tail	Cd_wing&tail	Cd_Glider	CL glider
-10	-0.174532925	-0.7261503	0.03	-0.67915	-9.3208516	0.040436925	6.52809	0.113936664	-1.139366644	0.061439447	0.0138	0.048356758	0.049749758	-0.641958877
-9	-0.157079633	-0.63743293	0.03	-0.59617	-8.4038265	0.038042453			-1.025429979	0.049765952		0.044733513	0.046126513	-0.563527587
-8	-0.13962634	-0.54871555	0.03	-0.5132	-7.4868015	0.035959558			-0.911493315	0.039321246		0.041551191	0.042944191	-0.485096297
-7	-0.122173048	-0.45999818	0.03	-0.43022	-6.5697764	0.034188242			-0.797556651	0.030105329		0.038809792	0.040202792	-0.406665007
-6	-0.104719755	-0.37128081	0.03	-0.34725	-5.6527513	0.032728504			-0.683619986	0.022118201		0.036509315	0.037902315	-0.328233717
-5	-0.087266463	-0.28256344	0.03	-0.26427	-4.7357262	0.031580343			-0.569683322	0.015359862		0.03464976	0.03604276	-0.249802427
-4	-0.06981317	-0.19384607	0.03	-0.1813	-3.8187011	0.030743761			-0.455746657	0.009830311		0.033231128	0.034624128	-0.171371137
-3	-0.052359878	-0.10512869	0.03	-0.09832	-2.901676	0.030218757			-0.341809993	0.00552955		0.032253419	0.033646419	-0.092939847
-2	-0.034906585	-0.01641132	0.03	-0.01535	-1.9846509	0.030005331			-0.227873329	0.002457578		0.031716631	0.033109631	-0.014508557
-1	-0.017453293	0.07230605	0.03	0.067626	-1.0676259	0.030103483			-0.113936664	0.000614394		0.031620767	0.033013767	0.063922733
0	0	0.16102342	0.03	0.150601	-0.1506008	0.030513213			0	0		0.031965825	0.033358825	0.142354023
1	0.017453293	0.2497408	0.03	0.233576	0.76642431	0.031234521			0.113936664	0.000614394		0.032751805	0.034144805	0.220785313
2	0.034906585	0.33845817	0.03	0.316551	1.6834494	0.032267407			0.227873329	0.002457578		0.033978708	0.035371708	0.299216603
3	0.052359878	0.42717554	0.03	0.399526	2.60047448	0.033611871			0.341809993	0.00552955		0.035646533	0.037039533	0.377647893
4	0.06981317	0.51589291	0.03	0.4825	3.51749956	0.035267914			0.455746657	0.009830311		0.037755281	0.039148281	0.456079183
5	0.087266463	0.60461028	0.03	0.565475	4.43452465	0.037235534			0.569683322	0.015359862		0.040304951	0.041697951	0.534510473
6	0.104719755	0.69332766	0.03	0.64845	5.35154973	0.039514732			0.683619986	0.022118201		0.043295543	0.044688543	0.612941763
7	0.122173048	0.78204503	0.03	0.731425	6.26857482	0.042105509			0.797556651	0.030105329		0.046727059	0.048120059	0.691373053
8	0.13962634	0.8707624	0.03	0.8144	7.1855999	0.045007863			0.911493315	0.039321246		0.050599496	0.051992496	0.769804343
9	0.157079633	0.95947977	0.03	0.897375	8.10262499	0.048221796			1.025429979	0.049765952		0.054912856	0.056305856	0.848235633
10	0.174532925	1.04819715	0.03	0.98035	9.01965007	0.051747306			1.139366644	0.061439447		0.059667139	0.061060139	0.926666923
11	0.191986218	1.13691452	0.03	1.063325	9.93667516	0.055584395			1.253303308	0.07434173		0.064862344	0.066255344	1.005098212
12	0.20943951	1.22563189	0.03	1.1463	10.8537002	0.059733061			1.367239972	0.088472803		0.070498471	0.071891471	1.083529502
13	0.226892803	1.31434926	0.03	1.229275	11.7707253	0.064193306			1.481176637	0.103832665		0.076575521	0.077968521	1.161960792
14	0.244346095	1.40306663	0.03	1.31225	12.6877504	0.068965129			1.595113301	0.120421316		0.083093494	0.084486494	1.240392082
15	0.261799388	1.49178401	0.03	1.395225	13.6047755	0.07404853			1.709049965	0.138238755		0.090052389	0.091445389	1.318823372

CdMIN	
wings	0.030005331
Wings+Tail Plane	0.031620767
Glider	0.033013767

Re=		400000												
alpha [°]	alpha rad	CL_wings	Cd_0	alpha_i	alpha_eff	Cd_wings	a_tail[1/rad]	a_tail[1/°]	Cl_tail	Cd_i_tail	Cd0_tail	Cd_wings&tail	Cd_Glider	CL glider
-10	-0.174532925	-0.39589473	0.033278	-0.37027	-9.6297306	0.036380266	4.66929	0.081494484	-0.814944842	0.031432341	0.0061	0.040330984	0.041723984	-0.369469649
-9	-0.157079633	-0.29914634	0.033278	-0.27978	-8.7202167	0.035049279			-0.733450358	0.025460196		0.038371359	0.039764359	-0.27917899
-8	-0.13962634	-0.20239794	0.033278	-0.1893	-7.8107028	0.034088834			-0.651955874	0.020116698		0.036848448	0.038241448	-0.18888833
-7	-0.122173048	-0.10564954	0.033278	-0.09881	-6.9011889	0.03349893			-0.57046139	0.015401847		0.035762251	0.037155251	-0.09859767
-6	-0.104719755	-0.00890114	0.033278	-0.00832	-5.991675	0.033279568			-0.488966905	0.011315643		0.035112769	0.036505769	-0.008307011
-5	-0.087266463	0.08784726	0.033278	0.082161	-5.0821611	0.033430748			-0.407472421	0.007858085		0.0349	0.036293	0.081983649
-4	-0.06981317	0.18459565	0.033278	0.172647	-4.1726472	0.03395247			-0.325977937	0.005029175		0.035123946	0.036516946	0.172274309
-3	-0.052359878	0.28134405	0.033278	0.263133	-3.2631333	0.034844733			-0.244483453	0.002828911		0.035784605	0.037177605	0.262564968
-2	-0.034906585	0.37809245	0.033278	0.353619	-2.3536195	0.036107538			-0.162988968	0.001257294		0.036881979	0.038274979	0.352855628
-1	-0.017453293	0.47484085	0.033278	0.444106	-1.4441056	0.037740885			-0.081494484	0.000314323		0.038416067	0.039809067	0.443146287
0	0	0.57158925	0.033278	0.534592	-0.5345917	0.039744773			0	0		0.040386869	0.041779869	0.533436947
1	0.017453293	0.66833764	0.033278	0.625078	0.37492221	0.042119203			0.081494484	0.000314323		0.042794386	0.044187386	0.623727607
2	0.034906585	0.76508604	0.033278	0.715564	1.28443609	0.044864175			0.162988968	0.001257294		0.045638616	0.047031616	0.714018266
3	0.052359878	0.86183444	0.033278	0.80605	2.19394998	0.047979688			0.244483453	0.002828911		0.048919561	0.050312561	0.804308926
4	0.06981317	0.95858284	0.033278	0.896536	3.10346387	0.051465743			0.325977937	0.005029175		0.052637219	0.054030219	0.894599586
5	0.087266463	1.05533123	0.033278	0.987022	4.01297776	0.05532234			0.407472421	0.007858085		0.056791592	0.058184592	0.984890245
6	0.104719755	1.15207963	0.033278	1.077508	4.92249164	0.059549479			0.488966905	0.011315643		0.061382679	0.062775679	1.075180905
7	0.122173048	1.24882803	0.033278	1.167994	5.83200553	0.064147159			0.57046139	0.015401847		0.06641048	0.06780348	1.165471565
8	0.13962634	1.34557643	0.033278	1.258481	6.74151942	0.069115381			0.651955874	0.020116698		0.071874995	0.073267995	1.255762224
9	0.157079633	1.44232483	0.033278	1.348967	7.6510333	0.074454145			0.733450358	0.025460196		0.077776225	0.079169225	1.346052884
10	0.174532925	1.53907322	0.033278	1.439453	8.56054719	0.08016345			0.814944842	0.031432341		0.084114168	0.085507168	1.436343544
11	0.191986218	1.63582162	0.033278	1.529939	9.47006108	0.086243297			0.896439327	0.038033132		0.090888826	0.092281826	1.526634203
12	0.20943951	1.73257002	0.033278	1.620425	10.379575	0.092693685			0.977933811	0.045262571		0.098100197	0.099493197	1.616924863
13	0.226892803	1.82931842	0.033278	1.710911	11.2890889	0.099514616			1.059428295	0.053120656		0.105748283	0.107141283	1.707215523
14	0.244346095	1.92606682	0.033278	1.801397	12.1986027	0.106706088			1.140922779	0.061607388		0.113833083	0.115226083	1.797506182
15	0.261799388	2.02281521	0.033278	1.891883	13.1081166	0.114268102			1.222417263	0.070722767		0.122354597	0.123747597	1.887796842

CdMIN	
wings	0.033279568
Wings+Tail Plane	0.0349
Glider	0.036293

Re=		750000												
alpha [°]	alpha rad	CL_wings	Cd_0	alpha_i	alpha_eff	Cd_wings	a_tail[1/rad]	a_tail[1/°]	Cl_tail	Cd_i_tail	Cd0_tail	Cd_wings&tail	Cd_Glider	CL glider
-10	-0.174532925	-0.35914095	0.018882	-0.33589	-9.6641054	0.021434991	4.54375	0.079303398	-0.793033979	0.029764863	0.0049	0.025083874	0.026476874	-0.336243218
-9	-0.157079633	-0.26186606	0.018882	-0.24492	-8.7550839	0.020239307			-0.713730581	0.024109539		0.0232929	0.0246859	-0.245170279
-8	-0.13962634	-0.16459117	0.018882	-0.15394	-7.8460624	0.019418207			-0.634427183	0.019049512		0.021939174	0.023332174	-0.15409734
-7	-0.122173048	-0.06731628	0.018882	-0.06296	-6.9370409	0.018971693			-0.555123785	0.014584783		0.021022695	0.022415695	-0.0630244
-6	-0.104719755	0.02995861	0.018882	0.028019	-6.0280195	0.018899765			-0.475820387	0.010715351		0.020543463	0.021936463	0.028048539
-5	-0.087266463	0.1272335	0.018882	0.118998	-5.118998	0.019202422			-0.396516989	0.007441216		0.02050148	0.02189448	0.119121478
-4	-0.06981317	0.22450838	0.018882	0.209977	-4.2099765	0.019879665			-0.317213592	0.004762378		0.020896743	0.022289743	0.210194417
-3	-0.052359878	0.32178327	0.018882	0.300955	-3.300955	0.020931493			-0.237910194	0.002678838		0.021729254	0.023122254	0.301267356
-2	-0.034906585	0.41905816	0.018882	0.391934	-2.3919336	0.022357907			-0.158606796	0.001190595		0.022999013	0.024392013	0.392340295
-1	-0.017453293	0.51633305	0.018882	0.482912	-1.4829121	0.024158906			-0.079303398	0.000297649		0.02470602	0.02609902	0.483413234
0	0	0.61360794	0.018882	0.573891	-0.5738906	0.026334491			0	0		0.026850273	0.028243273	0.574486174
1	0.017453293	0.71088283	0.018882	0.664869	0.33513087	0.028884661			0.079303398	0.000297649		0.029431775	0.030824775	0.665559113
2	0.034906585	0.80815771	0.018882	0.755848	1.24415234	0.031809417			0.158606796	0.001190595		0.032450524	0.033843524	0.756632052
3	0.052359878	0.9054326	0.018882	0.846826	2.15317382	0.035108759			0.237910194	0.002678838		0.03590652	0.03729952	0.847704991
4	0.06981317	1.00270749	0.018882	0.937805	3.06219529	0.038782686			0.317213592	0.004762378		0.039799764	0.041192764	0.93877793
5	0.087266463	1.09998238	0.018882	1.028783	3.97121677	0.042831198			0.396516989	0.007441216		0.044130256	0.045523256	1.029850869
6	0.104719755	1.19725727	0.018882	1.119762	4.88023825	0.047254296			0.475820387	0.010715351		0.048897995	0.050290995	1.120923808
7	0.122173048	1.29453216	0.018882	1.21074	5.78925972	0.05205198			0.555123785	0.014584783		0.054102981	0.055495981	1.211996747
8	0.13962634	1.39180704	0.018882	1.301719	6.6982812	0.057224249			0.634427183	0.019049512		0.059745215	0.061138215	1.303069687
9	0.157079633	1.48908193	0.018882	1.392697	7.60730267	0.062771103			0.713730581	0.024109539		0.065824697	0.067217697	1.394142626
10	0.174532925	1.58635682	0.018882	1.483676	8.51632415	0.068692544			0.793033979	0.029764863		0.072341426	0.073734426	1.485215565
11	0.191986218	1.68363171	0.018882	1.574654	9.42534562	0.074988569			0.872337377	0.036015484		0.079295403	0.080688403	1.576288504
12	0.20943951	1.7809066	0.018882	1.665633	10.3343671	0.081659181			0.951640775	0.042861403		0.086686627	0.088079627	1.667361443
13	0.226892803	1.87818148	0.018882	1.756611	11.2433886	0.088704377			1.030944173	0.050302618		0.094515099	0.095908099	1.758434382
14	0.244346095	1.97545637	0.018882	1.84759	12.15241	0.09612416			1.11024757	0.058339131		0.102780819	0.104173819	1.849507321
15	0.261799388	2.07273126	0.018882	1.938568	13.0614315	0.103918527			1.189550968	0.066970941		0.111483785	0.112876785	1.940580261

CdMIN	
wings	0.018899765
Wings+Tail Plane	0.02050148
Glider	0.02189448

Re=		1.00E+06												
alpha [°]	alpha rad	CL_wings	Cd_0	alpha_i	alpha_eff	Cd_wings	a_tail[1/rad]	a_tail[1/°]	Cl_tail	Cd_i_tail	Cd0_tail	Cd_wings&tail	Cd_Glider	CL glider
-10	-0.174532925	-0.3569924	0.02878	-0.33389	-9.6661148	0.031302537	4.4722	0.078054615	-0.780546148	0.028834835	0.0044	0.034800892	0.036193892	-0.334828677
-9	-0.157079633	-0.25926666	0.02878	-0.24248	-8.757515	0.030110494			-0.702491533	0.023356216		0.033032161	0.034425161	-0.243170197
-8	-0.13962634	-0.16154092	0.02878	-0.15108	-7.8489152	0.029296517			-0.624436918	0.018454294		0.031702199	0.033095199	-0.151511717
-7	-0.122173048	-0.06381518	0.02878	-0.05968	-6.9403154	0.028860606			-0.546382304	0.014129069		0.030811007	0.032204007	-0.059853237
-6	-0.104719755	0.03391057	0.02878	0.031716	-6.0317156	0.028802761			-0.468327689	0.01038054		0.030358586	0.031751586	0.031805242
-5	-0.087266463	0.13163631	0.02878	0.123116	-5.1231158	0.029122982			-0.390273074	0.007208709		0.030344934	0.031737934	0.123463722
-4	-0.06981317	0.22936205	0.02878	0.214516	-4.214516	0.029821268			-0.312218459	0.004613574		0.030770052	0.032163052	0.215122202
-3	-0.052359878	0.32708779	0.02878	0.305916	-3.3059162	0.030897621			-0.234163844	0.002595135		0.031633941	0.033026941	0.306780682
-2	-0.034906585	0.42481354	0.02878	0.397316	-2.3973164	0.032352039			-0.15610923	0.001153393		0.032936599	0.034329599	0.398439162
-1	-0.017453293	0.52253928	0.02878	0.488717	-1.4887166	0.034184523			-0.078054615	0.000288348		0.034678027	0.036071027	0.490097642
0	0	0.62026502	0.02878	0.580117	-0.5801168	0.036395074			0	0		0.036858225	0.038251225	0.581756122
1	0.017453293	0.71799076	0.02878	0.671517	0.32848301	0.03898369			0.078054615	0.000288348		0.039477193	0.040870193	0.673414602
2	0.034906585	0.81571651	0.02878	0.762917	1.23708281	0.041950371			0.15610923	0.001153393		0.042534931	0.043927931	0.765073082
3	0.052359878	0.91344225	0.02878	0.854317	2.14568262	0.045295119			0.234163844	0.002595135		0.046031439	0.047424439	0.856731561
4	0.06981317	1.01116799	0.02878	0.945718	3.05428242	0.049017933			0.312218459	0.004613574		0.049966717	0.051359717	0.948390041
5	0.087266463	1.10889373	0.02878	1.037118	3.96288223	0.053118812			0.390273074	0.007208709		0.054340765	0.055733765	1.040048521
6	0.104719755	1.20661948	0.02878	1.128518	4.87148203	0.057597758			0.468327689	0.01038054		0.059153582	0.060546582	1.131707001
7	0.122173048	1.30434522	0.02878	1.219918	5.78008183	0.062454769			0.546382304	0.014129069		0.06440517	0.06579817	1.223365481
8	0.13962634	1.40207096	0.02878	1.311318	6.68868164	0.067689846			0.624436918	0.018454294		0.070095528	0.071488528	1.315023961
9	0.157079633	1.4997967	0.02878	1.402719	7.59728144	0.073302989			0.702491533	0.023356216		0.076224655	0.077617655	1.406682441
10	0.174532925	1.59752245	0.02878	1.494119	8.50588125	0.079294198			0.780546148	0.028834835		0.082792553	0.084185553	1.498340921
11	0.191986218	1.69524819	0.02878	1.585519	9.41448105	0.085663472			0.858600763	0.03489015		0.089799221	0.091192221	1.5899994
12	0.20943951	1.79297393	0.02878	1.676919	10.3230809	0.092410813			0.936655378	0.041522162		0.097244658	0.098637658	1.68165788
13	0.226892803	1.89069967	0.02878	1.768319	11.2316807	0.099536219			1.014709992	0.04873087		0.105128866	0.106521866	1.77331636
14	0.244346095	1.98842542	0.02878	1.85972	12.1402805	0.107039692			1.092764607	0.056516276		0.113451843	0.114844843	1.86497484
15	0.261799388	2.08615116	0.02878	1.95112	13.0488803	0.11492123			1.170819222	0.064878378		0.12221359	0.12360659	1.95663332

CdMIN	
wings	0.028802761
Wings+Tail Plane	0.030344934
Glider	0.031737934

Preliminary Performance Estimation - Spiral Flight - Reference to CL_wings **Re=100k**																
			phi	0.174533	0.349066	0.523599	0.698132	0.872665	1.047198	rad						
			0	10	20	30	40	50	60	[°]						
α [°]	Vx [m/s]	Vz [m/s]	Vx(0)	Vx(10)	Vx(20)	Vx(30)	Vx(40)	Vx(50)	Vx(60)	Vz(0)	Vz(10)	Vz(20)	Vz(30)	Vz(40)	Vz(50)	Vz(60)
-1	58.88985	70.7517	58.88985	59.34235	60.75018	63.28127	67.28426	73.45253	83.28283	70.7517	72.39518	77.67086	87.78916	105.5251	137.289	200.116
0	39.46238	21.52181	39.46238	39.7656	40.70899	42.40509	45.08751	49.2209	55.80823	21.52181	22.02174	23.62653	26.7044	32.09947	41.76164	60.87287
1	31.68714	11.41635	31.68714	31.93062	32.68814	34.05005	36.20396	39.52295	44.81239	11.41635	11.68154	12.53282	14.16549	17.02733	22.15268	32.29033
2	27.2192	7.507162	27.2192	27.42834	28.07905	29.24893	31.09914	33.95014	38.49376	7.507162	7.681545	8.241325	9.314935	11.19682	14.56715	21.23346
3	24.22839	5.554362	24.22839	24.41456	24.99377	26.0351	27.68201	30.21975	34.26412	5.554362	5.683384	6.097551	6.891888	8.28425	10.77787	15.71011
4	22.04693	4.432664	22.04693	22.21633	22.74339	23.69096	25.18959	27.49883	31.17906	4.432664	4.53563	4.866156	5.500078	6.611254	8.601289	12.53747
5	20.36526	3.72968	20.36526	20.52175	21.0086	21.8839	23.26821	25.40132	28.80083	3.72968	3.816316	4.094424	4.627811	5.562763	7.237195	10.54913
6	19.01772	3.262585	19.01772	19.16385	19.61849	20.43587	21.72859	23.72055	26.89512	3.262585	3.338371	3.58165	4.048237	4.866098	6.330829	9.227984
7	17.90655	2.939322	17.90655	18.04414	18.47222	19.24184	20.45903	22.3346	25.32369	2.939322	3.0076	3.226774	3.64713	4.383957	5.70356	8.313659
8	16.96985	2.709088	16.96985	17.10024	17.50593	18.23529	19.3888	21.16626	23.99899	2.709088	2.772017	2.974023	3.361454	4.040566	5.256805	7.662458
9	16.16627	2.541831	16.16627	16.29049	16.67696	17.37179	18.47068	20.16397	22.86256	2.541831	2.600875	2.79041	3.153921	3.791105	4.932254	7.189385
10	15.46701	2.418784	15.46701	15.58585	15.95561	16.62038	17.67174	19.29179	21.87365	2.418784	2.47497	2.65533	3.001243	3.607582	4.69349	6.841356
11	14.85128	2.327702	14.85128	14.96539	15.32043	15.95874	16.96824	18.5238	21.00288	2.327702	2.381772	2.55534	2.888227	3.471734	4.51675	6.583735
12	14.30368	2.2603	14.30368	14.41359	14.75553	15.3703	16.34259	17.84079	20.22846	2.2603	2.312804	2.481346	2.804595	3.371204	4.385961	6.393093
13	13.8125	2.210804	13.8125	13.91864	14.24884	14.8425	15.7814	17.22815	19.53383	2.210804	2.262158	2.42701	2.74318	3.297382	4.289918	6.253097
14	13.36868	2.175084	13.36868	13.47141	13.791	14.36559	15.27431	16.67458	18.90617	2.175084	2.225609	2.387796	2.698858	3.244106	4.220605	6.152066
15	12.96507	2.15012	12.96507	13.06469	13.37463	13.93187	14.81316	16.17116	18.33538	2.15012	2.200065	2.360391	2.667883	3.206873	4.172165	6.081458

Preliminary Performance Estimation - Spiral Flight - Reference to CL_Glider **Re = 100k**																
			phi	0.174533	0.349066	0.523599	0.698132	0.872665	1.047198	rad						
			0	10	20	30	40	50	60	[°]						
α [°]	Vx [m/s]	Vz [m/s]	Vx(0)	Vx(10)	Vx(20)	Vx(30)	Vx(40)	Vx(50)	Vx(60)	Vz(0)	Vz(10)	Vz(20)	Vz(30)	Vz(40)	Vz(50)	Vz(60)
-1	62.63256	88.86659	62.63256	63.11381	64.61111	67.30306	71.56047	78.12075	88.57581	88.86659	90.93086	97.5573	110.2662	132.5432	172.4397	251.3527
0	41.97038	27.01983	41.97038	42.29287	43.29622	45.10011	47.95302	52.3491	59.35509	27.01983	27.64747	29.66223	33.52637	40.29968	52.43017	76.42361
1	33.70099	14.31844	33.70099	33.95995	34.76561	36.21408	38.50488	42.0348	47.6604	14.31844	14.65104	15.71872	17.76642	21.35575	27.78399	40.49867
2	28.94909	9.401647	28.94909	29.17153	29.86359	31.10783	33.07562	36.10782	40.9402	9.401647	9.620037	10.32108	11.66562	14.02242	18.24327	26.59187
3	25.76821	6.943226	25.76821	25.96621	26.58223	27.68975	29.44132	32.14034	36.44175	6.943226	7.10451	7.62224	8.6152	10.35572	13.47287	19.63841
4	23.4481	5.529409	23.4481	23.62827	24.18883	25.19662	26.79049	29.2465	33.16062	5.529409	5.657852	6.070158	6.860927	8.247034	10.72945	15.63953
5	21.65956	4.642018	21.65956	21.82599	22.34379	23.27472	24.74701	27.01568	30.63125	4.642018	4.749847	5.095984	5.759846	6.923503	9.007527	13.12961
6	20.22638	4.051294	20.22638	20.3818	20.86533	21.73466	23.10954	25.22809	28.60442	4.051294	4.145402	4.447491	5.026872	6.042447	7.861267	11.45879
7	19.04459	3.64153	19.04459	19.19092	19.64621	20.46474	21.75928	23.75406	26.93311	3.64153	3.726119	3.997654	4.518434	5.431289	7.066147	10.2998
8	18.04836	3.348857	18.04836	18.18703	18.6185	19.39422	20.62104	22.51147	25.52423	3.348857	3.426647	3.676358	4.155283	4.994771	6.498233	9.471997
9	17.19371	3.135489	17.19371	17.32582	17.73686	18.47584	19.64457	21.44548	24.31558	3.135489	3.208323	3.442124	3.890535	4.676536	6.084207	8.868501
10	16.45	2.977822	16.45	16.5764	16.96966	17.67668	18.79486	20.51787	23.26382	2.977822	3.046994	3.269038	3.694901	4.441378	5.778265	8.422552
11	15.79514	2.860451	15.79514	15.91651	16.29411	16.97299	18.04665	19.70107	22.33771	2.860451	2.926897	3.14019	3.549267	4.266322	5.550516	8.090579
12	15.21274	2.772954	15.21274	15.32963	15.69331	16.34715	17.38123	18.97465	21.51406	2.772954	2.837367	3.044135	3.440699	4.135821	5.380733	7.843099
13	14.69035	2.708061	14.69035	14.80323	15.15441	15.78581	16.78437	18.32307	20.77529	2.708061	2.770967	2.972896	3.36018	4.039034	5.254813	7.659554
14	14.21832	2.660573	14.21832	14.32757	14.66748	15.27858	16.24506	17.73432	20.10774	2.660573	2.722376	2.920764	3.301257	3.968207	5.162665	7.525238
15	13.78905	2.626687	13.78905	13.89501	14.22465	14.8173	15.7546	17.1989	19.50067	2.626687	2.687702	2.883564	3.25921	3.917665	5.096911	7.429392

Preliminary Performance Estimation - Spiral Flight - Reference to CL_wings **Re = 400k**																
			phi	0.174533	0.349066	0.523599	0.698132	0.872665	1.047198	rad						
			0	10	20	30	40	50	60	[°]						
α [°]	Vx [m/s]	Vz [m/s]	Vx(0)	Vx(10)	Vx(20)	Vx(30)	Vx(40)	Vx(50)	Vx(60)	Vz(0)	Vz(10)	Vz(20)	Vz(30)	Vz(40)	Vz(50)	Vz(60)
-5	75.97171	41.00826	75.97171	76.55546	78.37165	81.63692	86.80104	94.7585	107.4402	41.00826	41.96084	45.01866	50.88331	61.16323	79.5738	115.9889
-4	52.40893	13.54906	52.40893	52.81163	54.06452	56.31706	59.87952	65.36895	74.11742	13.54906	13.86379	14.8741	16.81177	20.20823	26.29106	38.32254
-3	42.4519	7.336313	42.4519	42.77809	43.79295	45.61754	48.50318	52.94969	60.03606	7.336313	7.506727	8.053768	9.102944	10.942	14.23563	20.75023
-2	36.61989	4.853504	36.61989	36.90127	37.77671	39.35063	41.83984	45.6755	51.78834	4.853504	4.966246	5.328153	6.02226	7.238932	9.417902	13.72778
-1	32.67699	3.591939	32.67699	32.92807	33.70925	35.11371	37.3349	40.75757	46.21224	3.591939	3.675376	3.943213	4.456902	5.357326	6.969919	10.15954
0	29.78338	2.859251	29.78338	30.01223	30.72424	32.00433	34.02883	37.14841	42.12006	2.859251	2.925669	3.138872	3.547778	4.264532	5.548187	8.087184
1	27.54343	2.396244	27.54343	27.75507	28.41353	29.59734	31.46959	34.35455	38.9523	2.396244	2.451907	2.630585	2.973276	3.573964	4.649753	6.777603
2	25.7431	2.086437	25.7431	25.94091	26.55633	27.66276	29.41263	32.10903	36.40624	2.086437	2.134903	2.29048	2.588864	3.111891	4.048592	5.901335
3	24.25516	1.870617	24.25516	24.44153	25.02138	26.06386	27.71259	30.25313	34.30197	1.870617	1.91407	2.053555	2.321074	2.789999	3.629809	5.290905
4	22.99859	1.715879	22.99859	23.17531	23.72511	24.71359	26.27691	28.68583	32.52492	1.715879	1.755737	1.883684	2.129074	2.559209	3.329549	4.853239
5	21.91904	1.602651	21.91904	22.08747	22.61147	23.55355	25.04348	27.33933	30.99821	1.602651	1.639879	1.759383	1.98858	2.390331	3.109838	4.532983
6	20.97852	1.518659	20.97852	21.13971	21.64123	22.54288	23.96888	26.16622	29.6681	1.518659	1.553936	1.667176	1.884362	2.265058	2.946857	4.295417
7	20.14952	1.455864	20.14952	20.30434	20.78604	21.65207	23.02172	25.13223	28.49572	1.455864	1.489682	1.598241	1.806446	2.1714	2.825008	4.117806
8	19.41162	1.408813	19.41162	19.56078	20.02483	20.85915	22.17864	24.21186	27.45218	1.408813	1.441539	1.546588	1.748065	2.101225	2.733709	3.984726
9	18.74928	1.373695	18.74928	18.89334	19.34156	20.14741	21.42188	23.38572	26.51548	1.373695	1.405605	1.508036	1.70449	2.048847	2.665565	3.885397
10	18.15041	1.347778	18.15041	18.28987	18.72378	19.50388	20.73764	22.63876	25.66855	1.347778	1.379086	1.479584	1.672332	2.010192	2.615274	3.812093
11	17.60549	1.329061	17.60549	17.74076	18.16164	18.91833	20.11505	21.95909	24.89792	1.329061	1.359933	1.459036	1.649107	1.982275	2.578954	3.759151
12	17.10687	1.316049	17.10687	17.23832	17.64728	18.38253	19.54536	21.33717	24.19277	1.316049	1.346619	1.444752	1.632962	1.962867	2.553705	3.722347
13	16.64836	1.307608	16.64836	16.77628	17.17428	17.88982	19.02148	20.76527	23.54433	1.307608	1.337982	1.435486	1.622488	1.950278	2.537326	3.698474
14	16.22484	1.302866	16.22484	16.34951	16.73738	17.43472	18.53759	20.23702	22.94538	1.302866	1.33313	1.43028	1.616604	1.943206	2.528124	3.685061
15	15.83208	1.30114	15.83208	15.95373	16.33221	17.01267	18.08885	19.74714	22.38994	1.30114	1.331365	1.428386	1.614464	1.940632	2.524776	3.680181

Preliminary Performance Estimation - Spiral Flight - Reference to CL_Glider **Re = 400k**																
			phi	0.174533	0.349066	0.523599	0.698132	0.872665	1.047198	rad						
			0	10	20	30	40	50	60	[°]						
α [°]	Vx [m/s]	Vz [m/s]	Vx(0)	Vx(10)	Vx(20)	Vx(30)	Vx(40)	Vx(50)	Vx(60)	Vz(0)	Vz(10)	Vz(20)	Vz(30)	Vz(40)	Vz(50)	Vz(60)
-5	78.64161	47.30099	78.64161	79.24588	81.12589	84.50591	89.85152	98.08863	111.216	47.30099	48.39974	51.92679	58.69137	70.54874	91.78442	133.7874
-4	54.25075	15.62435	54.25075	54.6676	55.96453	58.29623	61.98388	67.66624	76.72215	15.62435	15.98728	17.15233	19.38679	23.30349	30.31801	44.19233
-3	43.9438	8.454043	43.9438	44.28146	45.33198	47.22069	50.20774	54.81052	62.14592	8.454043	8.650421	9.280807	10.48983	12.60908	16.40451	23.91164
-2	37.90683	5.586729	37.90683	38.1981	39.10431	40.73354	43.31023	47.28068	53.60836	5.586729	5.716503	6.133083	6.932049	8.332525	10.84068	15.80166
-1	33.82536	4.128569	33.82536	34.08527	34.8939	36.34772	38.64697	42.18992	47.83629	4.128569	4.224471	4.532323	5.122755	6.157701	8.011213	11.67736
0	30.83007	3.280807	30.83007	31.06696	31.80399	33.12906	35.22472	38.45393	43.6003	3.280807	3.357016	3.601653	4.070846	4.893276	6.366187	9.279523
1	28.5114	2.744379	28.5114	28.73048	29.41207	30.63749	32.57553	35.56189	40.32121	2.744379	2.808128	3.012766	3.405243	4.093201	5.325285	7.762276
2	26.6478	2.384867	26.6478	26.85256	27.4896	28.63492	30.44629	33.23744	37.68568	2.384867	2.440265	2.618095	2.959158	3.556994	4.627675	6.745422
3	25.10756	2.133931	25.10756	25.30049	25.90071	26.97983	28.6865	31.31633	35.50746	2.133931	2.1835	2.342619	2.647795	3.182727	4.14075	6.035667
4	23.80684	1.953583	23.80684	23.98976	24.55889	25.58211	27.20036	29.69395	33.66795	1.953583	1.998963	2.144634	2.424019	2.913741	3.790798	5.525568
5	22.68935	1.821229	22.68935	22.86369	23.40611	24.3813	25.92359	28.30013	32.08759	1.821229	1.863534	1.999336	2.259792	2.716336	3.533973	5.151212
6	21.71577	1.722691	21.71577	21.88263	22.40177	23.33511	24.81123	27.08579	30.71074	1.722691	1.762707	1.891161	2.137526	2.569368	3.342767	4.872505
7	20.85764	1.648685	20.85764	21.01791	21.51653	22.41299	23.83078	26.01546	29.49716	1.648685	1.686982	1.809918	2.045699	2.45899	3.199163	4.663185
8	20.09381	1.592911	20.09381	20.24821	20.72857	21.59221	22.95807	25.06274	28.41694	1.592911	1.629912	1.748689	1.976494	2.375803	3.090937	4.505431
9	19.40819	1.550963	19.40819	19.55732	20.02129	20.85545	22.17471	24.20757	27.44732	1.550963	1.58699	1.702639	1.924445	2.313239	3.00954	4.386786
10	18.78827	1.519684	18.78827	18.93264	19.38179	20.18931	21.46643	23.43436	26.57063	1.519684	1.554984	1.668301	1.885634	2.266586	2.948845	4.298315
11	18.2242	1.496759	18.2242	18.36423	18.7999	19.58318	20.82196	22.7308	25.77291	1.496759	1.531527	1.643135	1.857188	2.232395	2.904361	4.233474
12	17.70806	1.480461	17.70806	17.84413	18.26746	19.02855	20.23225	22.08703	25.04299	1.480461	1.51485	1.625242	1.836965	2.208086	2.872735	4.187375
13	17.23343	1.469476	17.23343	17.36585	17.77784	18.51853	19.68996	21.49503	24.37176	1.469476	1.50361	1.613184	1.823335	2.191702	2.851421	4.156306
14	16.79503	1.462795	16.79503	16.92408	17.32559	18.04744	19.18907	20.94822	23.75176	1.462795	1.496774	1.605849	1.815045	2.181737	2.838456	4.137409
15	16.38847	1.459628	16.38847	16.5144	16.90618	17.61056	18.72455	20.44112	23.1768	1.459628	1.493533	1.602372	1.811116	2.177014	2.83231	4.128451

Preliminary Performance Estimation - Spiral Flight - Reference to CL_wings **Re = 750k**																
			phi	0.174533	0.349066	0.523599	0.698132	0.872665	1.047198	rad						
			0	10	20	30	40	50	60	[°]						
α [°]	Vx [m/s]	Vz [m/s]														
-6	148.3448	106.2949	Vx(0)	Vx(10)	Vx(20)	Vx(30)	Vx(40)	Vx(50)	Vx(60)	Vz(0)	Vz(10)	Vz(20)	Vz(30)	Vz(40)	Vz(50)	Vz(60)
-5	71.9834	12.12004	71.9834	72.53651	74.25735	77.3512	82.24422	89.78393	101.7999	12.12004	12.40158	13.30532	15.03863	18.07687	23.51814	34.28066
-4	54.18971	5.270489	54.18971	54.60609	55.90156	58.23063	61.91414	67.59009	76.63582	5.270489	5.392917	5.785917	6.539657	7.860858	10.22703	14.90719
-3	45.26384	3.193896	45.26384	45.61163	46.69372	48.63916	51.71593	56.45697	64.01273	3.193896	3.268087	3.506243	3.963007	4.76365	6.197543	9.033702
-2	39.66395	2.274673	39.66395	39.96872	40.91693	42.62169	45.31781	49.47231	56.09329	2.274673	2.327511	2.497124	2.822428	3.392641	4.413851	6.433746
-1	35.73289	1.786607	35.73289	36.00745	36.86169	38.39749	40.8264	44.56915	50.53394	1.786607	1.828108	1.961328	2.216834	2.664699	3.466792	5.053288
0	32.77839	1.498765	32.77839	33.03025	33.81386	35.22267	37.45076	40.88404	46.35564	1.498765	1.533579	1.645336	1.859677	2.235386	2.908253	4.239146
1	30.45328	1.317469	30.45328	30.68728	31.4153	32.72418	34.79422	37.98397	43.06744	1.317469	1.348073	1.446311	1.634725	1.964987	2.556462	3.726366
2	28.56176	1.198391	28.56176	28.78123	29.46403	30.69161	32.63308	35.6247	40.39243	1.198391	1.226229	1.315588	1.486972	1.787383	2.325399	3.389563
3	26.98392	1.118176	26.98392	27.19126	27.83634	28.99611	30.83032	33.65668	38.16102	1.118176	1.14415	1.227528	1.38744	1.667744	2.169747	3.16268
4	25.64165	1.063507	25.64165	25.83867	26.45167	27.55375	29.29672	31.98249	36.26277	1.063507	1.088211	1.167512	1.319606	1.586205	2.063664	3.008051
5	24.48162	1.026311	24.48162	24.66974	25.255	26.30722	27.97134	30.5356	34.62224	1.026311	1.050151	1.126679	1.273453	1.530728	1.991488	2.902846
6	23.46601	1.001454	23.46601	23.64632	24.2073	25.21587	26.81096	29.26885	33.18596	1.001454	1.024717	1.099391	1.242611	1.493654	1.943255	2.832539
7	22.56715	0.985537	22.56715	22.74055	23.28004	24.24998	25.78396	28.1477	31.91477	0.985537	1.00843	1.081918	1.222861	1.469915	1.91237	2.787521
8	21.76424	0.976238	21.76424	21.93148	22.45177	23.3872	24.86661	27.14625	30.77929	0.976238	0.998915	1.071709	1.211323	1.456045	1.894325	2.761218
9	21.04136	0.971924	21.04136	21.20304	21.70605	22.61041	24.04068	26.2446	29.75698	0.971924	0.9945	1.066973	1.205969	1.44961	1.885953	2.749015
10	20.38603	0.97142	20.38603	20.54267	21.03002	21.90621	23.29194	25.42722	28.8302	0.97142	0.993985	1.06642	1.205344	1.448858	1.884975	2.74759
11	19.78835	0.973864	19.78835	19.9404	20.41346	21.26396	22.60906	24.68174	27.98495	0.973864	0.996486	1.069104	1.208377	1.452505	1.889719	2.754505
12	19.24033	0.978614	19.24033	19.38817	19.84813	20.67508	21.98293	23.99821	27.20994	0.978614	1.001346	1.074318	1.214271	1.459589	1.898936	2.767939
13	18.73546	0.985181	18.73546	18.87942	19.32731	20.13256	21.40609	23.36849	26.49594	0.985181	1.008066	1.081527	1.222419	1.469383	1.911678	2.786513
14	18.26835	0.993189	18.26835	18.40872	18.84545	19.63062	20.8724	22.78587	25.83535	0.993189	1.01626	1.090318	1.232356	1.481328	1.927218	2.809164
15	17.83453	1.002348	17.83453	17.97156	18.39792	19.16445	20.37674	22.24477	25.22183	1.002348	1.025631	1.100372	1.243719	1.494987	1.944989	2.835067

Preliminary Performance Estimation - Spiral Flight - Reference to CL_Glider **Re = 750k**																
			phi	0.174533	0.349066	0.523599	0.698132	0.872665	1.047198	rad						
			0	10	20	30	40	50	60	[°]						
α [°]	Vx [m/s]	Vz [m/s]	Vx(0)	Vx(10)	Vx(20)	Vx(30)	Vx(40)	Vx(50)	Vx(60)	Vz(0)	Vz(10)	Vz(20)	Vz(30)	Vz(40)	Vz(50)	Vz(60)
-6	74.39402	14.28797	74.39402	74.96565	76.74413	79.94158	84.99846	92.79067	105.209	14.28797	14.61987	15.68527	17.72861	21.31031	27.72486	40.41249
-5	56.00444	6.205752	56.00444	56.43477	57.77362	60.18069	63.98755	69.85359	79.20225	6.205752	6.349905	6.812644	7.700138	9.25579	12.04185	17.55252
-4	46.77966	3.751658	46.77966	47.1391	48.25742	50.26801	53.44783	58.34764	66.15643	3.751658	3.838805	4.118551	4.655081	5.595543	7.279842	10.61129
-3	40.99224	2.66302	40.99224	41.30721	42.28718	44.04903	46.83544	51.12907	57.97178	2.66302	2.724879	2.92345	3.304292	3.971856	5.167413	7.532158
-2	36.92953	2.083375	36.92953	37.21329	38.09613	39.68337	42.19362	46.06171	52.22625	2.083375	2.13177	2.287119	2.585066	3.107324	4.042651	5.892676
-1	33.87609	1.740271	33.87609	34.13639	34.94623	36.40223	38.70493	42.25319	47.90803	1.740271	1.780695	1.910461	2.159339	2.595589	3.376879	4.922229
0	31.47312	1.523145	31.47312	31.71495	32.46735	33.82007	35.95943	39.256	44.50971	1.523145	1.558526	1.672101	1.889928	2.271748	2.955561	4.308103
1	29.51826	1.379652	29.51826	29.74507	30.45074	31.71943	33.72591	36.81773	41.74512	1.379652	1.4117	1.514575	1.711881	2.057731	2.677123	3.902246
2	27.88757	1.282204	27.88757	28.10185	28.76854	29.96715	31.86278	34.7838	39.43898	1.282204	1.311989	1.407598	1.590968	1.912389	2.488032	3.626622
3	26.50035	1.21506	26.50035	26.70398	27.3375	28.47648	30.27782	33.05353	37.47716	1.21506	1.243285	1.333887	1.507654	1.812245	2.357743	3.436709
4	25.30148	1.168673	25.30148	25.49589	26.10075	27.18821	28.90806	31.5582	35.7817	1.168673	1.19582	1.282963	1.450097	1.743059	2.267732	3.305506
5	24.25186	1.136965	24.25186	24.43821	25.01797	26.06032	27.70882	30.24902	34.29731	1.136965	1.163376	1.248155	1.410754	1.695767	2.206206	3.215824
6	23.32289	1.115913	23.32289	23.5021	24.05966	25.06208	26.64743	29.09033	32.98355	1.115913	1.141835	1.225044	1.384633	1.664369	2.165356	3.15628
7	22.4931	1.102764	22.4931	22.66593	23.20365	24.17041	25.69936	28.05534	31.81004	1.102764	1.12838	1.210608	1.368316	1.644756	2.139839	3.119087
8	21.746	1.09558	21.746	21.9131	22.43296	23.3676	24.84577	27.1235	30.7535	1.09558	1.121029	1.202722	1.359402	1.634041	2.125899	3.098767
9	21.06873	1.092967	21.06873	21.23062	21.73429	22.63982	24.07195	26.27874	29.79568	1.092967	1.118356	1.199854	1.356161	1.630145	2.120831	3.091379
10	20.45103	1.093903	20.45103	20.60817	21.09708	21.97606	23.36621	25.5083	28.92213	1.093903	1.119313	1.200881	1.357322	1.63154	2.122645	3.094024
11	19.88466	1.09762	19.88466	20.03745	20.51282	21.36746	22.71911	24.80187	28.12116	1.09762	1.123116	1.204962	1.361934	1.637084	2.129858	3.104538
12	19.36288	1.103538	19.36288	19.51166	19.97455	20.80677	22.12295	24.15106	27.38325	1.103538	1.129172	1.211458	1.369277	1.645911	2.141342	3.121276
13	18.88013	1.111209	18.88013	19.0252	19.47656	20.28802	21.57139	23.54894	26.70054	1.111209	1.137021	1.219879	1.378795	1.657352	2.156227	3.142973
14	18.43178	1.120285	18.43178	18.57341	19.01404	19.80624	21.05912	22.98971	26.06647	1.120285	1.146308	1.229843	1.390056	1.670888	2.173838	3.168643

Preliminary Performance Estimation - Spiral Flight - Reference to CL_wings **Re = 1E6**

			phi	0.174533	0.349066	0.523599	0.698132	0.872665	1.047198	rad						
			0	10	20	30	40	50	60	[°]						
α [°]	Vx [m/s]	Vz [m/s]	Vx(0)	Vx(10)	Vx(20)	Vx(30)	Vx(40)	Vx(50)	Vx(60)	Vz(0)	Vz(10)	Vz(20)	Vz(30)	Vz(40)	Vz(50)	Vz(60)
-5	74.41014	16.21276	74.41014	74.98189	76.76075	79.9589	85.01687	92.81077	105.2318	16.21276	16.58936	17.79829	20.1169	24.1811	31.45978	45.85661
-4	56.37145	7.147928	56.37145	56.80459	58.15221	60.57506	64.40687	70.31135	79.72126	7.147928	7.313967	7.84696	8.869195	10.66103	13.87008	20.21739
-3	47.20498	4.315102	47.20498	47.56769	48.69618	50.72505	53.93377	58.87813	66.75792	4.315102	4.415337	4.737098	5.354207	6.435912	8.373168	12.20495
-2	41.42102	3.035397	41.42102	41.73929	42.72951	44.50978	47.32535	51.66388	58.57817	3.035397	3.105906	3.332244	3.76634	4.527251	5.889986	8.585399
-1	37.34741	2.342665	37.34741	37.63438	38.52721	40.1324	42.67107	46.58292	52.81721	2.342665	2.397083	2.571766	2.906794	3.494051	4.545786	6.626058
0	34.27925	1.925319	34.27925	34.54264	35.36213	36.83545	39.16556	42.75605	48.47818	1.925319	1.970042	2.113606	2.388949	2.871586	3.735954	5.445625
1	31.86108	1.655779	31.86108	32.1059	32.86757	34.23696	36.4027	39.7399	45.05837	1.655779	1.694241	1.817706	2.054501	2.46957	3.212928	4.683249
2	29.89168	1.473232	29.89168	30.12136	30.83596	32.1207	34.15257	37.28349	42.27322	1.473232	1.507454	1.617307	1.827996	2.197304	2.858709	4.166929
3	28.24746	1.345449	28.24746	28.46451	29.1398	30.35387	32.27397	35.23268	39.94794	1.345449	1.376702	1.477027	1.669442	2.006718	2.610754	3.805504
4	26.84777	1.25395	26.84777	27.05407	27.69589	28.84981	30.67477	33.48687	37.96849	1.25395	1.283078	1.37658	1.555909	1.870248	2.433206	3.546705
5	25.63746	1.187477	25.63746	25.83445	26.44734	27.54924	29.29193	31.97726	36.25684	1.187477	1.215061	1.303606	1.473429	1.771104	2.30422	3.358692
6	24.57733	1.138832	24.57733	24.76618	25.35373	26.41006	28.08069	30.65498	34.7576	1.138832	1.165286	1.250205	1.413071	1.698552	2.209829	3.221105
7	23.6387	1.10323	23.6387	23.82034	24.38545	25.40144	27.00827	29.48424	33.43018	1.10323	1.128857	1.211121	1.368895	1.645452	2.140745	3.120407
8	22.80001	1.077382	22.80001	22.9752	23.52026	24.5002	26.05001	28.43814	32.24408	1.077382	1.102408	1.182744	1.336822	1.606899	2.090588	3.047296
9	22.04468	1.058964	22.04468	22.21406	22.74107	23.68855	25.18702	27.49603	31.17588	1.058964	1.083563	1.162525	1.313969	1.579429	2.054849	2.995202
10	21.35976	1.046297	21.35976	21.52389	22.03452	22.95256	24.40448	26.64175	30.20727	1.046297	1.070602	1.14862	1.298252	1.560537	2.03027	2.959376
11	20.73496	1.038142	20.73496	20.89429	21.38998	22.28117	23.69061	25.86244	29.32367	1.038142	1.062257	1.139668	1.288134	1.548374	2.014446	2.93631
12	20.16197	1.033568	20.16197	20.31689	20.79888	21.66545	23.03594	25.14775	28.51333	1.033568	1.057577	1.134646	1.282458	1.541552	2.00557	2.923372
13	19.63399	1.031864	19.63399	19.78486	20.25423	21.0981	22.43271	24.48922	27.76666	1.031864	1.055833	1.132775	1.280343	1.53901	2.002263	2.918552
14	19.14544	1.032481	19.14544	19.29255	19.75024	20.57311	21.87451	23.87985	27.07574	1.032481	1.056464	1.133452	1.281109	1.53993	2.00346	2.920296
15	18.69163	1.034988	18.69163	18.83525	19.28209	20.08546	21.35601	23.31381	26.43395	1.034988	1.059029	1.136204	1.284219	1.543669	2.008324	2.927387

Preliminary Performance Estimation - Spiral Flight - Reference to CL_Glider **Re = 1E6**

			phi	0.174533	0.349066	0.523599	0.698132	0.872665	1.047198	rad						
			0	10	20	30	40	50	60	[°]						
α [°]	Vx [m/s]	Vz [m/s]	Vx(0)	Vx(10)	Vx(20)	Vx(30)	Vx(40)	Vx(50)	Vx(60)	Vz(0)	Vz(10)	Vz(20)	Vz(30)	Vz(40)	Vz(50)	Vz(60)
-5	76.83344	18.66826	76.83344	77.42381	79.2606	82.5629	87.7856	95.83332	108.6589	18.66826	19.10191	20.49393	23.1637	27.84344	36.22452	52.80182
-4	58.20728	8.225526	58.20728	58.65454	60.04605	62.5478	66.5044	72.60116	82.31753	8.225526	8.416596	9.029942	10.20629	12.26825	15.96109	23.2653
-3	48.74229	4.959759	48.74229	49.11682	50.28206	52.377	55.69022	60.79561	68.93201	4.959759	5.074969	5.444799	6.154102	7.39741	9.624083	14.02832
-2	42.76997	3.483052	42.76997	43.09861	44.12107	45.95932	48.86658	53.34641	60.48587	3.483052	3.56396	3.823678	4.321794	5.194922	6.758631	9.851559
-1	38.5637	2.68268	38.5637	38.86001	39.78192	41.43939	44.06073	48.09998	54.5373	2.68268	2.744996	2.945033	3.328687	4.001178	5.205562	7.587765
0	35.39562	2.199724	35.39562	35.66759	36.51376	38.03506	40.44106	44.14848	50.05696	2.199724	2.250821	2.414846	2.729432	3.280857	4.268418	6.221759
1	32.8987	1.887197	32.8987	33.15148	33.93796	35.35195	37.58821	41.0341	46.52578	1.887197	1.931034	2.071755	2.341646	2.814727	3.66198	5.337798
2	30.86516	1.675023	30.86516	31.10232	31.84018	33.16677	35.26481	38.4977	43.64992	1.675023	1.713931	1.838831	2.078379	2.498272	3.25027	4.737679
3	29.16739	1.526052	29.16739	29.39151	30.08879	31.3424	33.32503	36.38009	41.24892	1.526052	1.561501	1.675292	1.893535	2.276085	2.961202	4.316327
4	27.72212	1.41898	27.72212	27.93513	28.59786	29.78936	31.67375	34.57743	39.205	1.41898	1.451942	1.55775	1.76068	2.116389	2.753437	4.013483
5	26.47239	1.340825	26.47239	26.6758	27.30865	28.44643	30.24588	33.01866	37.43761	1.340825	1.371971	1.471952	1.663705	1.999822	2.601783	3.792427
6	25.37774	1.283284	25.37774	25.57274	26.17942	27.27016	28.99519	31.65331	35.88954	1.283284	1.313094	1.408783	1.592308	1.914	2.490128	3.629676
7	24.40854	1.240834	24.40854	24.59609	25.17961	26.22869	27.88784	30.44445	34.51889	1.240834	1.269657	1.362182	1.539635	1.850686	2.407756	3.509609
8	23.54253	1.209679	23.54253	23.72343	24.28624	25.29809	26.89838	29.36428	33.29416	1.209679	1.237779	1.32798	1.500978	1.804219	2.347302	3.421489
9	22.7626	1.187137	22.7626	22.93751	23.48167	24.46001	26.00728	28.39149	32.19118	1.187137	1.214713	1.303233	1.473007	1.770597	2.30356	3.357729
10	22.05538	1.171267	22.05538	22.22485	22.75211	23.70005	25.19925	27.50938	31.19102	1.171267	1.198474	1.285811	1.453316	1.746928	2.272766	3.312843
11	21.41024	1.160638	21.41024	21.57475	22.08658	23.0068	24.46214	26.7047	30.27865	1.160638	1.187598	1.274142	1.440127	1.731074	2.25214	3.282779
12	20.81858	1.154172	20.81858	20.97855	21.47624	22.37102	23.78615	25.96674	29.44192	1.154172	1.180982	1.267044	1.432104	1.721431	2.239594	3.264492
13	20.27341	1.151049	20.27341	20.42919	20.91385	21.7852	23.16327	25.28675	28.67093	1.151049	1.177786	1.263616	1.428229	1.716773	2.233533	3.255657
14	19.76894	1.150632	19.76894	19.92084	20.39344	21.24311	22.58689	24.65754	27.95751	1.150632	1.17736	1.263158	1.427711	1.71615	2.232724	3.254478
15	19.30035	1.152423	19.30035	19.44865	19.91005	20.73958	22.05151	24.07307	27.29482	1.152423	1.179192	1.265124	1.429933	1.718822	2.236199	3.259543

Spiral Performance Estimation Re=1E6

Spiral radius	With Cl Glider						With Cl wings only				
	20°	30°	40°	50°	60°		20°	30°	40°	50°	60°
r [m]	443.389011	303.2959	235.9224	197.96237	175.1079963	r [m]	1650.790055	1129.206902	878.3670417	737.0374607	651.947909
	373.530936	255.5102	198.7517	166.772444	147.5188878		947.4274754	648.0785618	504.1156302	423.0032393	374.1683321
	322.68963	220.7327	171.6996	144.073043	127.4400879		664.3595794	454.4487171	353.4983487	296.620334	262.3760892
	284.030263	194.2881	151.1293	126.812579	112.1723115		511.5277422	349.9055834	272.1782266	228.3846496	202.0180828
	253.642936	173.502	134.9606	113.245379	100.1714188		415.8613866	284.4659421	221.275222	185.6719572	164.2364883
	229.129261	156.7336	121.9171	102.300621	90.49021216		350.3404215	239.6469624	186.4122447	156.4184458	138.3602382
	208.936318	142.9209	111.1727	93.2849656	82.51539645		302.6555772	207.0286078	161.039669	135.1283268	119.5280224
	192.014283	131.3455	102.1687	85.7296901	75.83236294		266.3963611	182.2258432	141.7465431	118.939472	105.2081396
	177.627955	121.5047	94.51386	79.3065458	70.1507582		237.8956188	162.7301873	126.5816148	106.2145863	93.95231742
	165.24711	113.0357	87.92615	73.7788005	65.26118048		214.9038645	147.0029011	114.3479579	95.9493293	84.8721645
	154.479719	105.6704	82.19694	68.9714236	61.00880594		195.9645928	134.0476762	104.2705819	87.49340682	77.39246195
	145.029683	99.20615	77.16868	64.7522131	57.27669509		180.0931555	123.1909737	95.82556653	80.40719753	71.12434183
	136.669177	93.48722	72.72015	61.019451	53.97487321		166.5999966	113.9611094	88.64600662	74.38283146	65.79547719
	129.220046	88.39172	68.75655	57.6935961	51.03298183		154.9878109	106.0179066	82.46729166	69.19827402	61.2094669
	122.540971	83.82296	65.20269	54.7115521	48.3952091		144.8889095	99.10985122	77.09377851	64.68936111	57.22109928
	116.518413	79.70329	61.99815	52.022627	46.01671519		136.0255748	93.04697315	72.37769658	60.7320985	53.720695
	111.060109	75.96959	59.09385	49.5856273	43.86106235		128.1841269	87.68310691	68.20534931	57.23108345	50.62386538
							121.1974726	82.90395391	64.48782822	54.11171288	47.86462011
							114.9330652	78.61884689	61.15460667	51.3148079	45.39061241
							109.2844153	74.75494275	58.14902281	48.79282359	43.15978632
							104.1649873	71.25304777	55.42503207	46.50712397	41.13796631

2D Draws of the Designed Aircraft

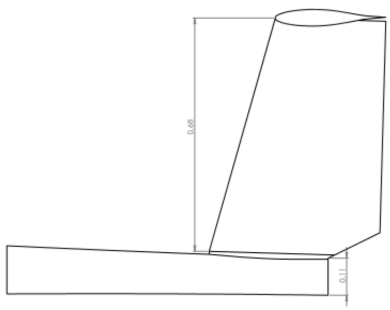
0,68
0,11

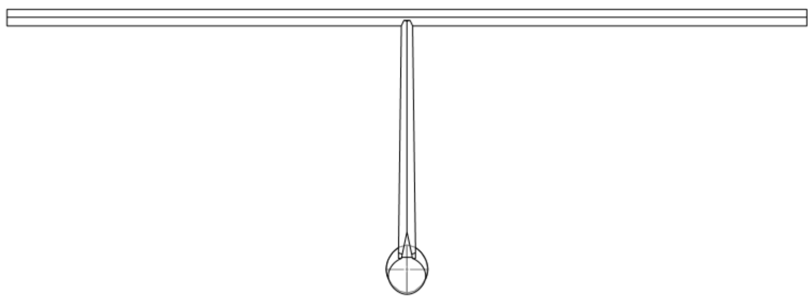

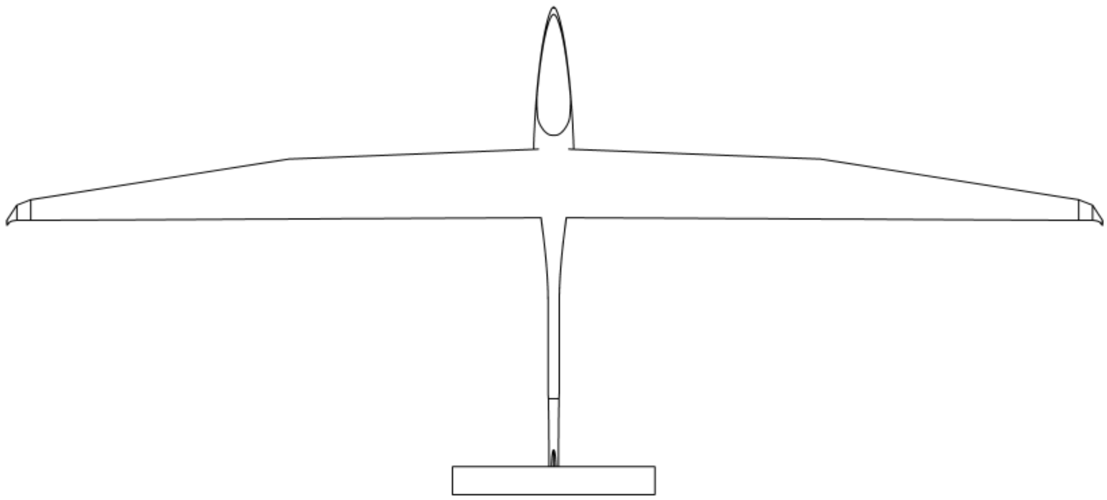

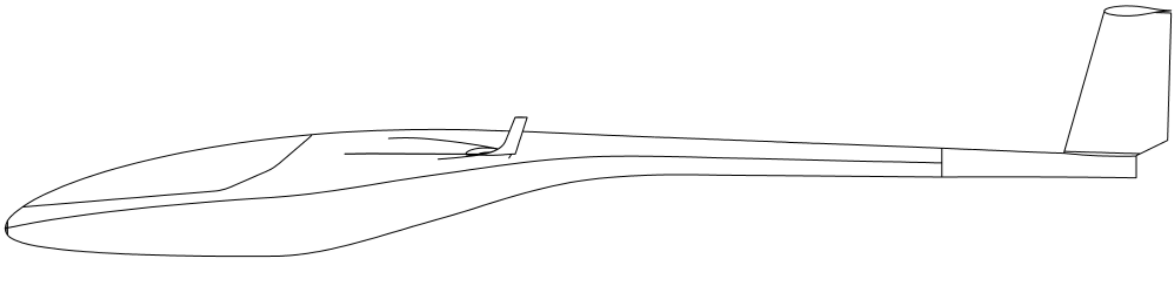

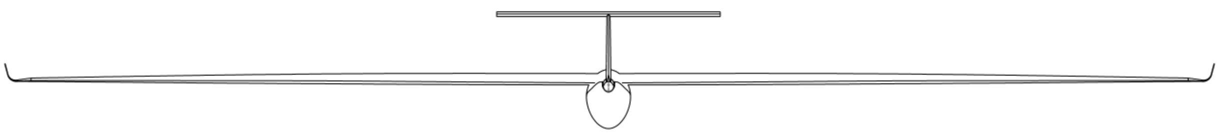

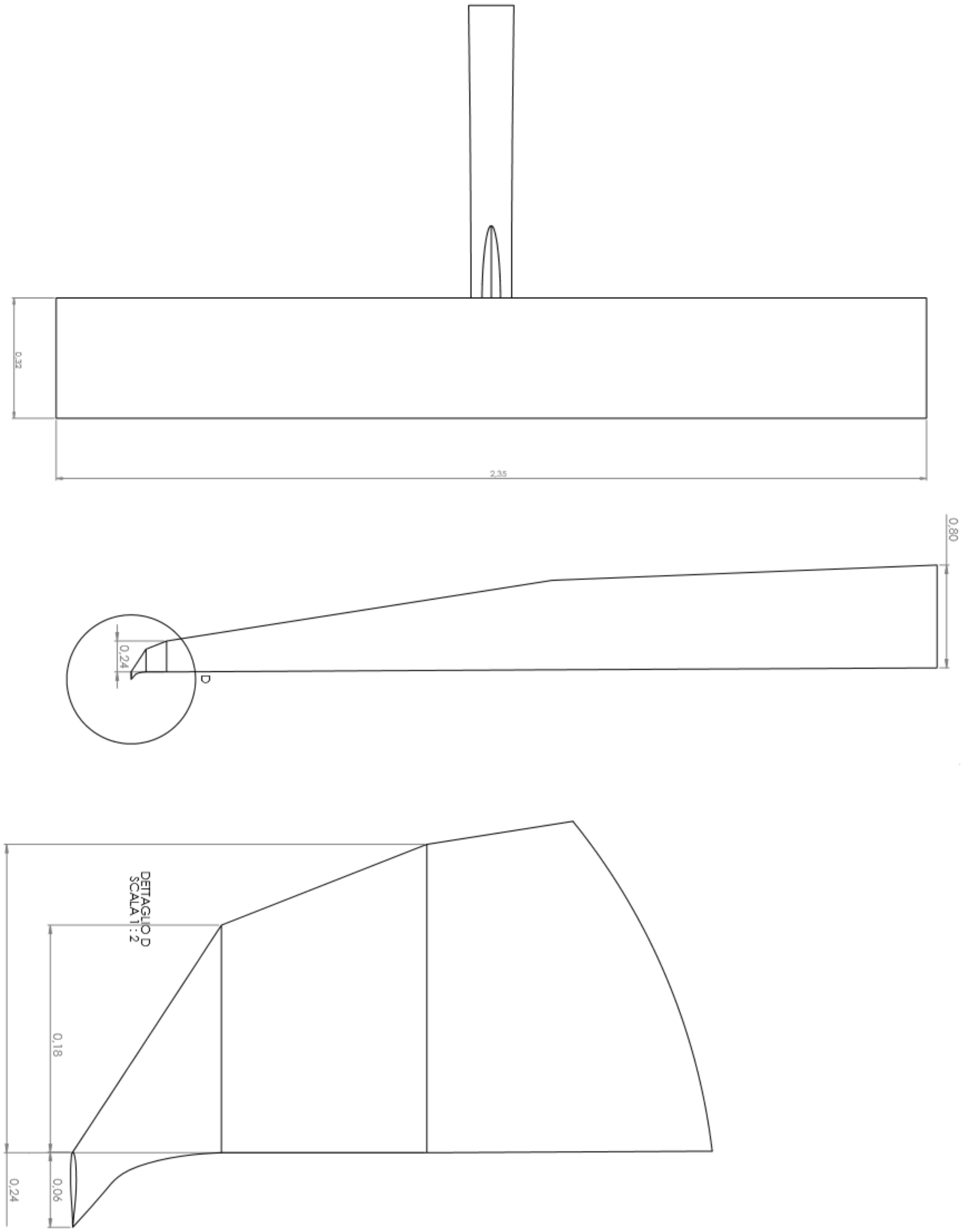
0,32
2,35
0,80
0,24
D
DETTAGLIO D
SCALA 1 : 2
0,18
0,06
0,24

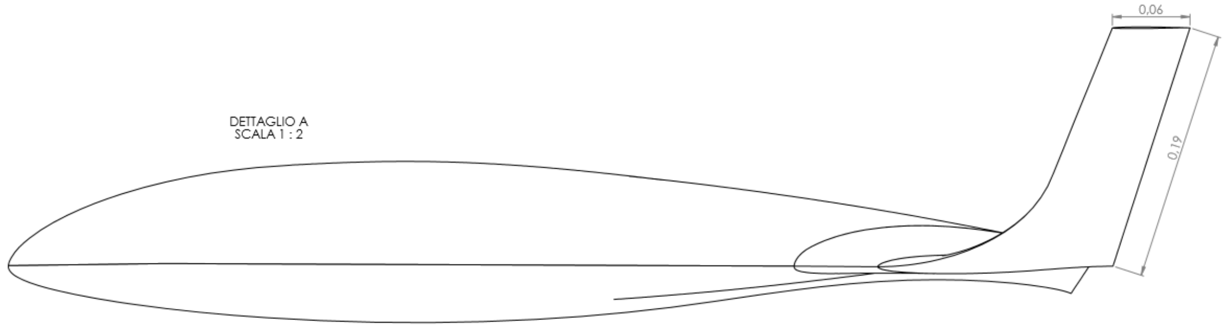
DETTAGLIO A
SCALA 1 : 2
0,06
0,19

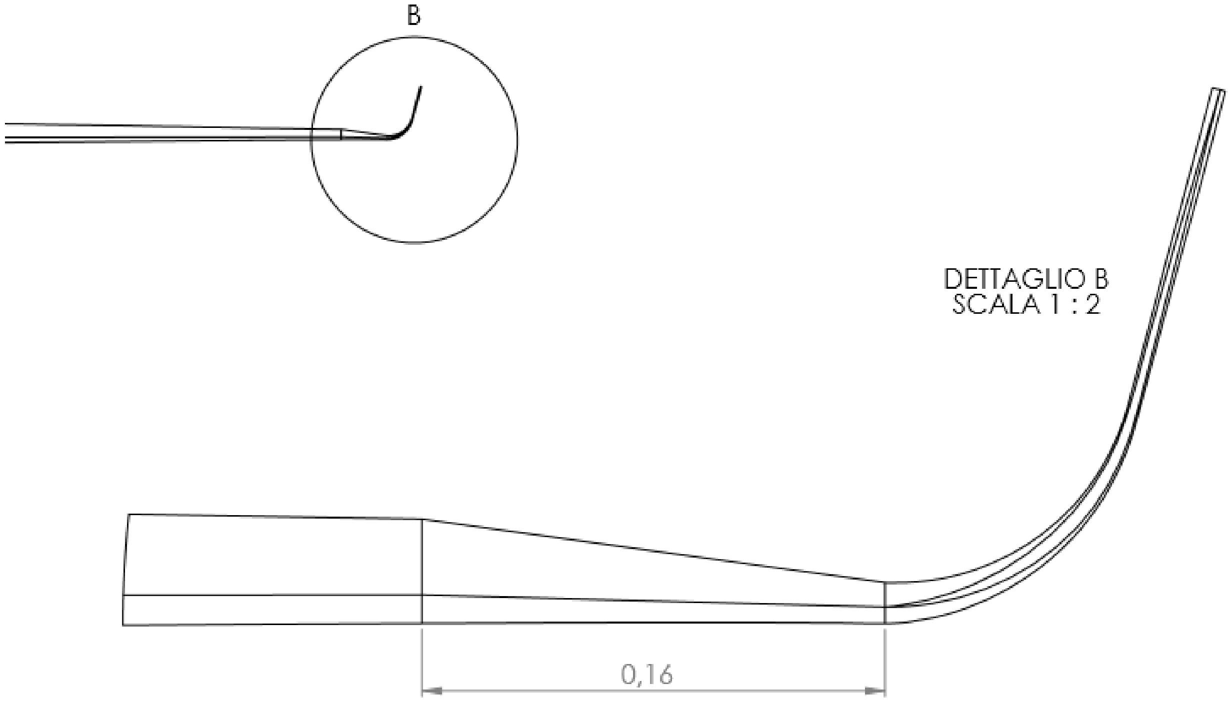
B
DETTAGLIO B
SCALA 1 : 2
0,16

```
%============EVALUATING MAXIMUM EFFICIENCY VELOCITY============
%Author : Marco Marzari
%Modified script of Lowry, J. T., "Performance of Light Aircraft"
%, AIAA(R) Education Series,Washington, DC, 1999.
%---------------------------------------------------------------

clc
clear all
W = 2500; % weight, N
S = 7.26;  % wing reference area, m^2;
A = 19.5; % wing aspect ratio
C_D0 = 0.03173; % flaps up parasite drag coefficient
e = 0.8247; % airplane efficiency factor
h_m=1500; % altitude, m
phi = 0; % bank angle, deg
i=0;

[T, a, P, rho] = atmoscoesa(h_m, 'Warning');

TAS_bg = sqrt((2*W) / (rho*S))*(1./(4*C_D0.^2 + ...
...C_D0.*pi*e*A*cos(phi)^2)).^(1/4);
CAS_bg = correctairspeed(TAS_bg,a,P,'TAS','CAS')';
gamma_bg_rad = asin( -sqrt((4.*C_D0')./(pi*e*A*cos(phi)^2 +...
4.*C_D0')) );
gamma_bg = convang(gamma_bg_rad,'rad','deg');
D_bg = -W*sin(gamma_bg_rad);
L_bg =  W*cos(gamma_bg_rad);
qbar = dpressure([TAS_bg' zeros(size(TAS_bg,2),2)], rho);
C_D_bg = D_bg./(qbar*S);
C_L_bg = L_bg./(qbar*S);

%PLOT
mTAS = (15:50)'; % true airspeed,m/s
mCAS = correctairspeed(mTAS,a,P,'TAS','CAS')'; % corrected airspeed, m/s
qbar = dpressure([mTAS zeros(size(mTAS,1),2)], rho);
Dp = qbar*S.*C_D0;
Di = (2*W^2)/(rho*S*pi*e*A).*(mTAS.^-2);
D = Dp + Di;
L = W;
KAPPA=max(L./D);
figure
```

```
plot(mCAS,L./D);
hold on

title('L/D vs. CAS');
xlabel('CAS'); ylabel('L/D');

hold on
plot(CAS_bg,L_bg/D_bg,'Marker','o','MarkerFaceColor','black',...
'MarkerEdgeColor','black','Color','white');
legend('L/D','L_{bg}/D_{bg}','Location','Best');
h2 = figure;
plot(mCAS,Dp,mCAS,Di,mCAS,D);
title('Parasite, induced, and total drag curves');
xlabel('CAS'); ylabel('Drag, [N]');
hold on
plot(CAS_bg,D_bg,'Marker','o','MarkerFaceColor','black',...
'MarkerEdgeColor','black','Color','white');
hold on
legend('Parasite, D_p','Induced, D_i','Total, D','D_{bg}','Location','Best');
```

K-ω SST Algorithm

Turbulent flows are characterized by fluctuating velocity fields. These fluctuations mix transported quantities such as momentum, energy, and species concentration, and cause the transported quantities to fluctuate as well. Since these fluctuations can be of small scale and high frequency, they are too computationally expensive to simulate directly in practical engineering calculations. Instead, the instantaneous (exact) governing equations can be time-averaged, ensemble-averaged, or otherwise manipulated to remove the resolution of small scales, resulting in a modified set of equations that are computationally less expensive to solve. However, the modified equations contain additional unknown variables, and turbulence models are needed to determine these variables in terms of known quantities.

The *standard* and *shear-stress transport* (SST) k- ω models have both similar forms, with transport equations for k and ω. The major ways in which the SST model differs from the standard model are as follows:

- gradual change from the standard k- ω model in the inner region of the boundary layer to a high-Reynolds-number version of the k- ϵ model in the outer part of the boundary layer
- modified turbulent viscosity formulation to account for the transport effects of the principal turbulent shear stress

The transport equations, methods of calculating turbulent viscosity, and methods of calculating model constants and other terms are presented separately for each model.

The shear-stress transport (SST) k- ω model was developed by Menter [224] to effectively blend the robust and accurate formulation of the k- ω model in the near-wall region with the free-stream independence of the k- ϵ model in the far field. To achieve this, the k- ϵ model is converted into a k- ω formulation. The SST k- ω model is similar to the standard k- ω model, but includes the following refinements:

- The standard k- ω model and the transformed k- ϵ model are both multiplied by a blending function and both models are added together. The blending function is designed to be one in the near-wall region, which activates the standard k- ω model, and zero away from the surface, which activates the transformed k- ϵ model.
- The SST model incorporates a damped cross-diffusion derivative term in the ω equation.

- The definition of the turbulent viscosity is modified to account for the transport of the turbulent shear stress.
- The modelling constants are different.

These features make the SST k- ω model more accurate and reliable for a wider class of flows (e.g., adverse pressure gradient flows, airfoils, transonic shock waves) than the standard k- ω model. Other modifications include the addition of a cross-diffusion term in the ω equation and a blending function to ensure that the model equations behave appropriately in both the near-wall and far-field zones.

The SST k-ω turbulence model [51] is a turbulence model and precisely a two-equation eddy-viscosity model which has become very popular. The shear stress transport (SST) formulation combines the best of two worlds. The use of a k-ω formulation in the inner parts of the boundary layer makes the model directly usable all the way down to the wall through the viscous sub-layer, hence the SST k-ω model can be used as a Low-Re turbulence model without any extra damping functions. The SST formulation also switches to a k-ϵ behaviour in the free-stream and thereby avoids the common k-ω problem that the model is too sensitive to the inlet free-stream turbulence properties. Authors who use the SST k-ω model often merit it for its good behaviour in adverse pressure gradients and separating flow. The SST k-ω model does produce a bit too large turbulence levels in regions with large normal strain, like stagnation regions and regions with strong acceleration. This tendency is much less pronounced than with a normal k-ϵ model though.

For other information or a deeply review of the main equation, please visit the *Ansys' Help Guide* or `www.cfd-online.com`

Bibliography

[1] Rodolfo Biancorosso. "*Per ora non voleremo elettrico*". VFR aviation,2017 May;number 23;Pag 27-31

[2] Kevin Bullis. "*Gli aerei elettrici stanno per diventare realtà*". Linkiesta.

[3] *The History of Solar*. U.S. Department of Energy. Energy Efficiency and Renewable Energy http://www1.eere.energy.gov/solar/pdfs/solar_timeline.pdf

[4] R. J. Boucher. *History of Solar Flight*. In Proc. of the 20th Joint Propulsion Conference, AIAA-84-1429, Cincinnati, Ohio, USA, June 1984.

[5] Solar Solitude Official Website. http://personalpages.tds.net/~dbeck/

[6] The World Air Sports Federation. http://www.fai.org

[7] Solar Flight of Wolfgang Schaeper.http://www.mfg-markdorf.de

[8] Sunseeker from Eric Raymond. www.solar-flight.com

[9] History of the Berblinger Contest. http://www.ifb.uni-stuttgart.de/icare

[10] Icare at Uni Stuttgart. http://www.ifb.uni-stuttgart.de/icare/Englisch/icare2eng.htm

[11] Solar-Power Research at NASA Dryden. http://trc.dfrc.nasa.gov/Newsroom/FactSheets/PDF/FS-054-DFRC.pdf

[12] Solar-Impulse Website. http://www.solar-impulse.com

[13] R.J.Boucher. *Project Sunrise-A Flight Demonstration of Astro Flight Model 7404 Solar Powered Remotely Piloted Vehicle*. In Proc. of the 15th Joint Propulsion Conference, AIAA-79-1264, Las Vegas, Nevada, June 18-20 1979

[14] P. B. MacCready, P. B. S. Lissaman, W. R. Morgan, and J. D. Burke. *Sun-Powered Aircraft Designs*. JournalofAircraft,20(6):487–493,June 1983.

[15] F.G.Irving ,D.Morgan. *The Feasibility of an Aircraft Propelled by Solar Energy*. In Proc. of the 2nd International Symposium on the Technology and Science of Low Speed and Motorless Flight, AIAA-19741042, Cambridge, Massachusetts, September 11-13 1974.

[16] W. Stender. *Sailplane Weight Estimation*. Organisation Scientific et Technique International a Voile (OSITIV), 1969.

[17] S.A.BrandtandF.T.Gilliam. *Design Analysis Methodology for Solar Powered Aircraft*. Journal of Aircraft, 32(4):703–709, July-August 1995.

[18] A. Noth. *Design of Solar Powered Airplanes for Continuous Flight*. DISS. ETH NO. 18010 Ecole Polytechnique Fédérale de Lausanne, Suisse

[19] M. Hajianmaleki. *Conceptual Design Method for Solar Powered Aircrafts*. 49th AIAA Aerospace Sciences Meeting 4-7 January2011, Orlando, Florida.

[20] F. Ferus. *Calcolo dei carichi aerodinamici e verifica strutturale di un aereo ultraleggero*. Tesi di Laurea in Ingegneria Aerospaziale, Dipartimento di Ingegneria Industriale, Università degli Studi di Padova, 2013-14

[21] M. Scalchi. *Aerodynamic and Structural design of some components of an ultralight aircraft*. Tesi di Laurea in Ingegneria Aerospaziale, Dipartimento di Ingegneria Industriale, Università degli Studi di Padova,2012-13

[22] Lloyd R. Jenkinson, James F. Marchman III. *Aircraft Design Projects for engineering students*. Chapter One : *Design Methodology*. Butterworth-Heinemann An imprint of Elsevier Science Linacre House, Jordan Hill, Oxford OX2 8DP 200 Wheeler Road, Burlington MA 01803

[23] Michelangelo Flaccavento. *Progettazione del Velivolo*. Chapter two, Section two, Pag 48. Ulrico Hoepli Editore S.p.A

[24] Fred Thomas. *Fundamental of Sailplane Design*. College Park Press P.O. Box 143 College Park, Maryland 20741, USA

[25] *Glider Flying Handbook*. FAA U.S. Department of Transportation

[26] Xiongfeng Zhu, Zheng Guo, Zhongxi Hou. *Solar-powered airplanes : A historical perspective and future challenge*. College of Aerospace Sciences and Engineering, National University of Defense Technology, Changsha 410073, China. *Progress in Aerospace Science* edited by Elseveir.

[27] Petrie G. *High-resolution imaging from a world-wide survey*. GEO Inf 2004:22–7, `http://web2.ges.gla.ac.uk/~gpetrie/ww_survey1.pdf`.

[28] Oodo M, Tsuji H, Miura R, Maruyama M, Suzuki M, Nishi Y, et al. *Experiments on IMT-2000 using unmanned solar powered aircraft at an altitude of 20 km*. IEEE Trans Veh Technol 2005;54(4):1278–94.

[29] Buoni GP, Howell KM. *Large unmanned aircraft system operations in the national airspace system – the NASA 2007 Western States Fire Missions*. In: Proceedings of the 26th congress of international council of the aeronautical sciences (ICAS), Anchorage, Alaska; 2008.

[30] Herwitz SR, Johnson LF, Arvesen JC. *Precision agriculture as a commercial application for solar-powered unmanned aerial vehicles*. In: Proceedings of the AIAA's 1st technical conference and workshop on unmanned aerospace vehicles, Portsmouth, Virginia; 2002.

[31] Herwitz SR, Johnson LF, Dunagand SE, Higgins RG, Sullivan DV, Zheng J, et al. *Imaging from an unmanned aerial vehicle: agricultural surveillance and decision support*. Comput Electron Agric 2004;44(1):49–61.

[32] Landis GA. *Solar airplane concept developed for Venus exploration*. NASA Technical Report 20050192264, 2005.

[33] John D. Anderson, Jr. *Fundamentals of Aerodynamics*. Published by McGraw-Hill

[34] Vittorio Pajno. *Sailplane Design : a guide for students and designers, from drafting to flight test*. IBN Istituto Bibliografico Napoleone Via dei Marsi 57-00185 Roma.

[35] *What is the Earth's Radiation Budjet?* https://science-edu.larc.nasa.gov/EDDOCS/whatis.html

[36] *Basic Photovoltaic Principles and Method* published by Technical Information Office, Energy Research Institute, 1617 Cole Boulevard, Golden, Colorado 80401 https://www.nrel.gov/docs/legosti/old/1448.pdf

[37] Colella NJ, Wenneker GS.*Pathfinder and the development of solar rechargeable aircraft*. Energy Technology Rev 1994:1–10.

[38] Rapinett A Zephyr. *A high altitude long endurance unmanned air vehicle*. (Master thesis). University of Surrey; 2009, http://personal.ph.surrey.ac.uk/~phs1pr/mphys-dissertations/2009/Rapinett-MPhys09.pdf.

[39] Daniel P. Raymar. *Aircraft Design : A Conceptual Approach.*Chapter 1, AIAA Eduaction Series, Fifth Edition,

[40] J.D. Anderson Jr., *Introduction to Flight*, 3rd edition. Tata McGraw-Hill Edition, University of Maryland, 1989

[41] J.D. Anderson Jr., *Aircraft Performance and Design*. Tata McGraw-Hill Edition, University of Maryland, 2010

[42] Jean Marie and Claude. *J2mc Planeurs*. Copyright 2003-2017 https://www.j2mcl-planeurs.net/

[43] M. D. Bailey and M. V. Bower. *High-Altitude Solar Power Platform*. Technical report, NASA-TM-103578, George C. Marshall Space Flight Center Huntsville, AL, USA, April 1992.

[44] A. J. Colozza. *Preliminary Design of a Long-Endurance Mars Aircraft*. In Proc. of the 26th Joint Propulsion Conference, AIAA 90-2000, Orlando, Florida, USA, July 16-18 1990.

[45] E. Rizzo and A. Frediani. *A Model for Solar Powered Aircraft Preliminary Design*. In Proc. of International Conference on Computational and Experimental Engineering and Sciences 04, volume 1, pages 39–54, Madeira, Portugal, July 2004.

[46] Lloyd R. Jenkinson James F. Marchman III. *Aircraft Design Projects for engineering students*. Butterworth-Heinemann, ISBN 0 7506 5772 3

[47] Harry Riblett. *What are Wortmann airfoil?*. EAA 29576, 416 Riblett Lane, Wilmington

[48] Mark Drela. *XFOIL : an Analysis and Design System for Low Reynolds Number Airfoils*. MIT Dept. of Aeronautics and Astronautics, Cambridge, Massachusetts.

[49] Althaus, D. *Wind-Tunnel Measurements on Bodies and Wing-Body Combinations*. In Motorless Flight Research, 1972, NASA CR-2315, November 1973.

[50] *A Hands-on Introduction to Engineering Simulations*, CornellX: ENGR2000X, Online Course on platform EdX. https://www.edx.org/

[51] Menter, F. R. (1993), "*Zonal Two Equation $k-\omega$ Turbulence Models for Aerodynamic Flows*", AIAA Paper 93-2906.

[52] Menter, F. R. (1994), "*Two-Equation Eddy-Viscosity Turbulence Models for Engineering Applications*", AIAA Journal, vol. 32, no 8. pp. 1598-1605.

[53] MichaelS. Selig, James J. Guglielmo, Andy P. Broeren and Philippe Giguere. *Summary of Low-Speed Airfoil Data* , Department of Aeronautical and Astronautical Engineering University of Illinois at Urbana-Champaign, SoarTech Publications.

[54] *Hybrid Initialization.* [Https://www.sharcnet.ca/Software/Ansys/16.2.3/en-us/help/flu_th/flu_th_sec_hybrid_initialization.html]

[55] *Solar radiationi in PVGIS* European Commission, Joint research Centre, Institute for Energy and Transport(IET) http://re.jrc.ec.europa.eu/pvgis/solres/solrespvgis.htm

[56] V.M. Sineglazov, D.P. Karabetsky. "*Energy System Design of Solar Aircraft*" Aviation Computer-Integrated Complexes Department National Aviation University Kyiv, Ukraine

[57] *Li-ion Battery and Gauge Introduction* http://www.richtek.com/Design%20Support/Technical%20Document/AN024ù

[58] *Principle Operation : Universal Motor*. Johnson Electric, http://www.johnsonelectric.com/en/resources-for-engineers/ac-motors/principle-of-operation